ECRIS-2014
NIZHNY NOVGOROD, RUSSIA
24-28 AUGUST 2014

THE 21ST INTERNATIONAL
WORKSHOP ON
ECR ION SOURCES

ECR ion source developments at INFN-LNS

L. Celona on behalf the INFN-LNS team

Istituto Nazionale di Fisica Nucleare
Laboratori Nazionali del Sud

Outline

- Sources under construction

  - AISHa and relative LEBT
  - ESS high intensity proton source and relative LEBT

- Upgrading of existing sources for K-800 LNS cyclotron and daily operation

  - SERSE
  - CAESAR

- R&D activities

  - Modelling and full wave computations
  - Plasma diagnostic

    - Advances in X-ray spectroscopy
    - Development of microwave interferometer for ECRIS

  - Flexible Plasma Trap completion

AISHa

Advanced Ion Source for Hadrontherapy

The AISHa project is supported by the incentives in favour of Research Development and Innovation Art.5 Regional law 16/12/2008 - Intervention line 4.1.1.1 POR FERS Sicilia 2007-13 devoted to small and medium companies integrated with Research Institutions (Partners: INFN-LNS, HITEC2000 srl, UNICO srl, C3SL)

Regione Siciliana

AISHa
Advanced Ion Source for Hadrontherapy

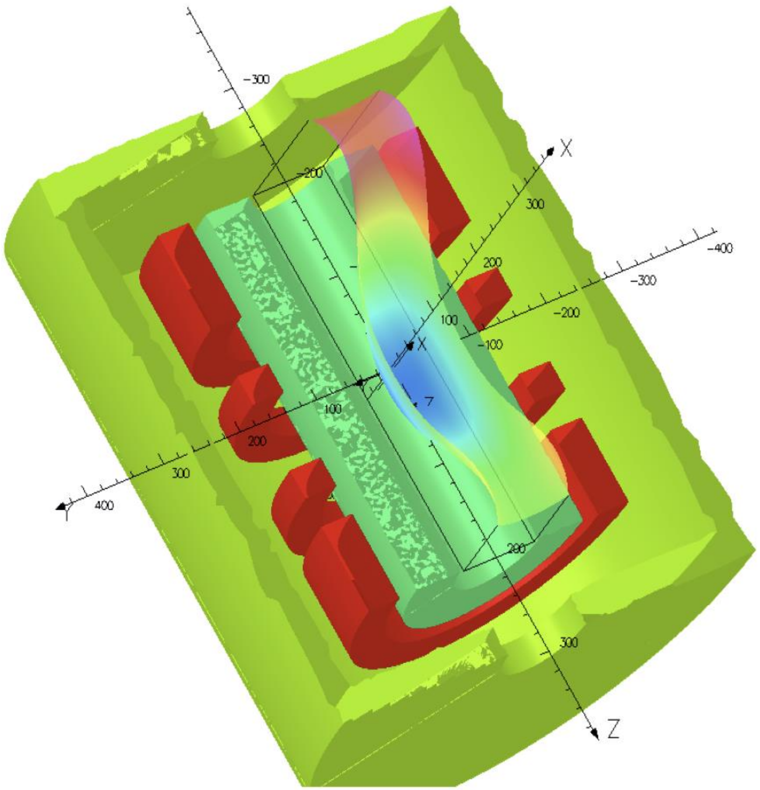

Radial field	1.3 T
Axial field	2.7 T - 0.4 T - 1.6 T
Operating frequencies	18 GHz (TFH)
Max operating power	1.5 kW + 1.5 kW
Extraction voltage	40 kV
Chamber diameter / length	Ø 92 mm / 360 mm
LHe	Free
Warm bore diameter	274 mm

INFN Istituto Nazionale di Fisica Nucleare

LABORATORI NAZIONALI DEL SUD

AISHa
Advanced Ion Source for Hadrontherapy

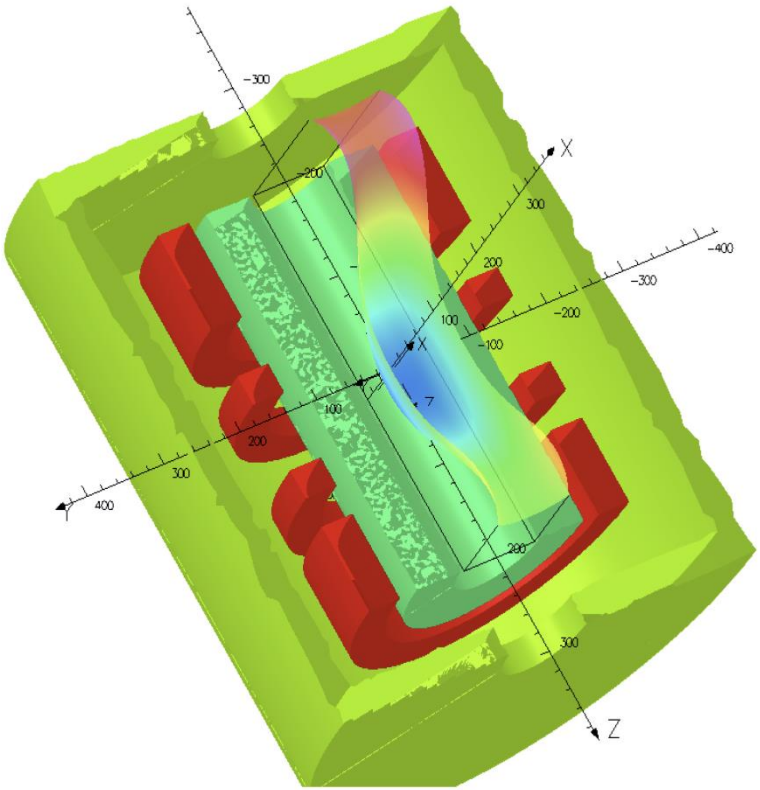

AISHA is a hybrid ECRIS: the radial confining field is obtained by means of a permanent magnet hexapole, while the axial field is obtained with a **Helium-free superconducting system.**

The **operating frequency of 18 GHz will permit** to maximize the plasma density by employing commercial microwave tubes meeting the **<u>needs of the installation in hospital</u>** environments.

Radial field	1.3 T
Axial field	2.7 T - 0.4 T - 1.6 T
Operating frequencies	18 GHz (TFH)
Max operating power	1.5 kW + 1.5 kW
Extraction voltage	40 kV
Chamber diameter / length	Ø 92 mm / 360 mm
LHe	Free
Warm bore diameter	274 mm

AISHa

AISHA render view

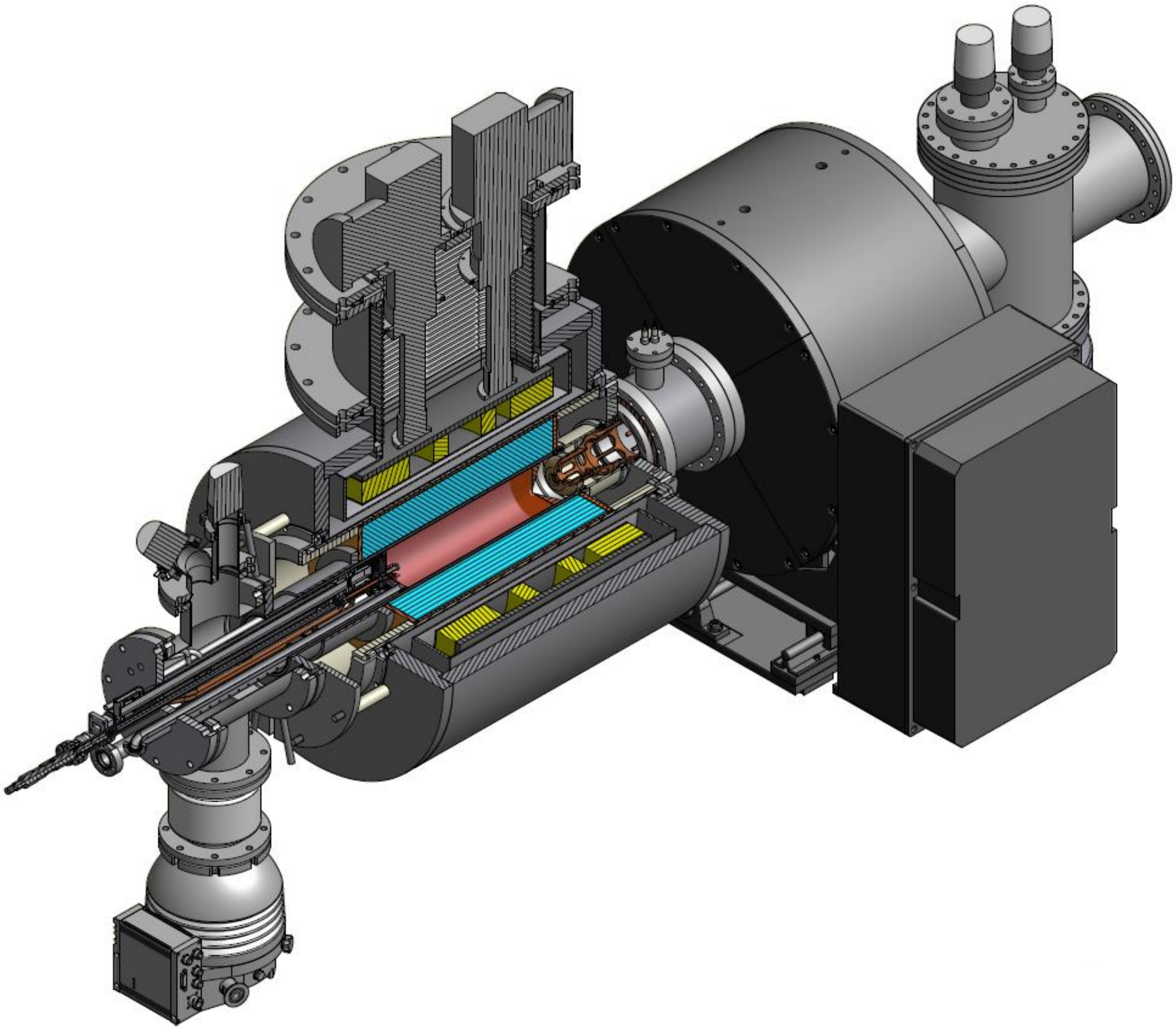

AISHA axial magnetic confinement

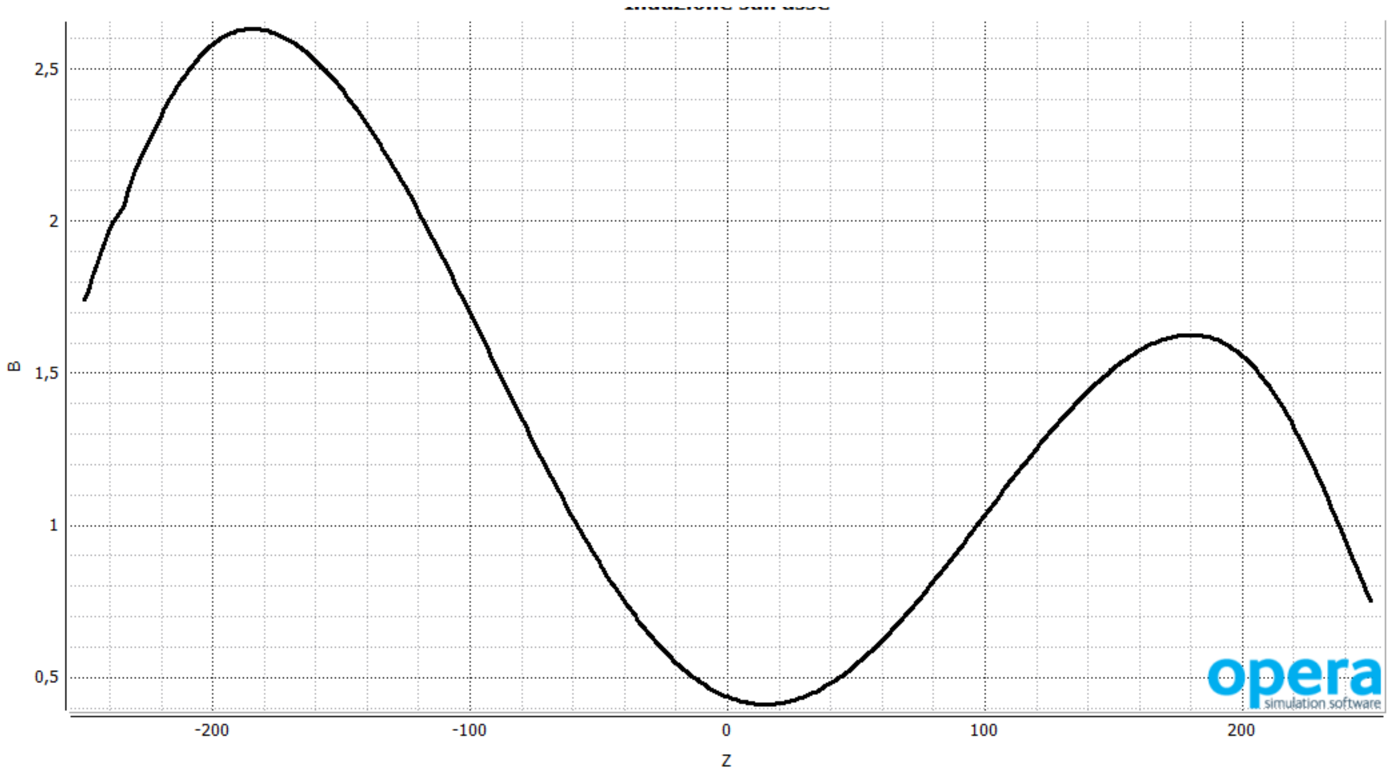

Demagnetisation induced by SC coils

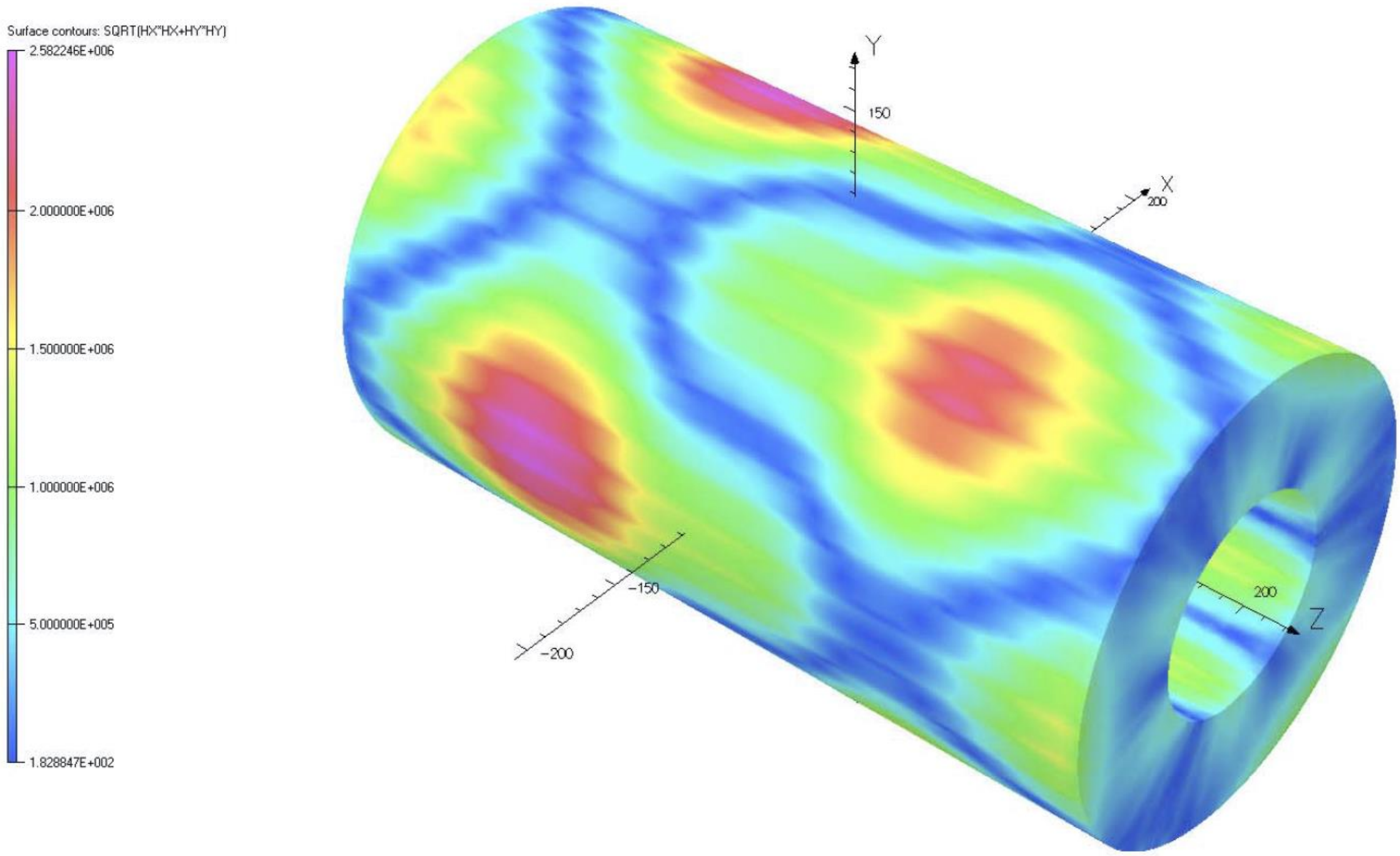

AISHa

Demagnetisation induced by SC coils

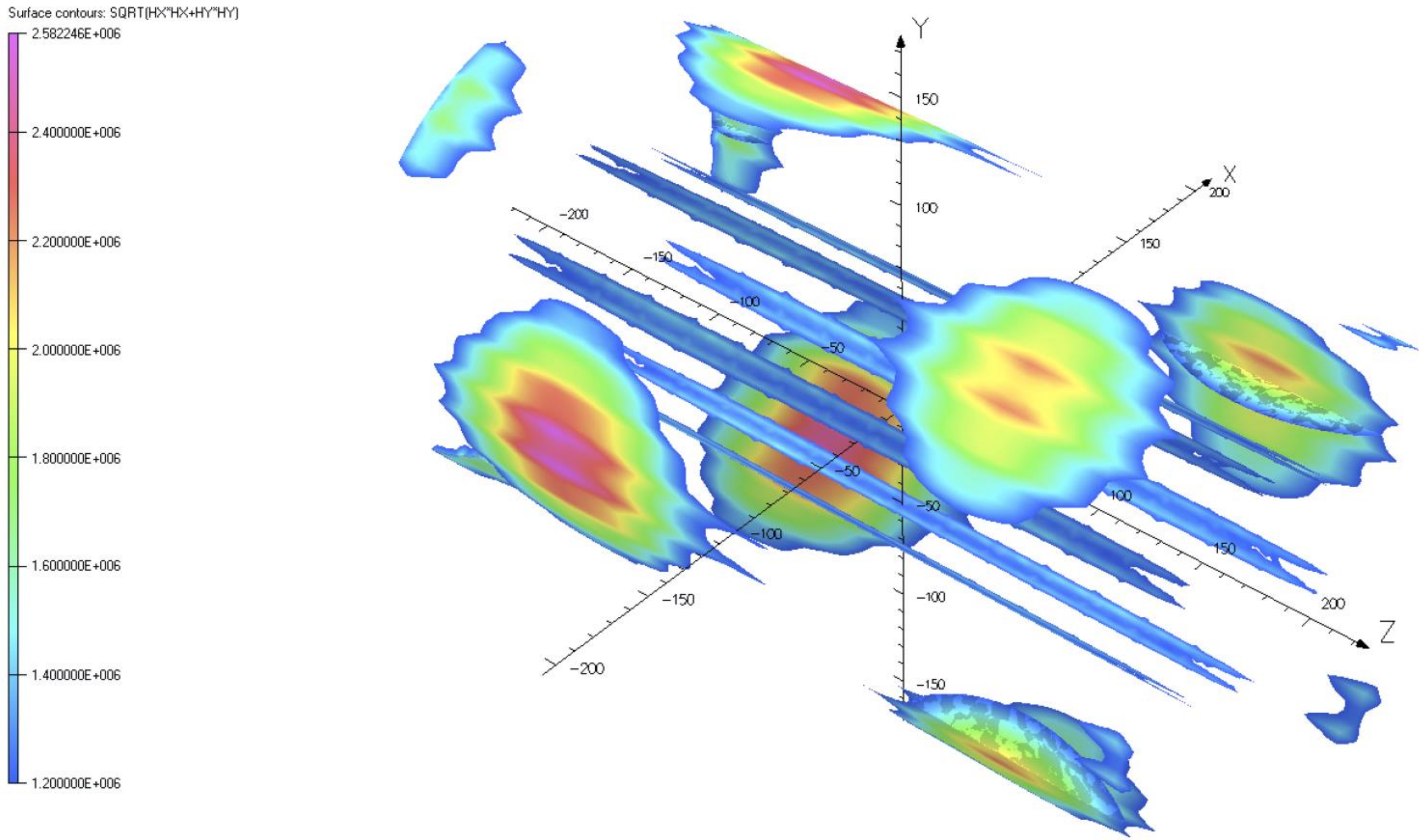

Demagnetization using normal VAC 745 HR

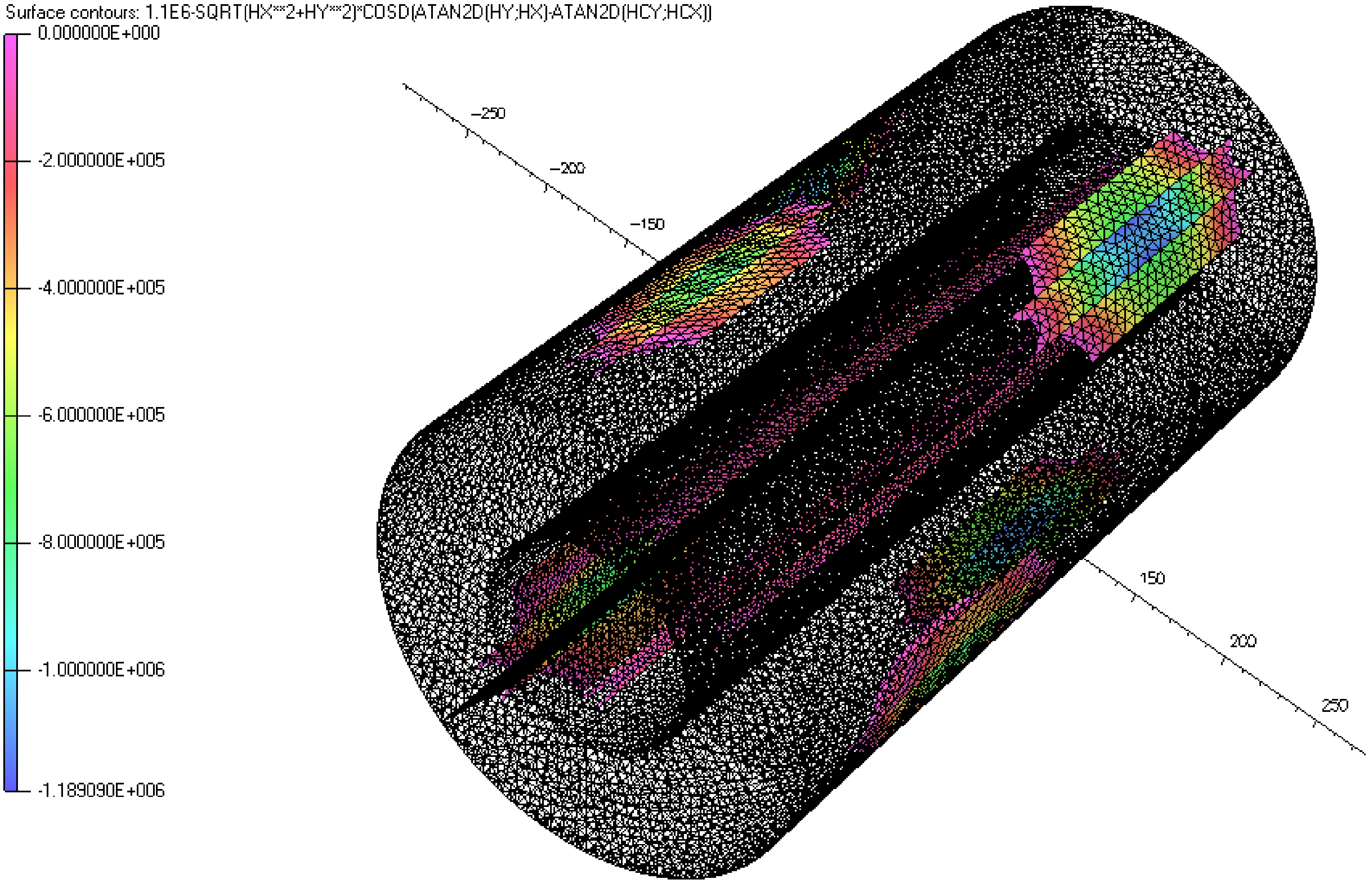

Hexapole configuration

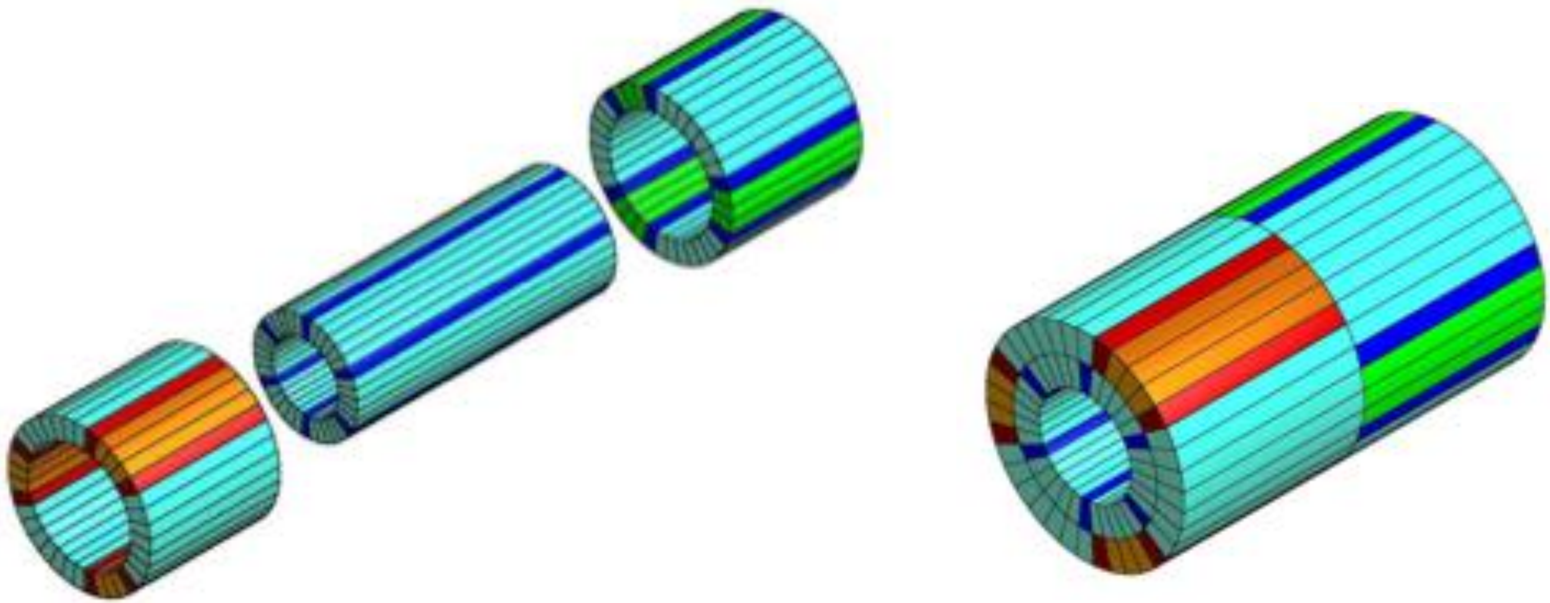

Further optimization: only 2 materials needed with the grain boundary diffusion (Tb) process.

AISHA radial magnetic confinement (plasma chamber wall)

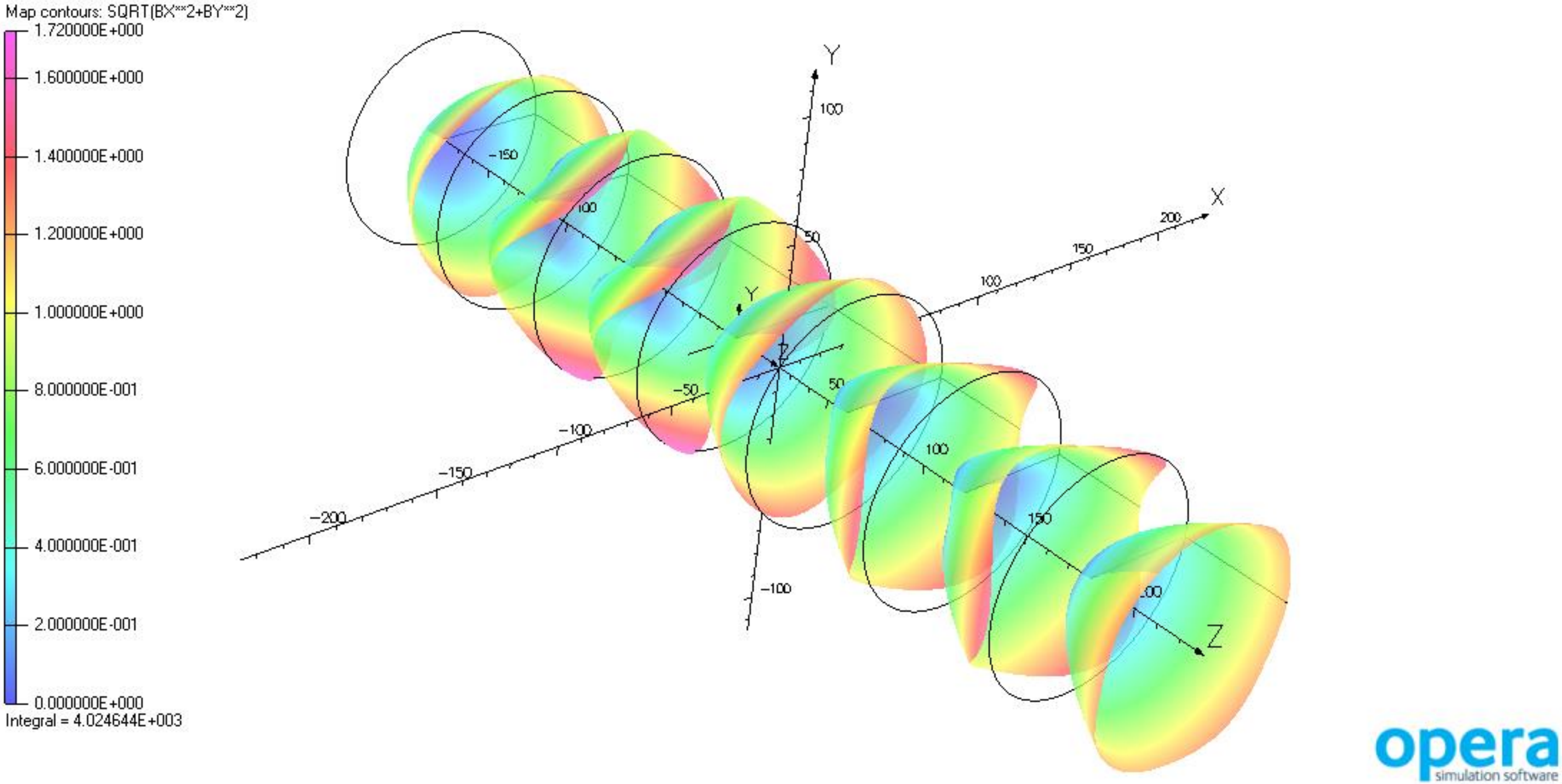

Integration of hexapole: forces conteinement

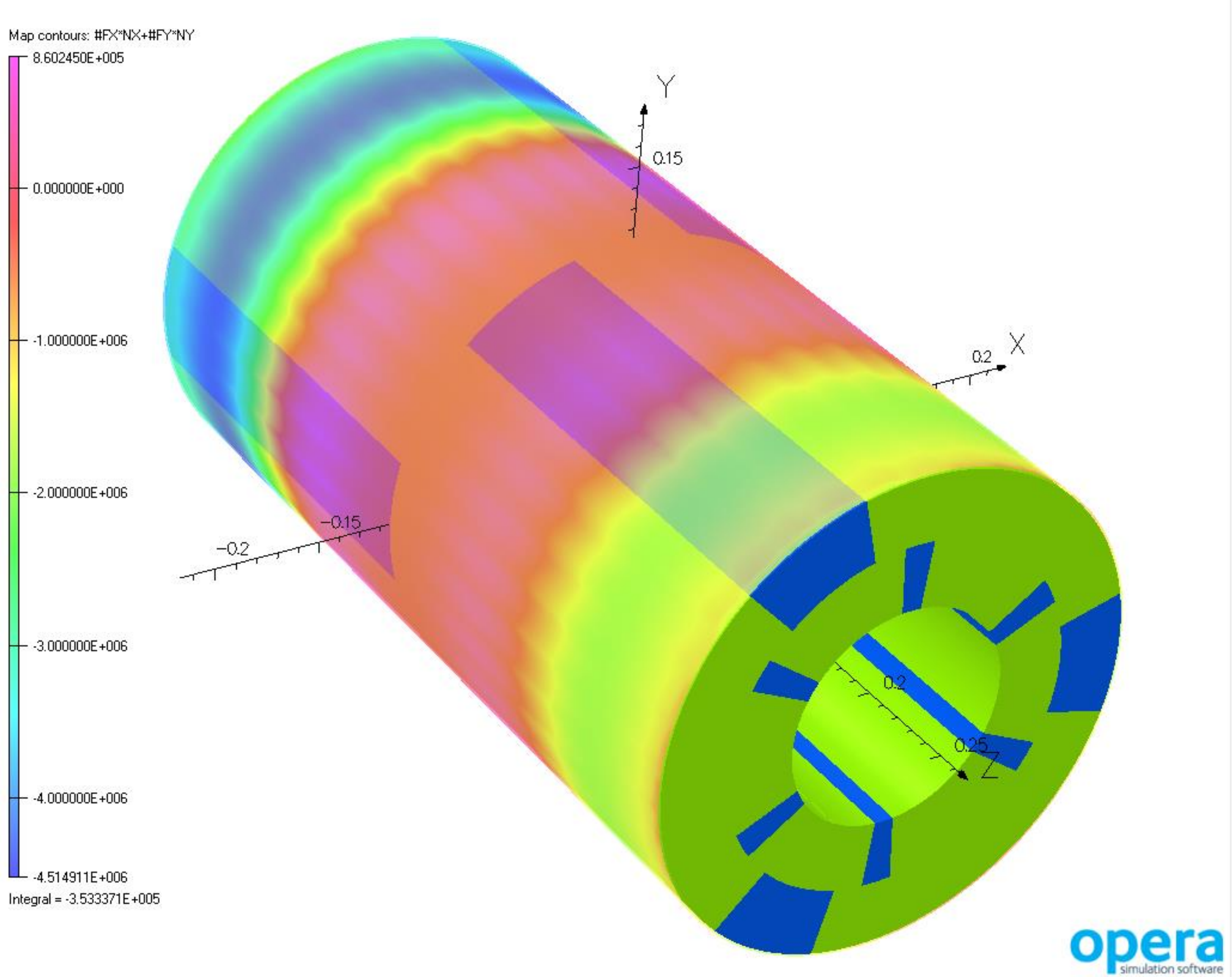

Due to simmetry reasons there is a high cancellation of the forces acting on the whole structure.

AISHa injection system

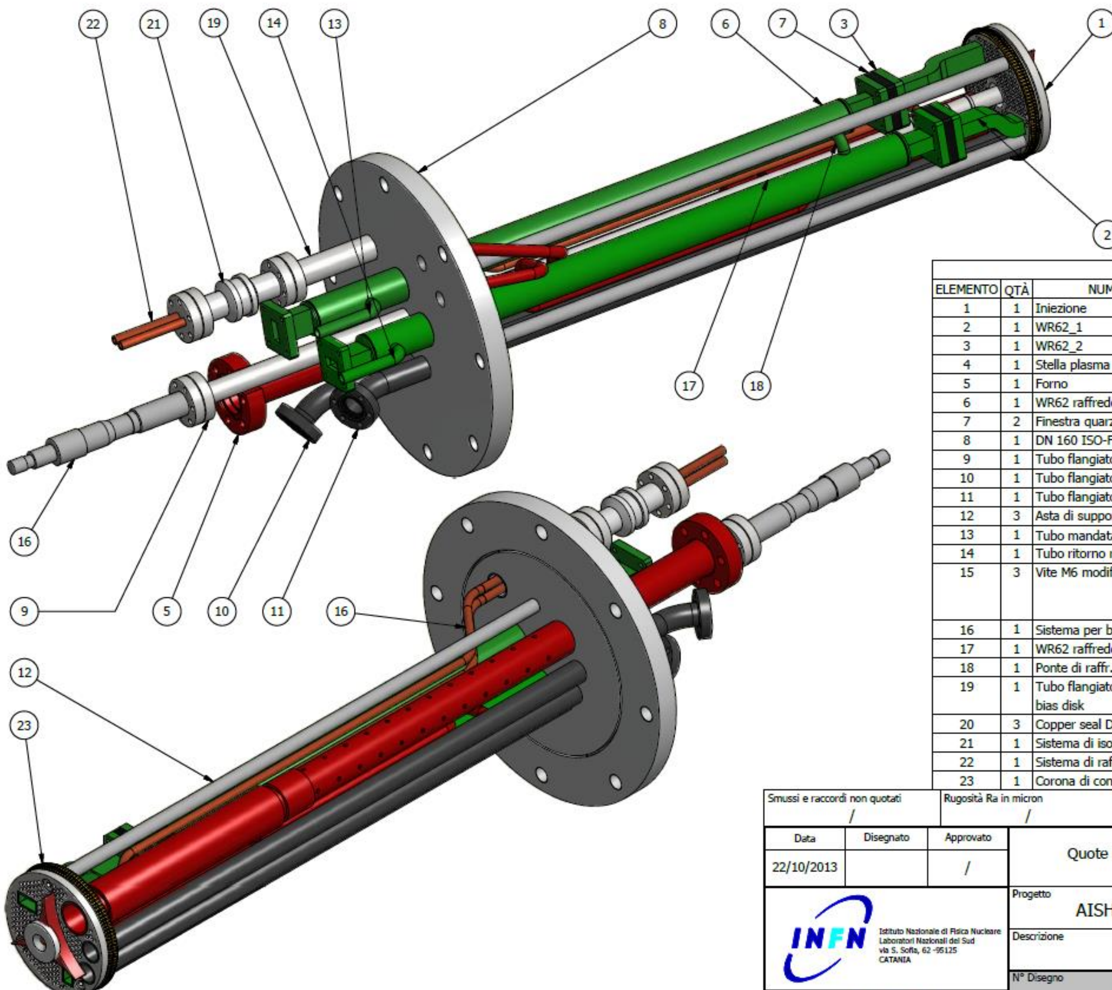

ELENCO PARTI			
ELEMENTO	QTÀ	NUMERO PARTE	DESCRIZIONE
1	1	Iniezione	
2	1	WR62_1	Guida d'onda WR62 a S
3	1	WR62_2	Guida d'onda WR62
4	1	Stella plasma	
5	1	Forno	Assieme forno
6	1	WR62 raffreddata	
7	2	Finestra quarzo	Finestra WR62
8	1	DN 160 ISO-F cieca	
9	1	Tubo flangiato bias disk	
10	1	Tubo flangiato gas-1	
11	1	Tubo flangiato gas-2	
12	3	Asta di supporto	
13	1	Tubo mandata raffr. WR62	
14	1	Tubo ritorno raffr. WR62	
15	3	Vite M6 modificata	Vite a testa svasata con impronta a croce ed esagono incassato 1 - Grado prodotto A
16	1	Sistema per bias disk	
17	1	WR62 raffreddata-1	
18	1	Ponte di raffr. WR62	
19	1	Tubo flangiato per sist. di raffr. bias disk	
20	3	Copper seal DN16	
21	1	Sistema di isolamento flangiato	
22	1	Sistema di raffr. bies disk	
23	1	Corona di contatti	

Smussi e raccordi non quotati	Rugosità Ra in micron	Trattamento termico superficiale	Materiale
/	/	/	/

Data	Disegnato	Approvato
22/10/2013		/

Quote senza indicazione di tolleranza
UNI-EN 22768-F

Istituto Nazionale di Fisica Nucleare
Laboratori Nazionali del Sud
via S. Sofia, 62 -95125
CATANIA

SERVIZIO SVILUPPO
NUOVE TECNICHE DI ACCELERAZIONE

Progetto	Gruppo	Scala
AISHa	Gruppo iniezione	/

Descrizione	N° di pezzi
Assieme iniezione	1

N° Disegno	Foglio
GRUPPO INIEZIONE-2	2/2

AISHa room @LNS

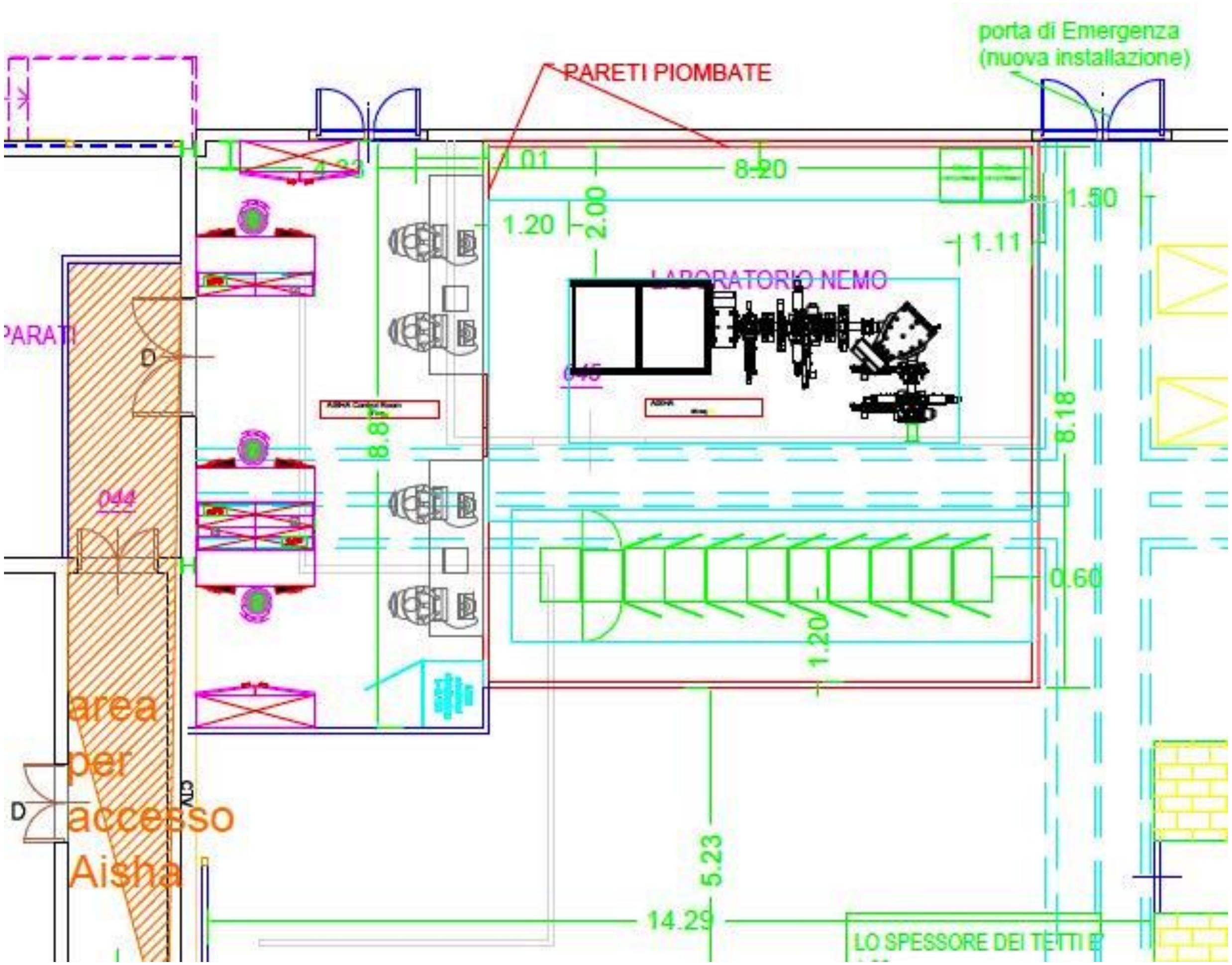

AISHa AISHa 2
important dates

- AISHa site ready for January 2015
- Magnetic system delivery for second half of 2015
- RF system and ancillaries ready for June 2015
- Mechanics ready for March 2015
- Solenoid+Dipole ready for April 2015
- Diagnostics ready for March 2015

- AISHa2 site @ CNAO to be confirmed
- Magnetic system call for tenders to be released in October 2014
- RF system and ancillaries ready for June 2015
- Mechanics ready for October 2015
- CNAO
- CNAO

O3: CNAO installation

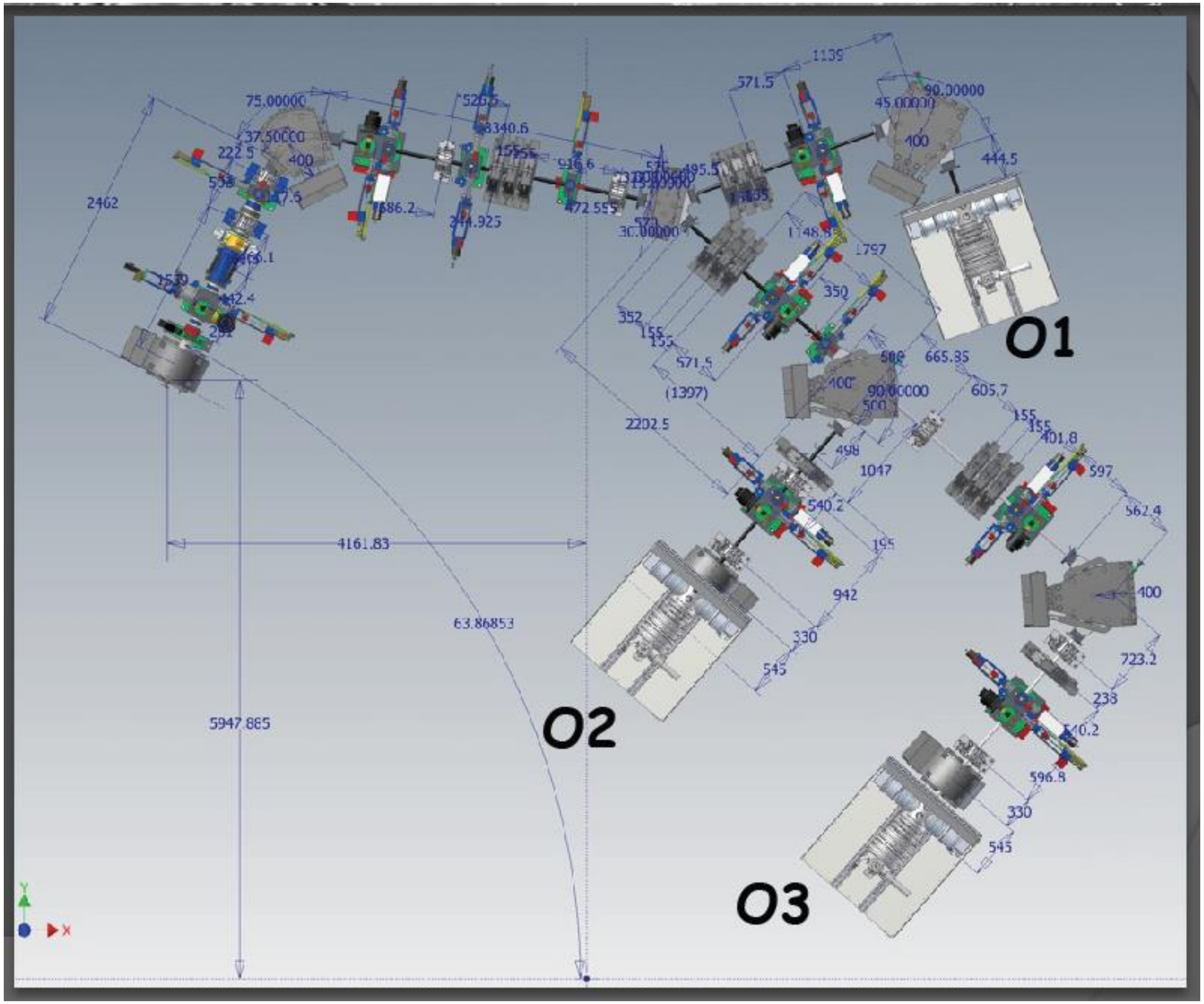

PS-ESS

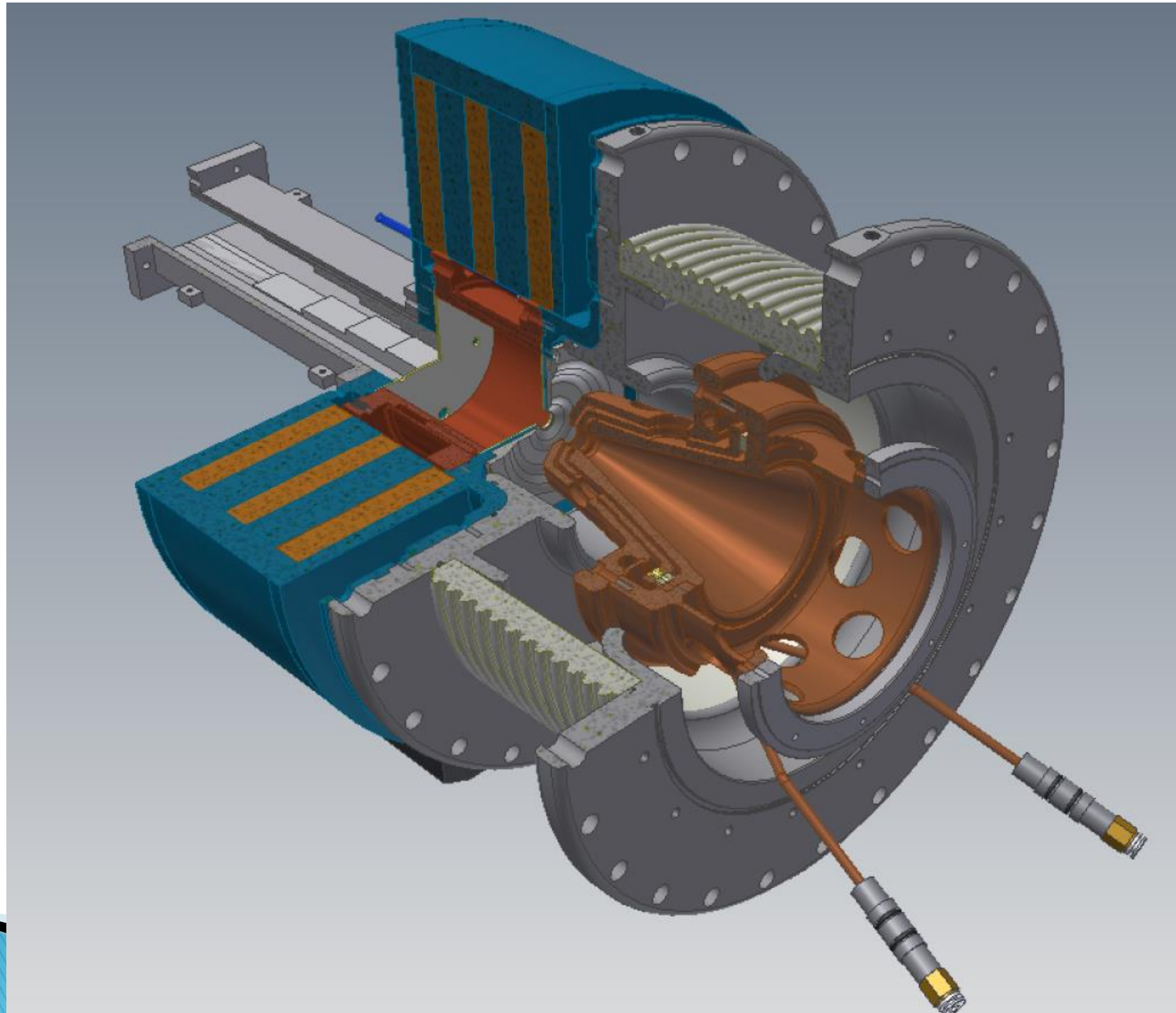

Name	Expectation	Consequences
Beam energy	75 keV	New isolation column + New HV platform + New HV electronics
Maximum proton current	62.5 mA	High proton fraction + High total current up to 80 mA
Minimum proton current	6.3 mA	Movable iris inside the LEBT + High precision iris movement + High power dissipation on the iris + Space charged transport of different beams
Proton current step	6.3 mA	
Proton current precision	1.6 mA	
Beam pulse frequency	From single pulse to 14 Hz	Pulsed ion source + Chopper inside the LEBT + Fast chopper electronics + Fast recovery of LEBT space charge compensation + High power dissipation on the LEBT collimator + test of LEBT chopping strategy before construction
Beam pulse modulation	From 5 us to 2.86 ms	
Beam pulse rise and fall time	< 100 ns	
Bem emittance	0.25 π mm mrad	Low emittance source + Test new plasma heating methods + LEBT solenoids with reduced fringing field + High precision alignment of IS and LEBT to reduce steerer use + High interaction with ESS Beam Instrumentation group and RFQ team to reduce LEBT length
Twiss parameter α	1.02	
Twiss parameter β	0.11	
Twiss parameter α mismatch	±10 %	
Twiss parameter β mismatch	±5 %	
Center displacement	±0.2 mm	
Center angle	±2 mrad	
Current beam stability	±5 %	Study of RF-Plasma coupling + New RF injection system + Test new plasma heating methods
Emittance stability	±5 %	
High reliability	> 99 %	New source assembly design + Definition of maintenance procedure
Fast IS and LEBT recovery time	Hours	
Second ion source		Upgrading study + double delivery time + double commissioning time

Body Source

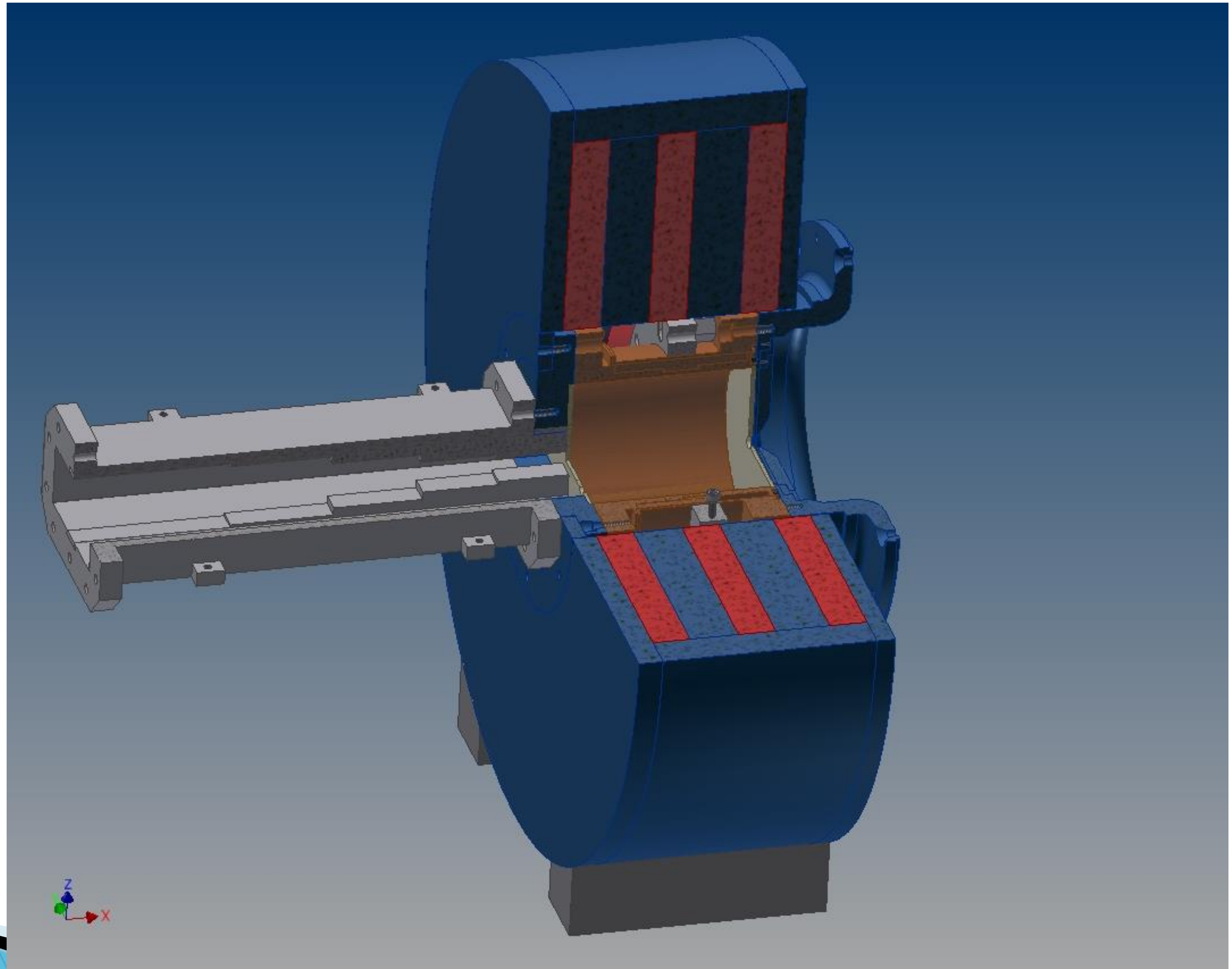

Body Source

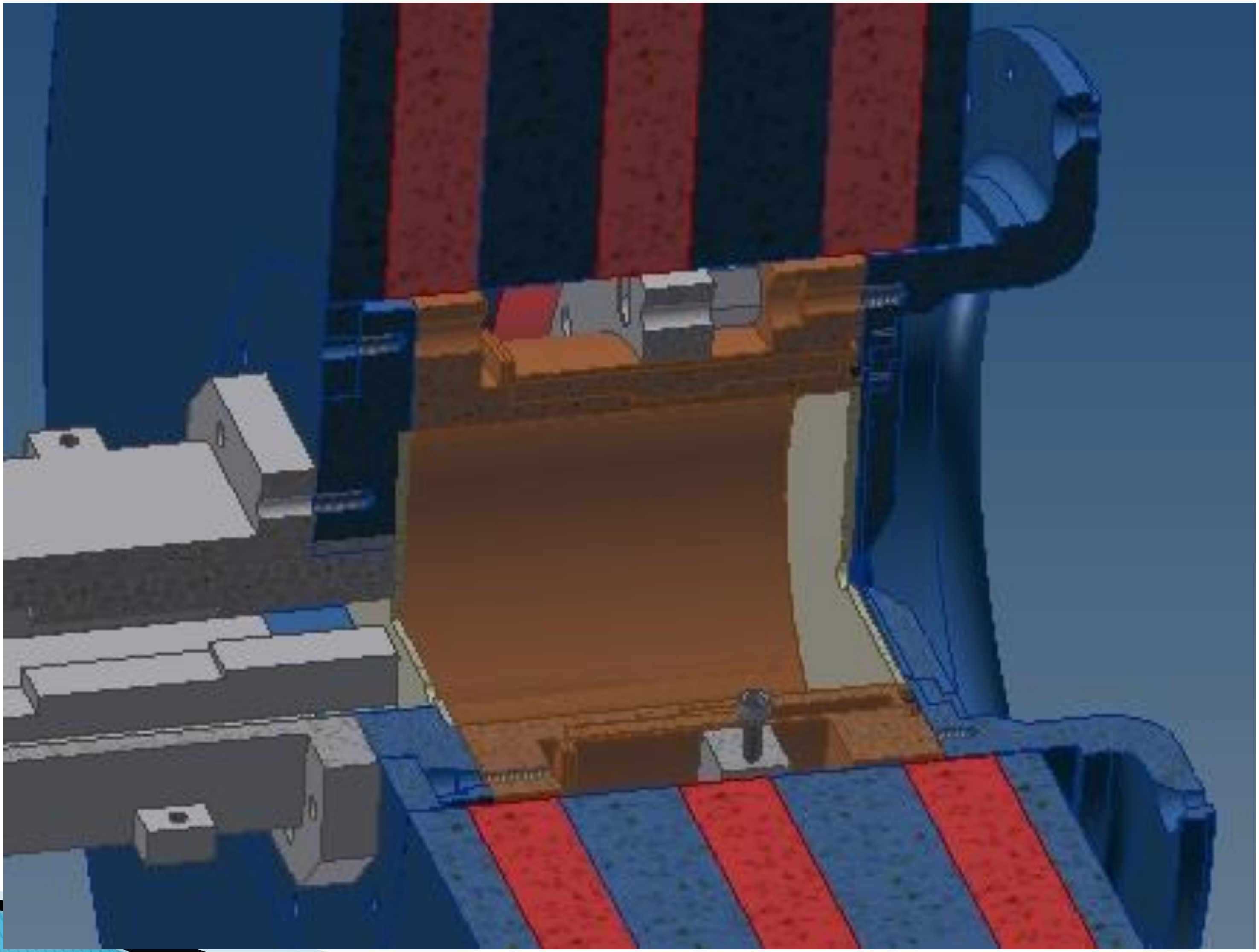

Body Source

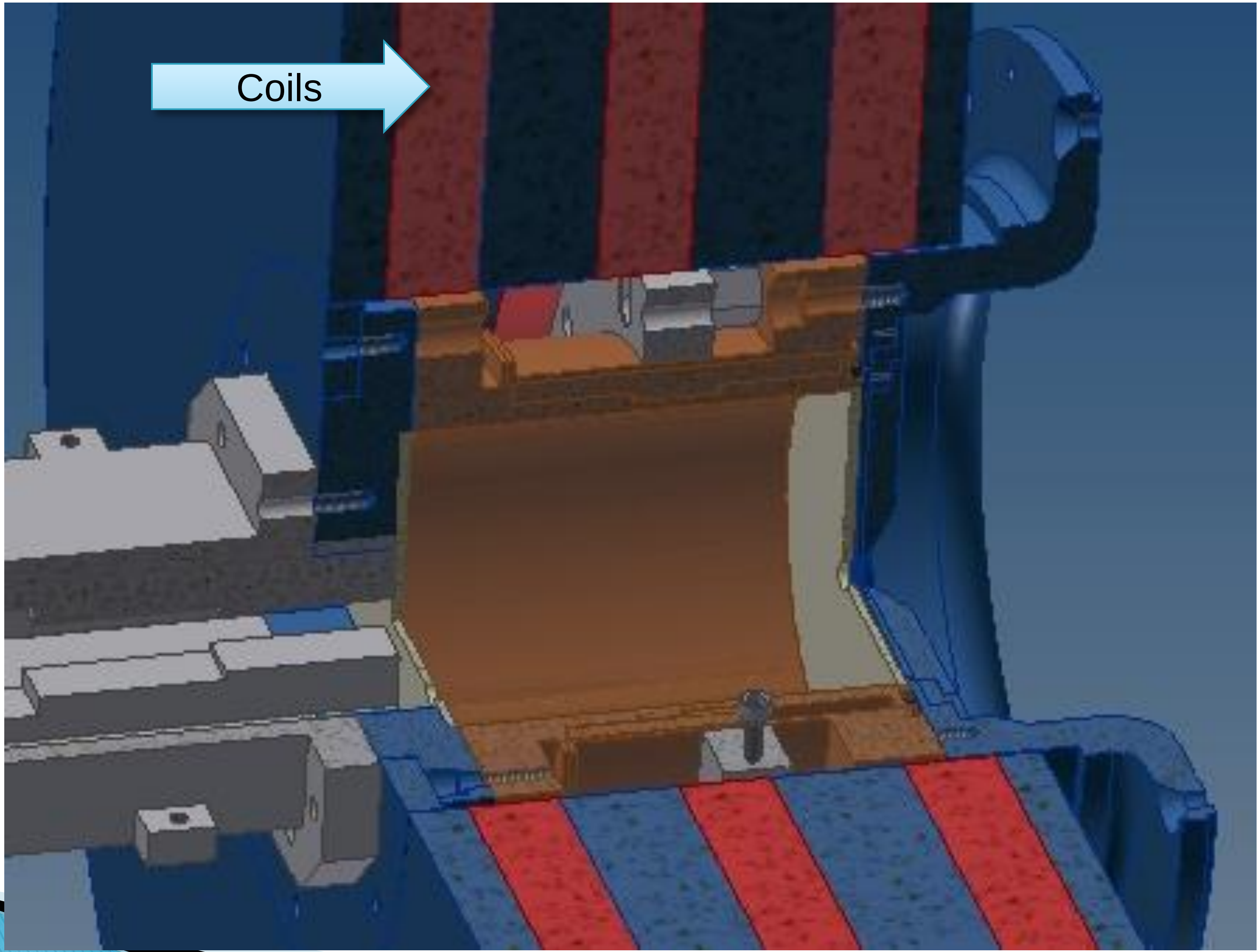

Body Source

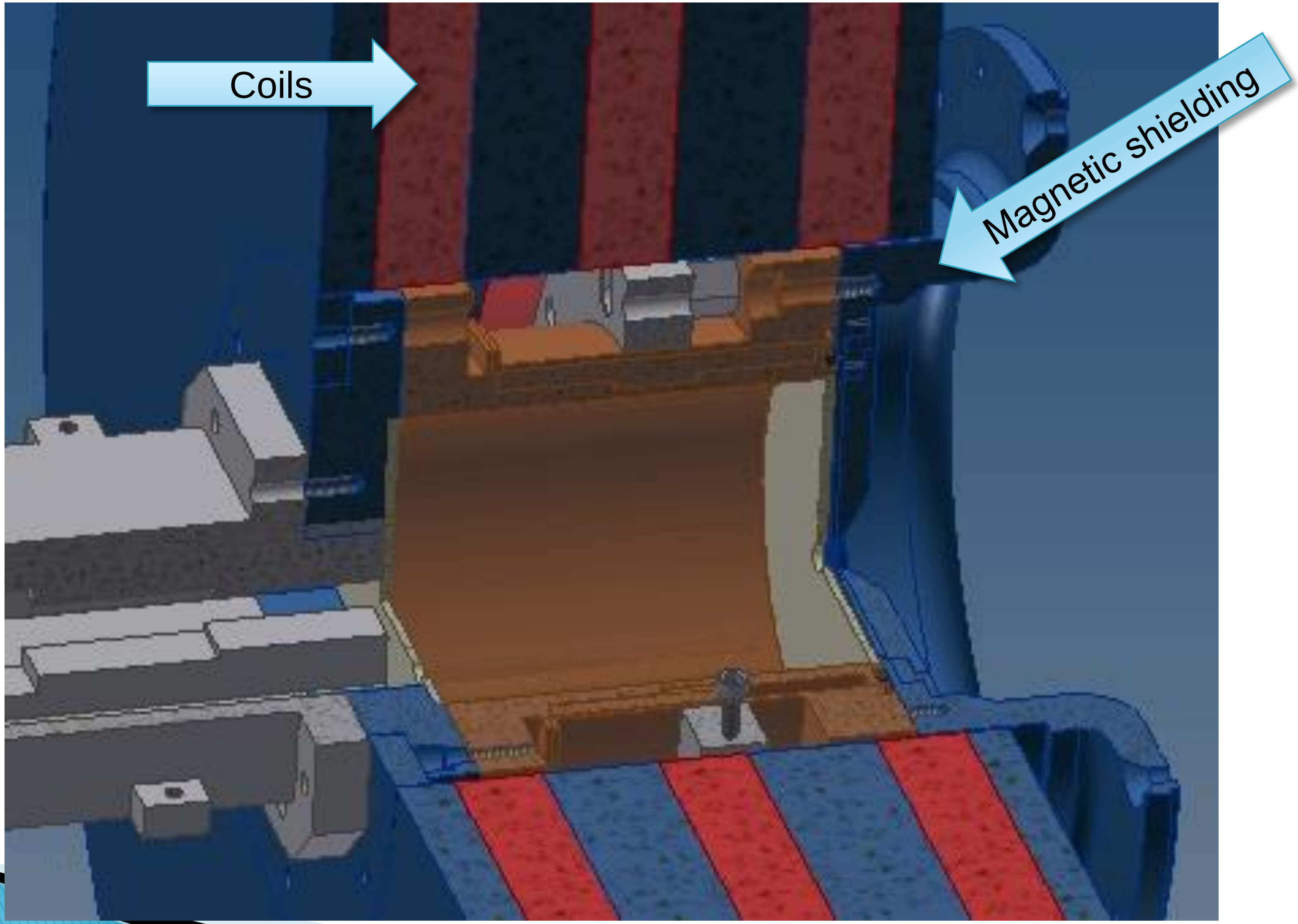

Body Source

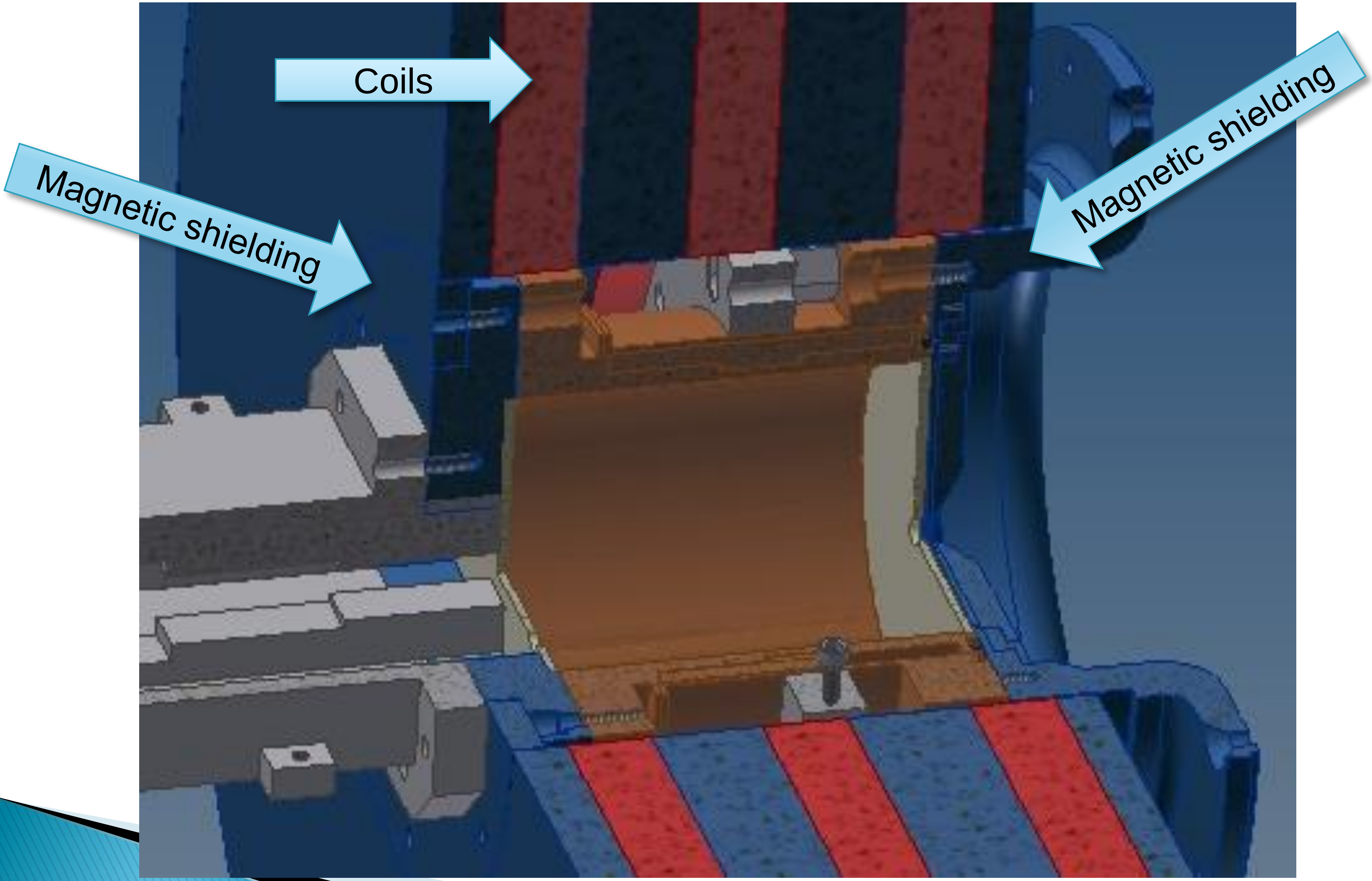

Body Source

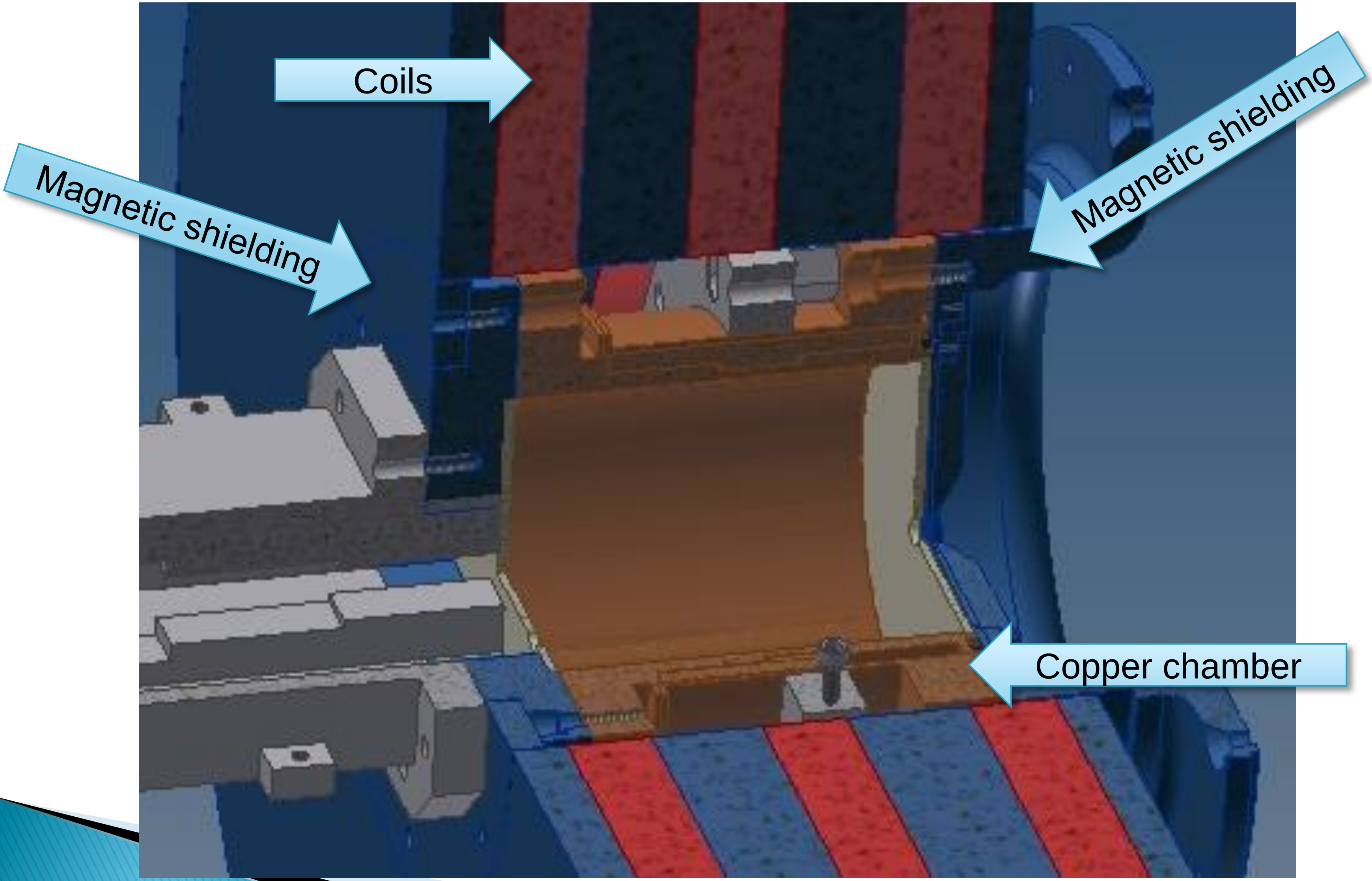

Coils
Magnetic shielding
Magnetic shielding
Copper chamber

Body Source

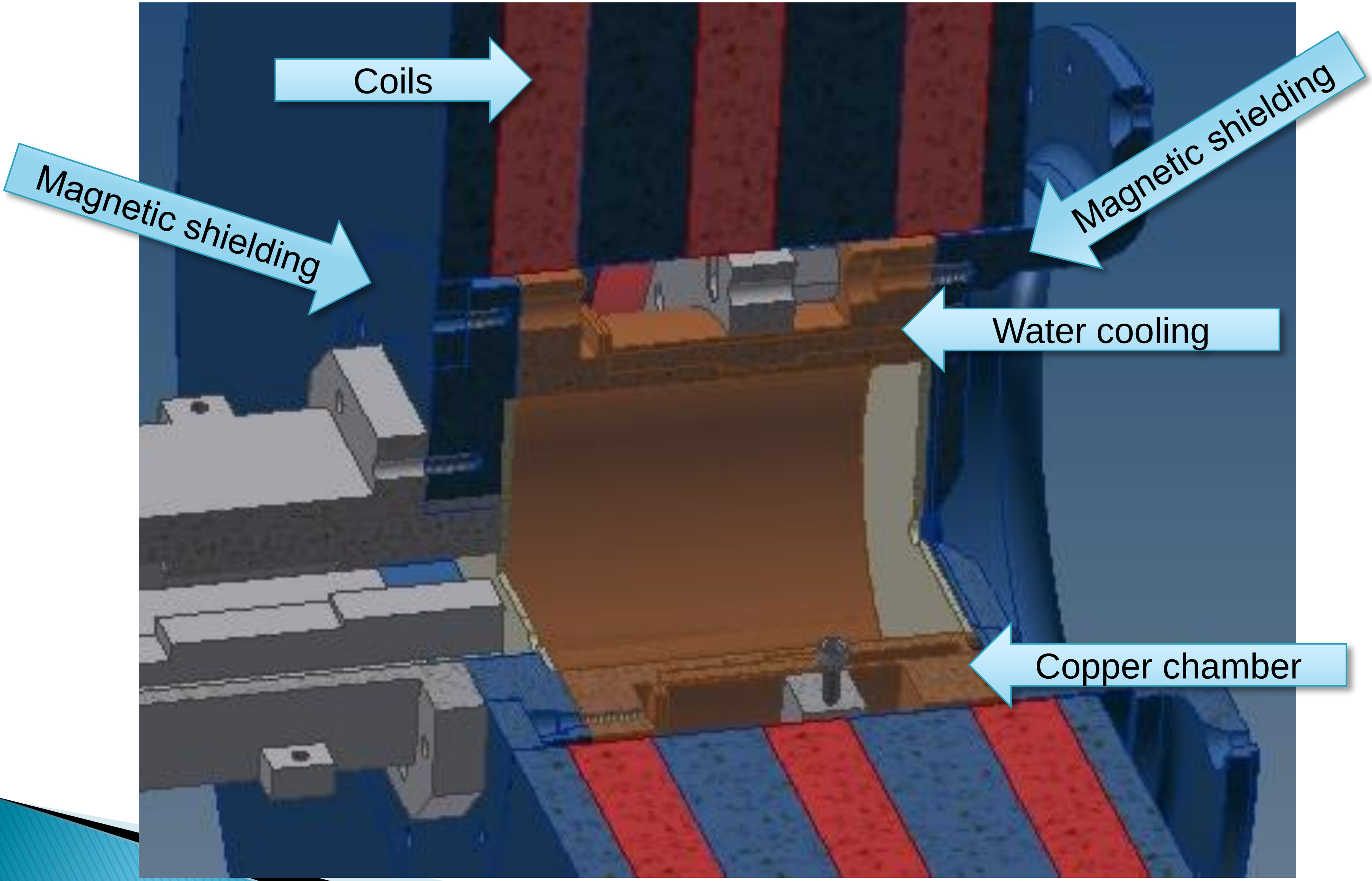

Coils
Magnetic shielding
Magnetic shielding
Water cooling
Copper chamber

Body Source

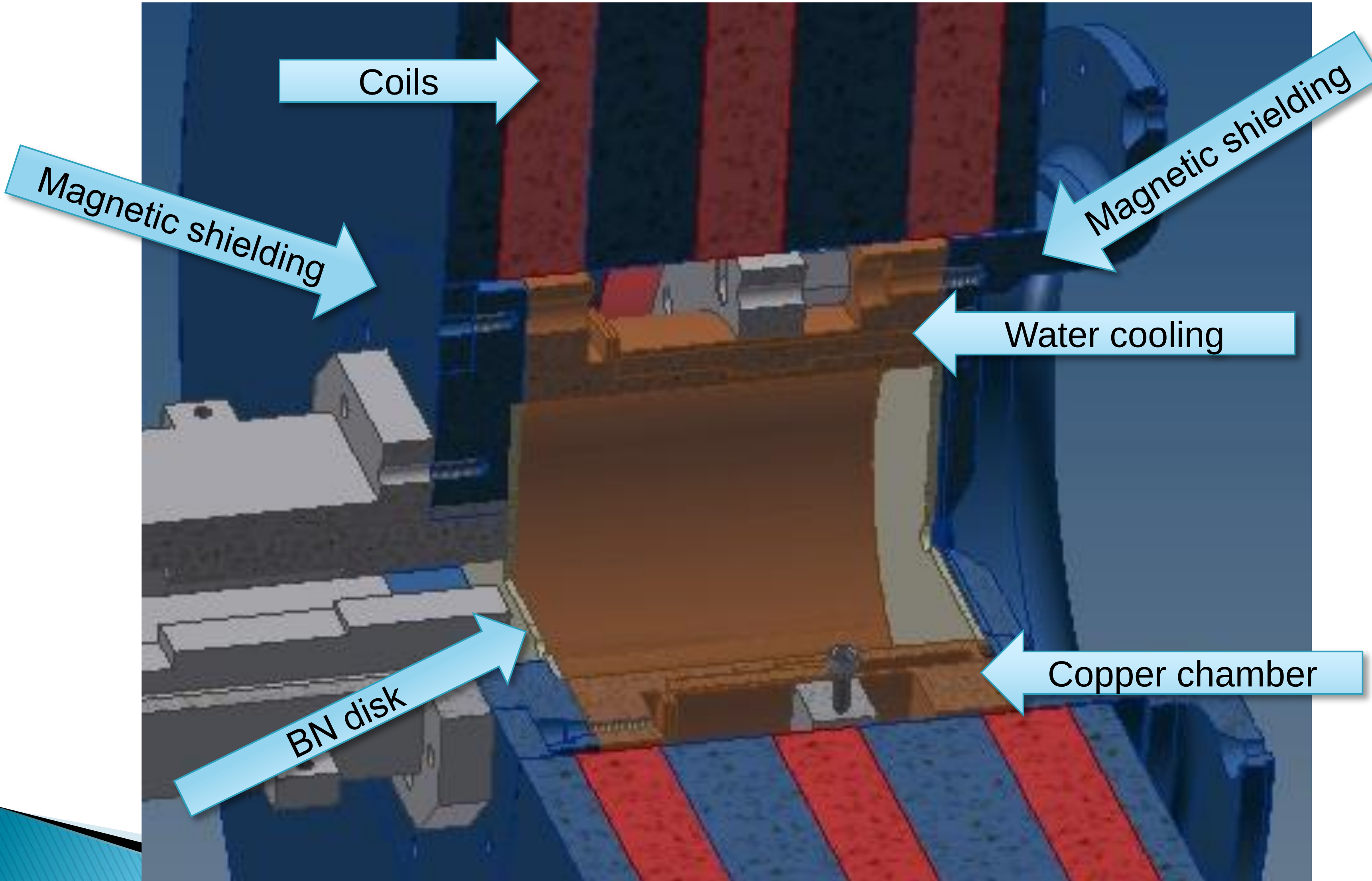
Coils
Magnetic shielding
Magnetic shielding
Water cooling
BN disk
Copper chamber

Body Source

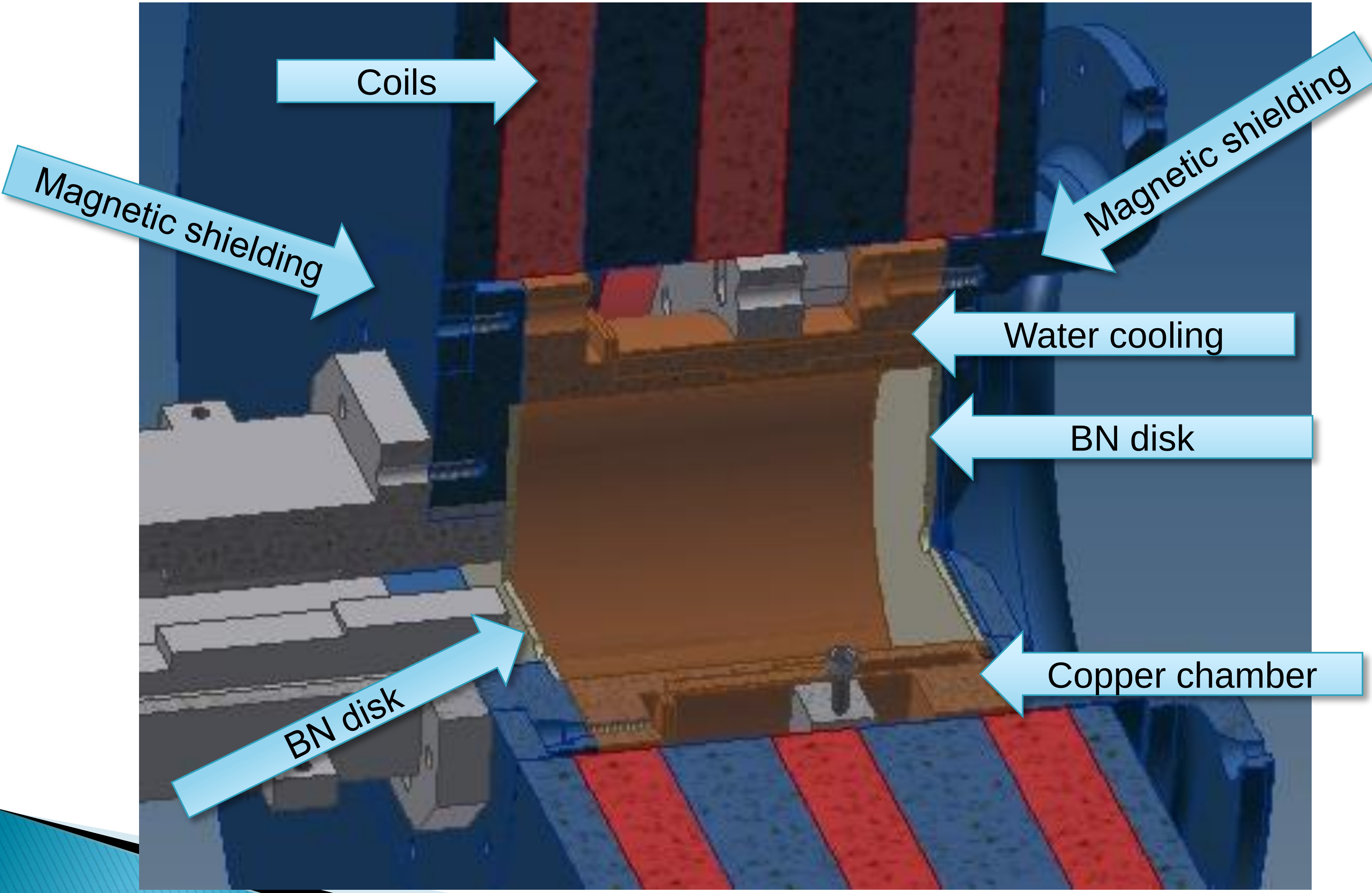
Coils
Magnetic shielding
Magnetic shielding
Water cooling
BN disk
BN disk
Copper chamber

Body Source

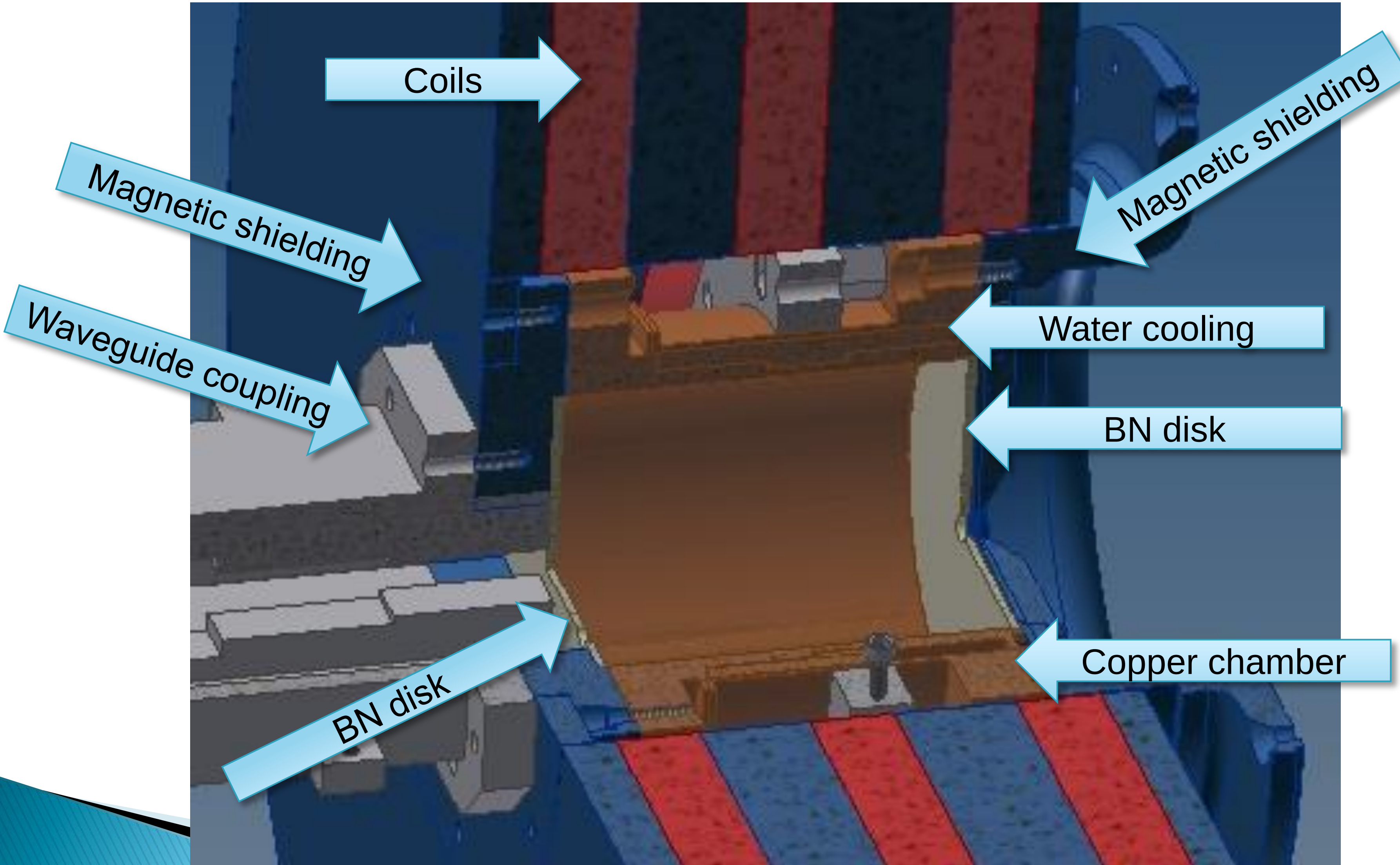

Coils
Magnetic shielding
Magnetic shielding
Waveguide coupling
Water cooling
BN disk
BN disk
Copper chamber

Body Source

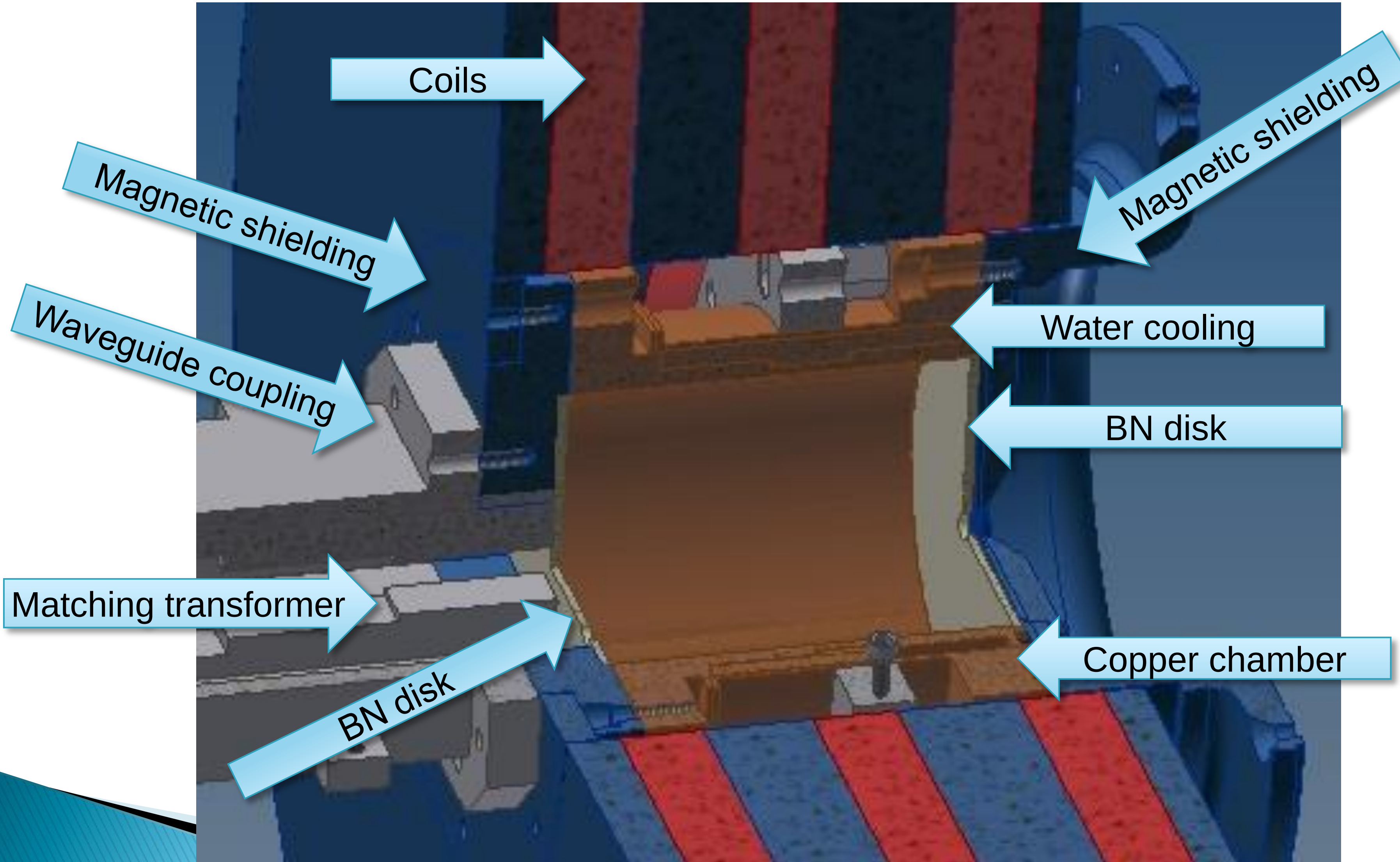

Coils
Magnetic shielding
Magnetic shielding
Waveguide coupling
Water cooling
BN disk
Matching transformer
BN disk
Copper chamber

MW coupling on TRIPS,VIS

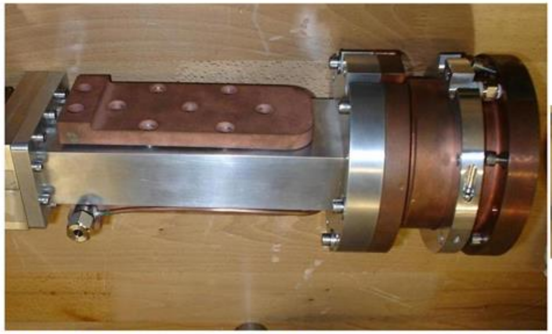

Matching transformer coupled to the plasma chamber

Four step double ridges

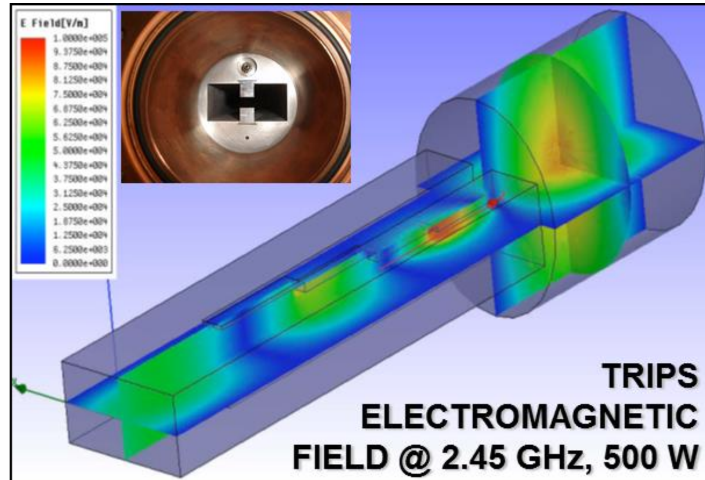

TRIPS ELECTROMAGNETIC FIELD @ 2.45 GHz, 500 W

S_{21} Vs FREQUENCY FOR THE TWO STRUCTURES

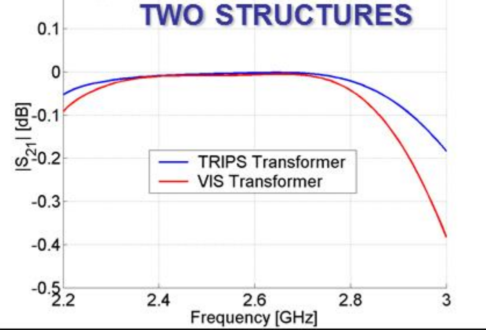

VIS TRANSFORMER INSERTION LOSS 0.0085 dB @ 2.45 GHz

ELECTROMAGNETIC FIELD @ 2.45 GHz, 500 W

10 % ENHANCEMENT WITH VIS TRANSFORMER

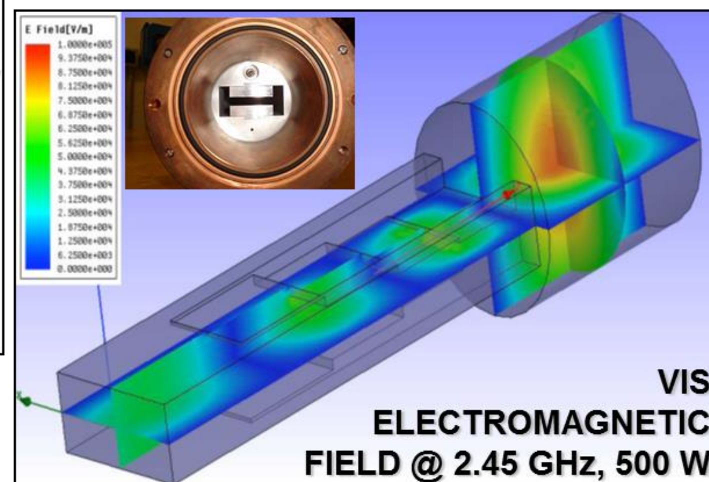

VIS ELECTROMAGNETIC FIELD @ 2.45 GHz, 500 W

ESS refinement

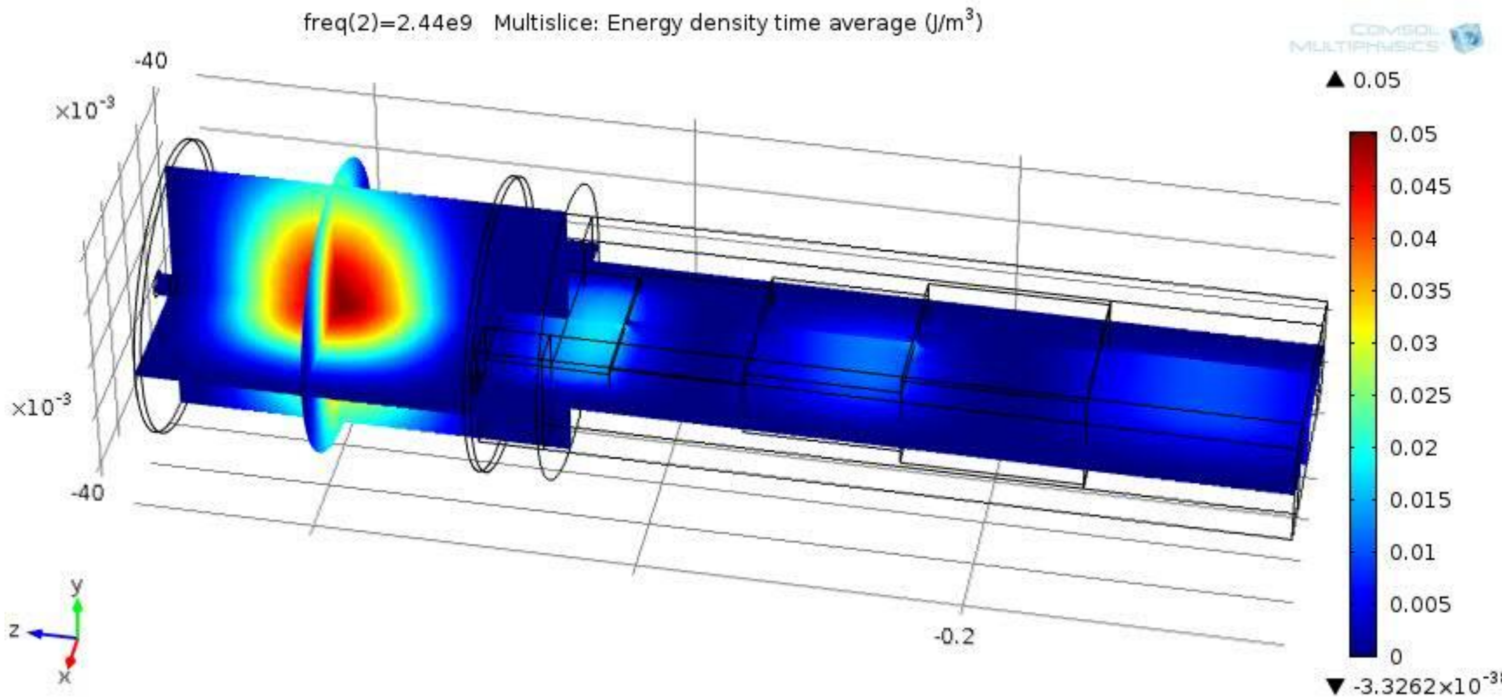

Optimization of all geometrical parameters of the matching transformer:
Step width, height, length, number

Cavity frequency domain study with real dimensions an real materials:

Copper chamber cylinder
Two Boro Nitride insulators disks
Aluminum waveguide
Extraction hole

Flexible magnetic system

- ✓ Classical MDIS flat profile (B-flat)
- ✓ Simple-mirror (B-min) for the prolongation of H_2^+ molecule lifetime, thus increasing ionization efficiency and proton fraction
- ✓ Magnetic beach (B-asymmetric) making possible Bernstein Waves (BWs) formation through inner-plasma conversion of the input electromagnetic waves.

Flexible magnetic system

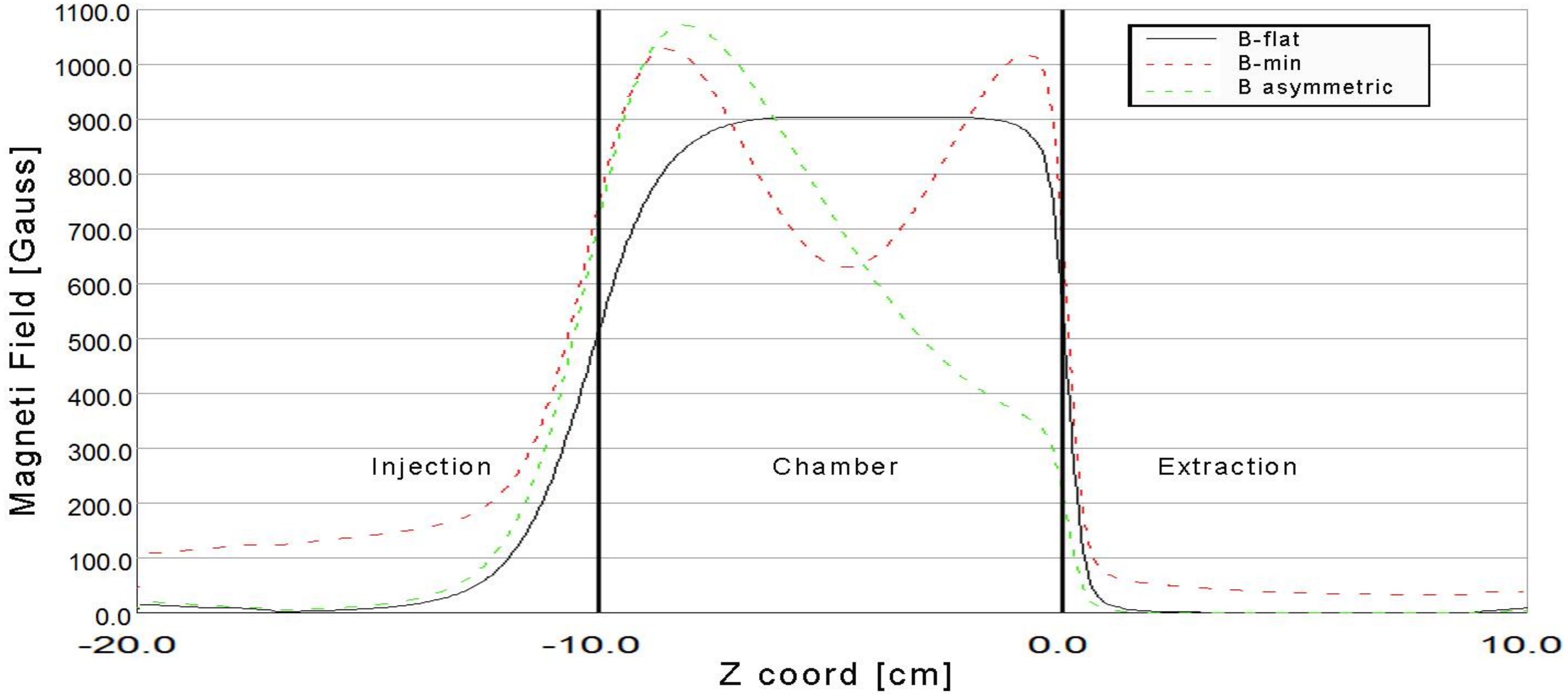

- Classical MDIS flat profile (B-flat)
- Simple-mirror (B-min) for the prolongation of H_2^+ molecule lifetime, thus increasing ionization efficiency and proton fraction
- Magnetic beach (B-asymmetric) making possible Bernstein Waves (BWs) formation through inner-plasma conversion of the input electromagnetic waves.

Flexible magnetic system

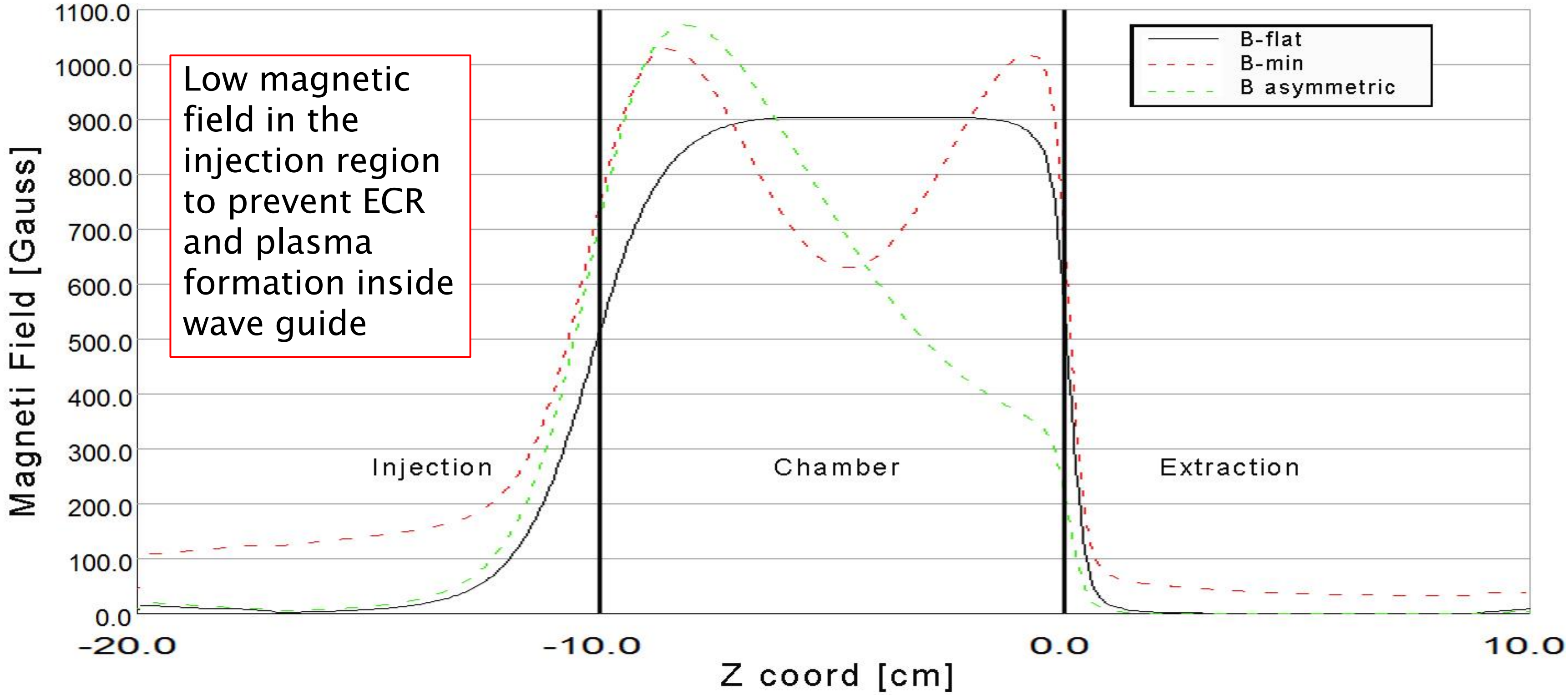

- ✓ Classical MDIS flat profile (B-flat)
- ✓ Simple-mirror (B-min) for the prolongation of H_2^+ molecule lifetime, thus increasing ionization efficiency and proton fraction
- ✓ Magnetic beach (B-asymmetric) making possible Bernstein Waves (BWs) formation through inner-plasma conversion of the input electromagnetic waves.

Flexible magnetic system

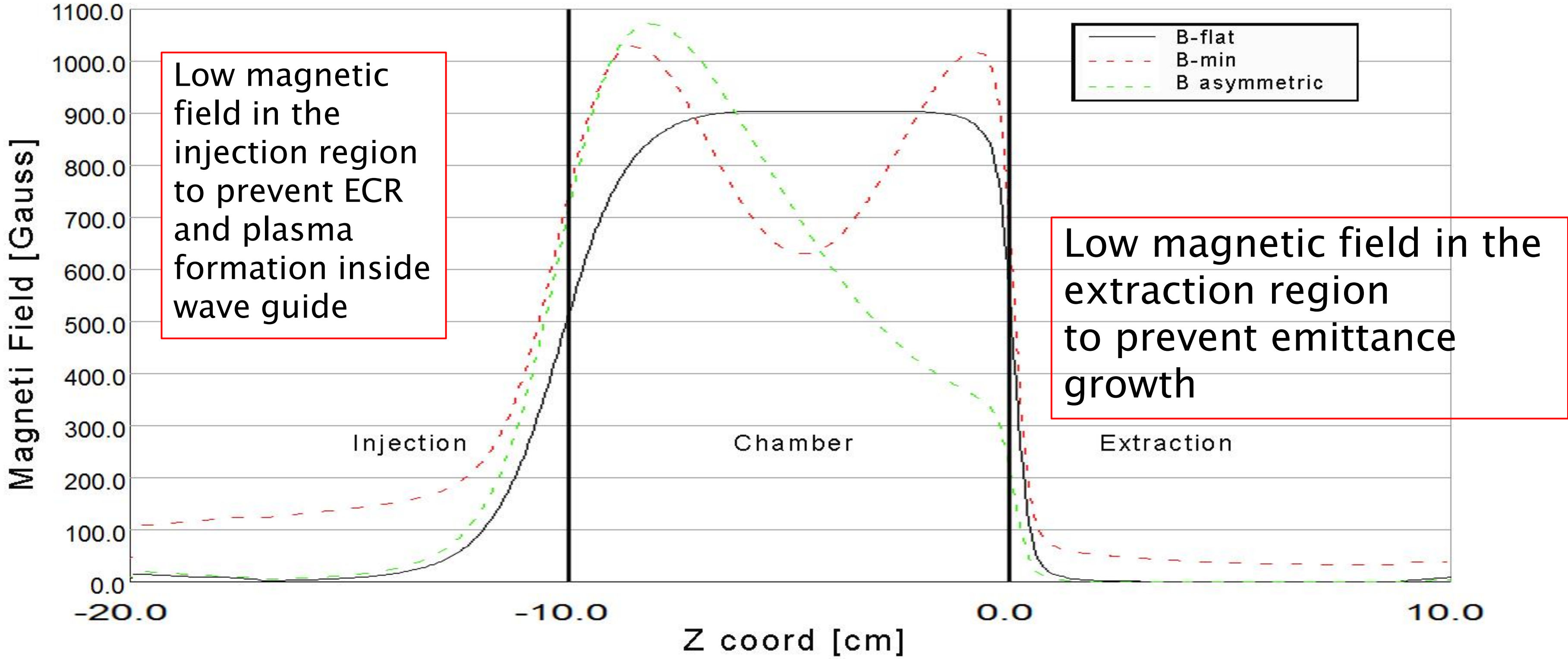

- ✓ <u>Classical</u> MDIS flat profile (B-flat)
- ✓ <u>Simple-mirror</u> (B-min) for the prolongation of H_2^+ molecule lifetime, thus increasing ionization efficiency and proton fraction
- ✓ <u>Magnetic beach</u> (B-asymmetric) making possible <u>Bernstein Waves</u> (BWs) formation through inner-plasma conversion of the input electromagnetic waves.

Ion beam extraction

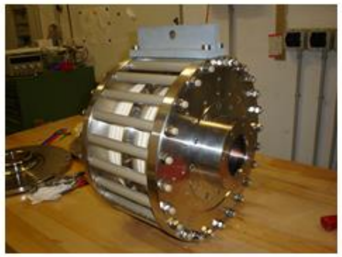


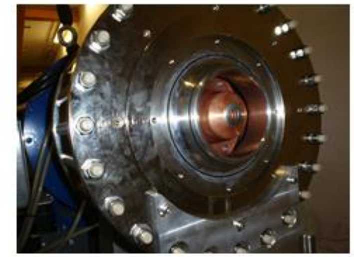

TRIPS Five-electrodes topology

- on-line optimisation of the extracted beam
- wide range of operations (10-60 mA)

VIS Four-electrodes topology

optimized for a 40 mA beam (90% proton, 10% H_2^+)

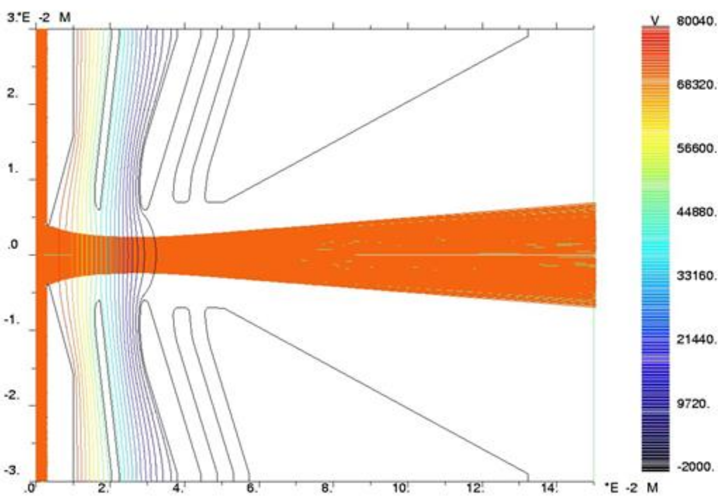

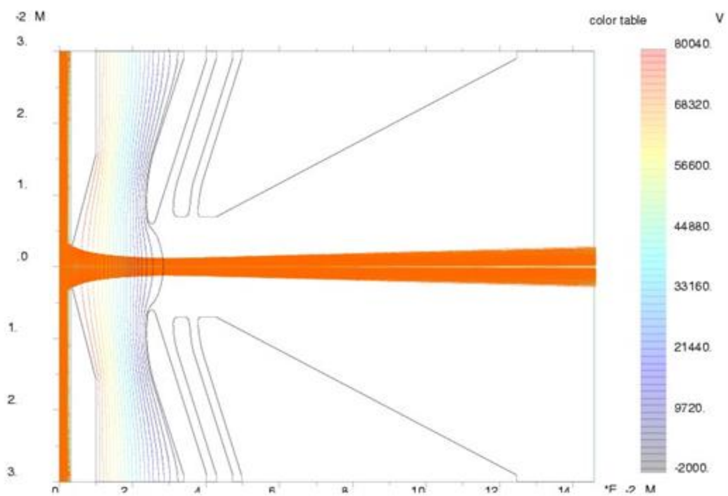

Upgrade of VIS extraction system

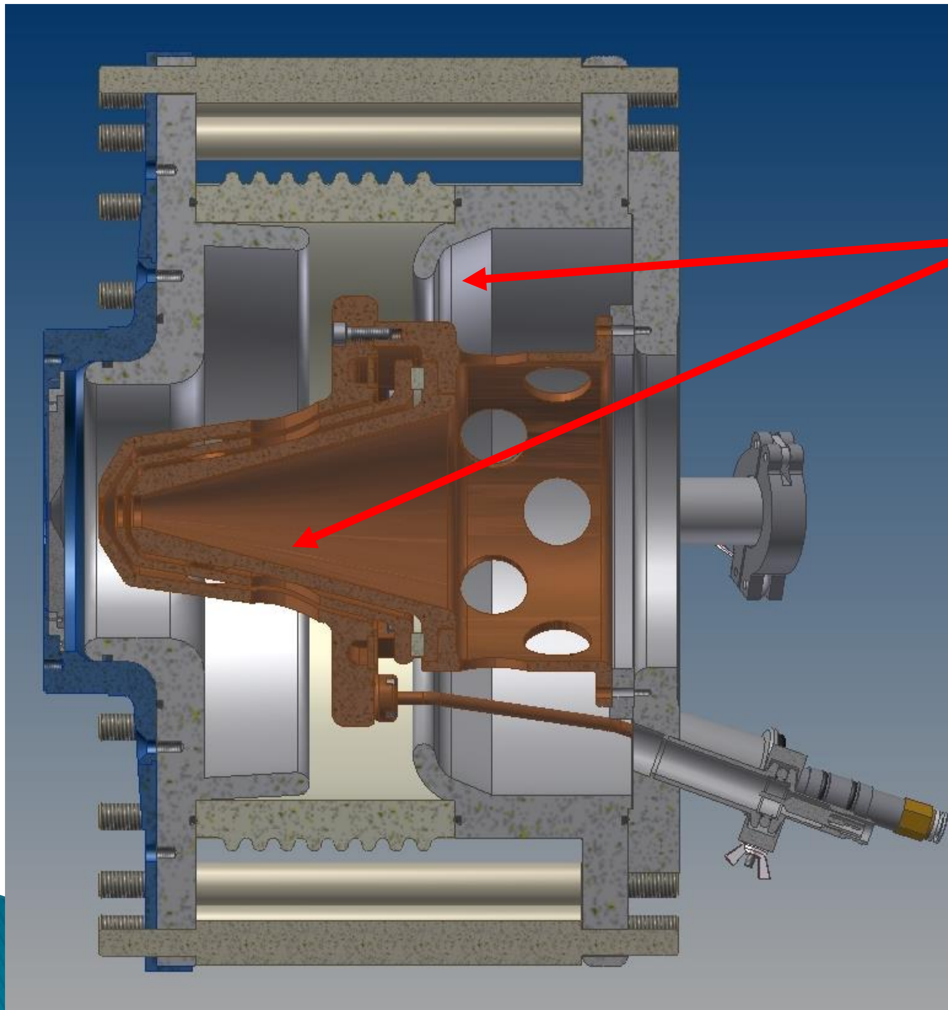

Improvements introduced:

- Improved ground shielding
- Single alumina
- All the electrodes are cooled, also repeller by using AlN insulator
- New triple point design (metal-vacuum-alumina)

Upgrade of VIS extraction system

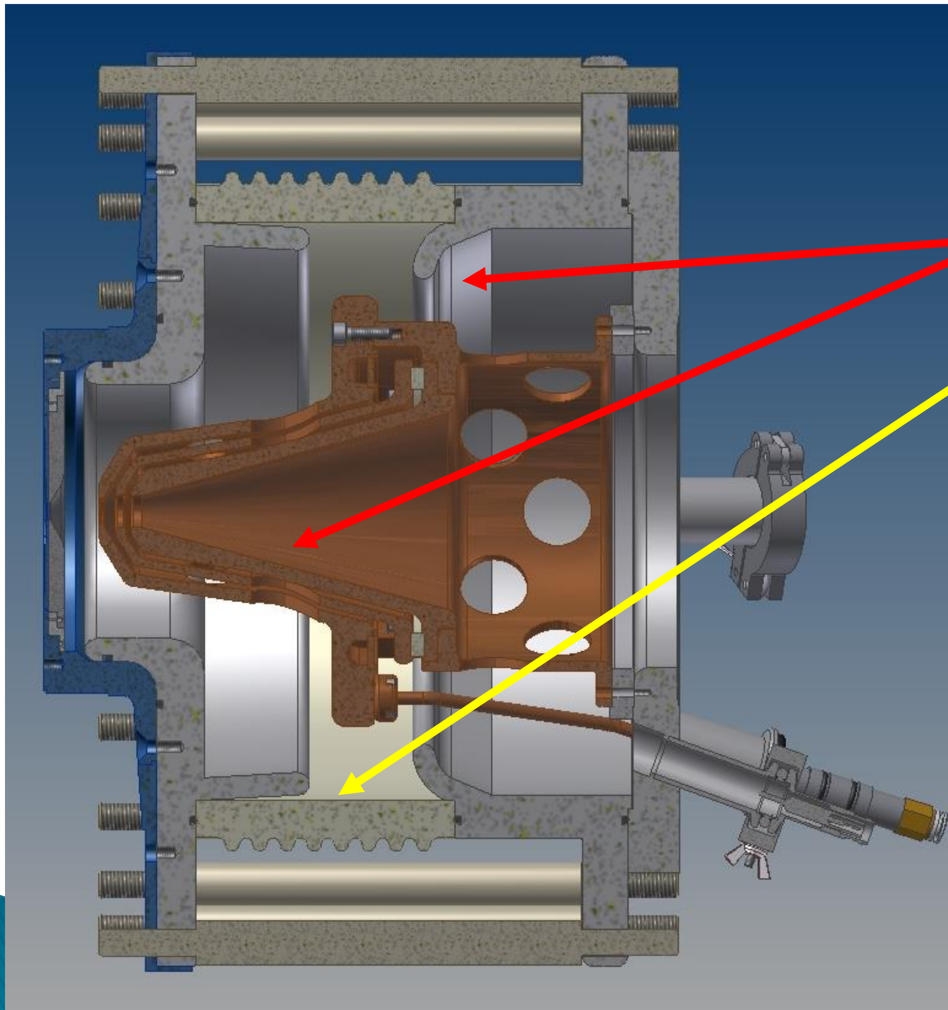

Improvements introduced:

- Improved ground shielding
- Single alumina
- All the electrodes are cooled, also repeller by using AlN insulator
- New triple point design (metal-vacuum-alumina)

Upgrade of VIS extraction system

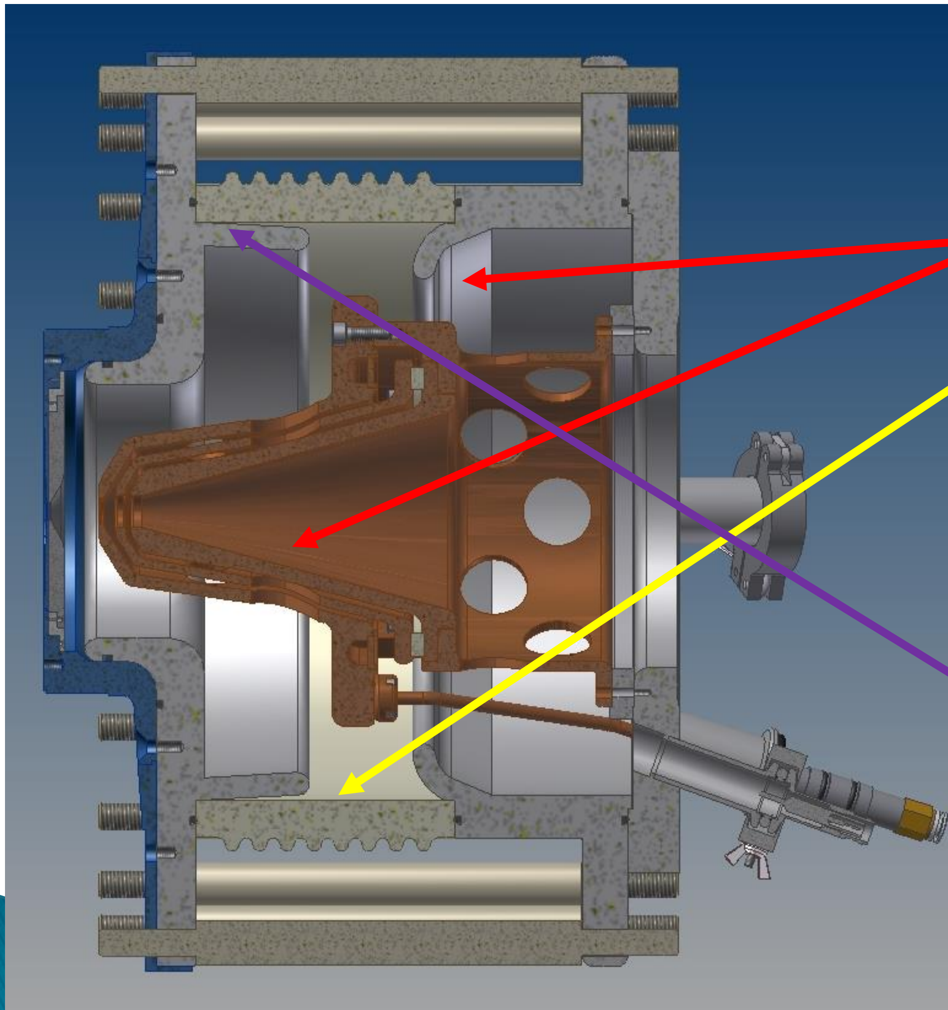

Improvements introduced:

- Improved ground shielding
- Single alumina
- All the electrodes are cooled, also repeller by using AlN insulator
- New triple point design (metal-vacuum-alumina)

Upgrade of VIS extraction system

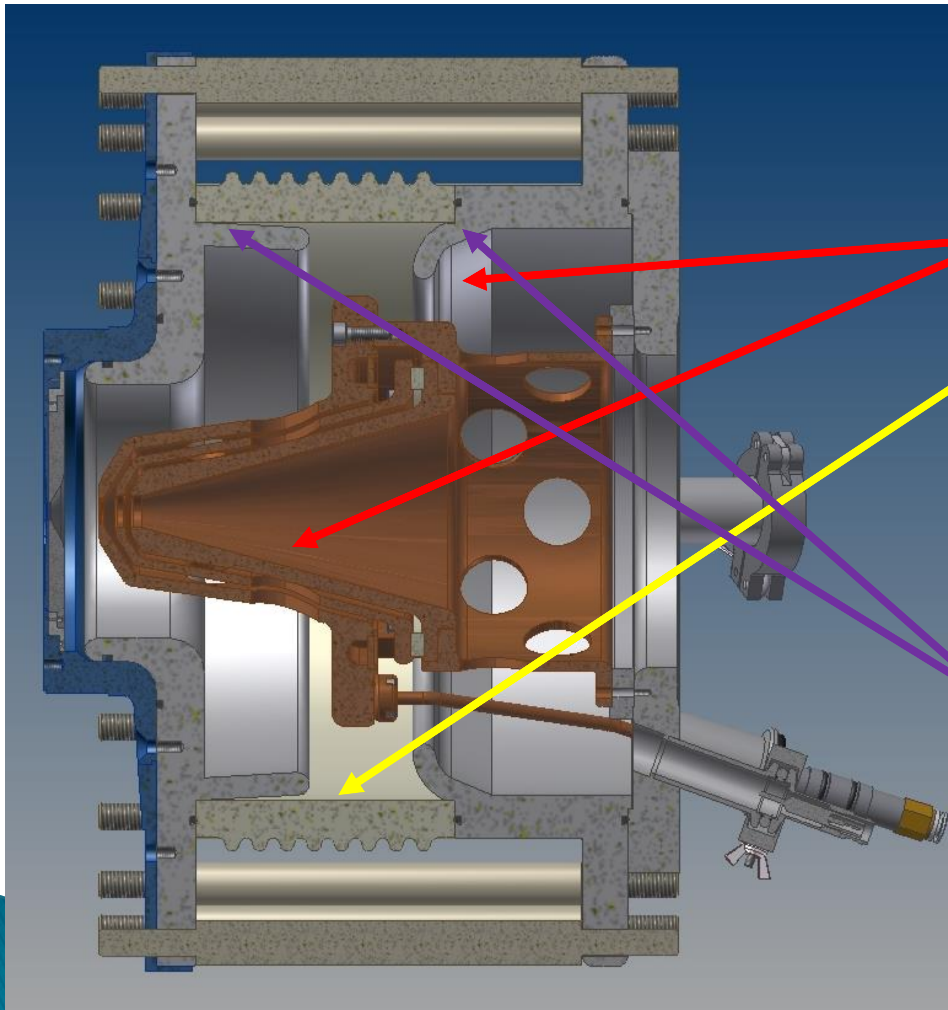

Improvements introduced:

- Improved ground shielding
- Single alumina
- All the electrodes are cooled, also repeller by using AlN insulator
- New triple point design (metal-vacuum-alumina)

Simulation of extraction

A multi-parametric optimization of the geometry was done using AXCEL 2D axial symmetric simulation

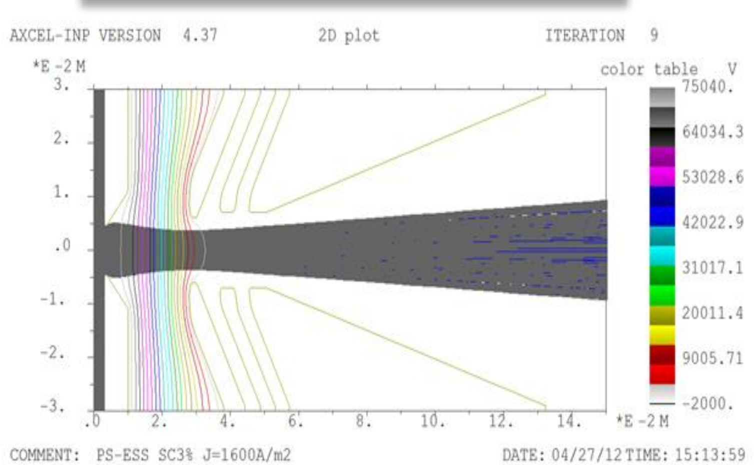

Own code for the conversion to a 3D beam distribution that take care about the representativeness the axial symmetry

3D beam distribution for TraceWin calculation

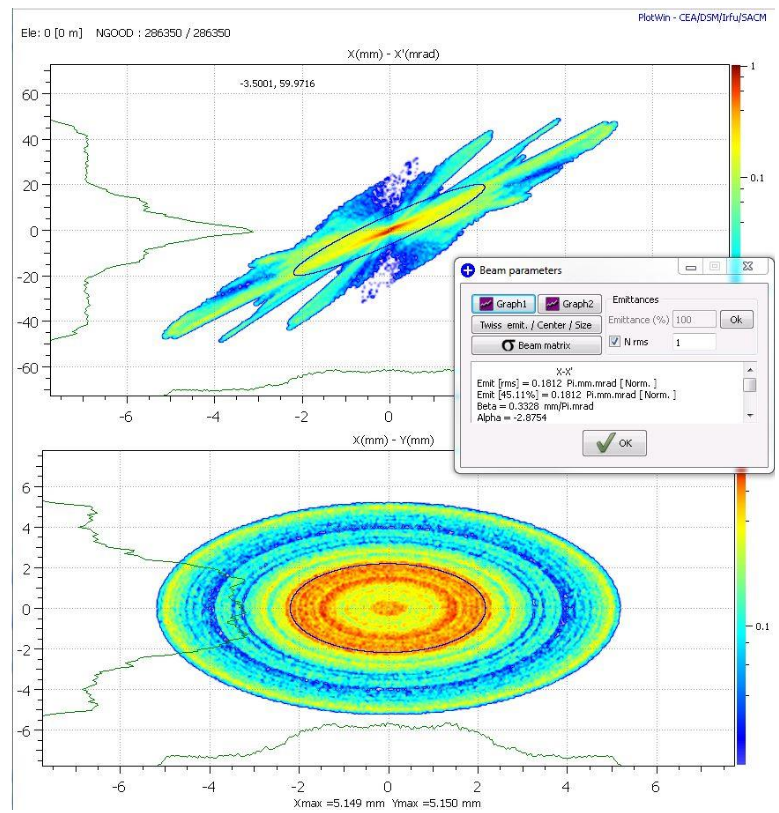

Beam transport optimization

The strength of the magnetic field of the two solenoid can be optimized to obtain the twiss parameters needed for the RFQ…

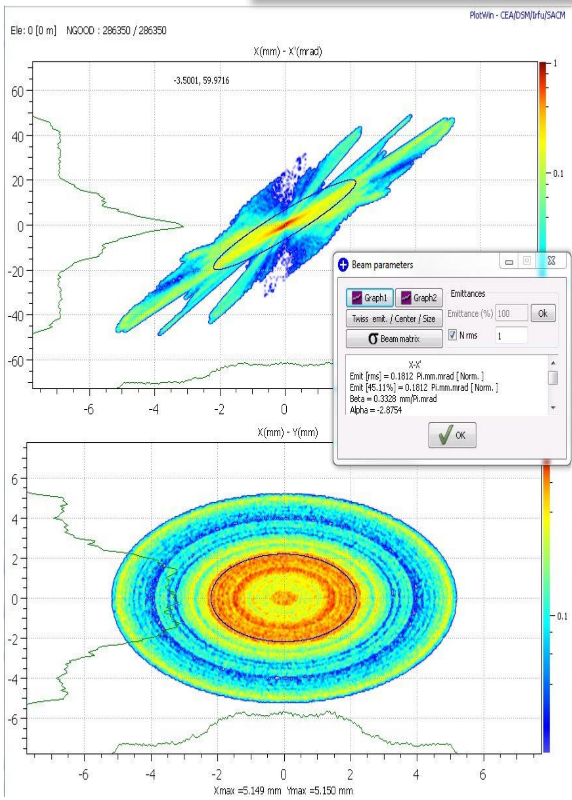

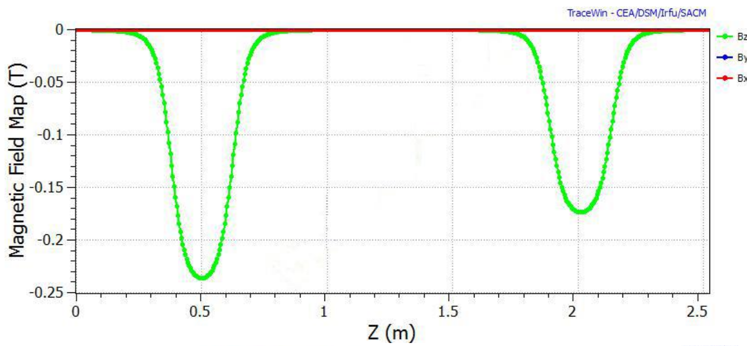

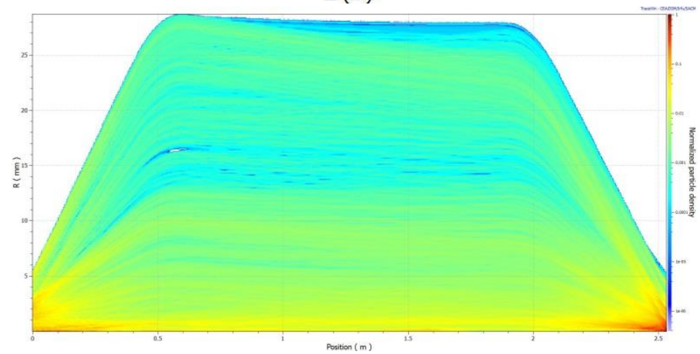

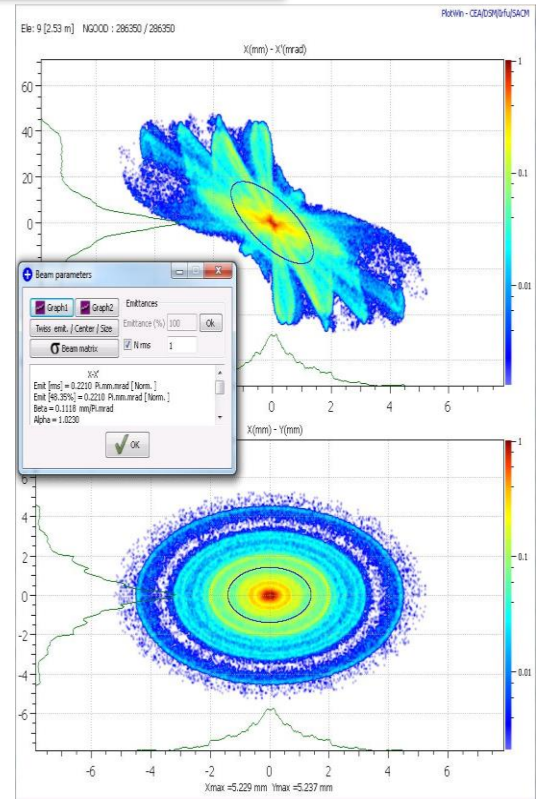

Beam transport optimization

The strength of the magnetic field of the two solenoid can be optimized to obtain the twiss parameters needed for the RFQ…

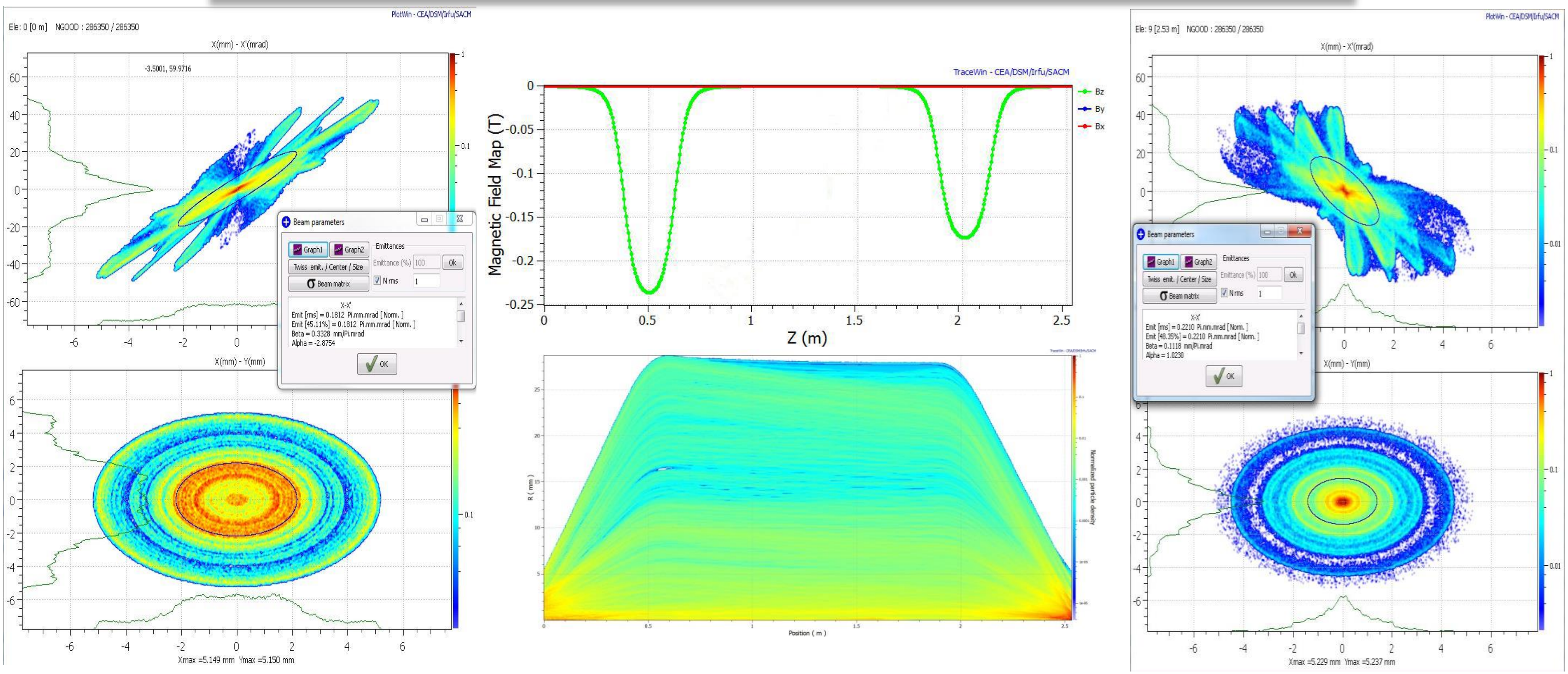

… not only for the full beam, but also when the iris is used:
same twiss parameters can be obtained from 100 % to 10 % of selected beam.
It is obvious that the emittance decrease a lot proportionally to the cut.
Experimental check is needed to measure the effect of a not ideal iris geometry.

PS-ESS#1 + LEBT

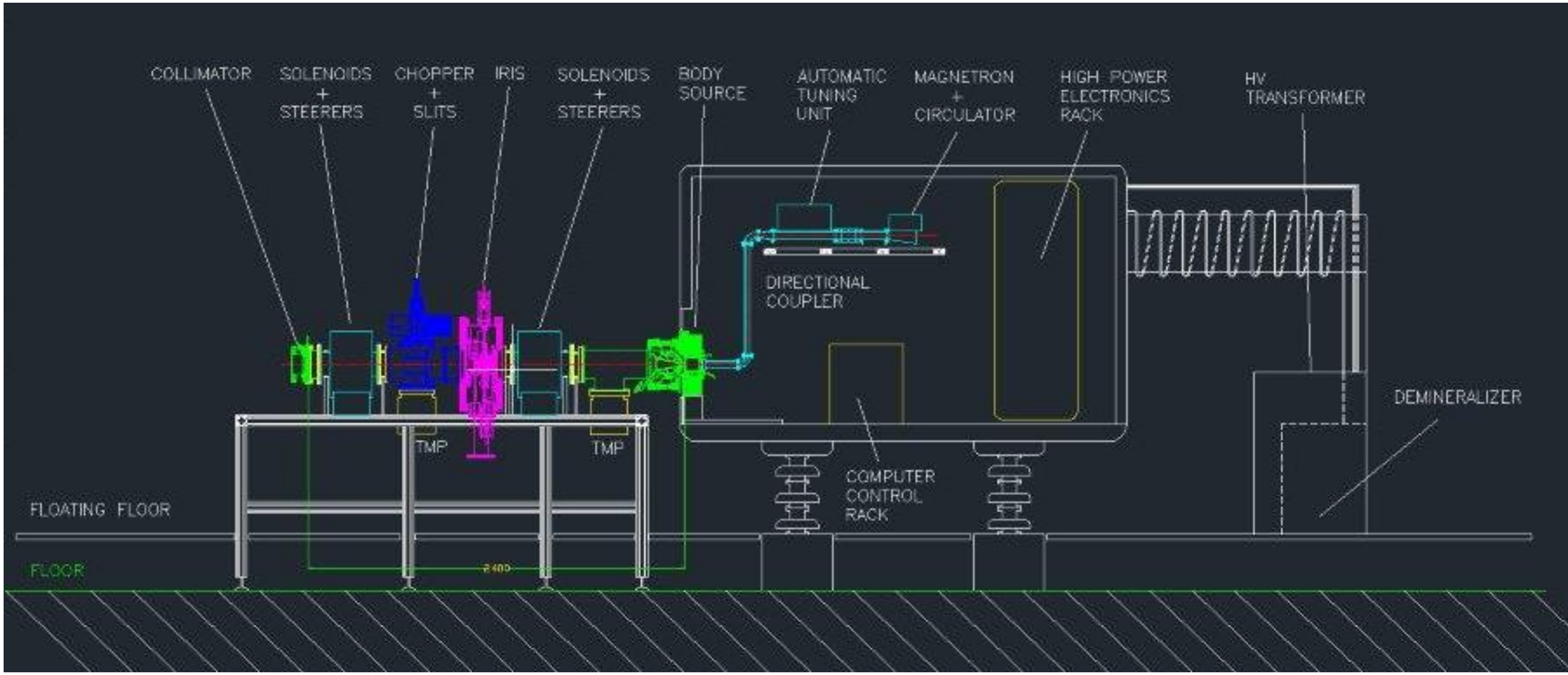

Picture to update with the new length:

- *270 mm : extraction system (starting from the plasma electrode)*
- *100 mm : cable from extraction system ; beam-current-transformer*
- *400 mm : first solenoid ; bellow*
- *60 mm : gate-valve*
- *300 mm : iris*
- *350 mm : chopper*
- *400 mm : diagnostic box*
- *400 mm : second solenoid ; bellow*
- *320 mm : gate-valve ; beam-current-transformer ; collimator ; repeller electrode with cable ;*

Movable iris: from 0 to 40 mm radius, 600 W, 300 mm length

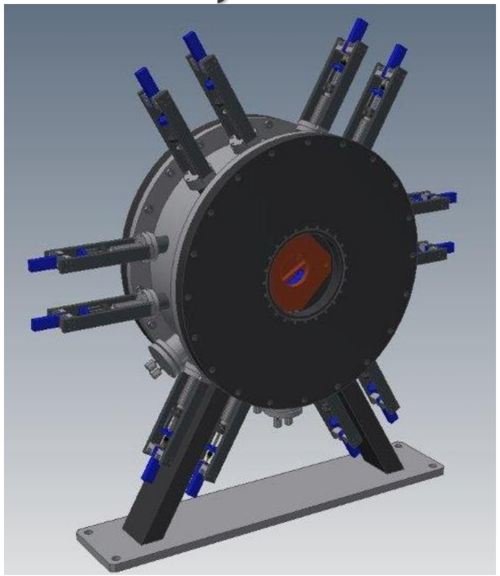

100 % of beam => 30 mm radius
10 % of beam => 5 mm radius

To increase the axial symmetry of the selected beam the shape of the six blades was chosen merging the minimum circumference of 5 mm radius and a dodecagonal shape

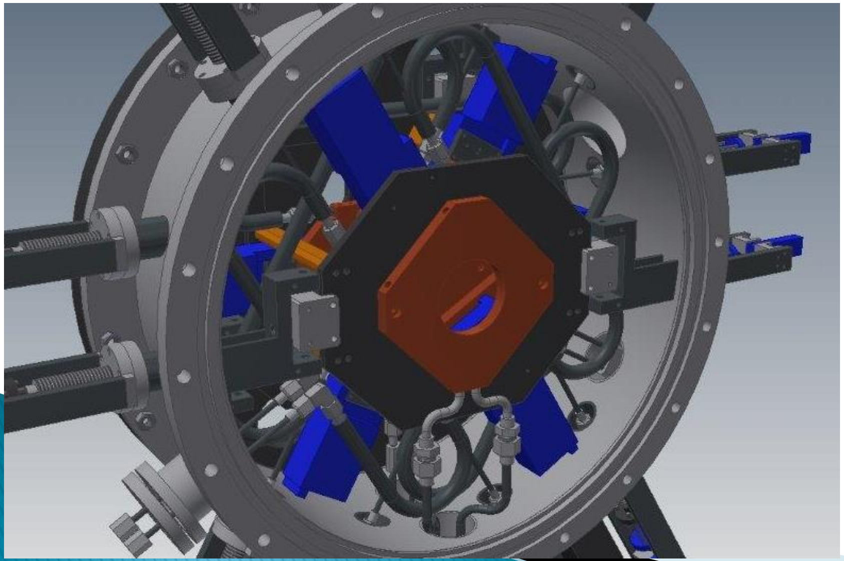

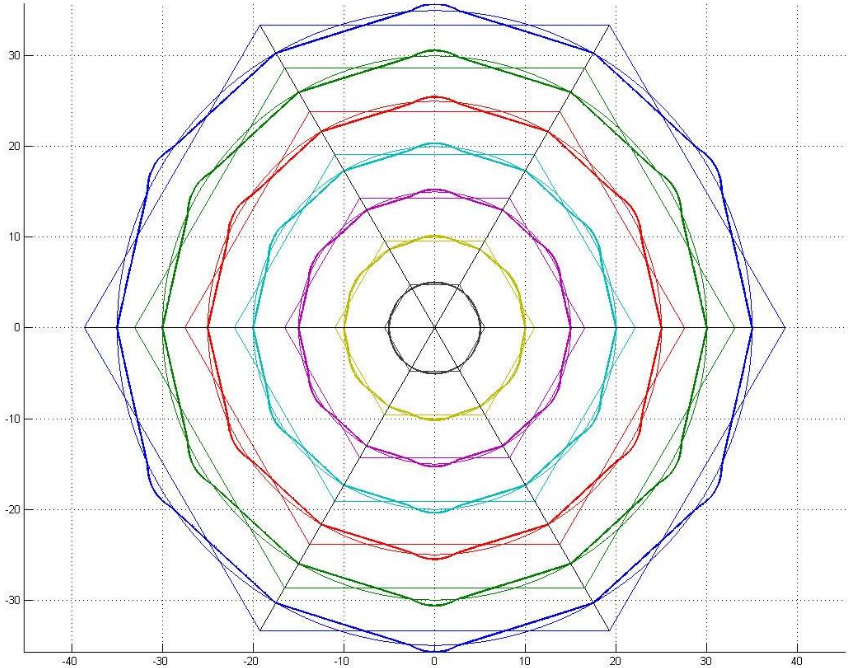

Chopper and collimator test at CEA-Saclay (12-2013 & 4-2014)

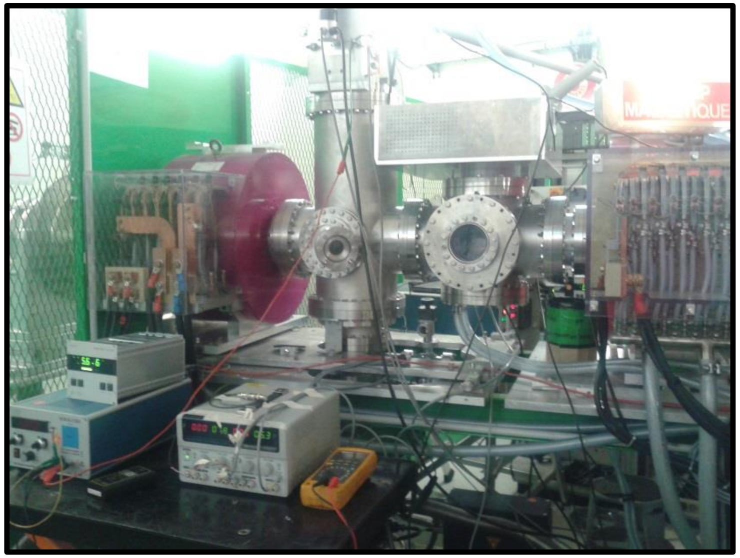

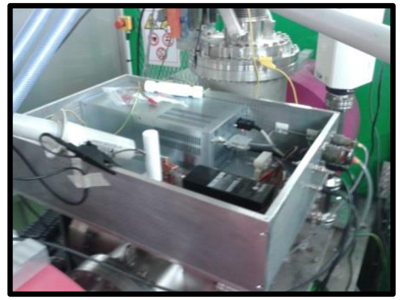

HV chopper electronics

Chopper

Collimator

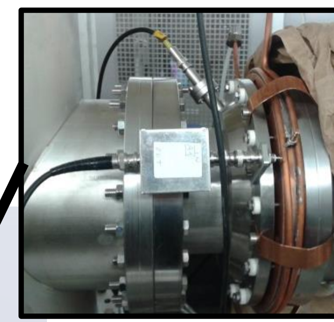

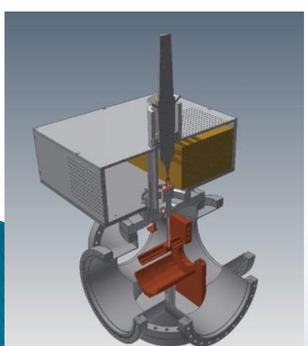

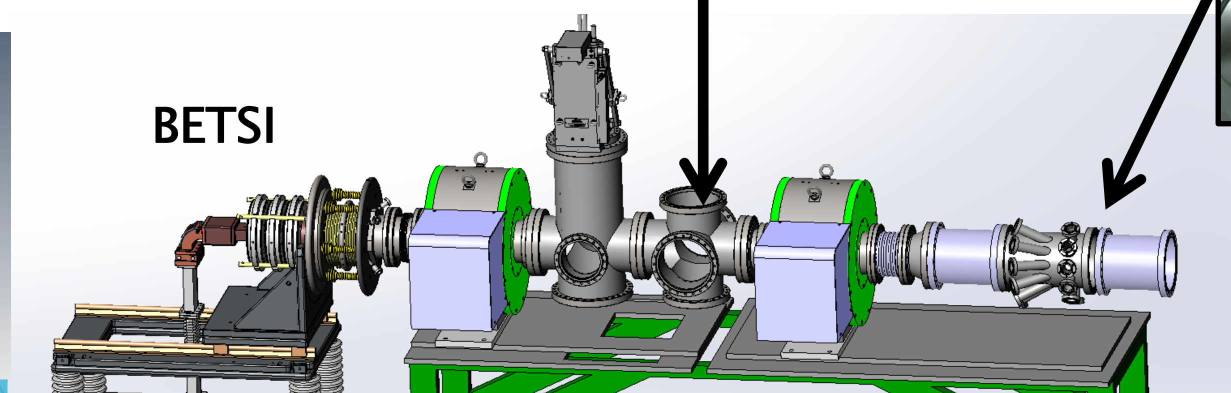

Defocusing chopper

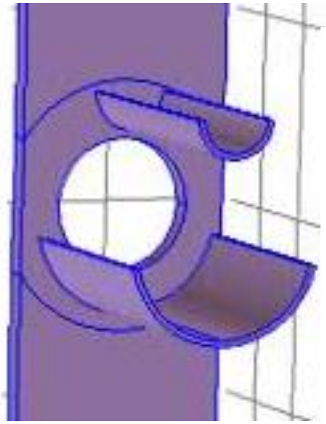

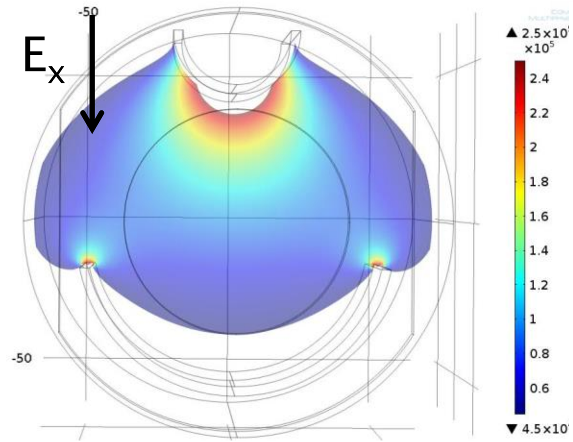

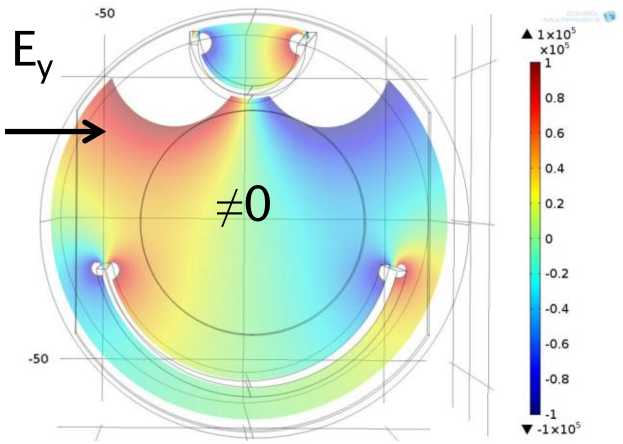

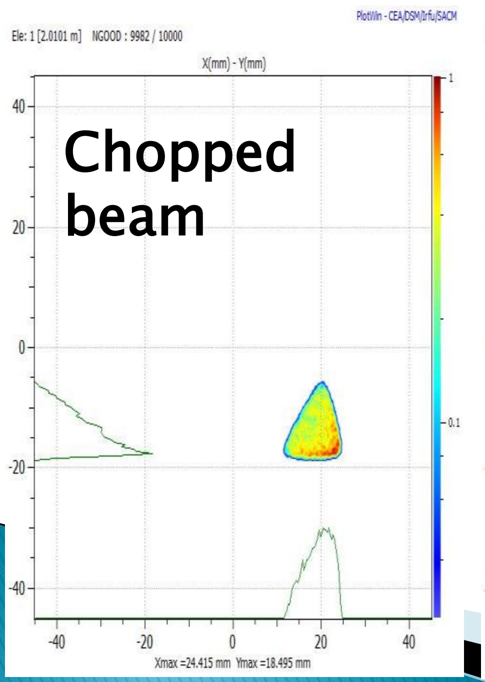

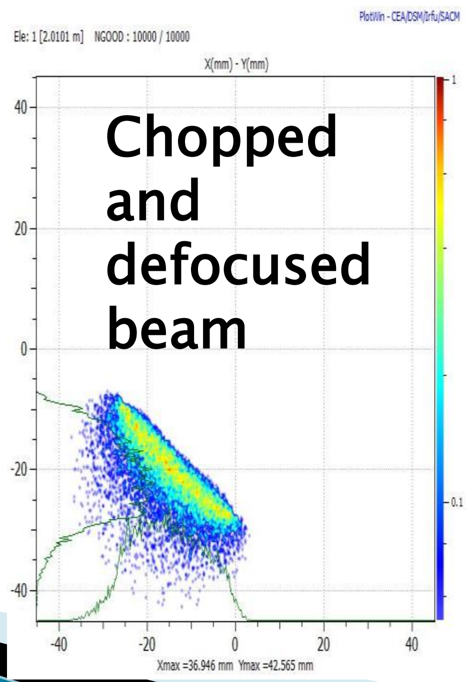

Experimental test done at CEA with our prototype

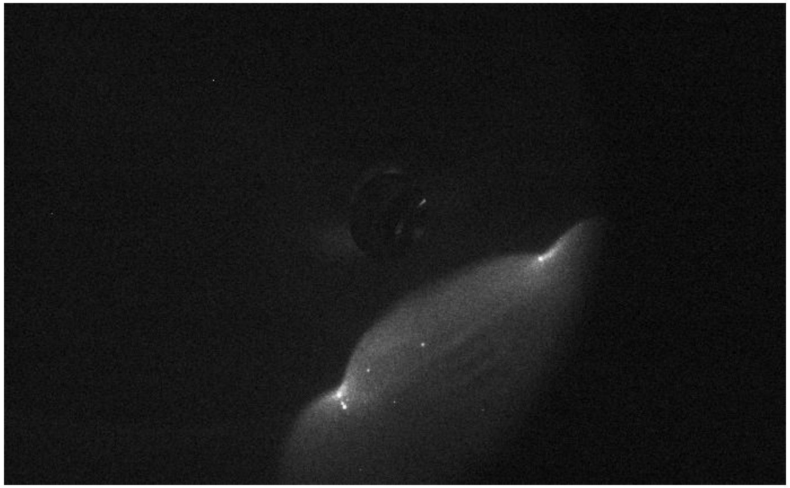

Beam pulse rise time

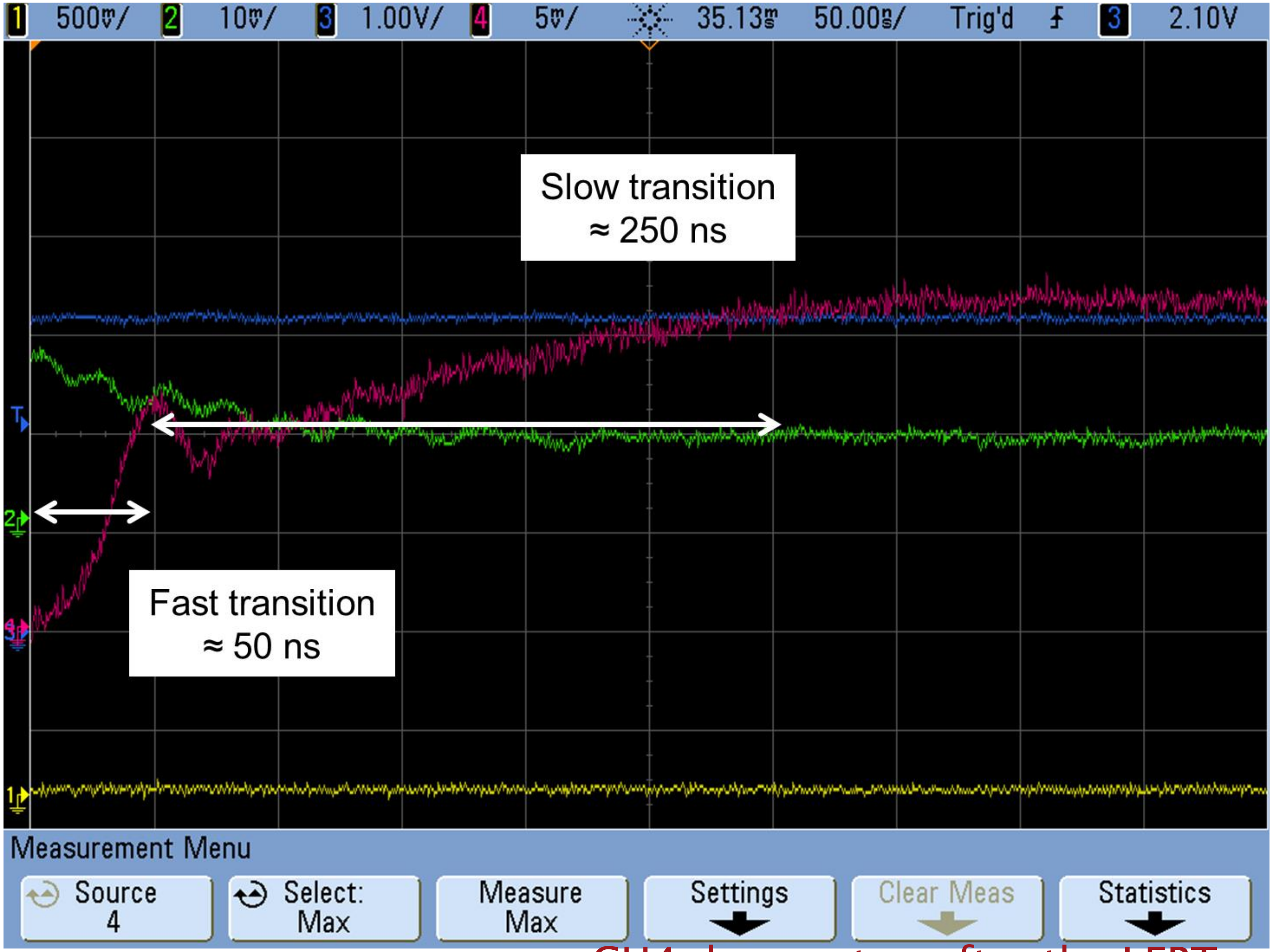

CH4: beam stop after the LEBT collimator
CH2: beam at LEBT collimator
CH1: chopper HV probe

Beam pulse fall time

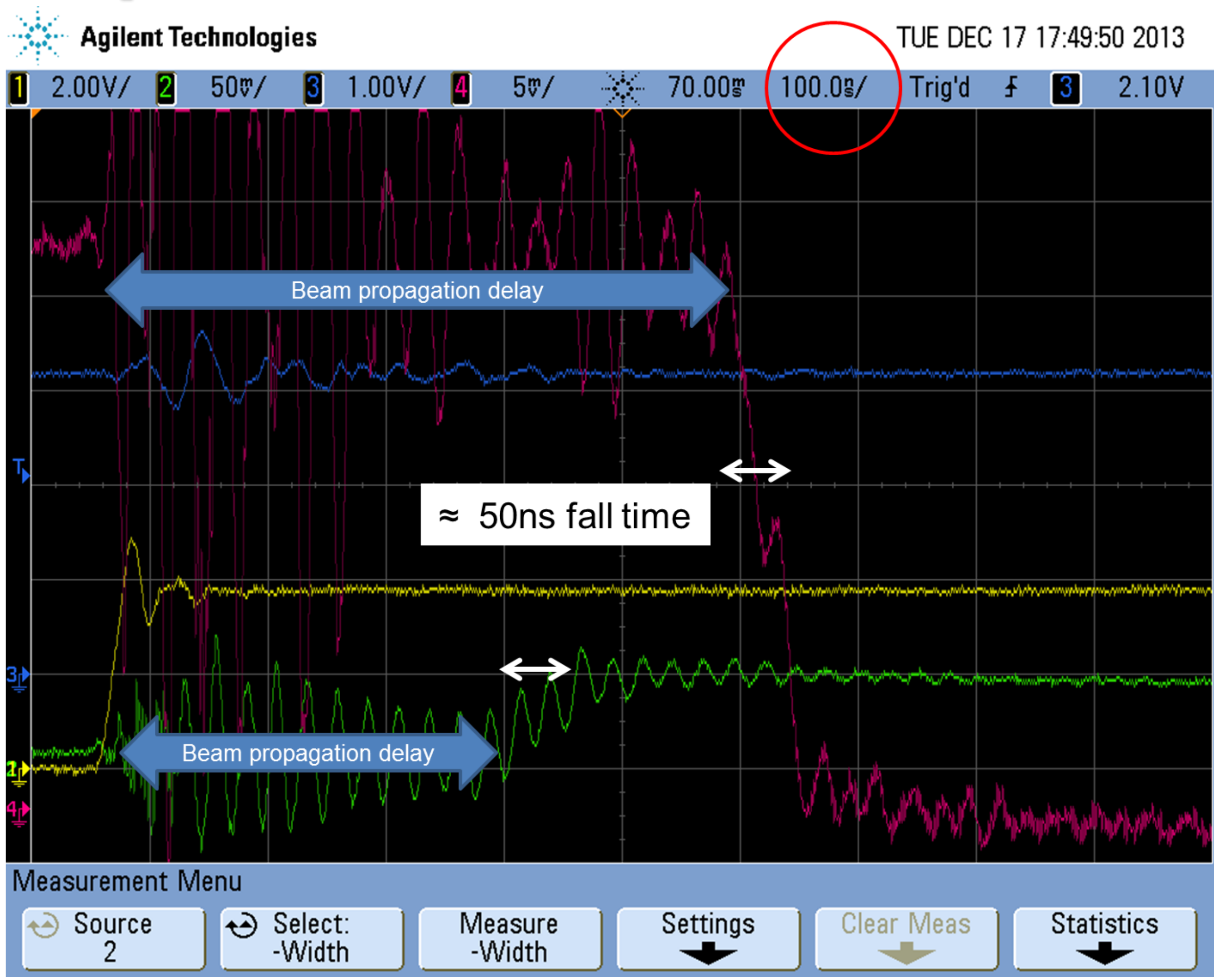

Ch4: Beam Stop (R_τ = 5,5 ohm; C = 183 pf ; R_τ * C = 1 ns)
Ch2: Collimator (R_τ = 5,5 ohm; C = 534 pf ; R_τ * C = 2,9 ns)

Chopper ON-OFF transition

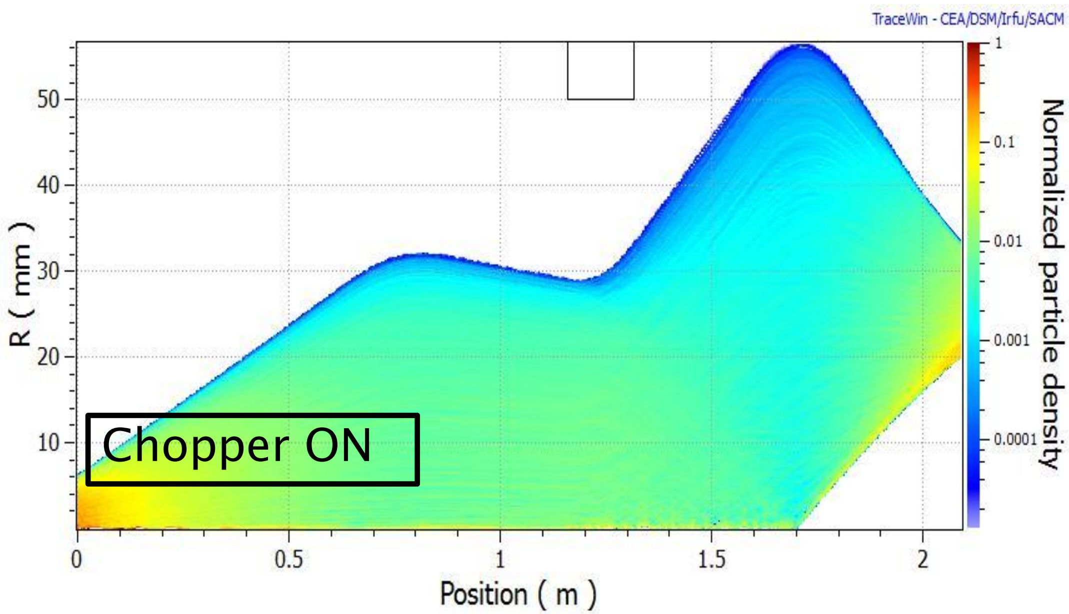

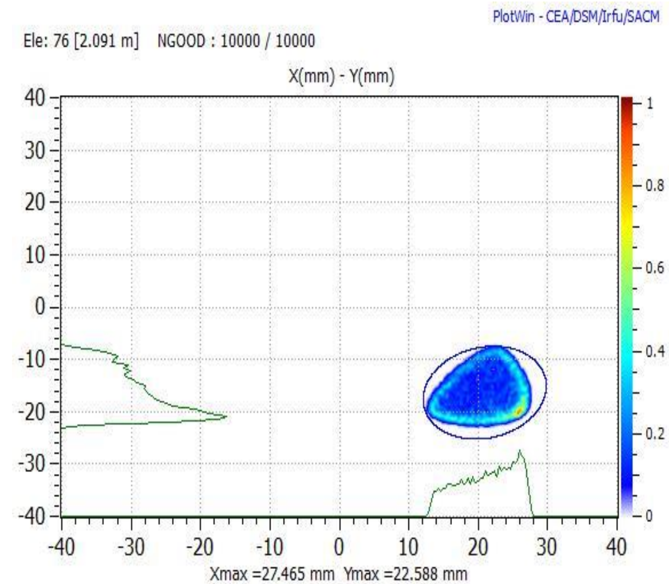

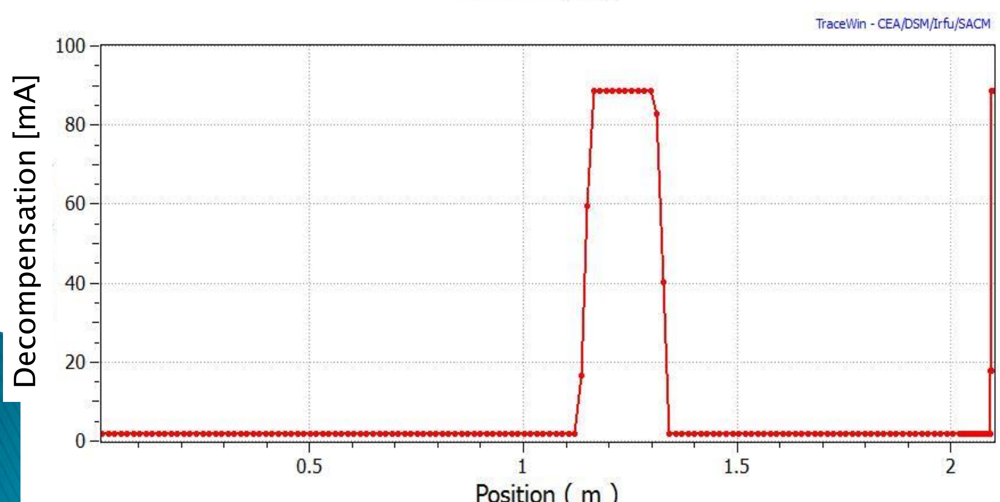

Chopper ON-OFF transition

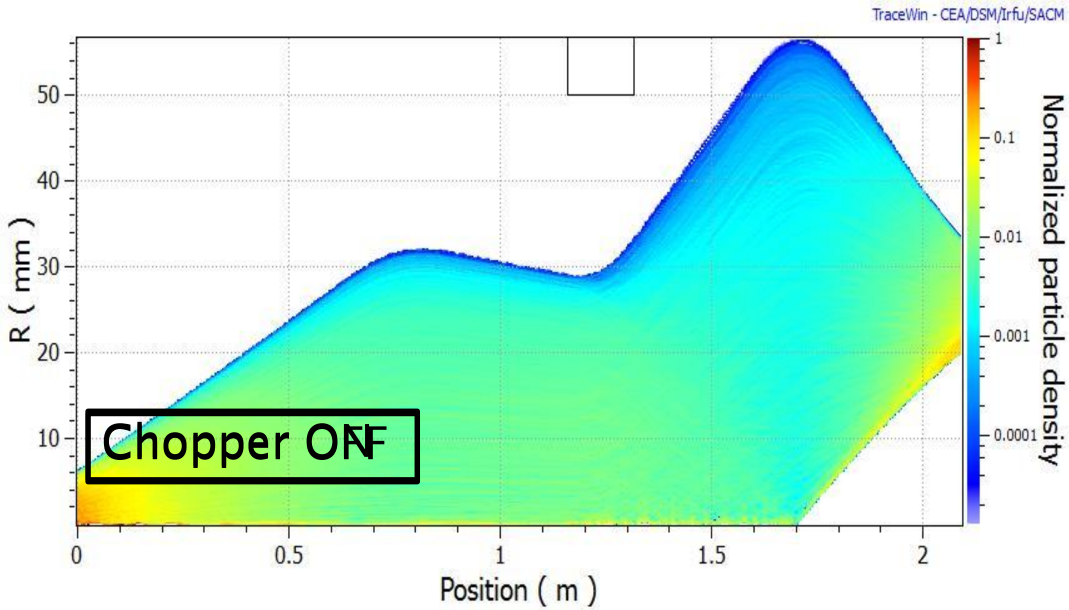

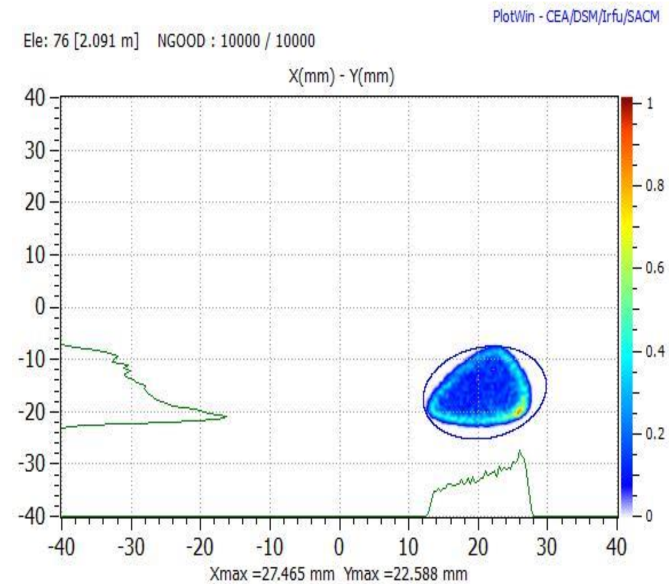

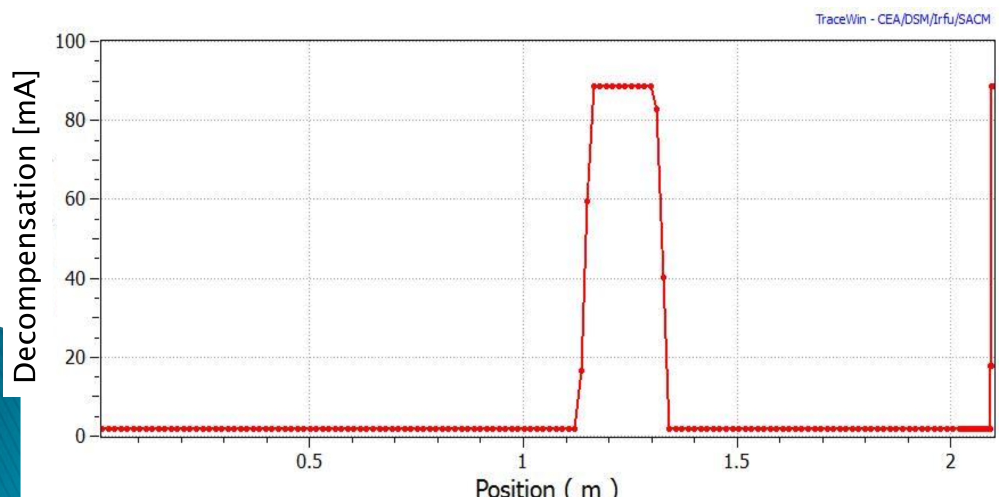

Chopper ON–OFF transition

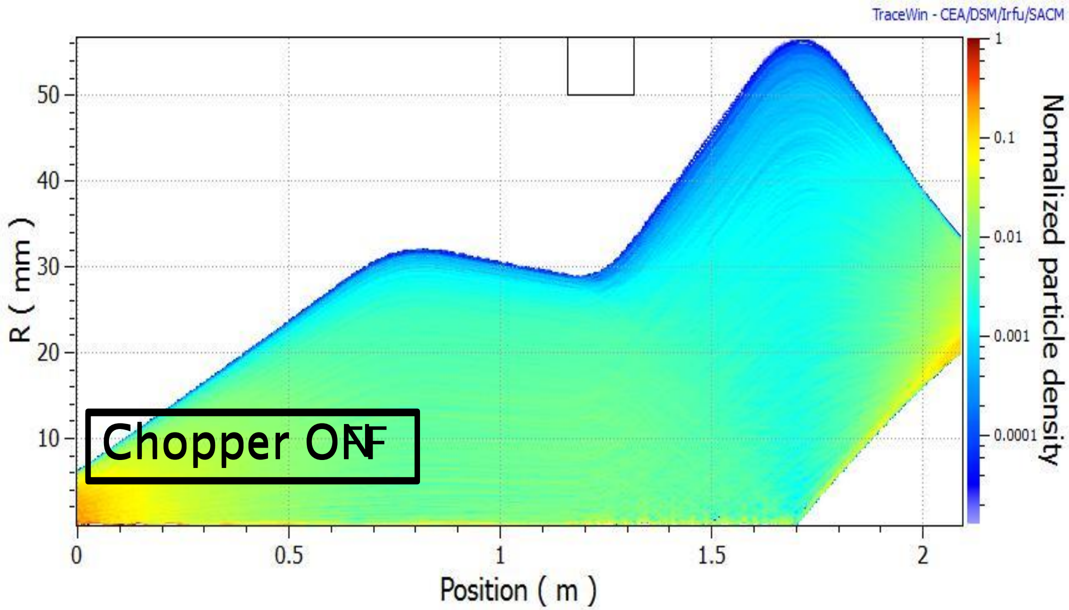

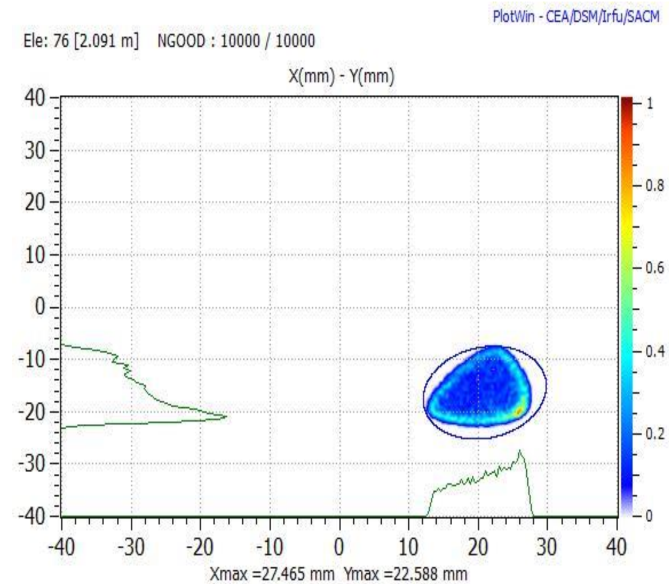

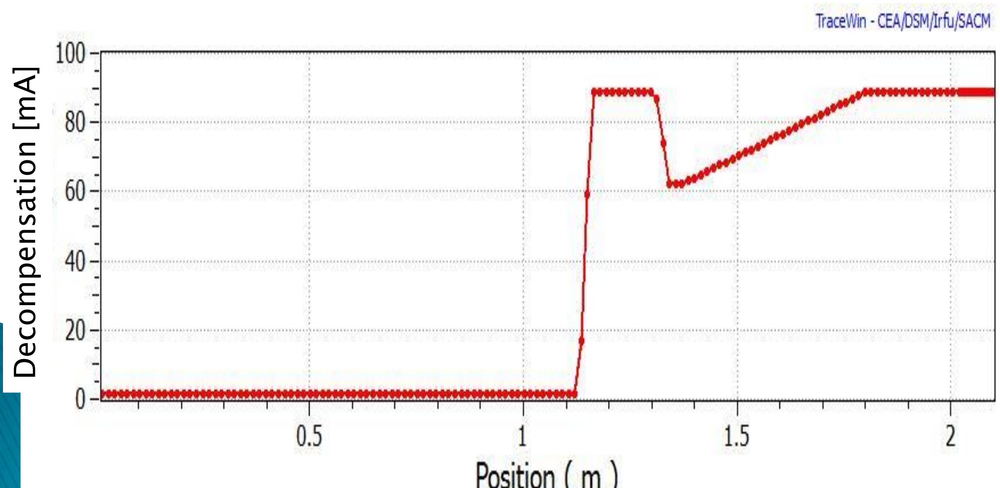

Chopper ON–OFF transition

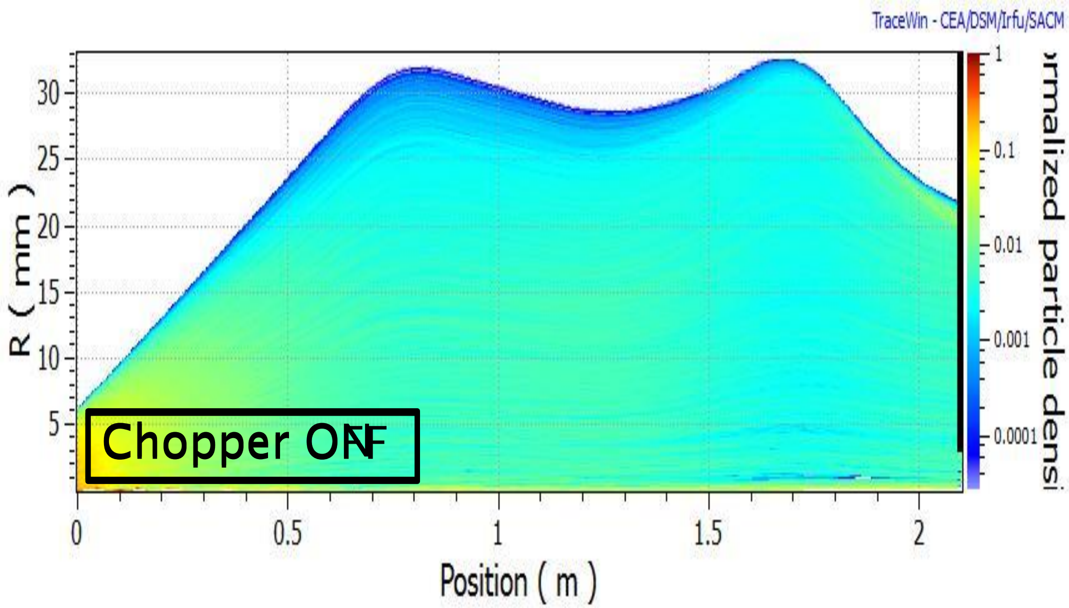

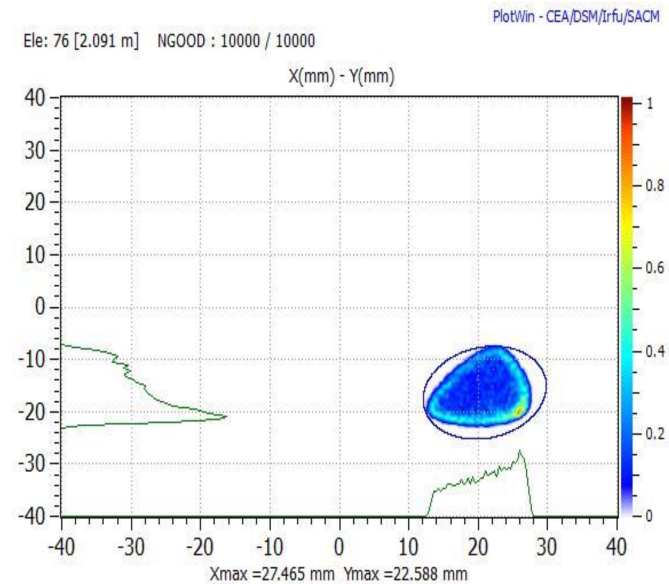

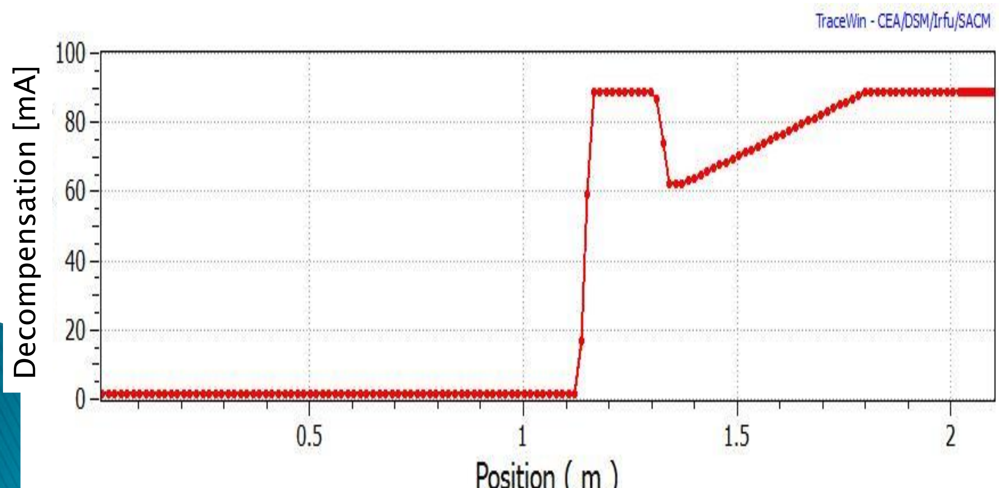

Chopper ON-OFF transition

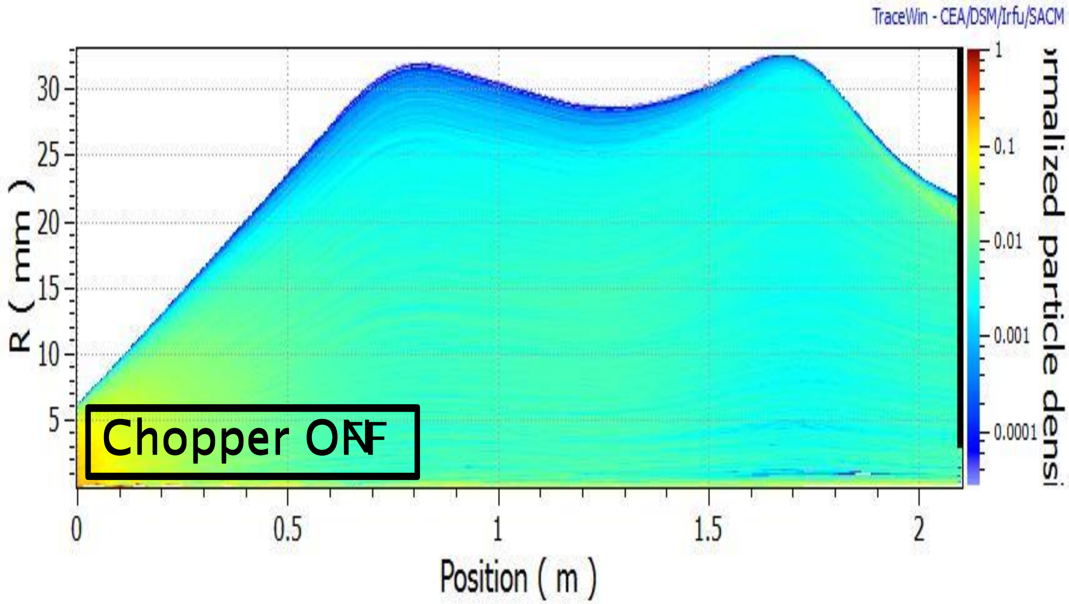

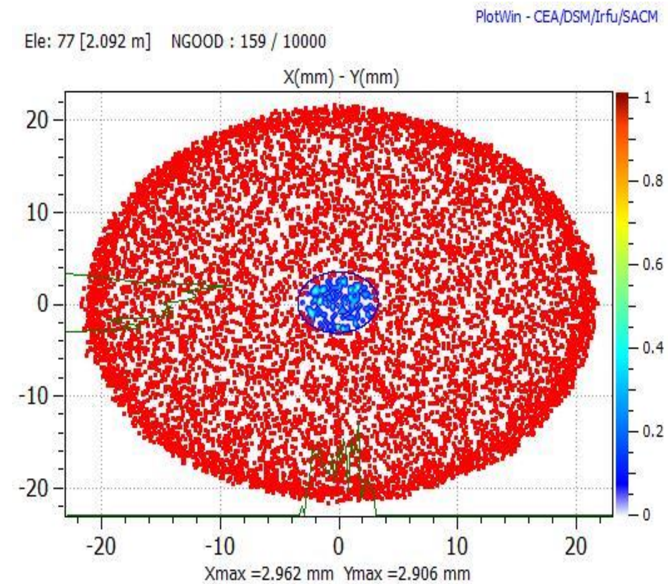

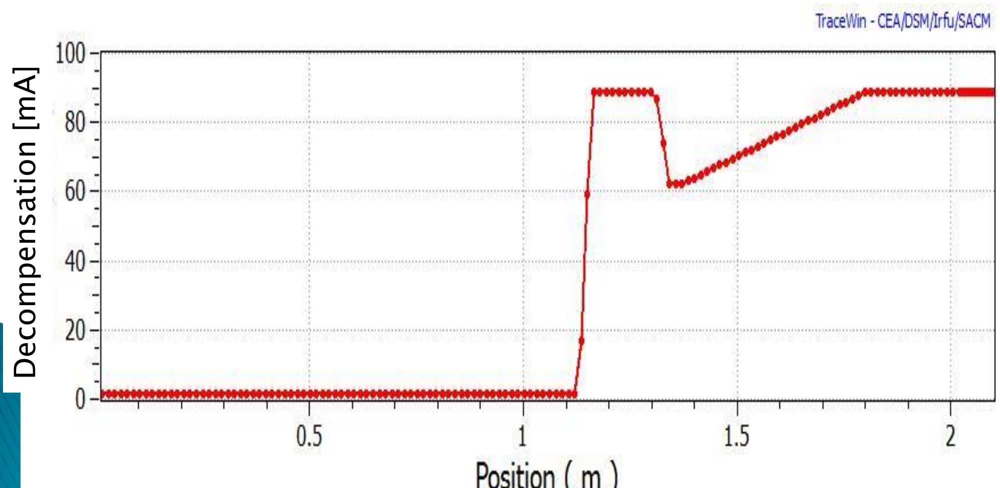

Chopper ON–OFF transition

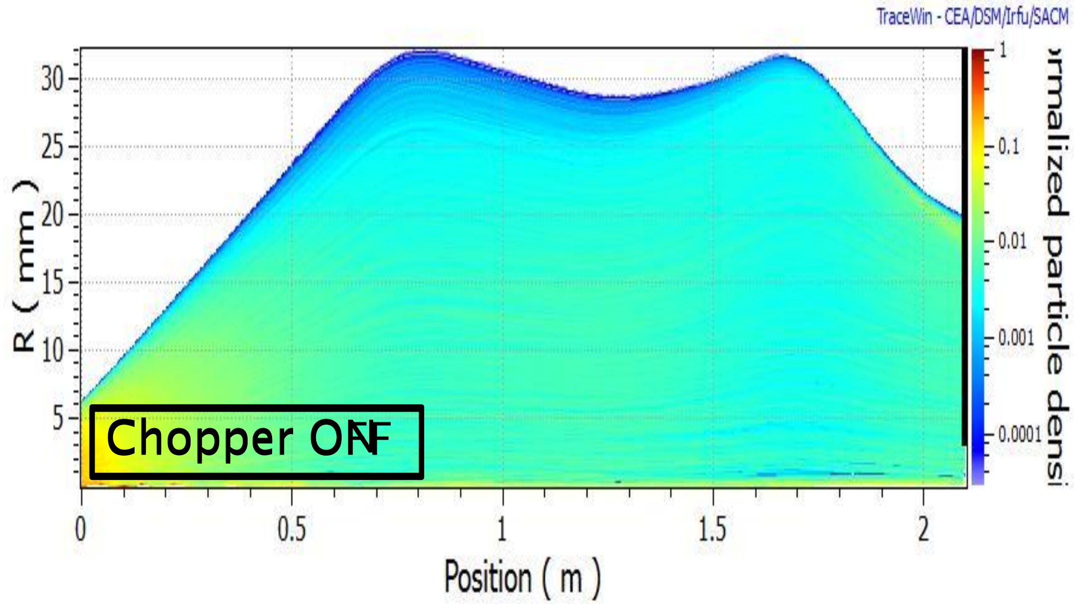

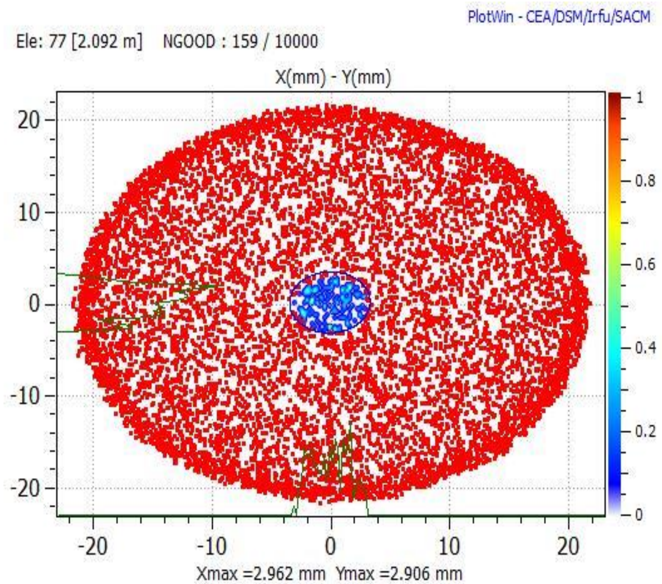

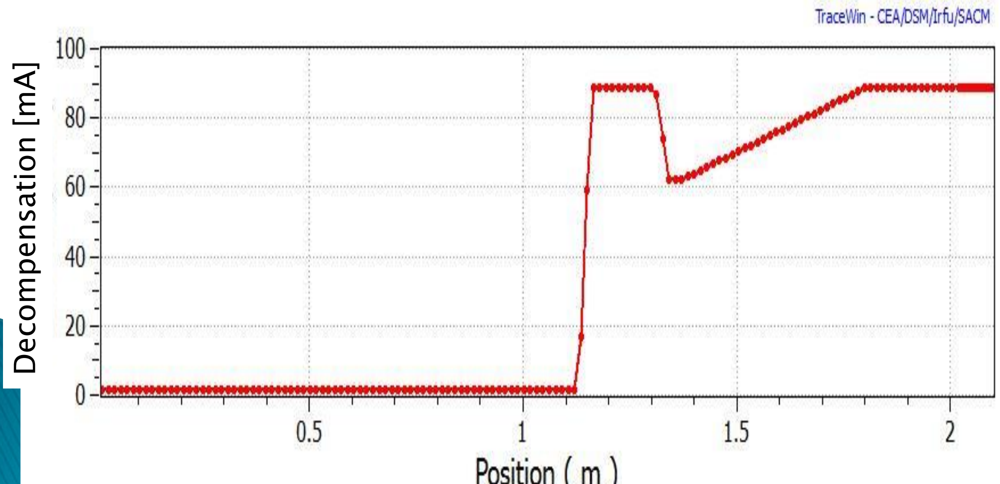

Chopper ON-OFF transition

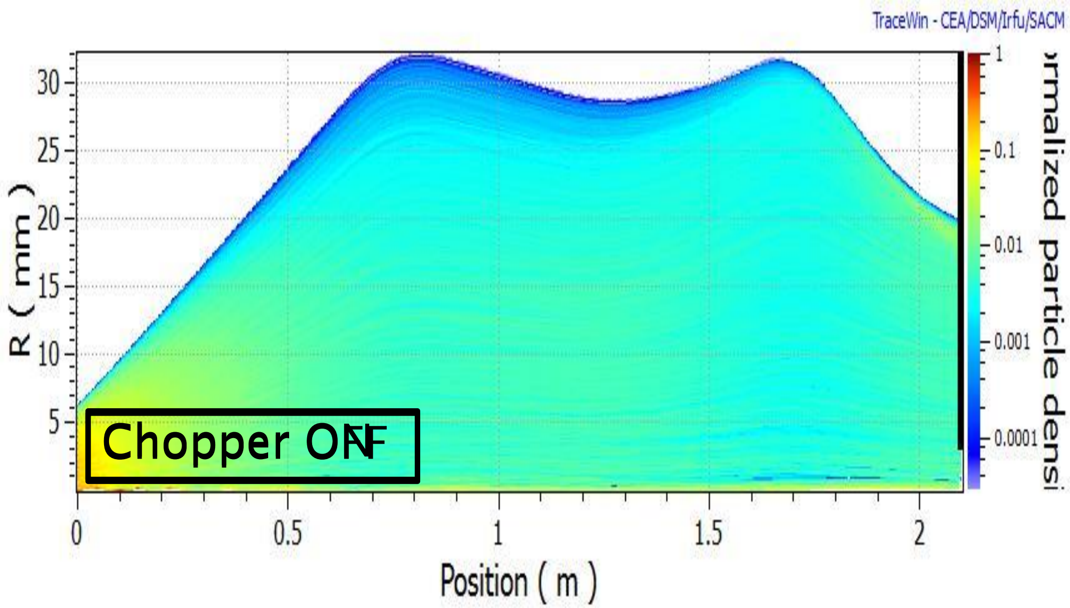

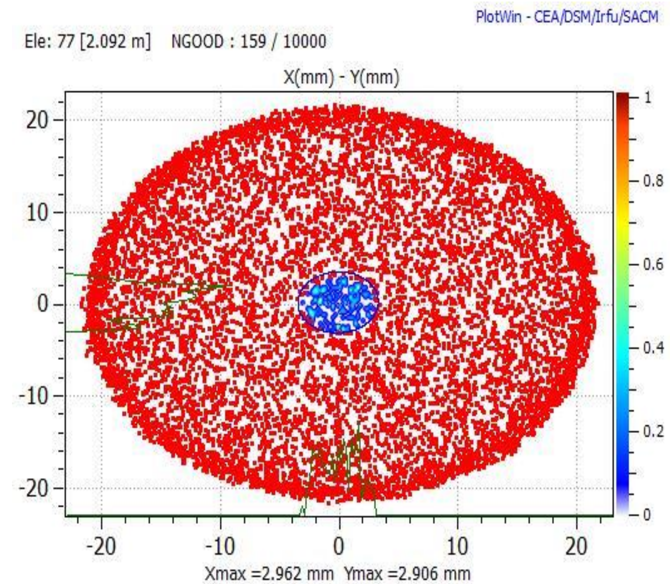

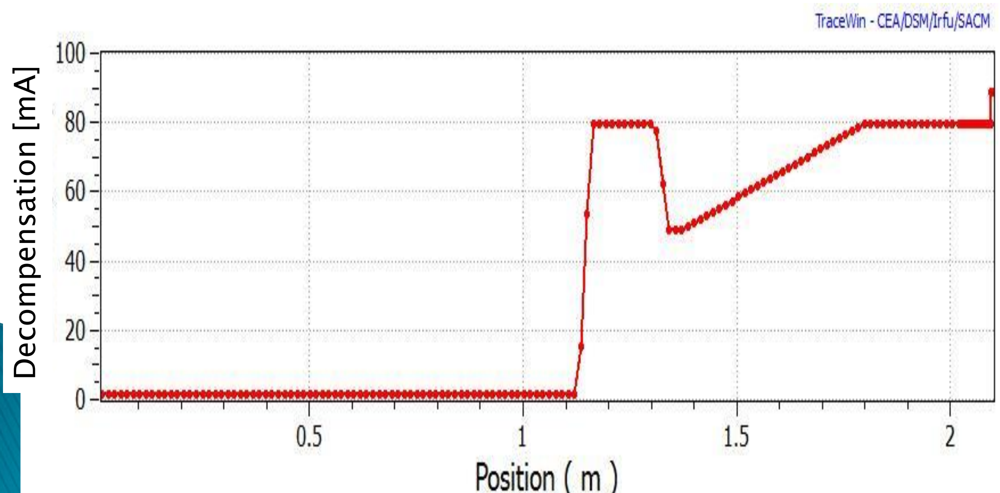

Chopper ON-OFF transition

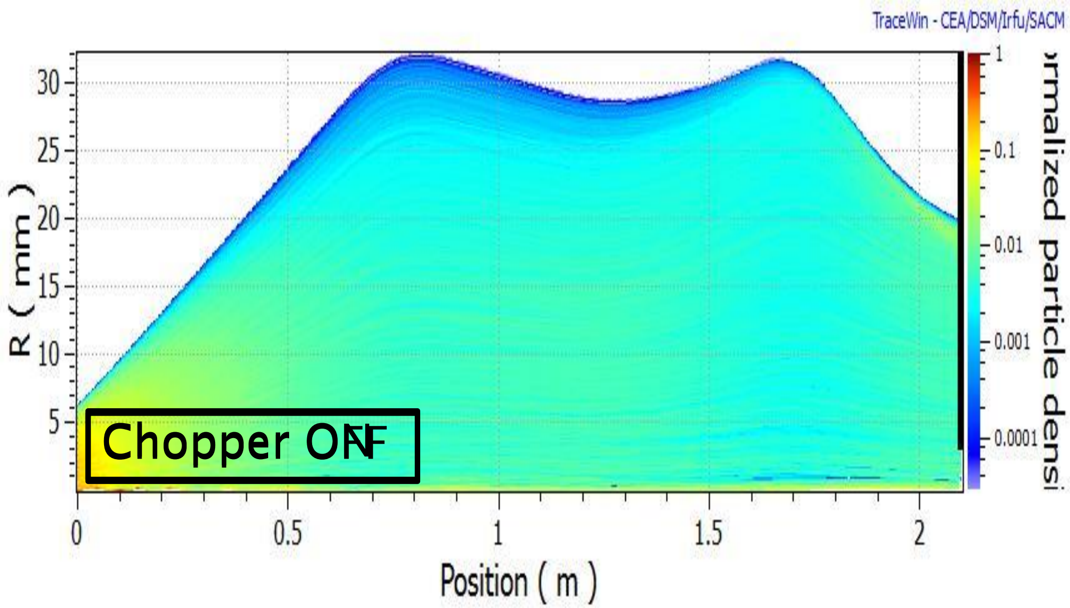

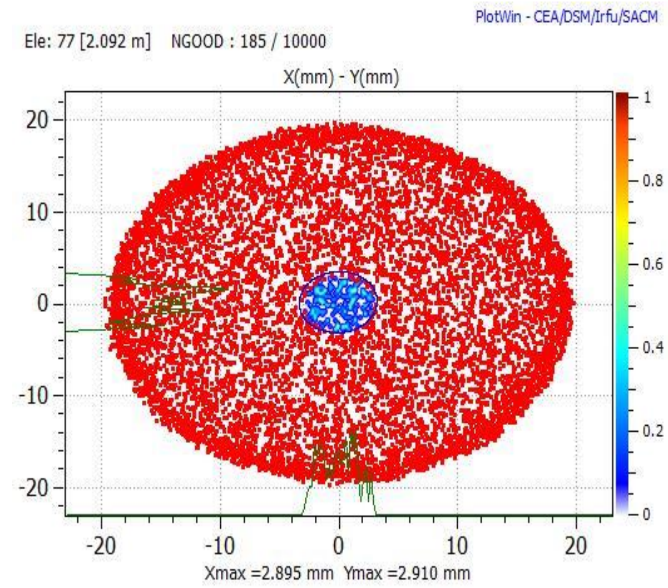

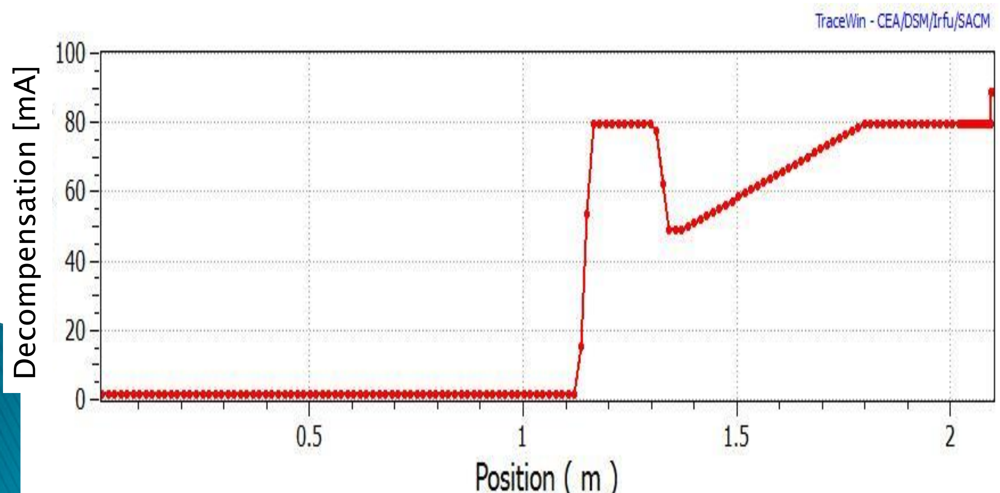

Chopper ON–OFF transition

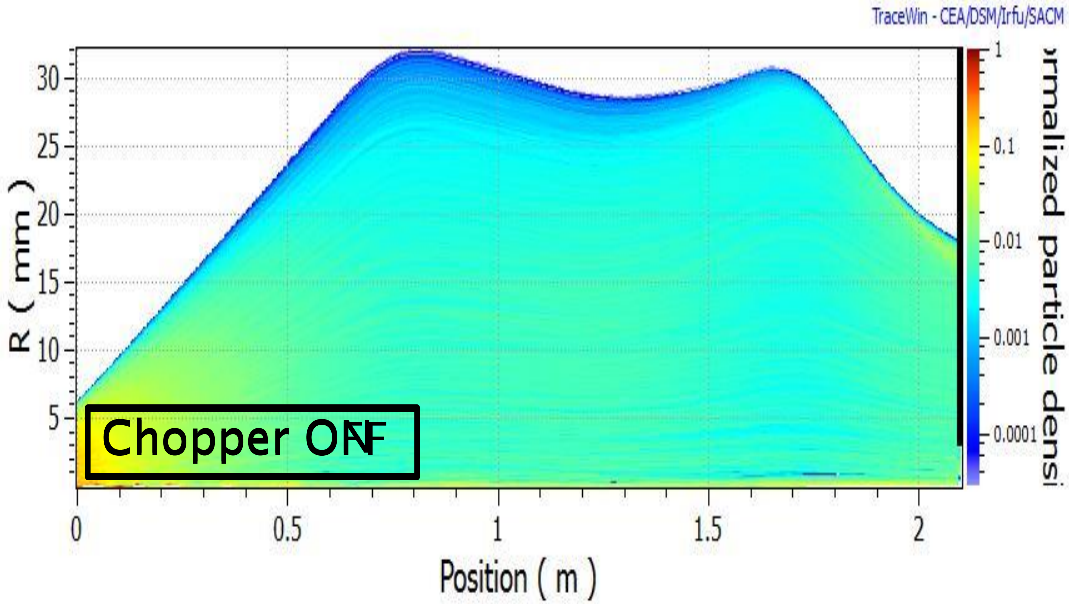

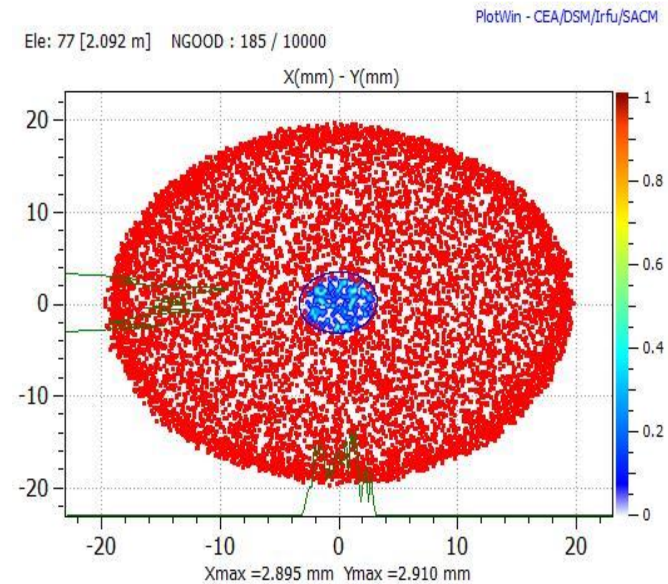

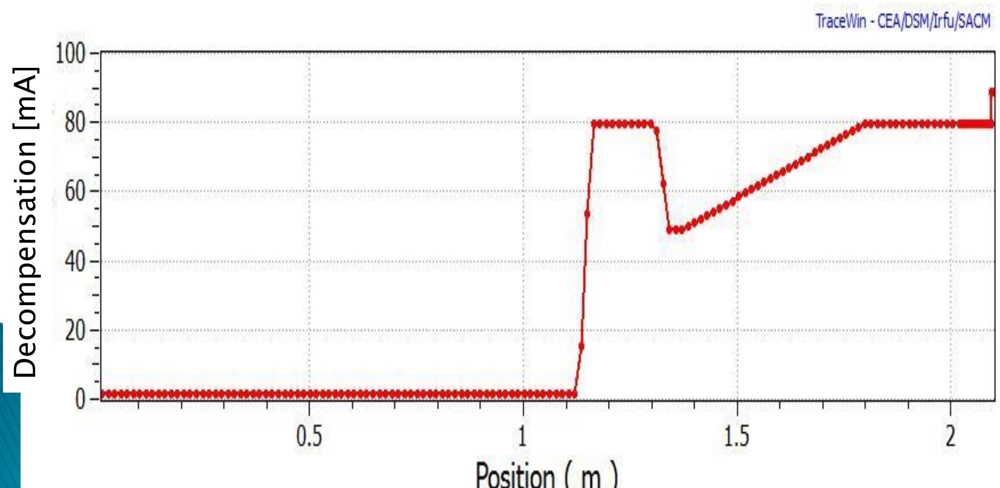

Chopper ON-OFF transition

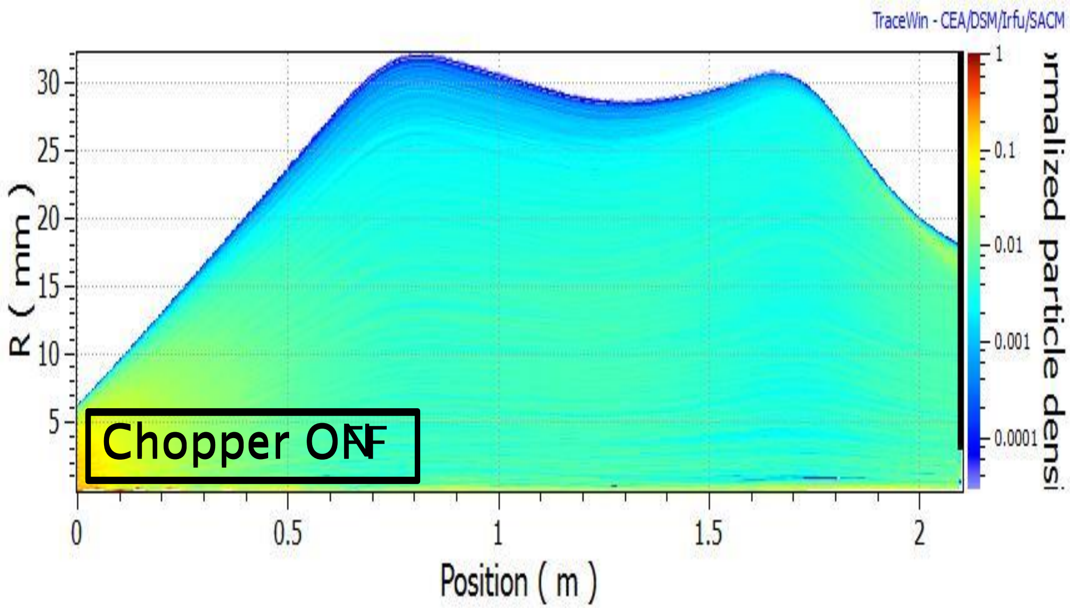

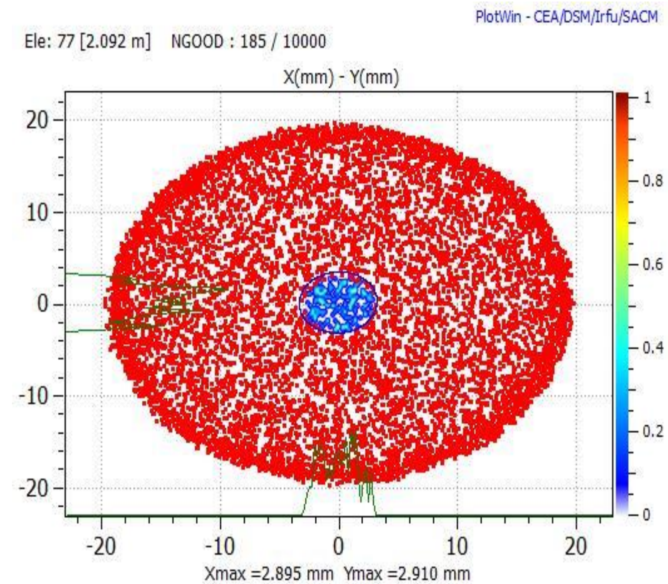

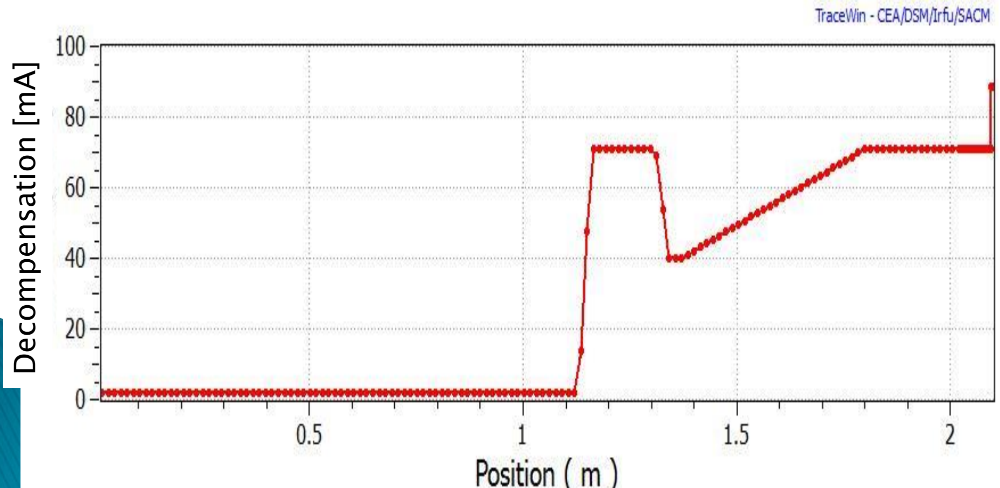

Chopper ON–OFF transition

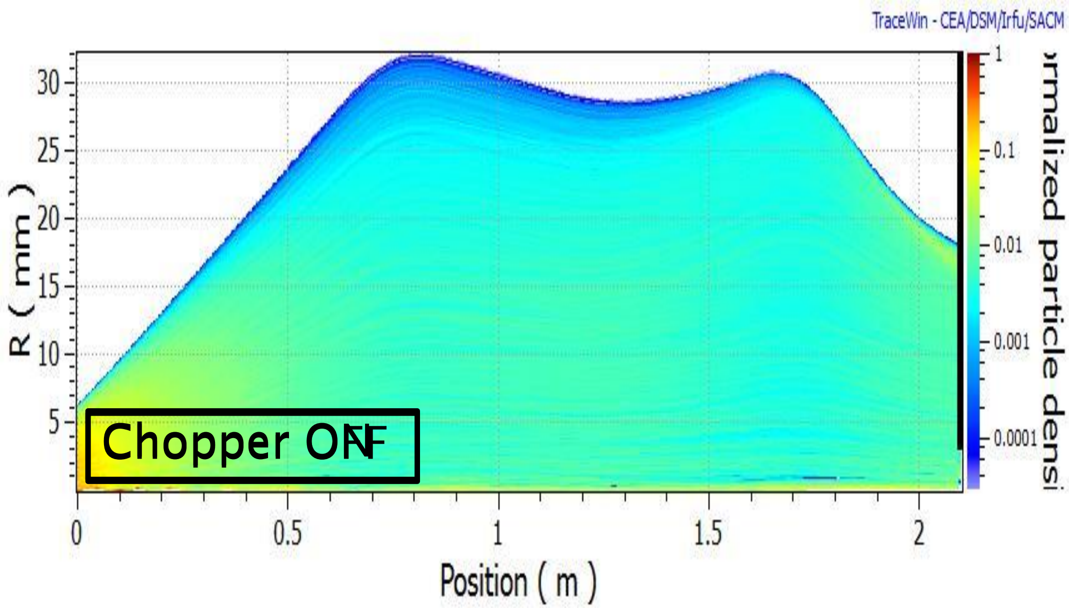

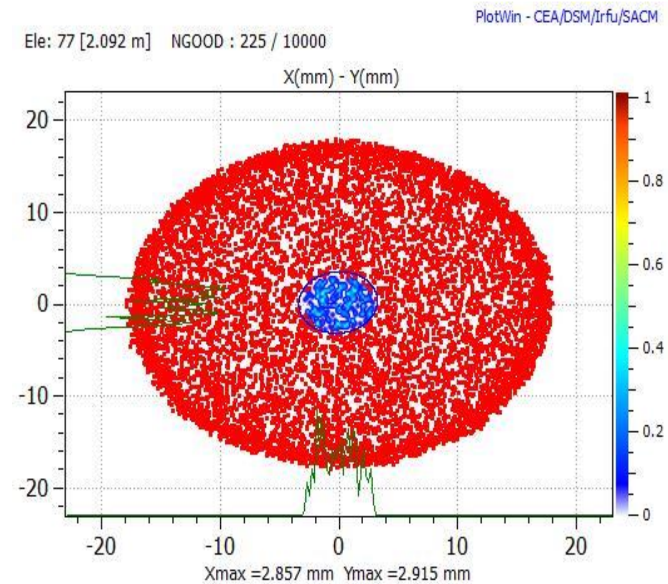

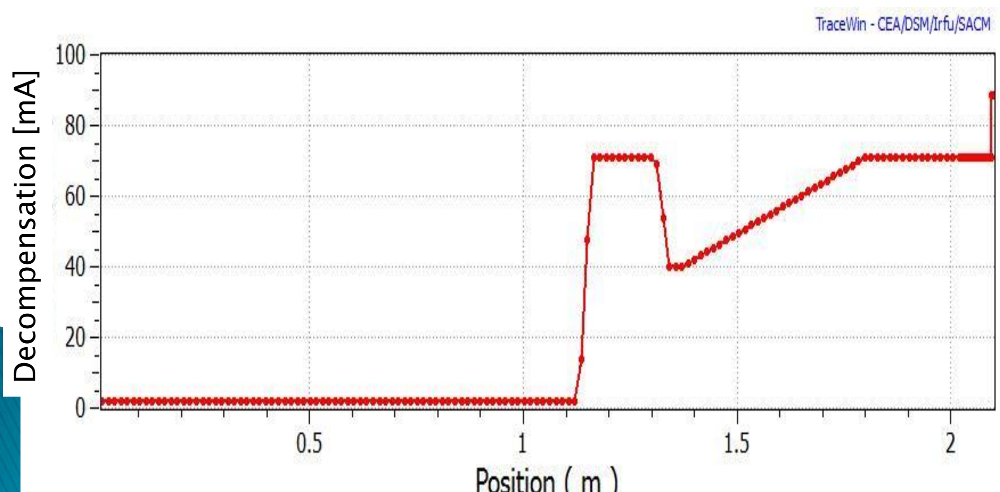

Chopper ON–OFF transition

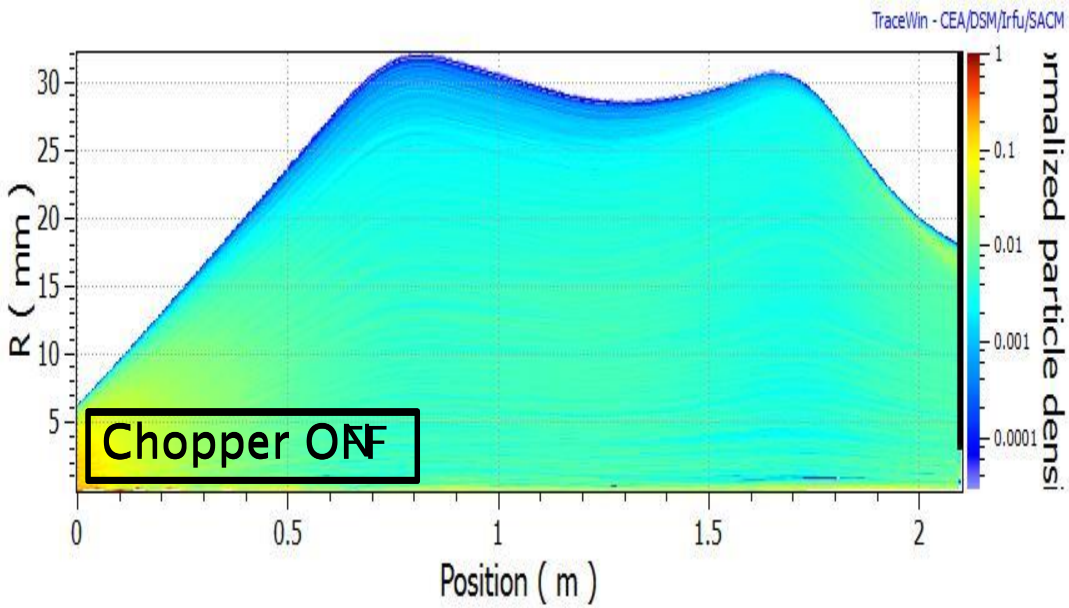

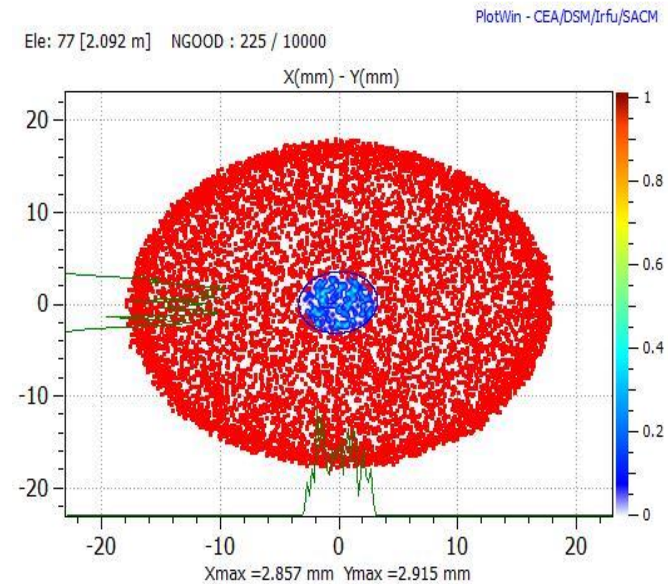

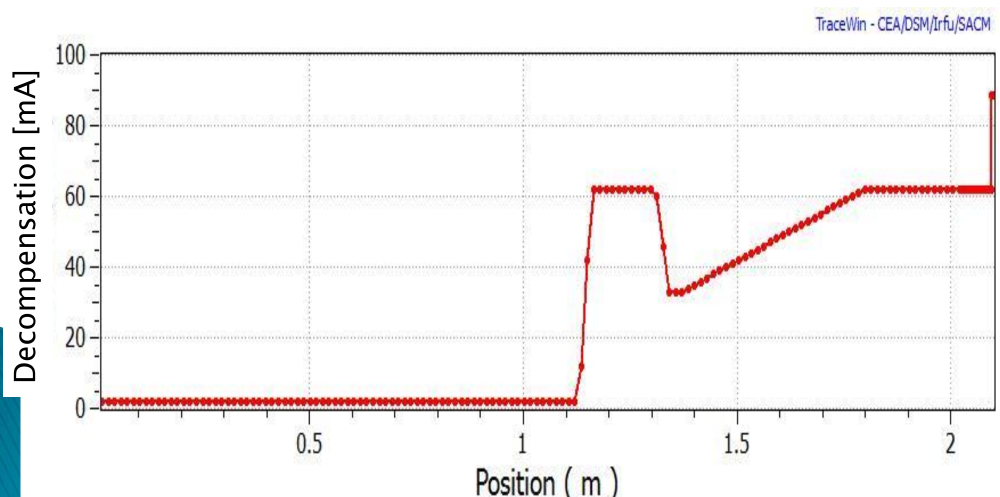

Chopper ON–OFF transition

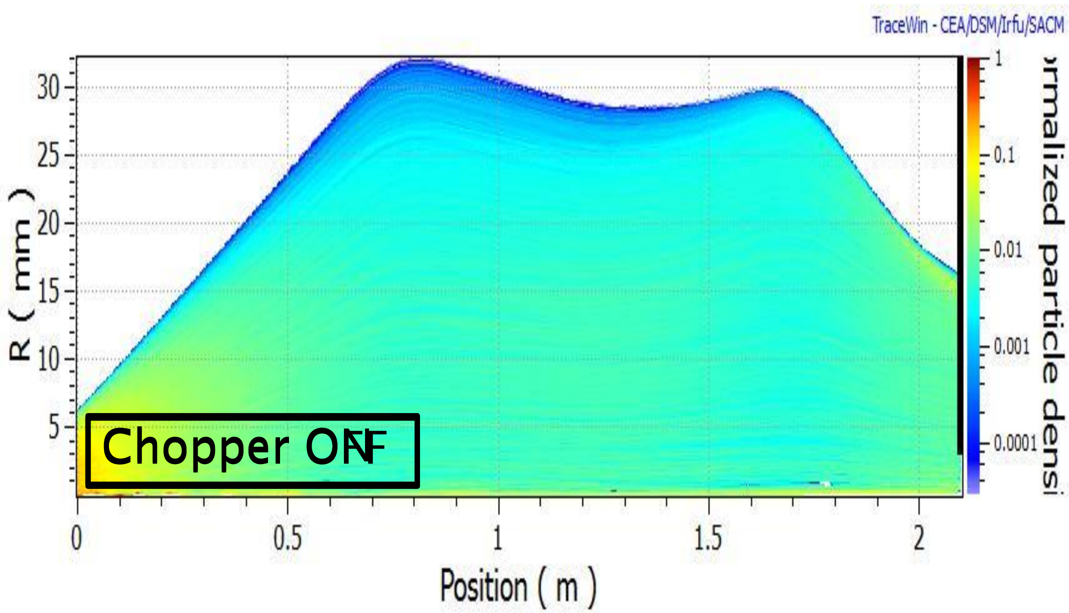

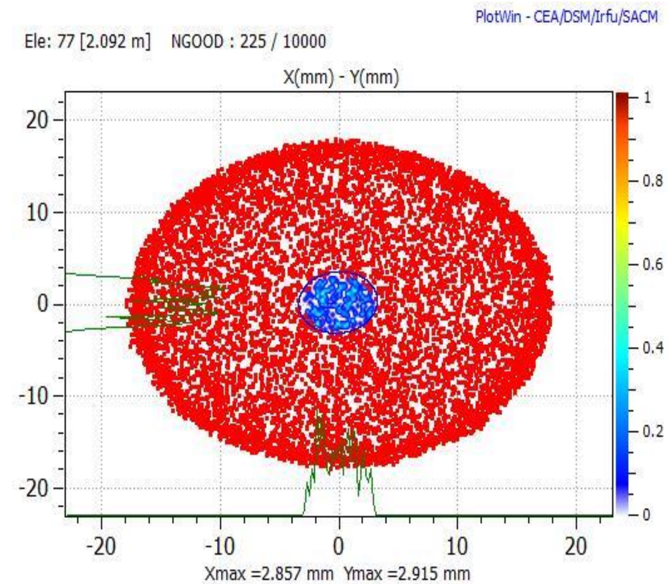

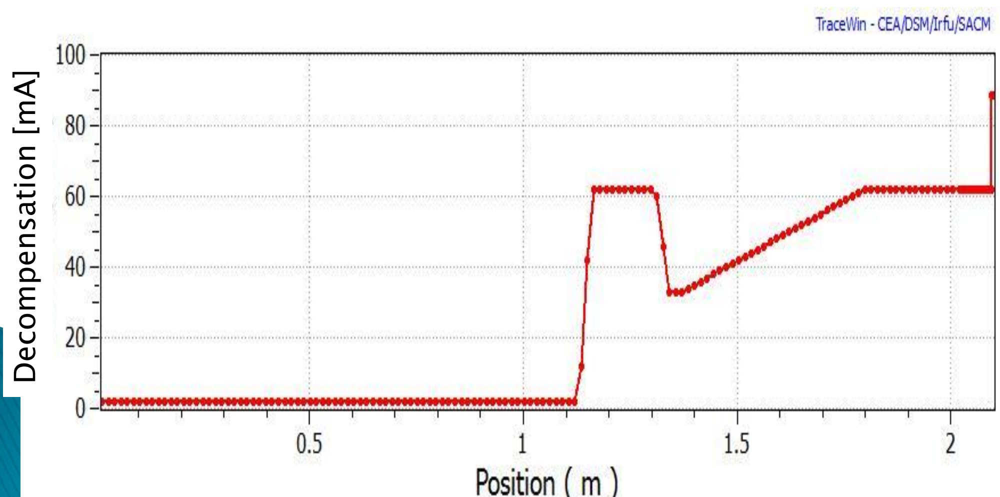

Chopper ON-OFF transition

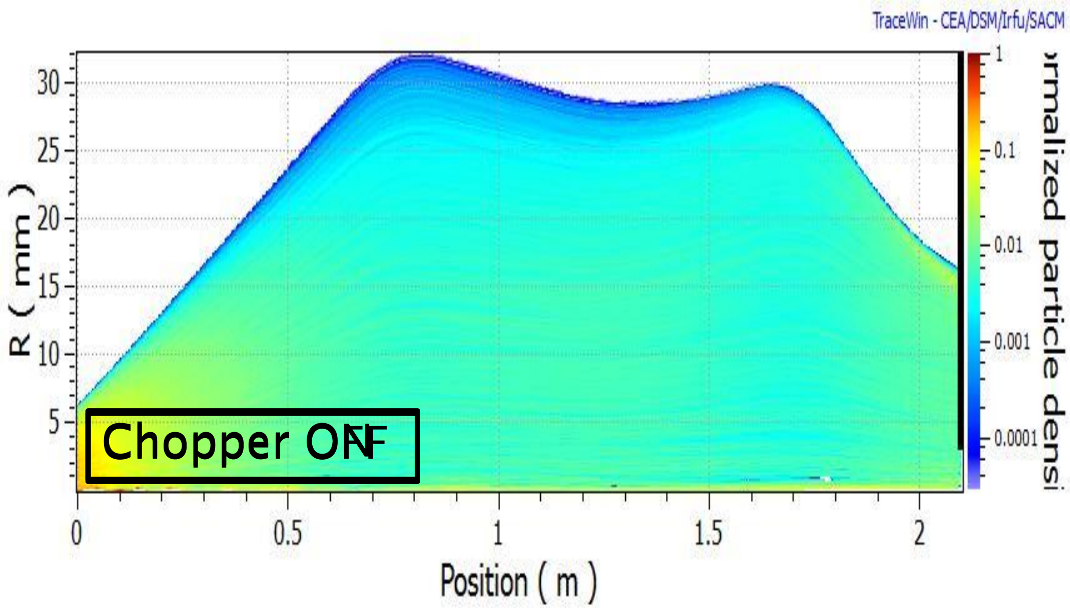

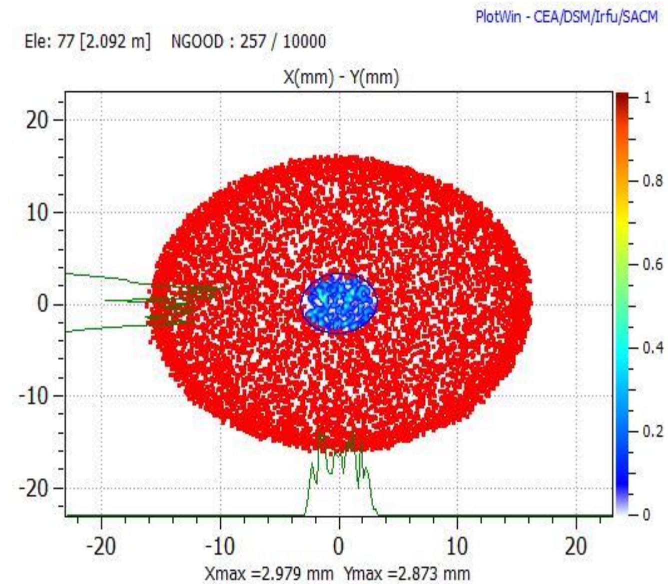

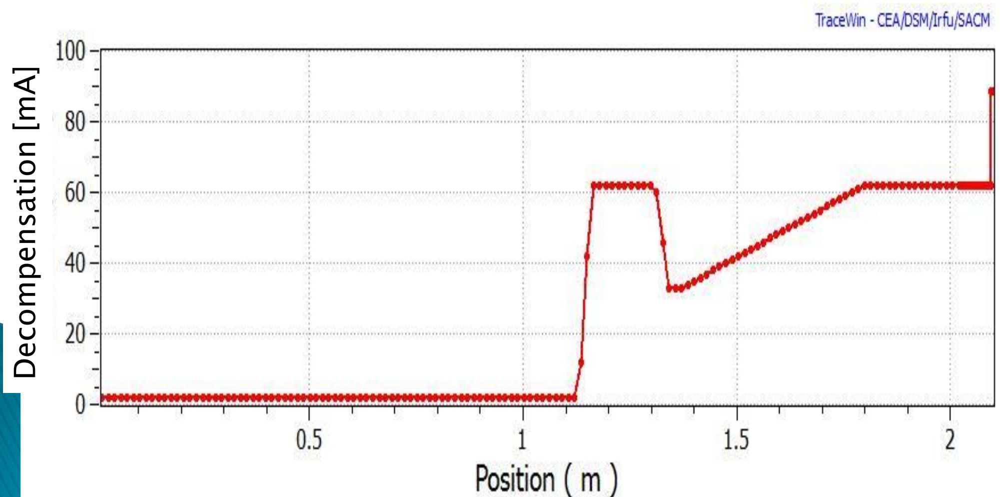

Chopper ON–OFF transition

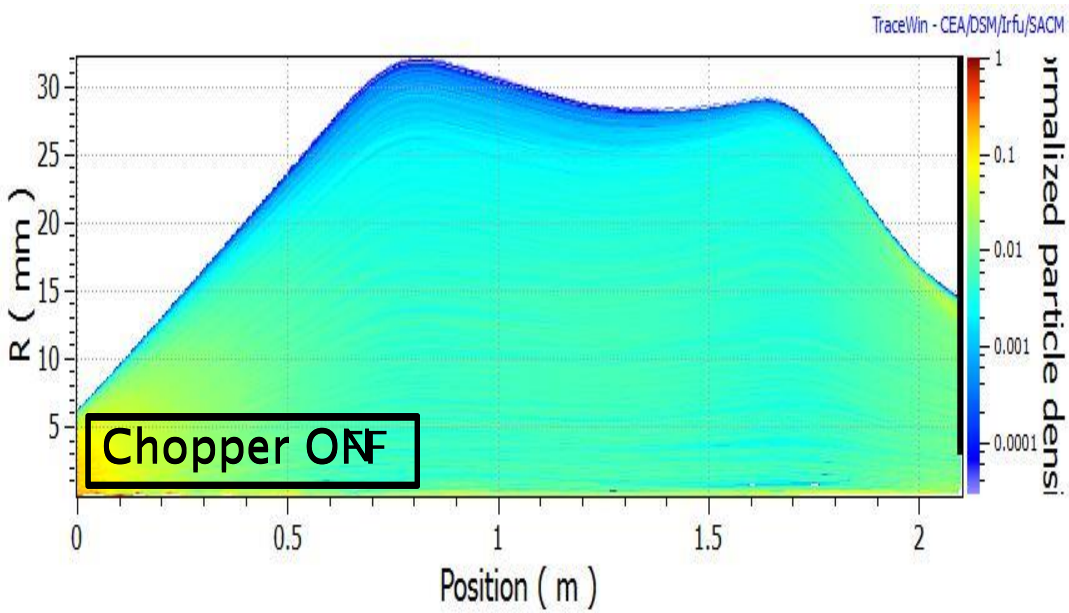

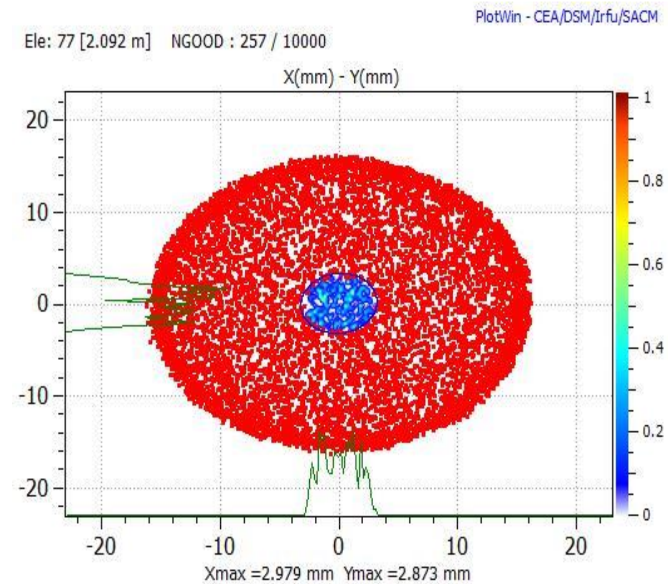

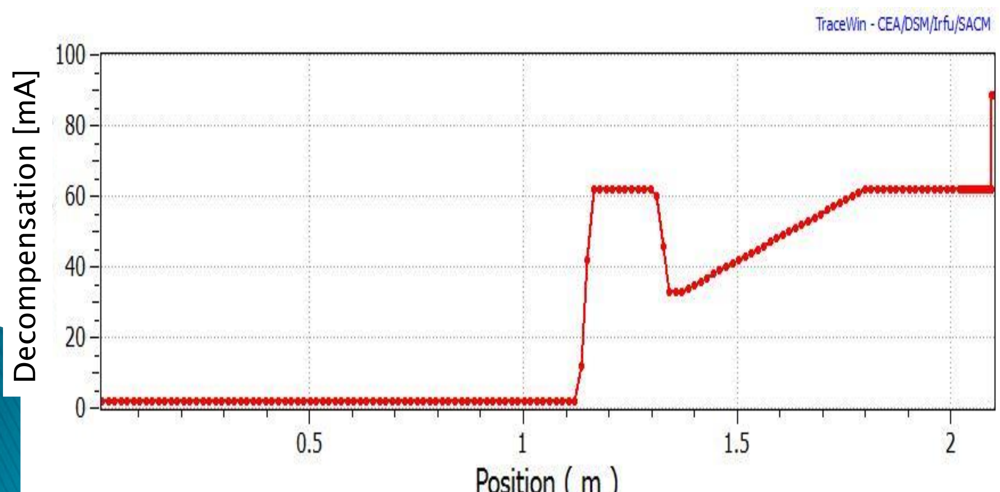

Chopper ON–OFF transition

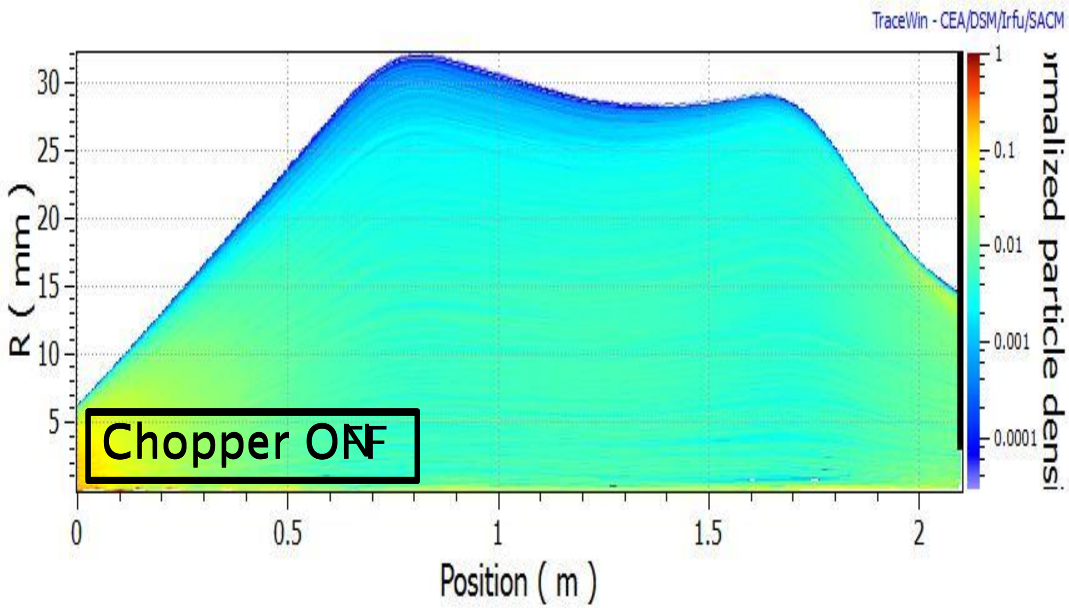

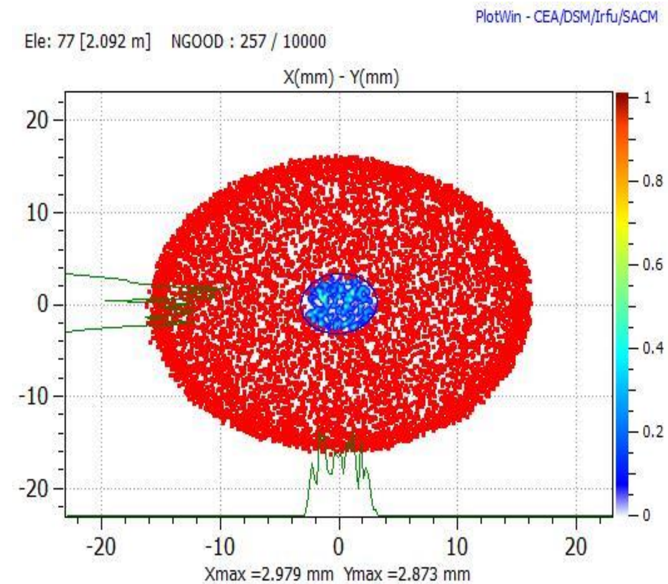

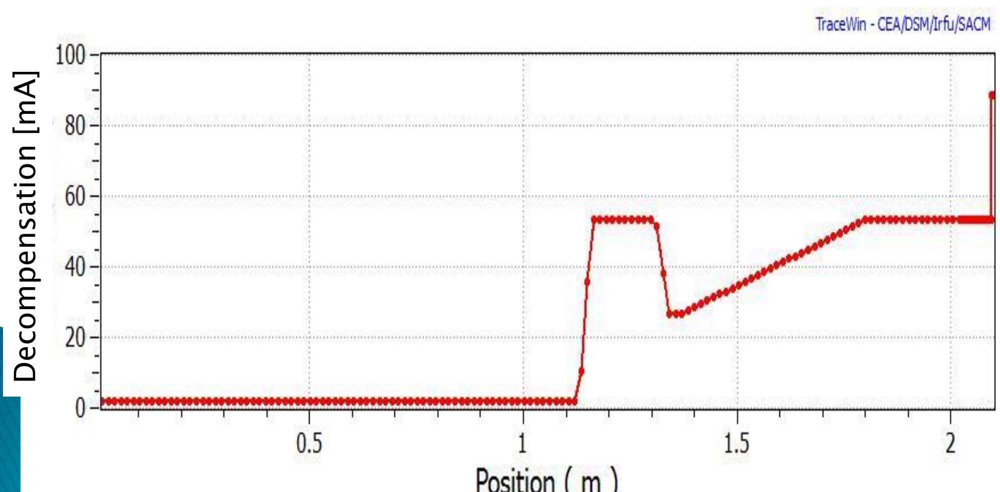

Chopper ON–OFF transition

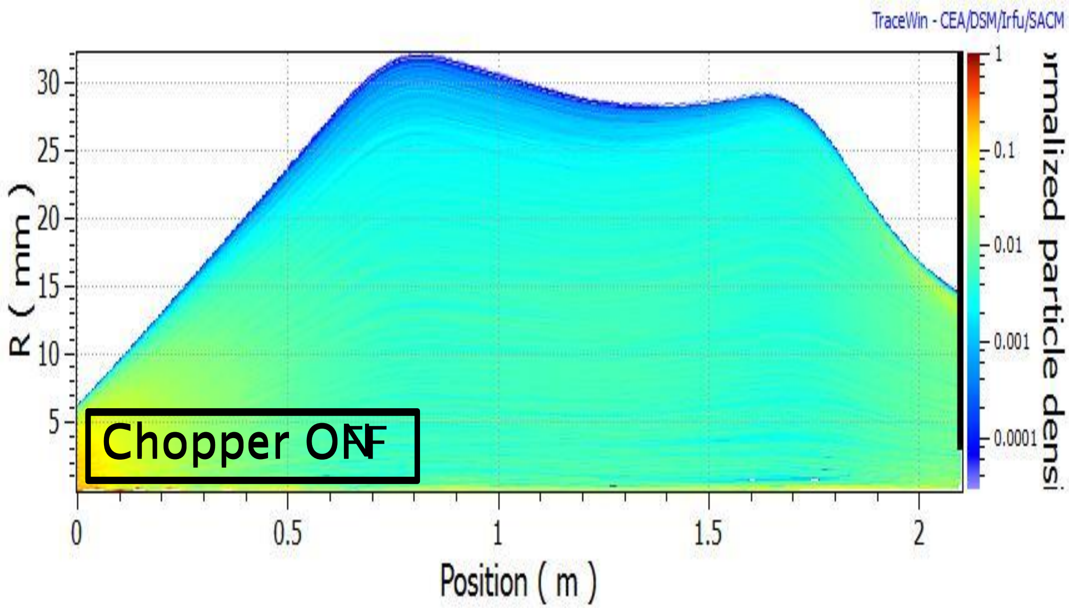

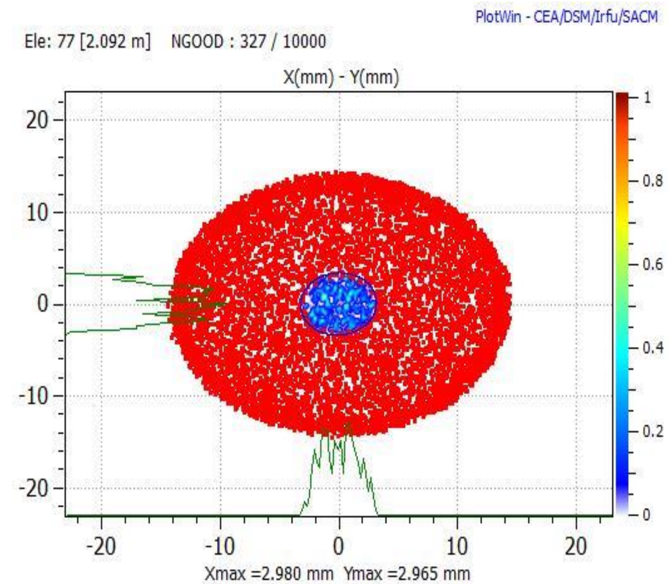

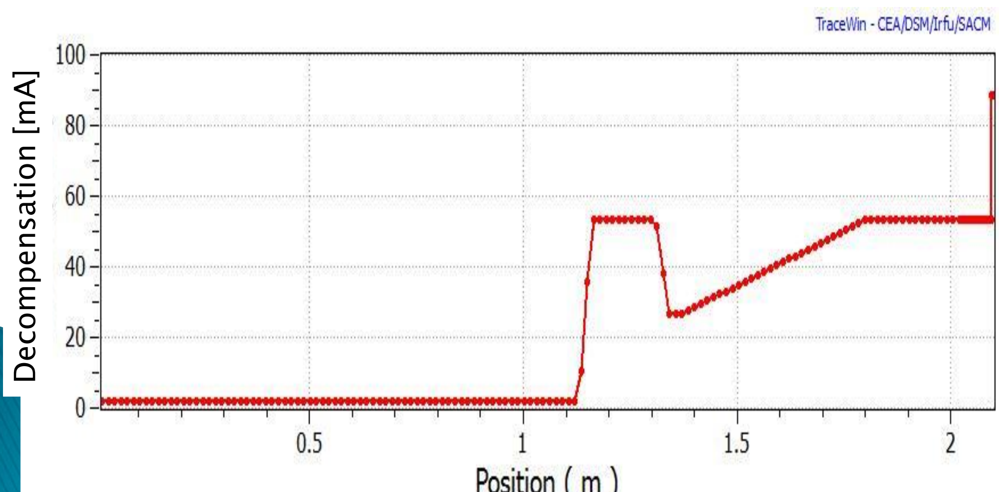

Chopper ON-OFF transition

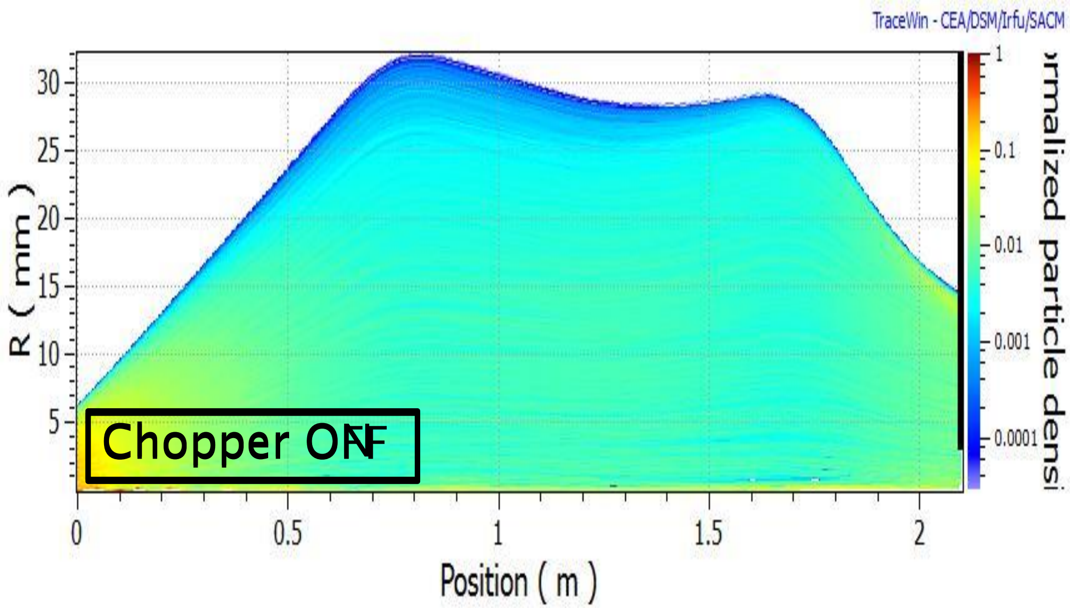

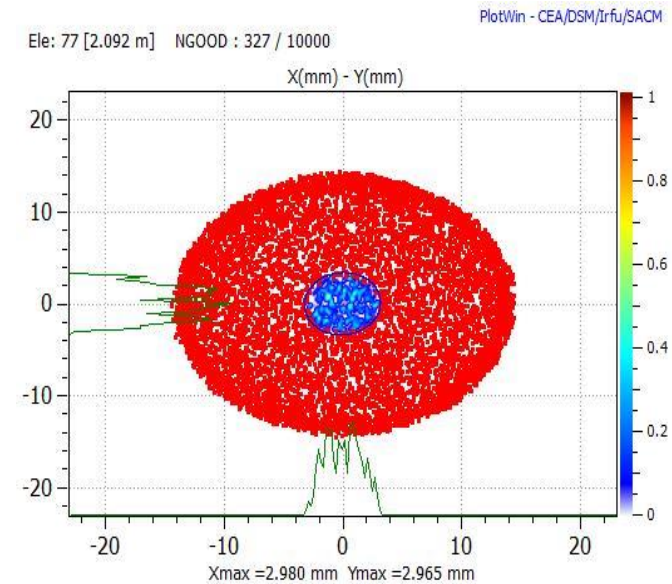

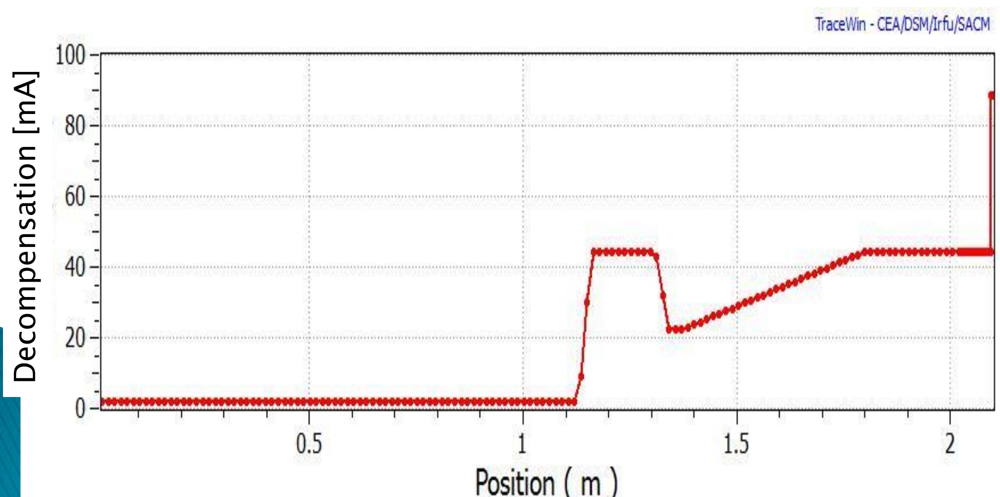

Chopper ON–OFF transition

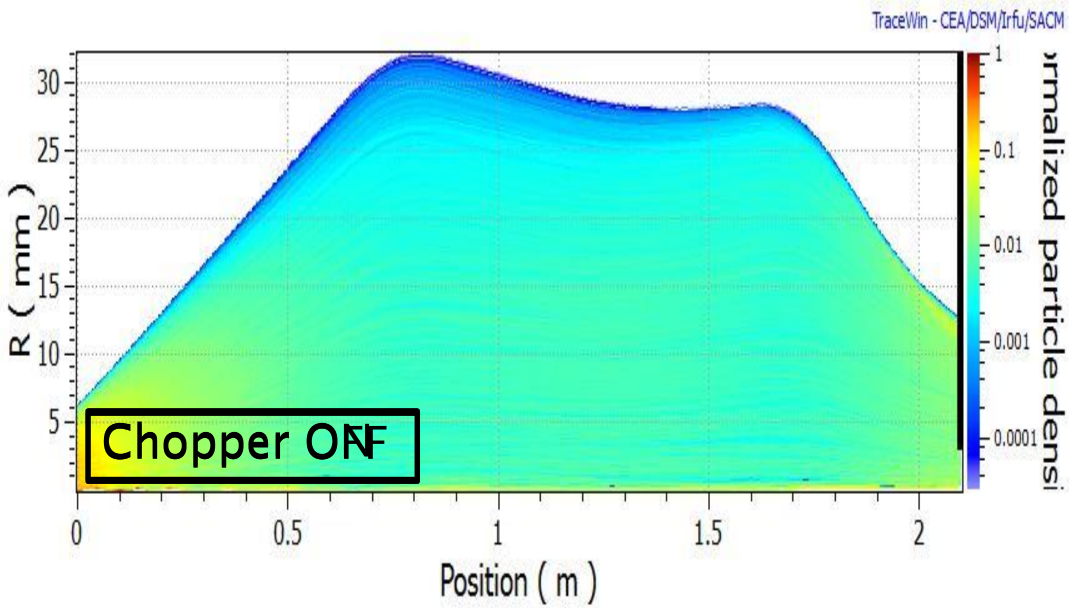

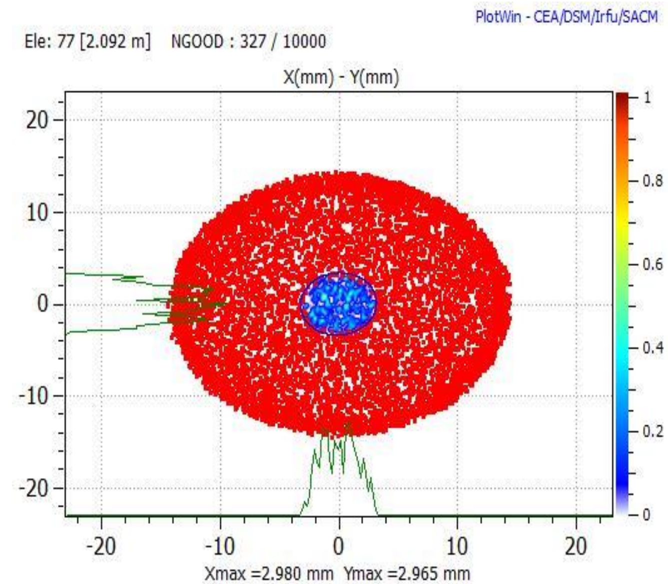

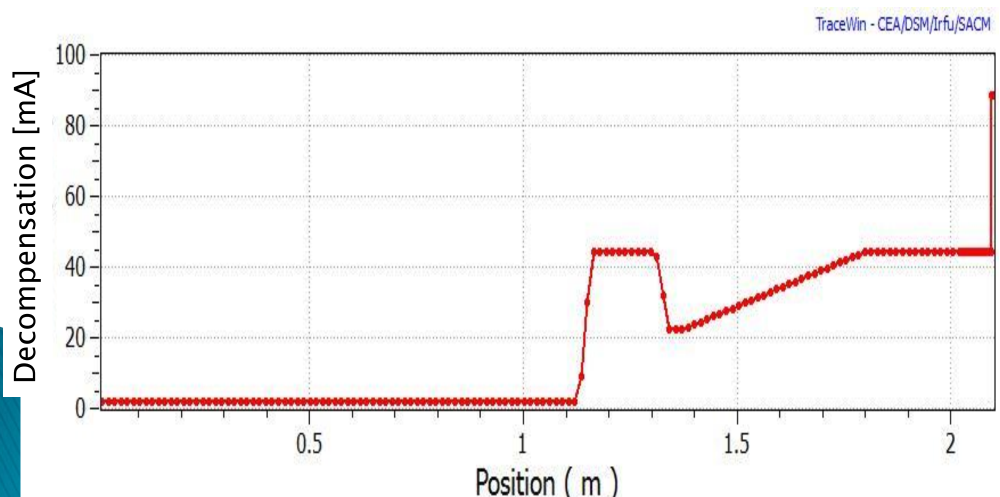

Chopper ON–OFF transition

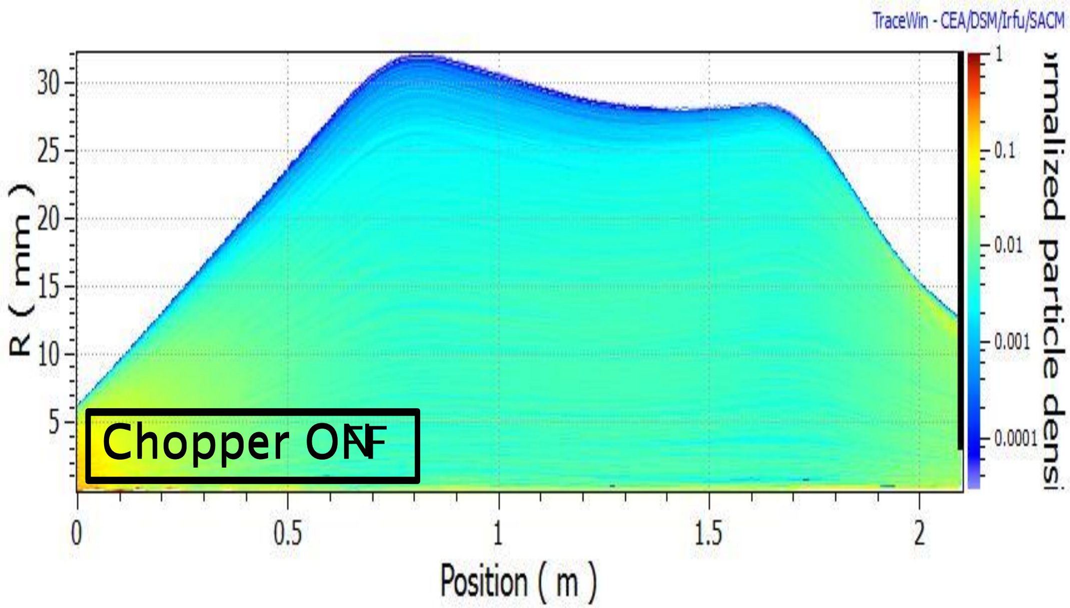

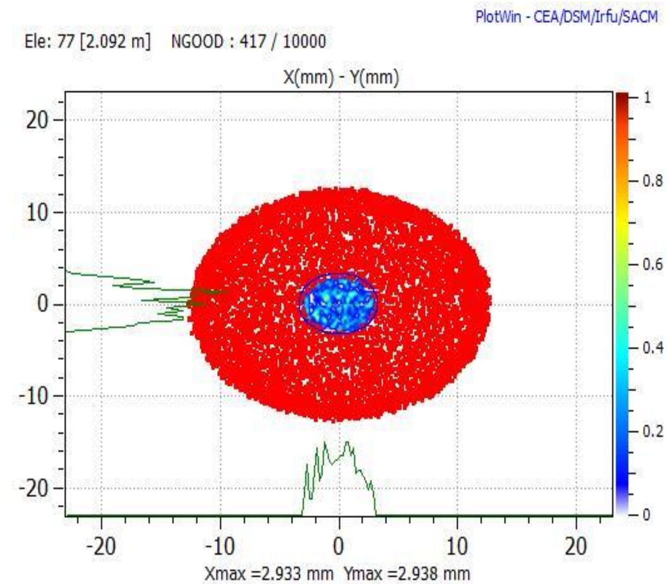

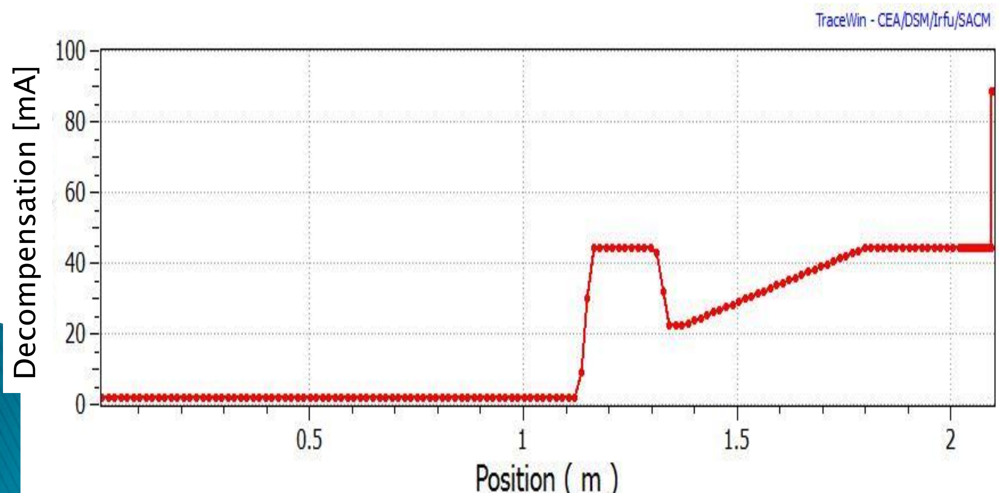

Chopper ON-OFF transition

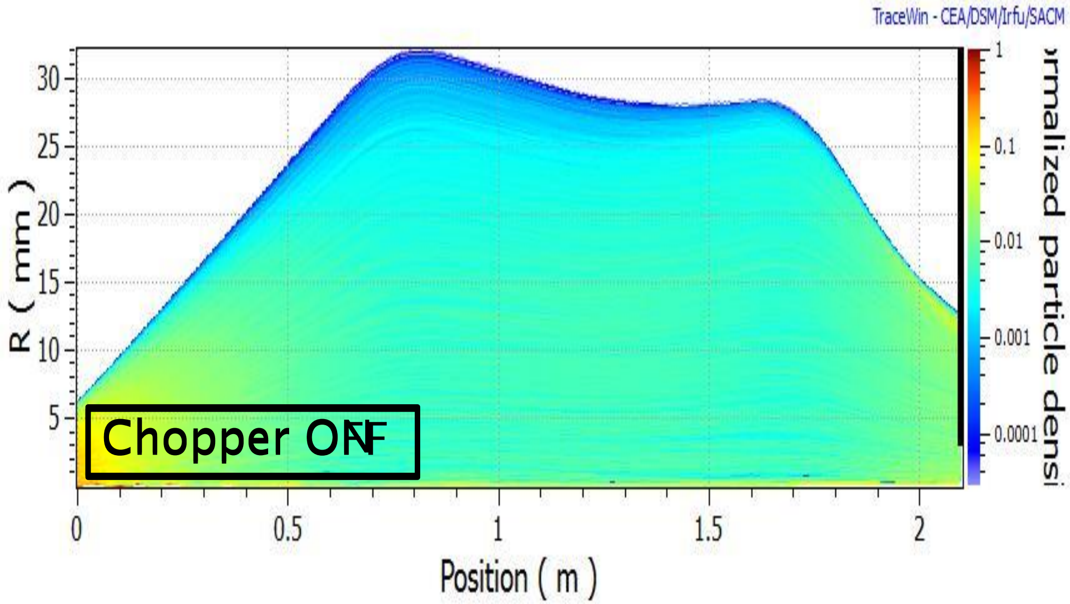

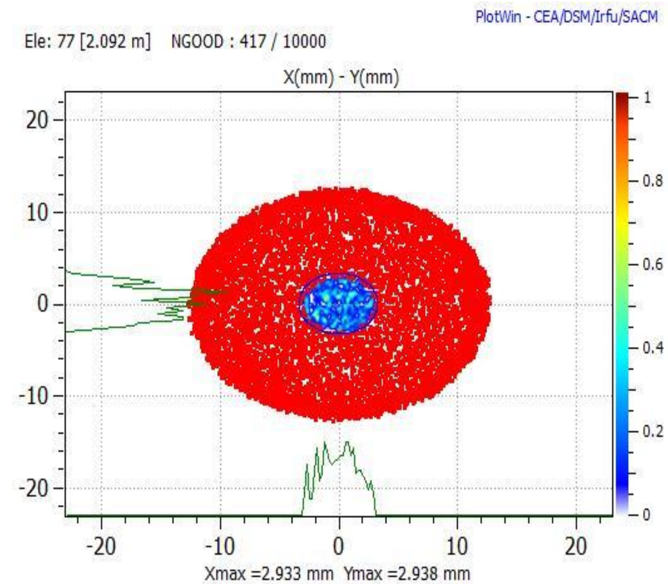

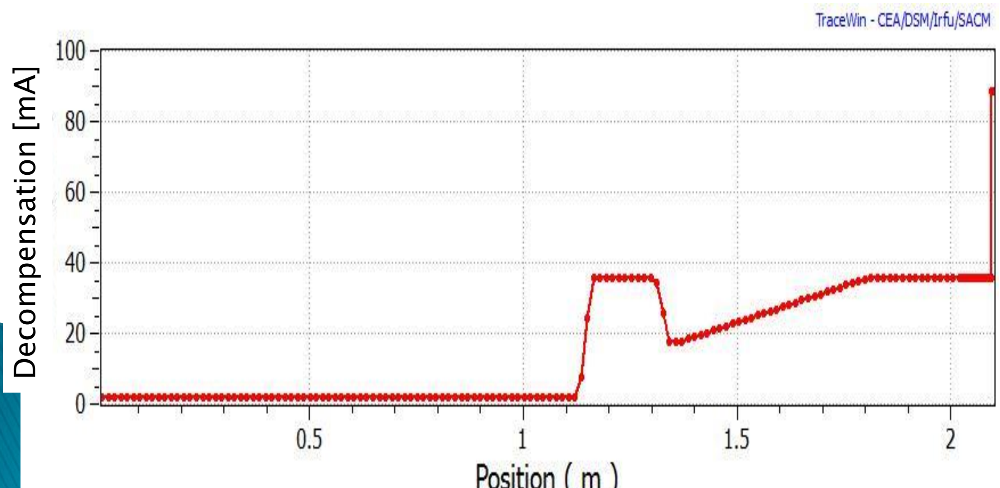

Chopper ON–OFF transition

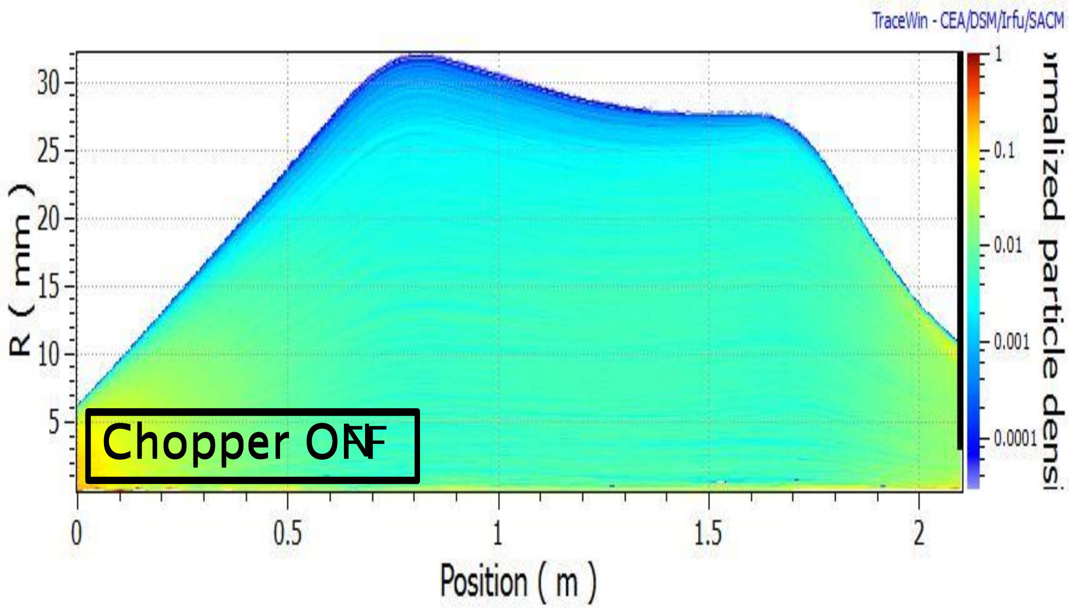

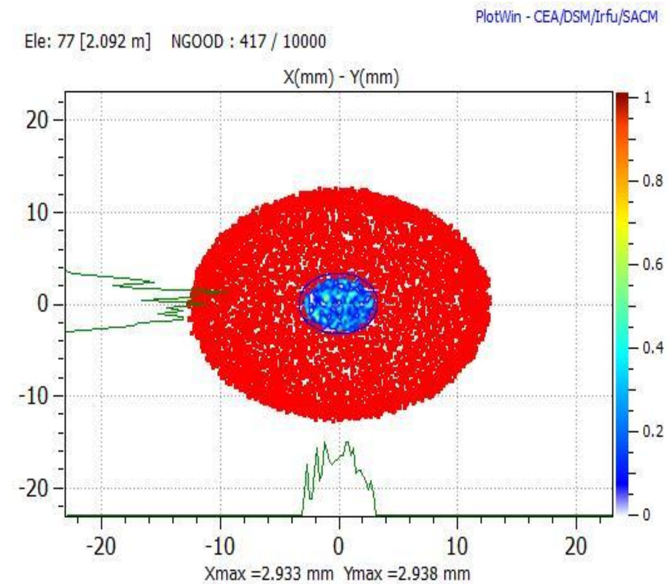

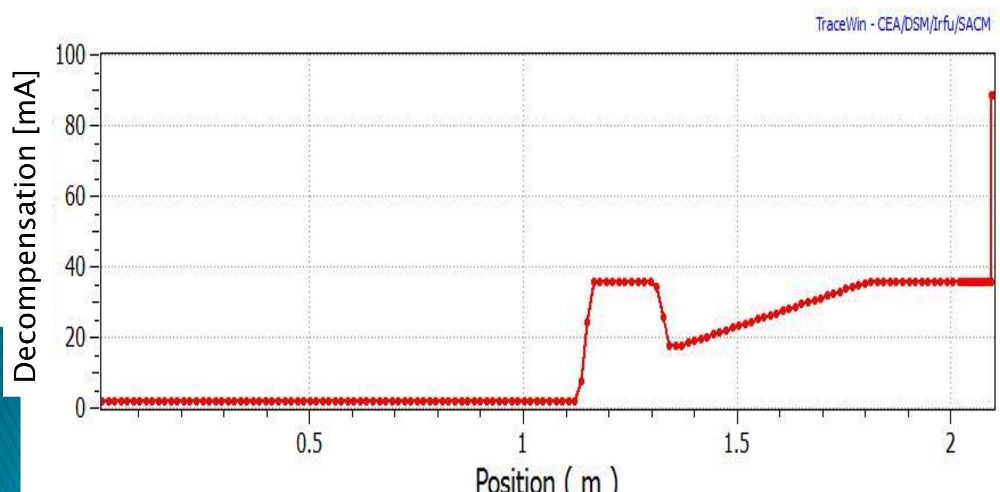

Chopper ON-OFF transition

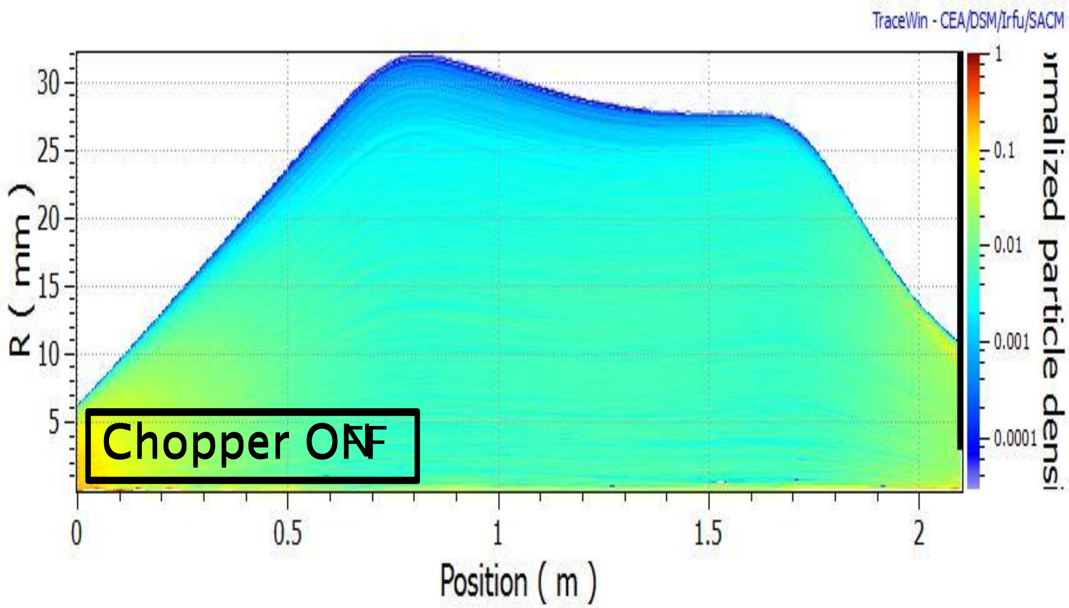

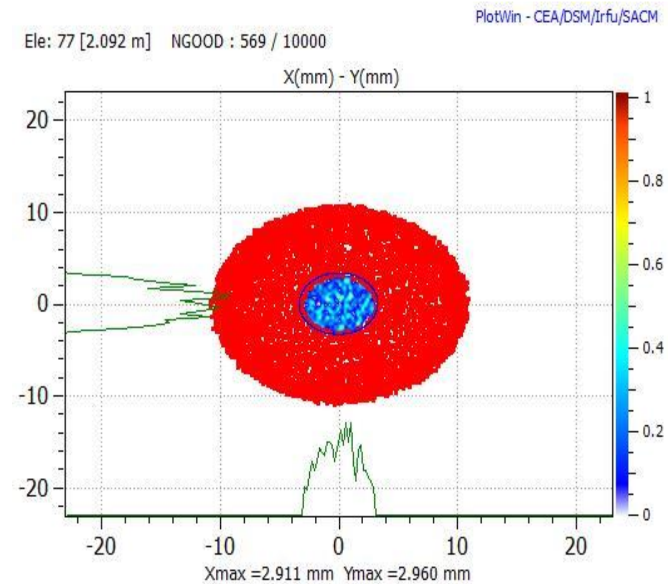

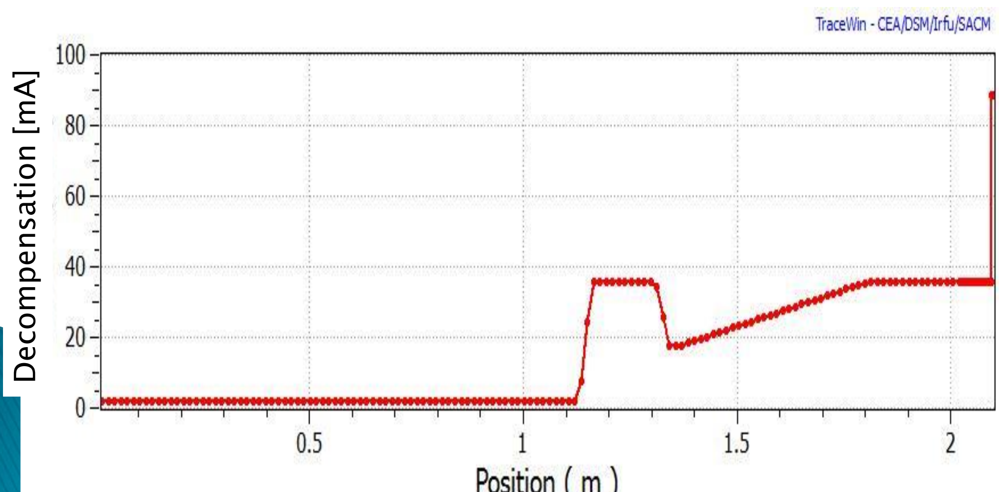

Chopper ON-OFF transition

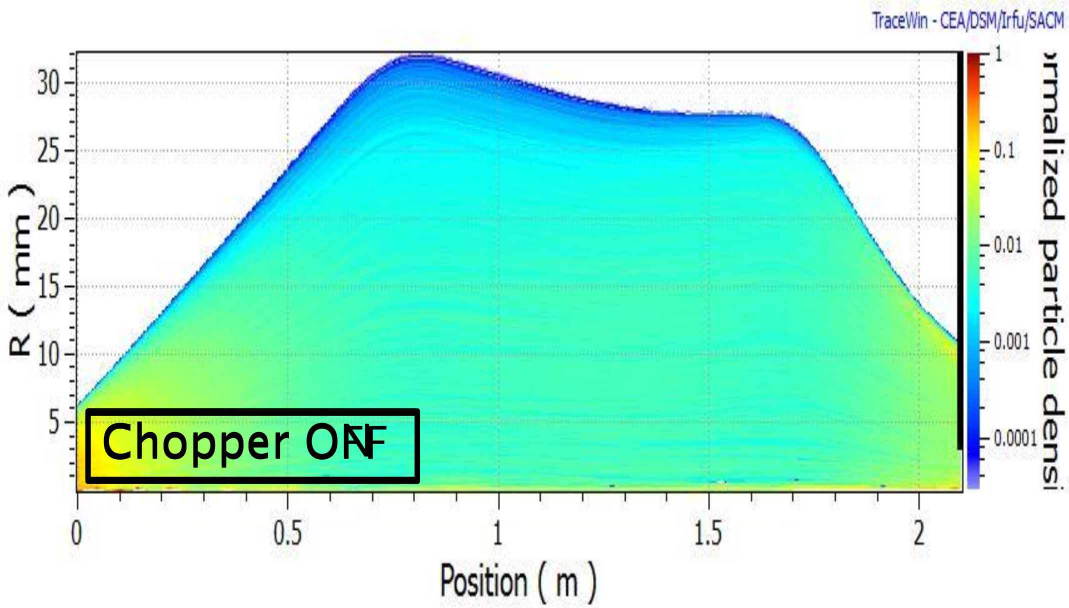

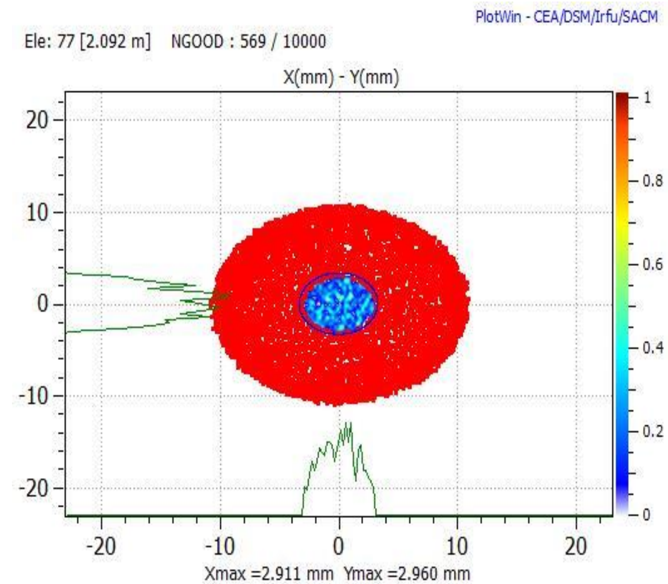

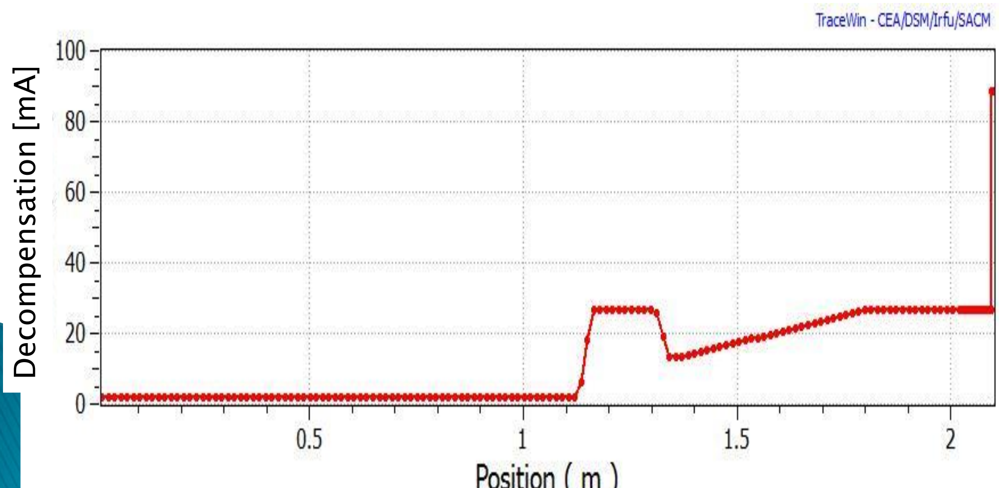

Chopper ON-OFF transition

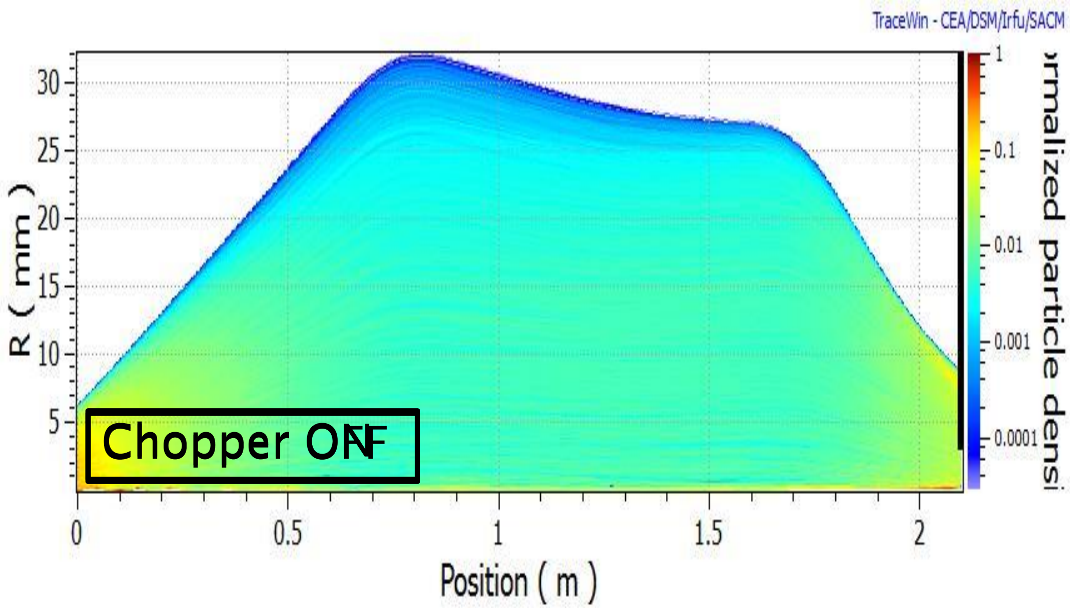

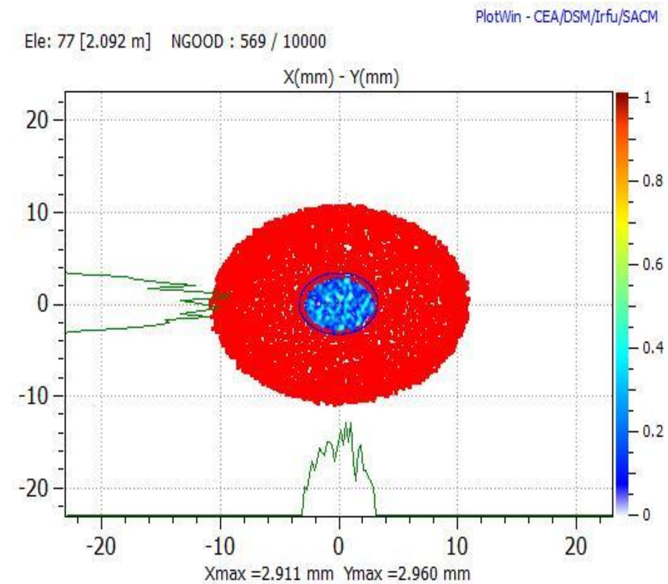

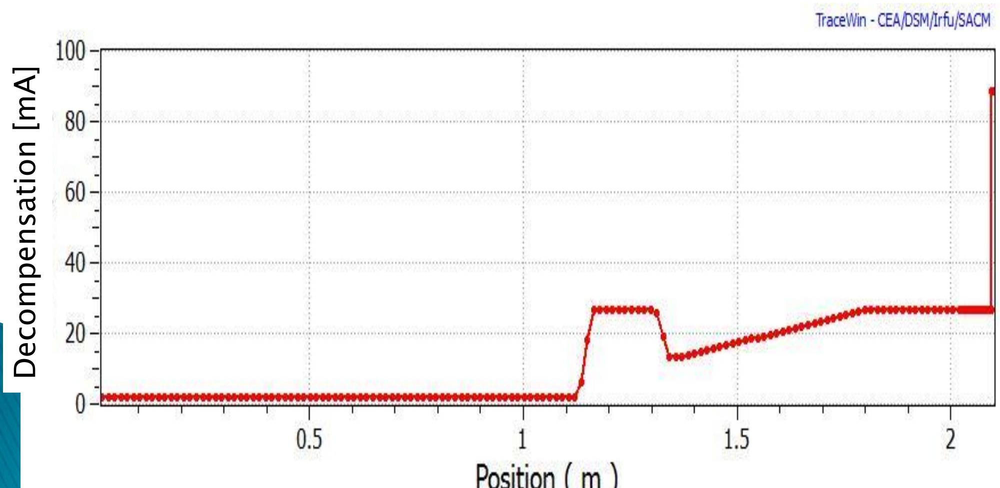

Chopper ON-OFF transition

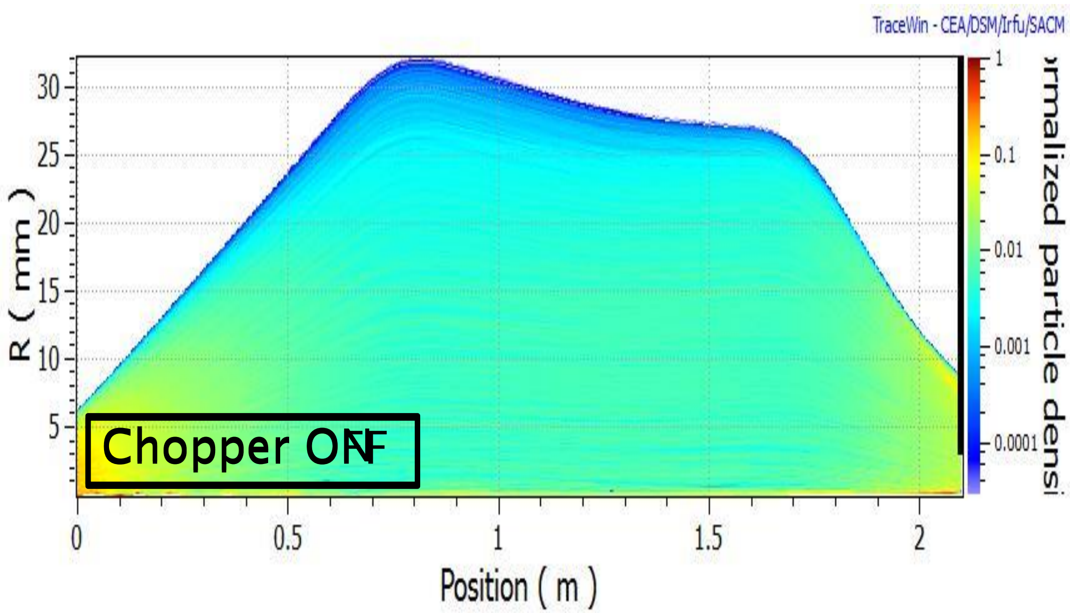

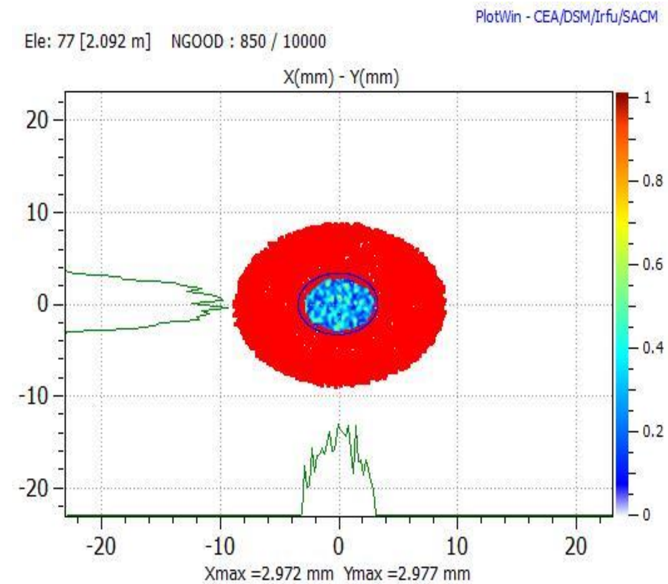

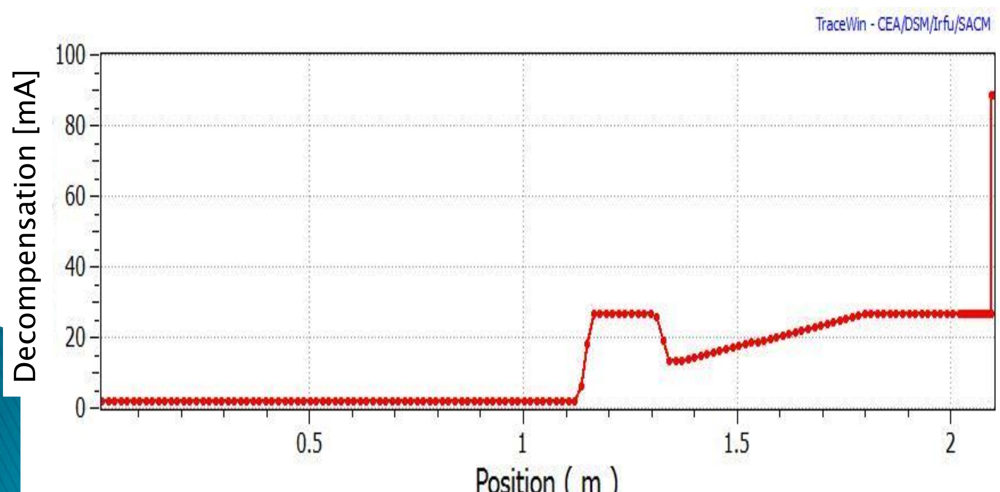

Chopper ON-OFF transition

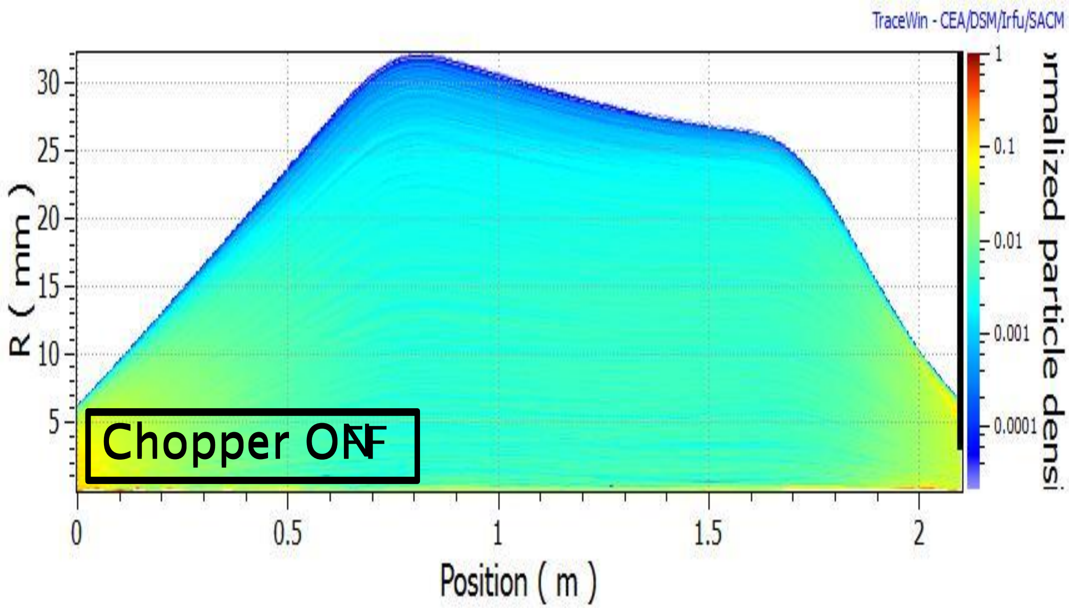

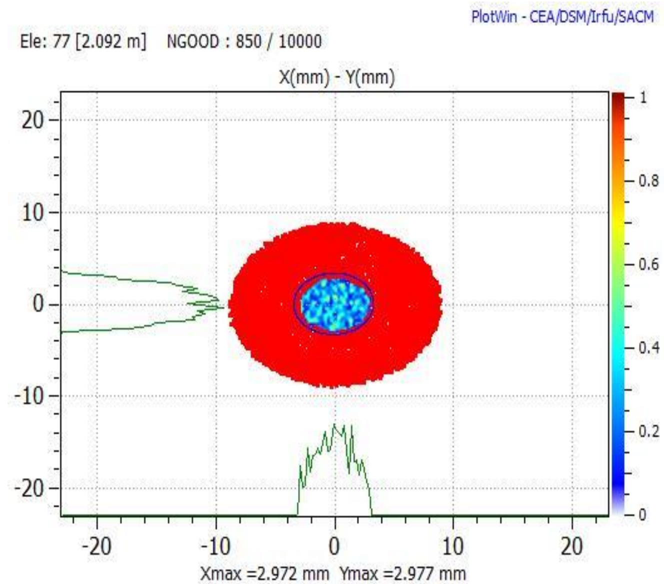

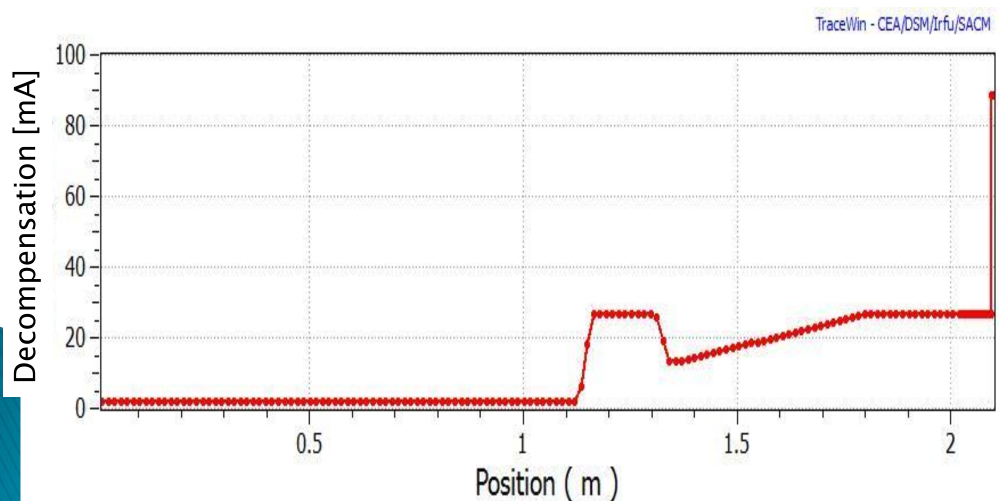

Chopper ON-OFF transition

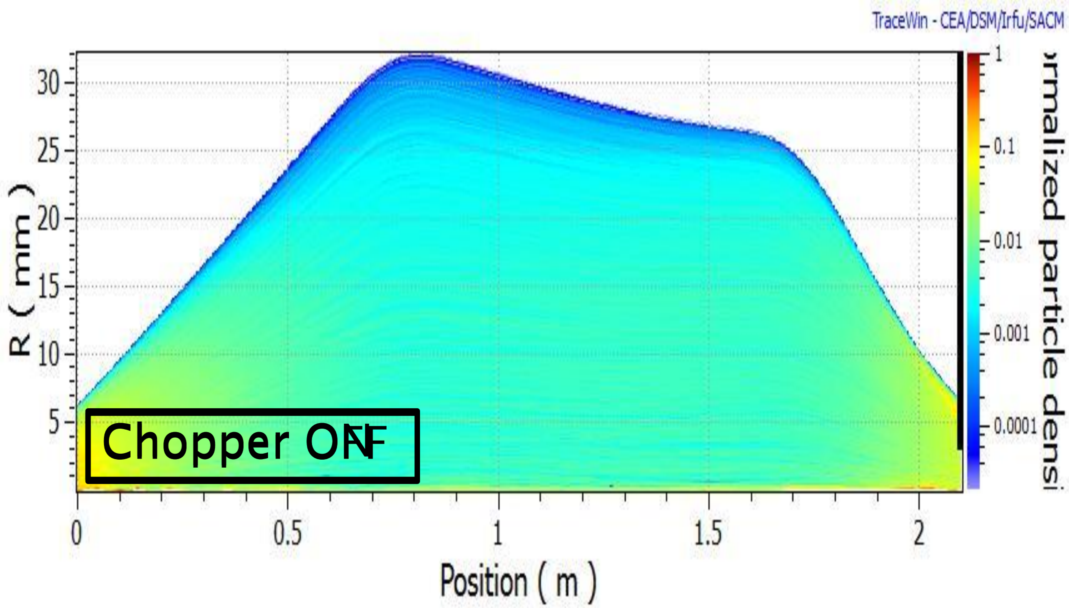

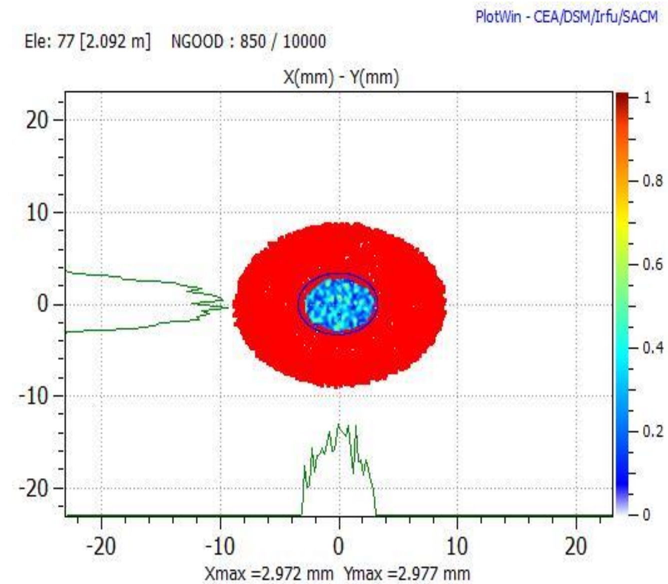

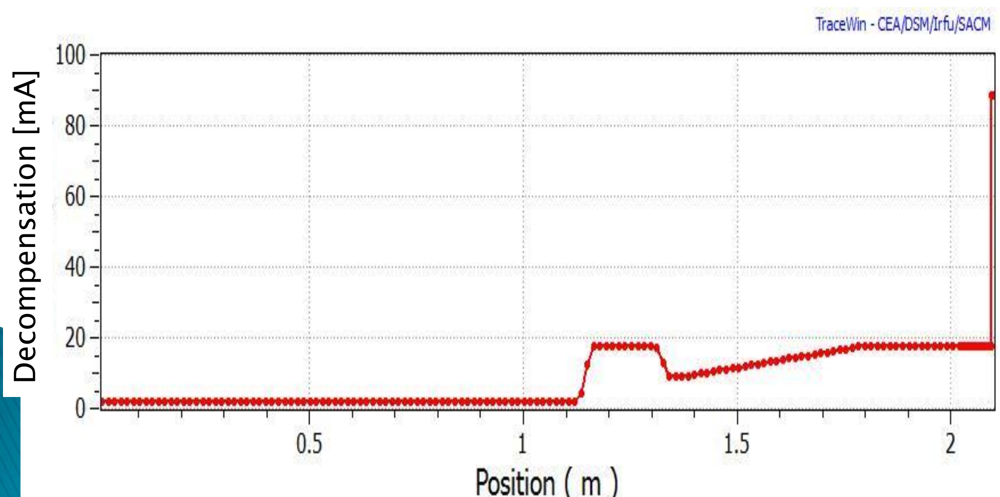

Chopper ON–OFF transition

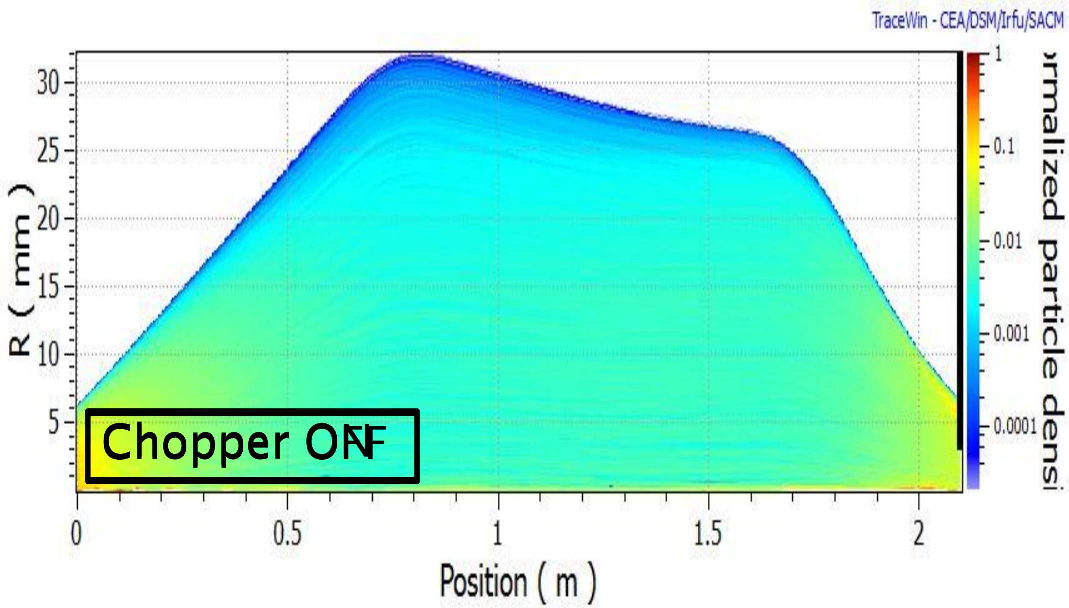

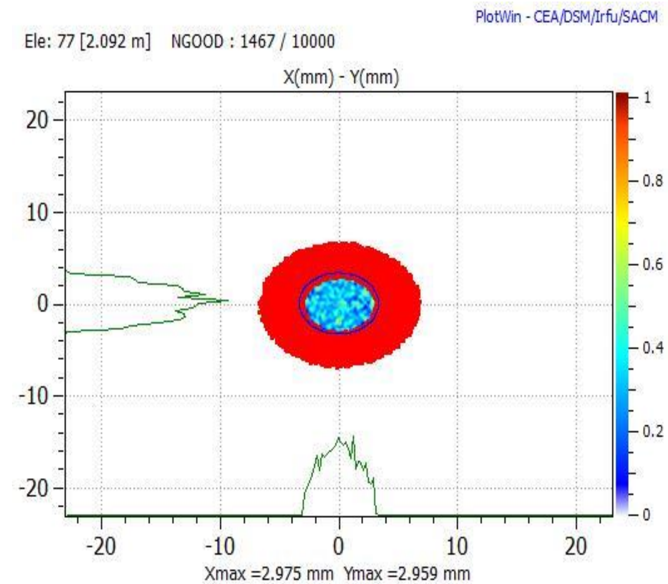

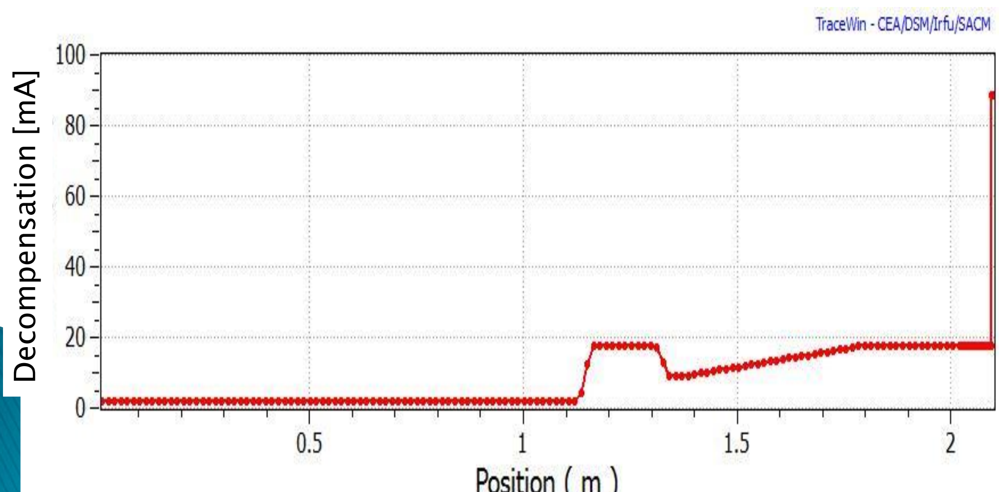

Chopper ON-OFF transition

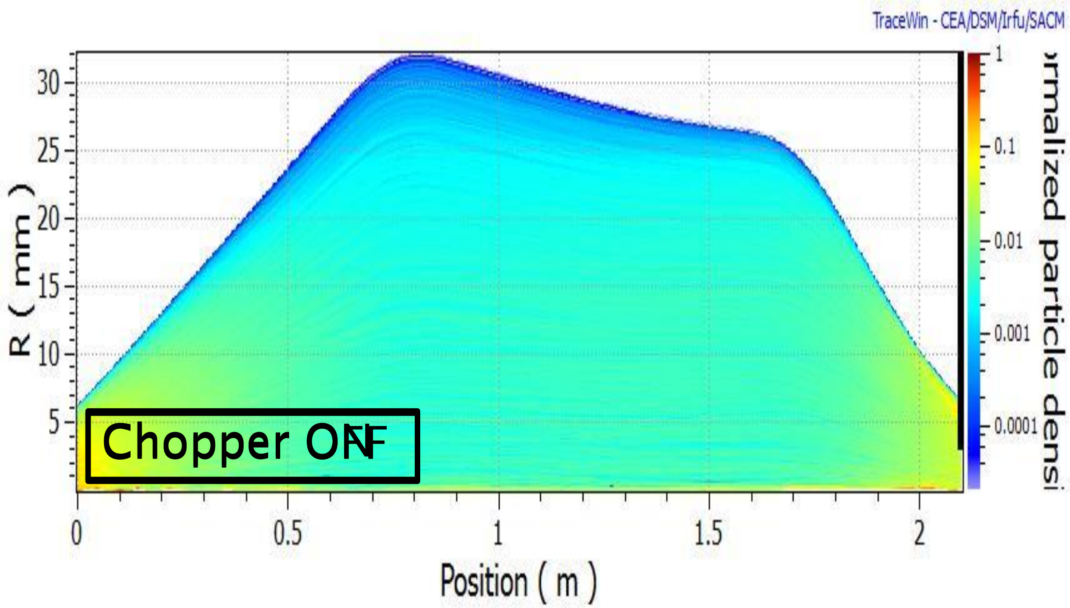

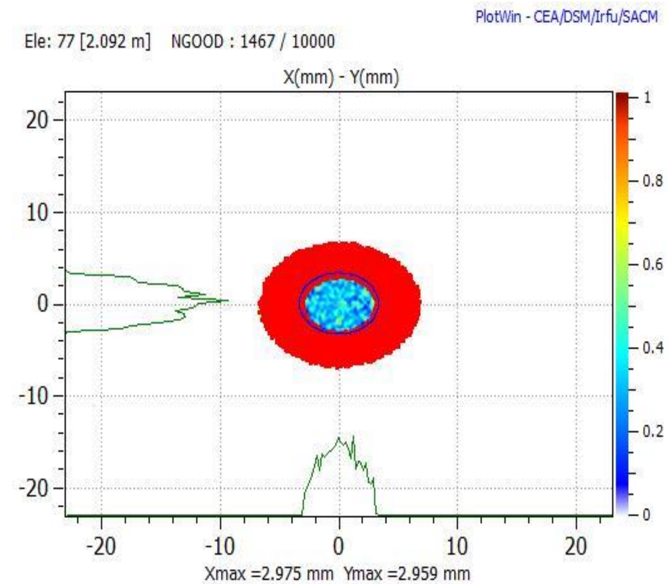

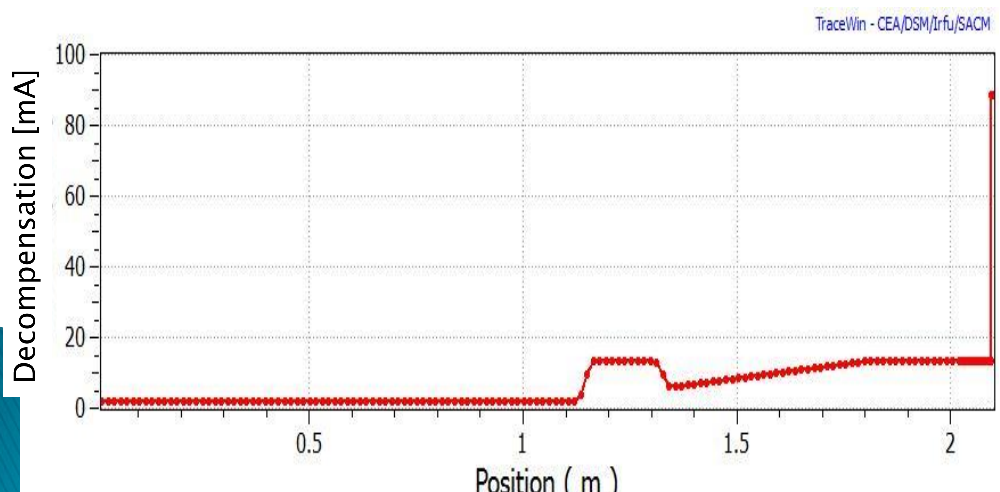

Chopper ON–OFF transition

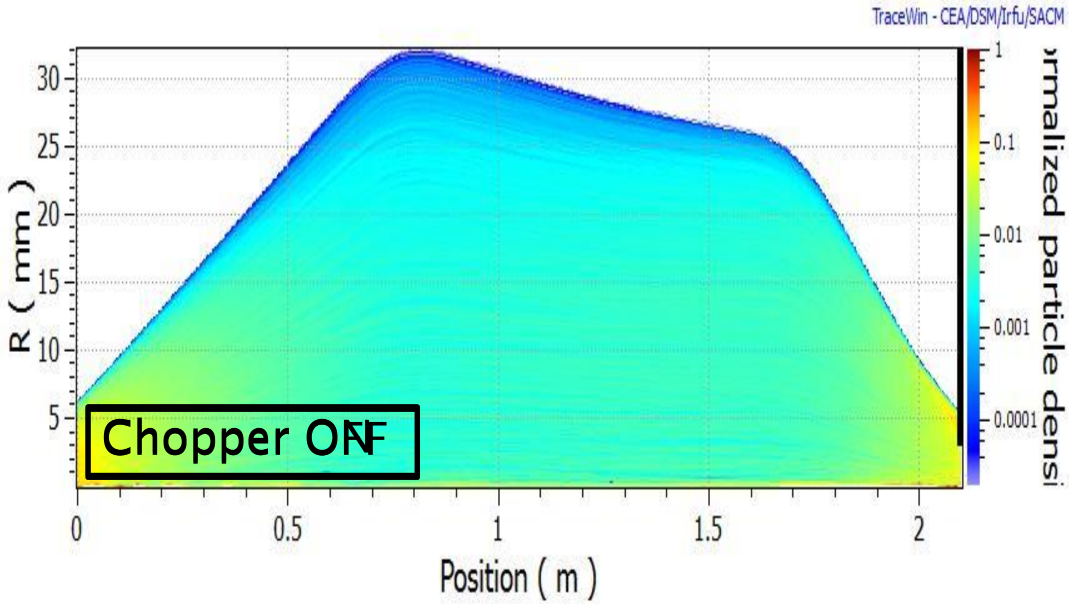

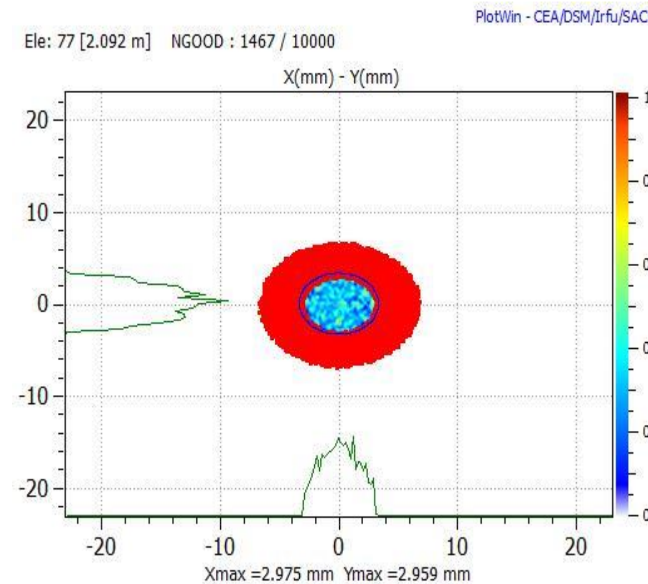

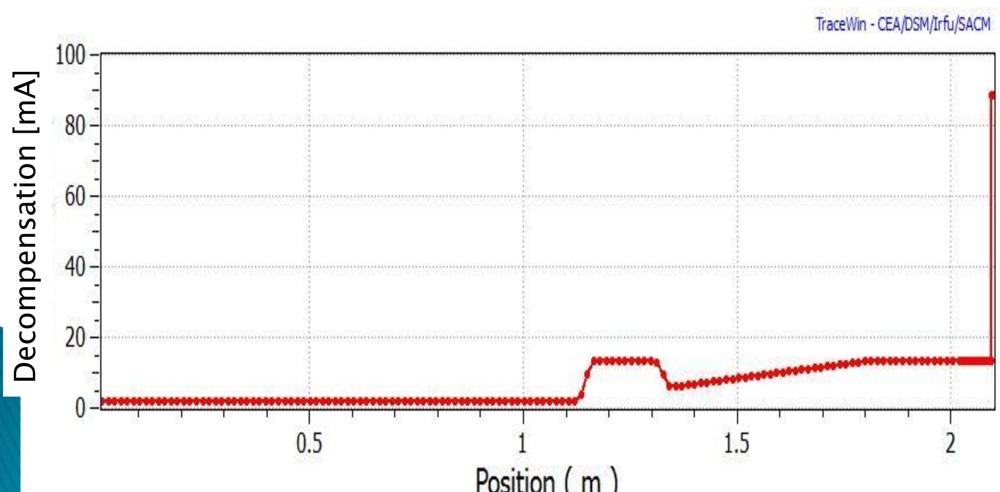

Chopper ON-OFF transition

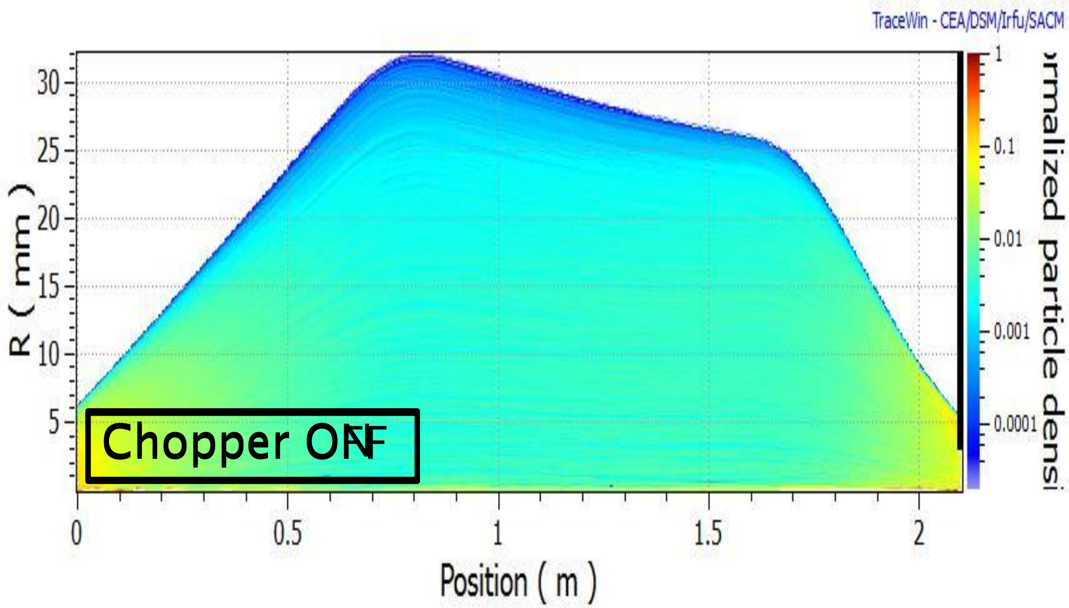

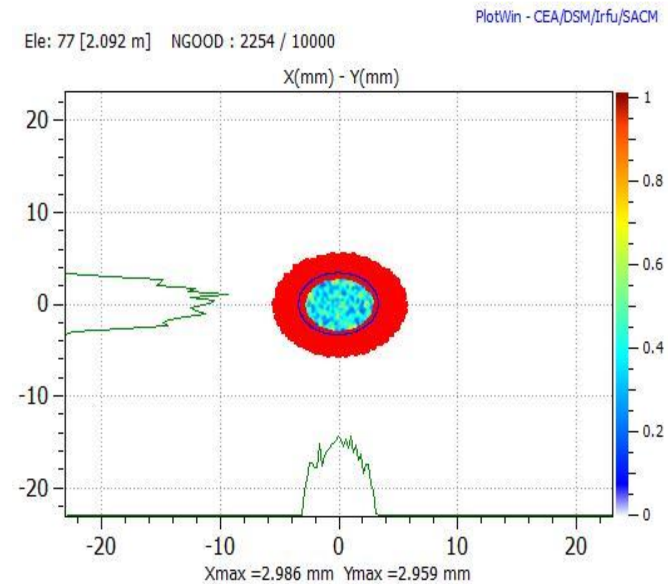

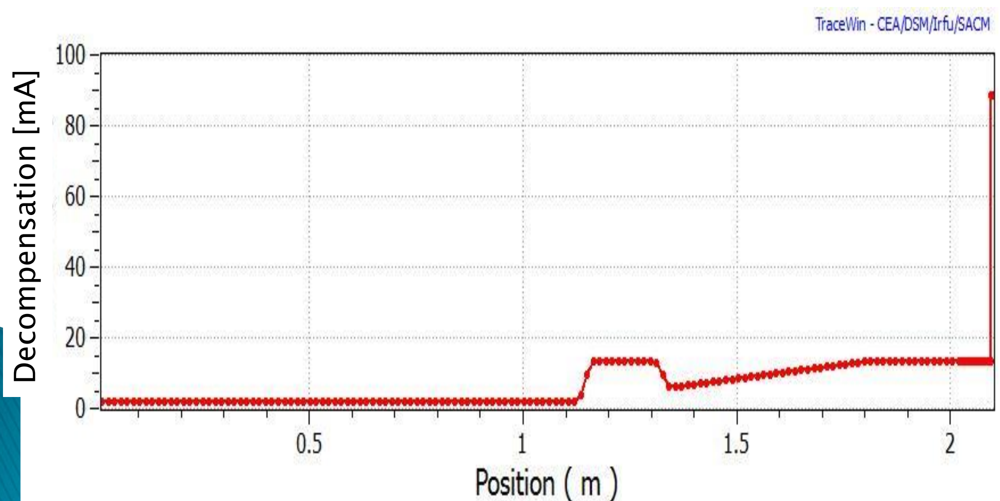

Chopper ON-OFF transition

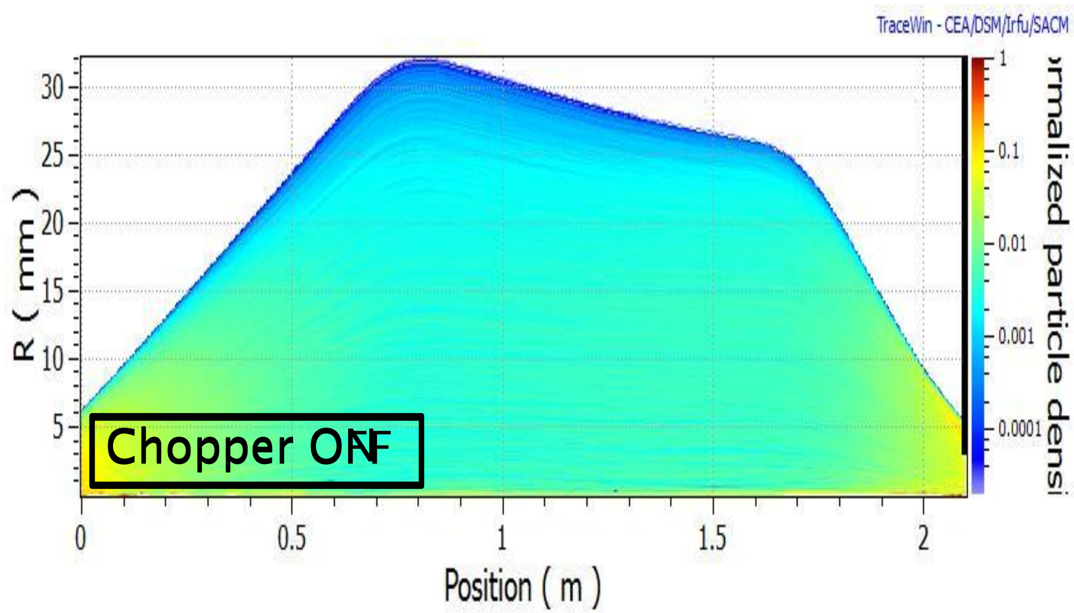

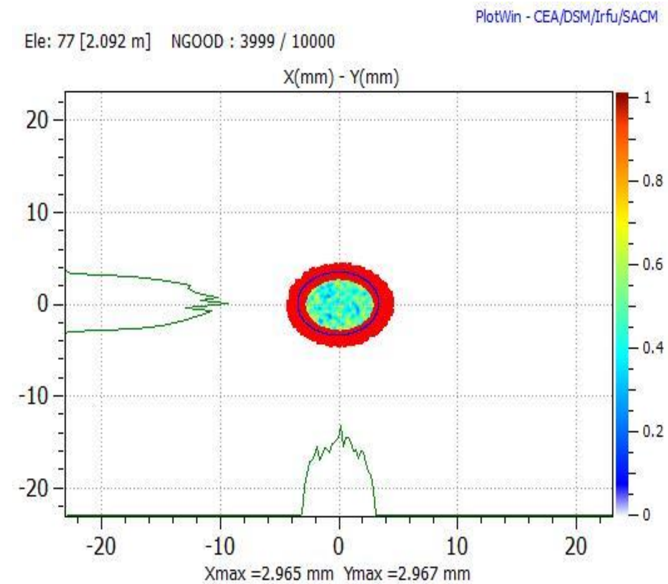

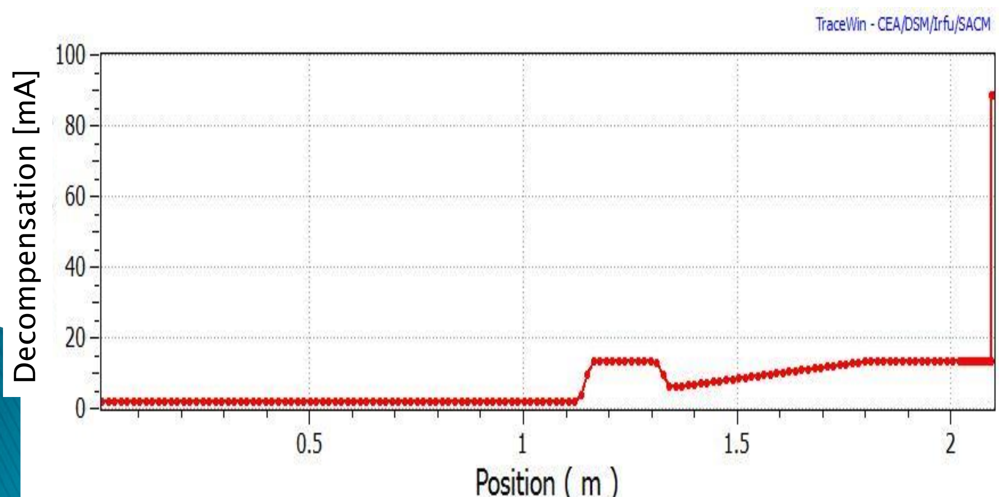

Chopper ON-OFF transition

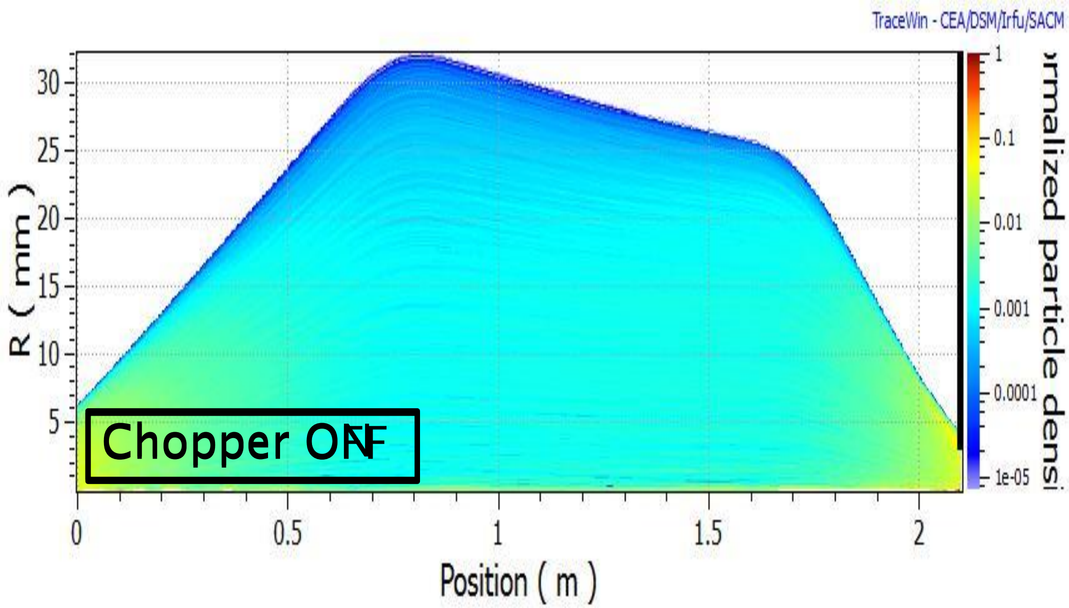

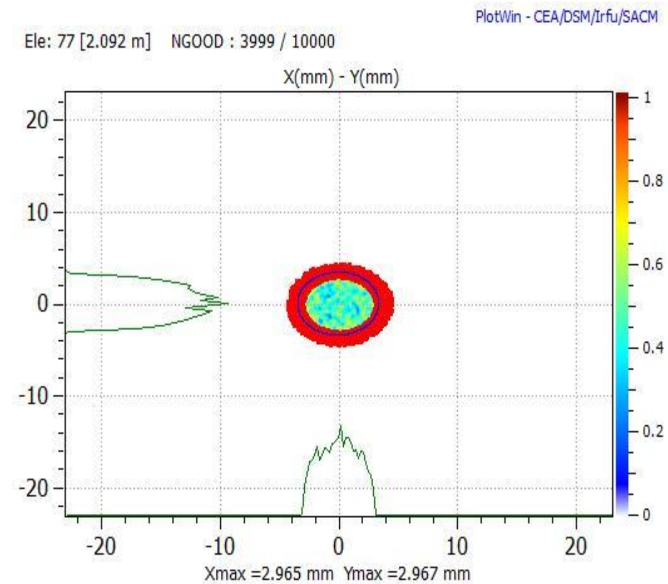

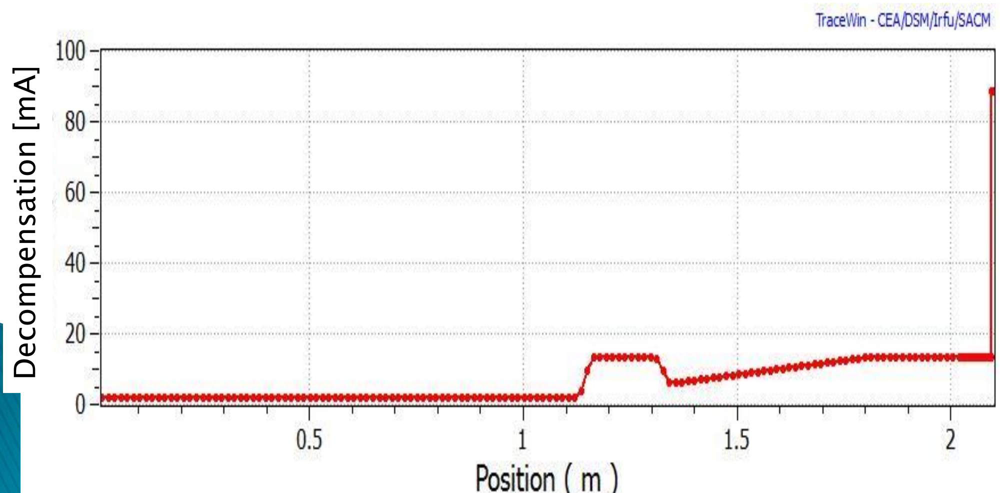

Chopper ON–OFF transition

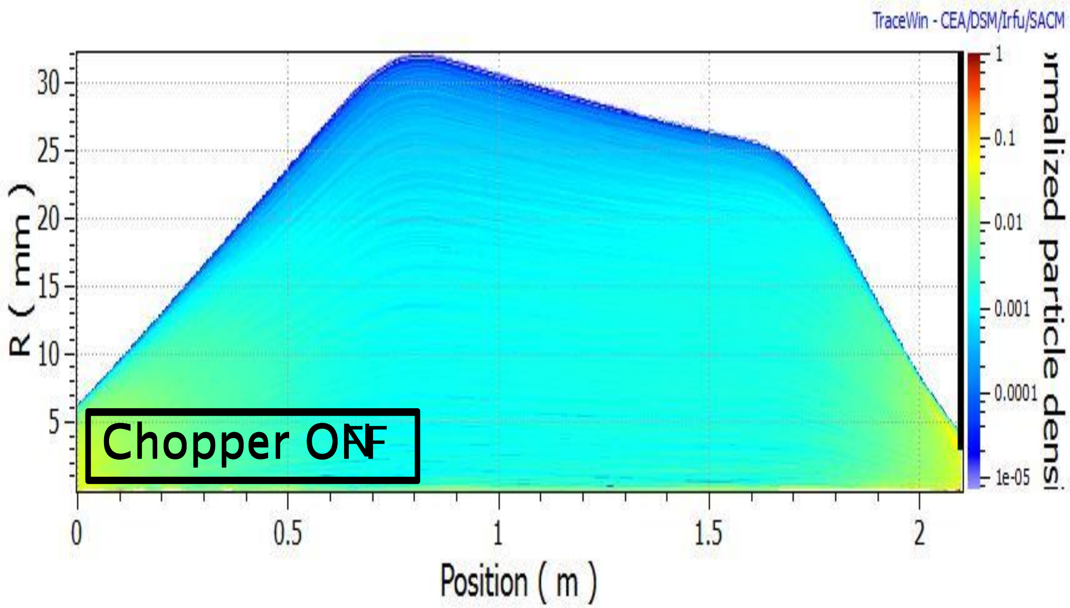

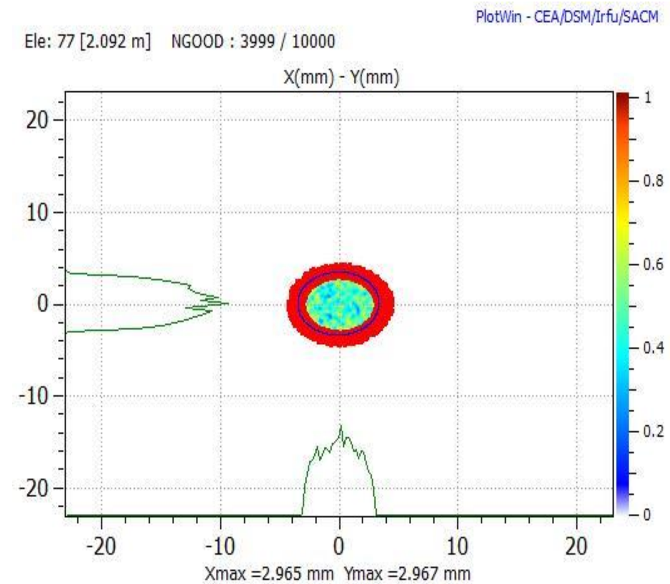

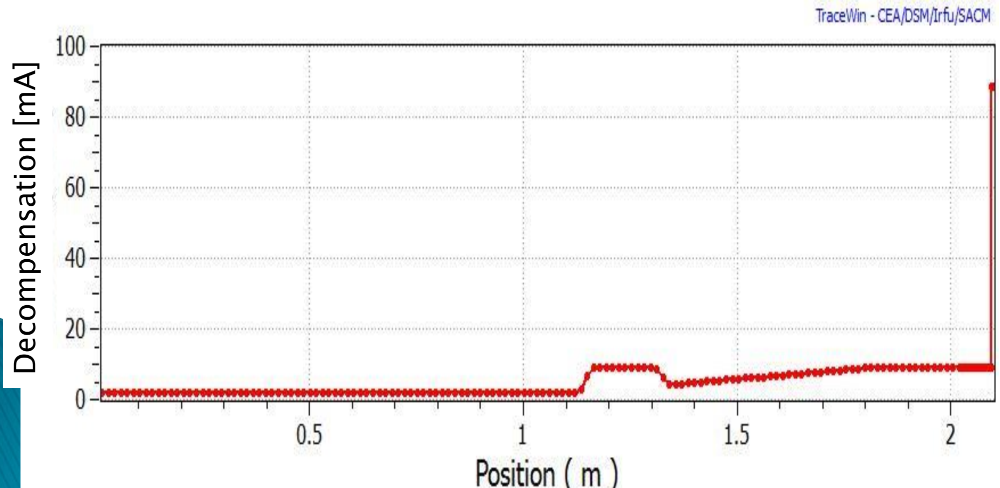

Chopper ON–OFF transition

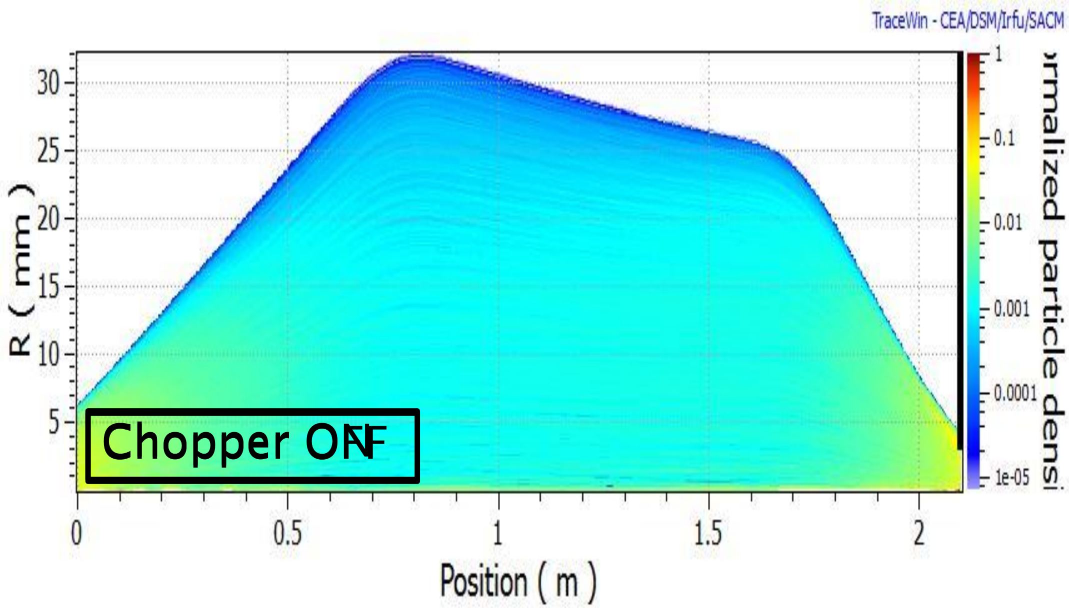

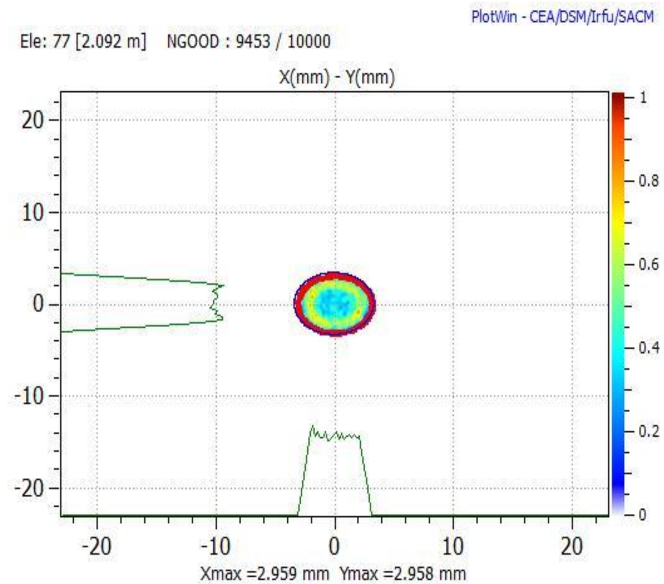

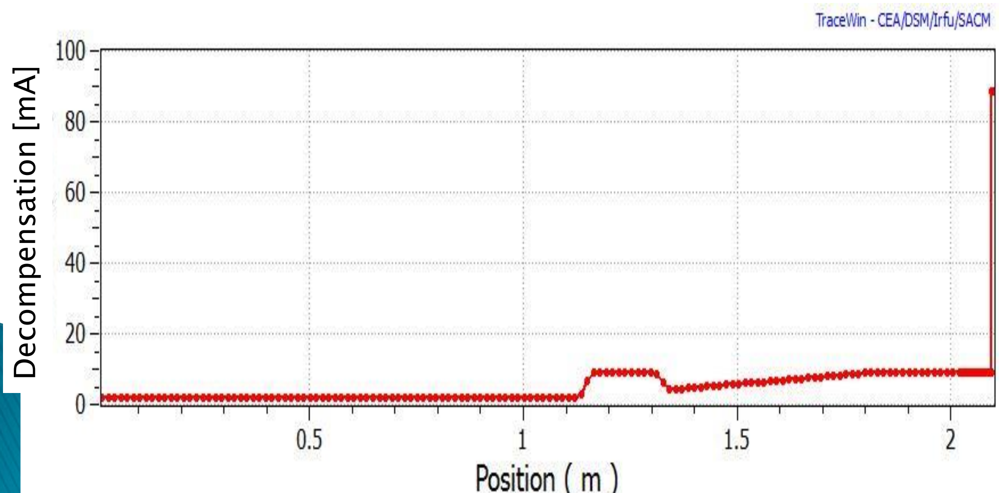

Chopper ON-OFF transition

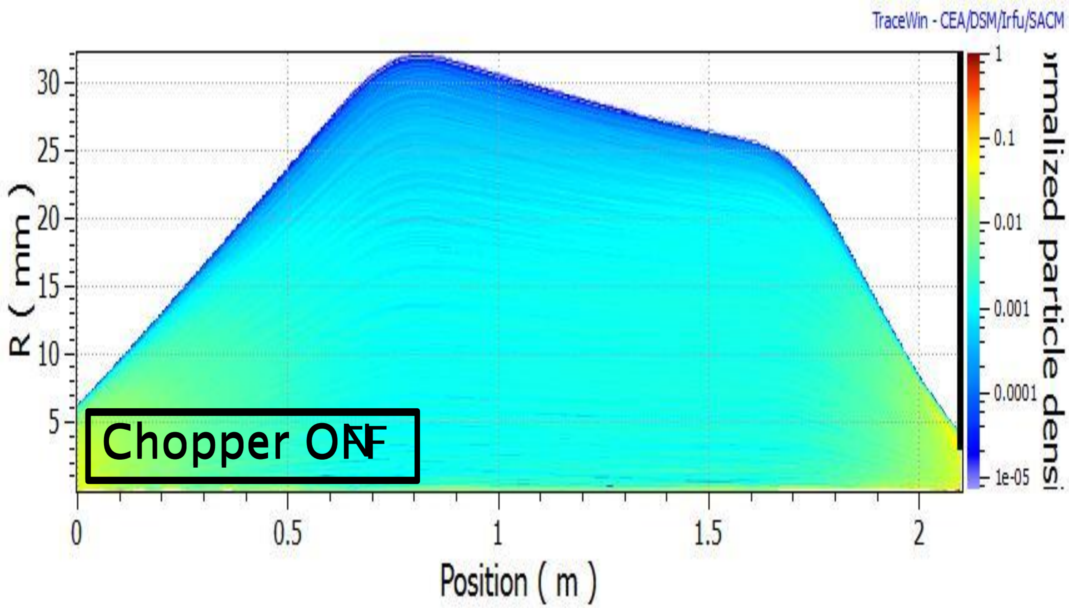

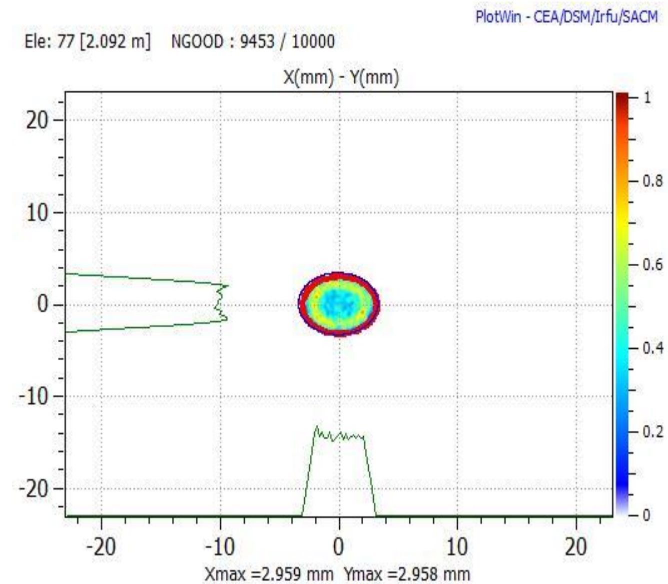

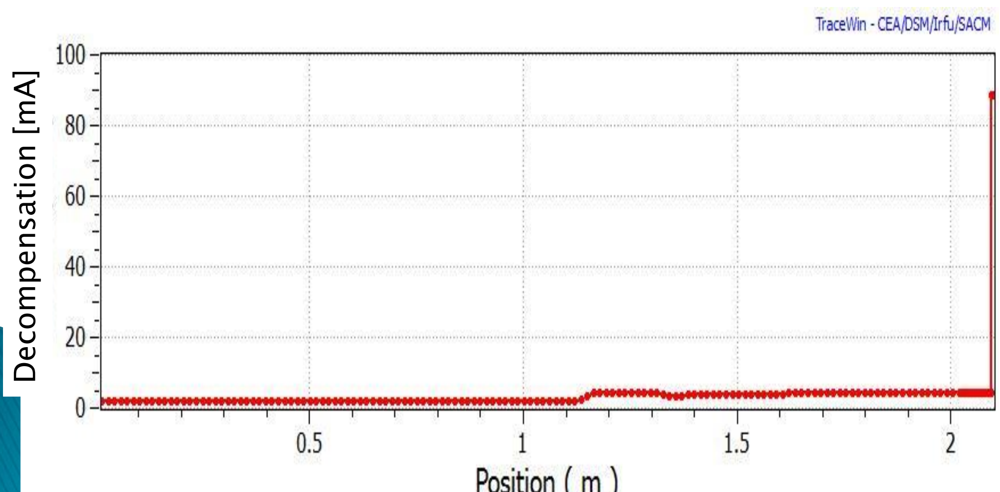

Chopper ON-OFF transition

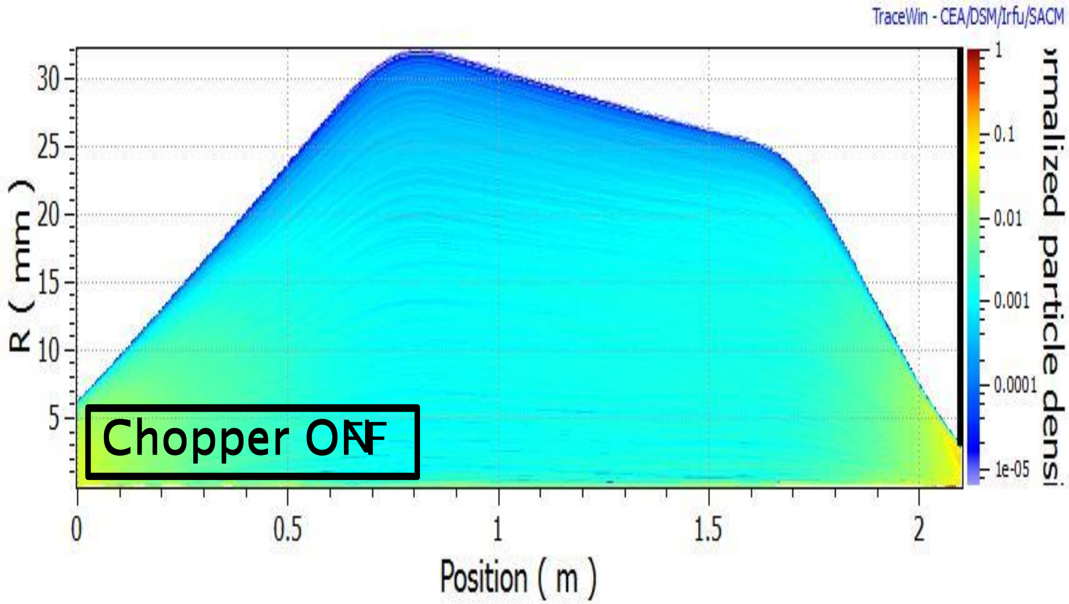

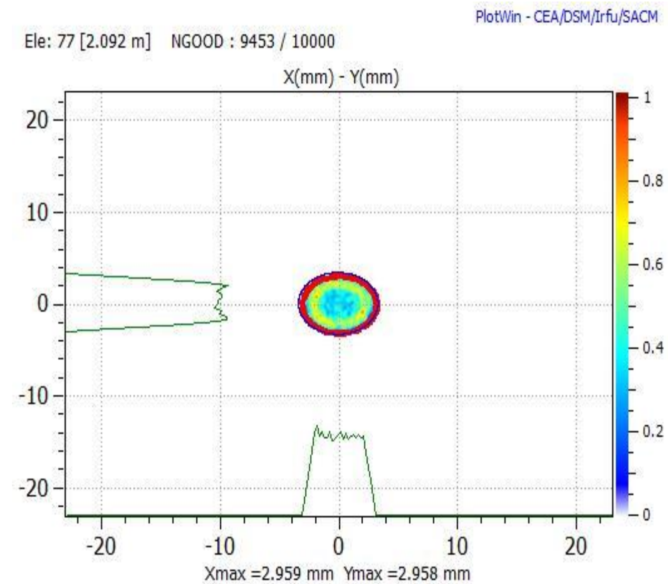

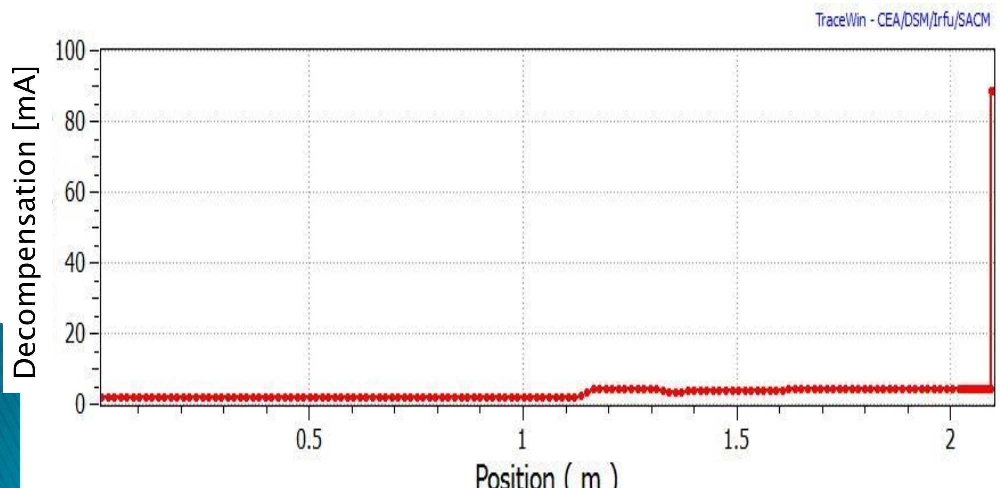

Chopper ON-OFF transition

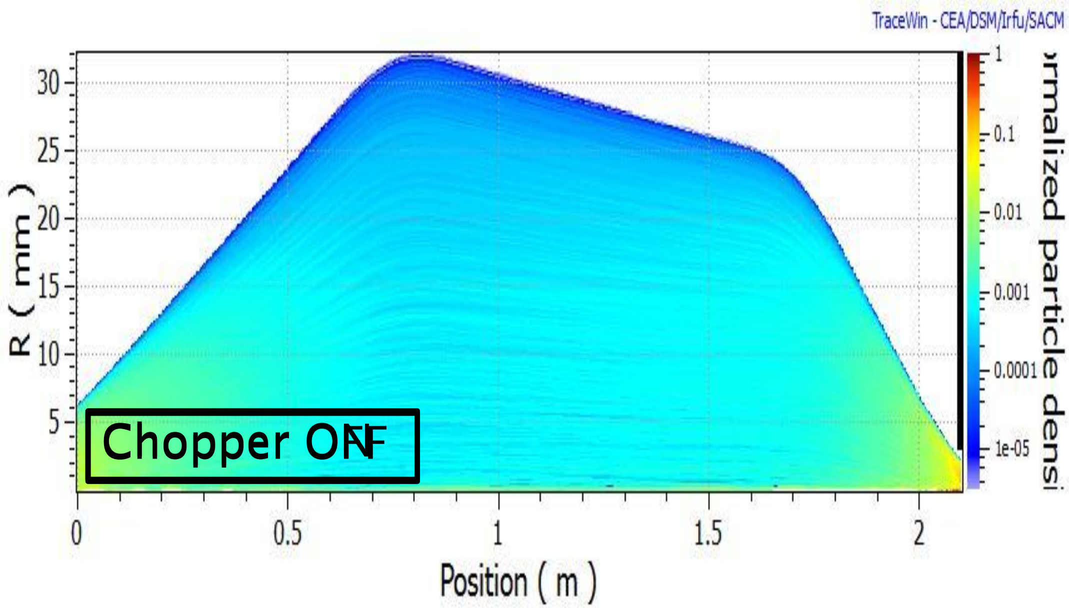

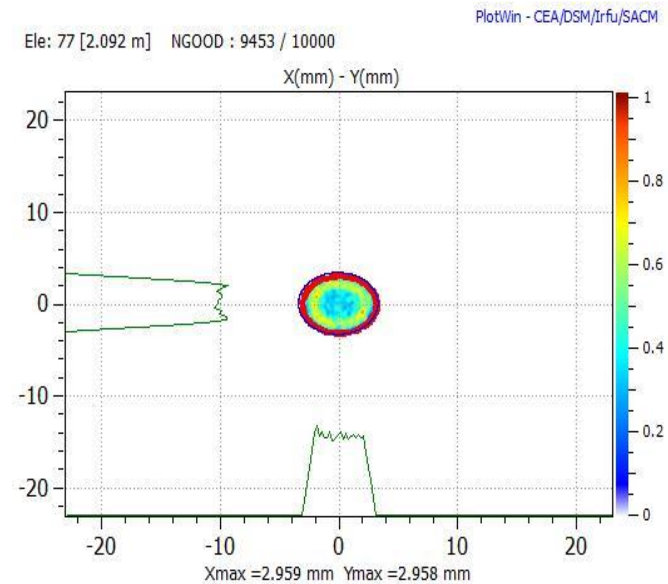

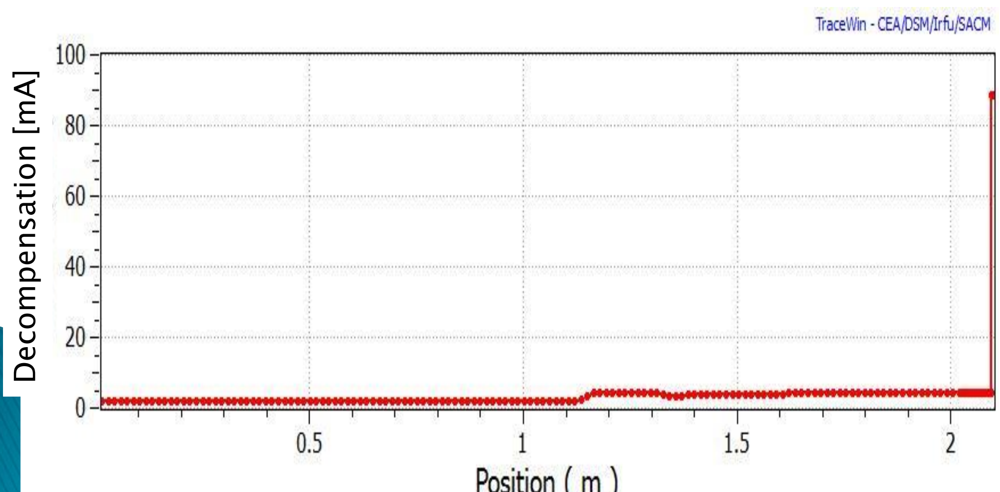

Chopper ON-OFF transition

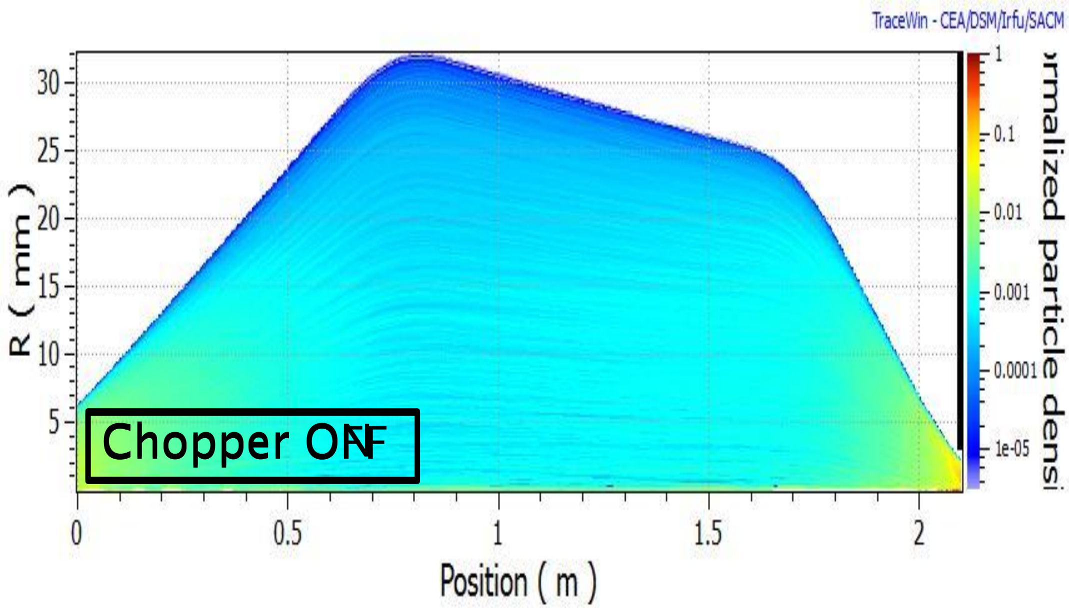

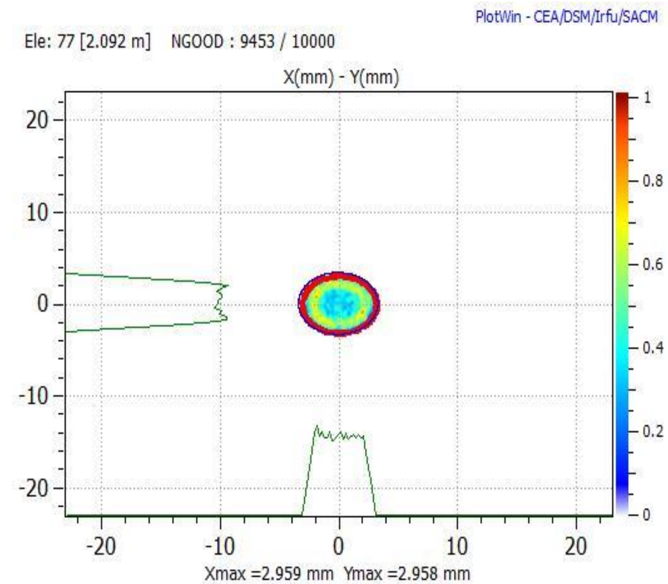

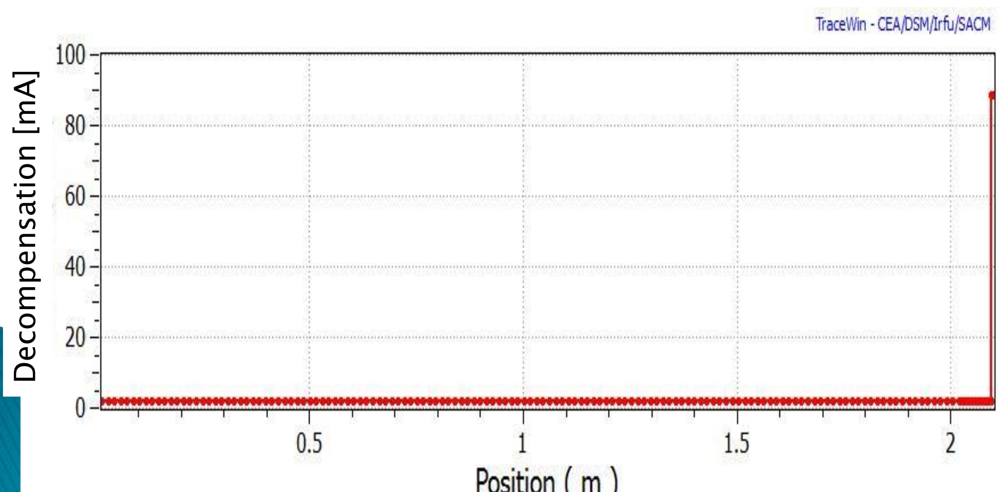

Chopper ON-OFF transition

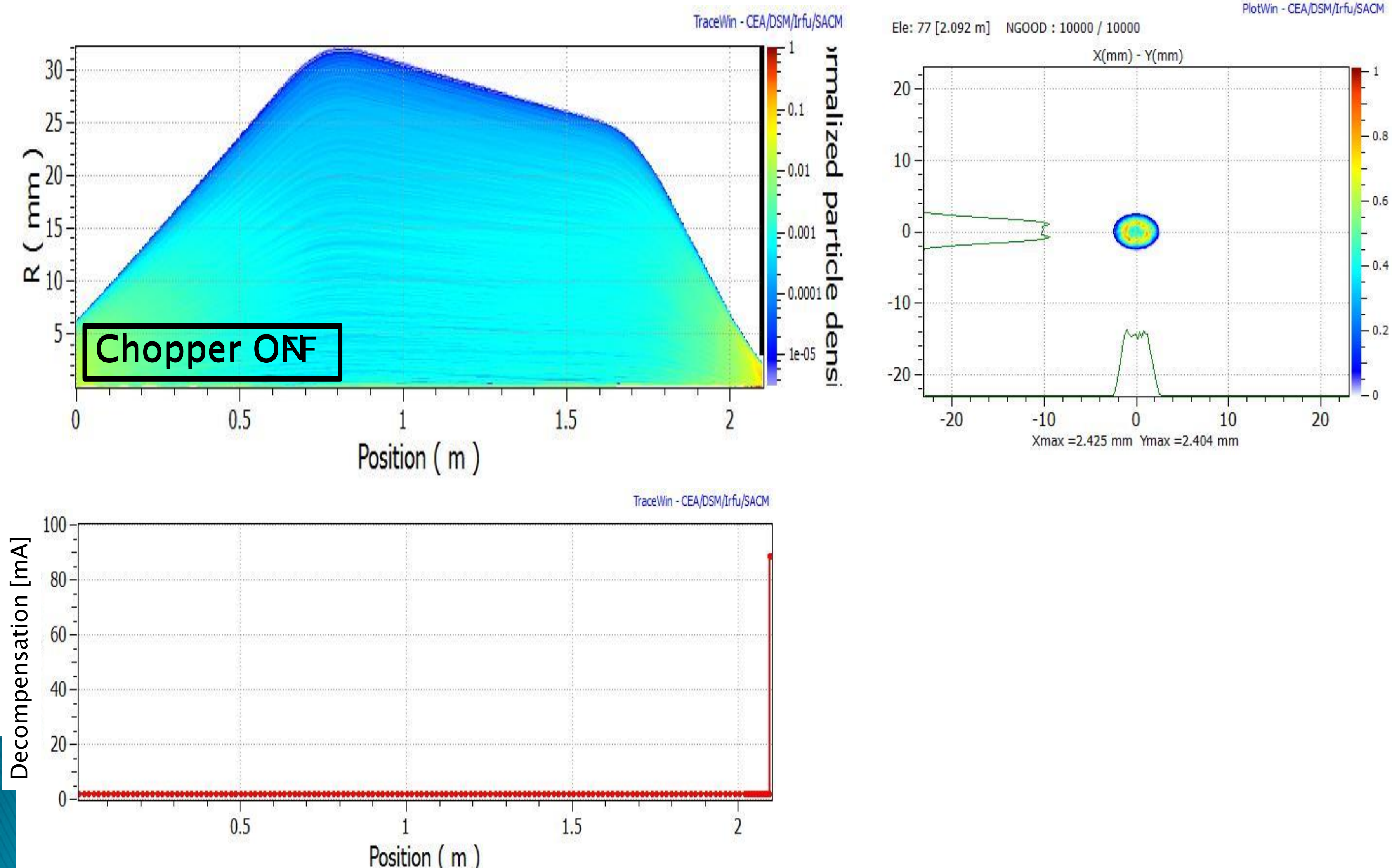

Chopper ON-OFF transition

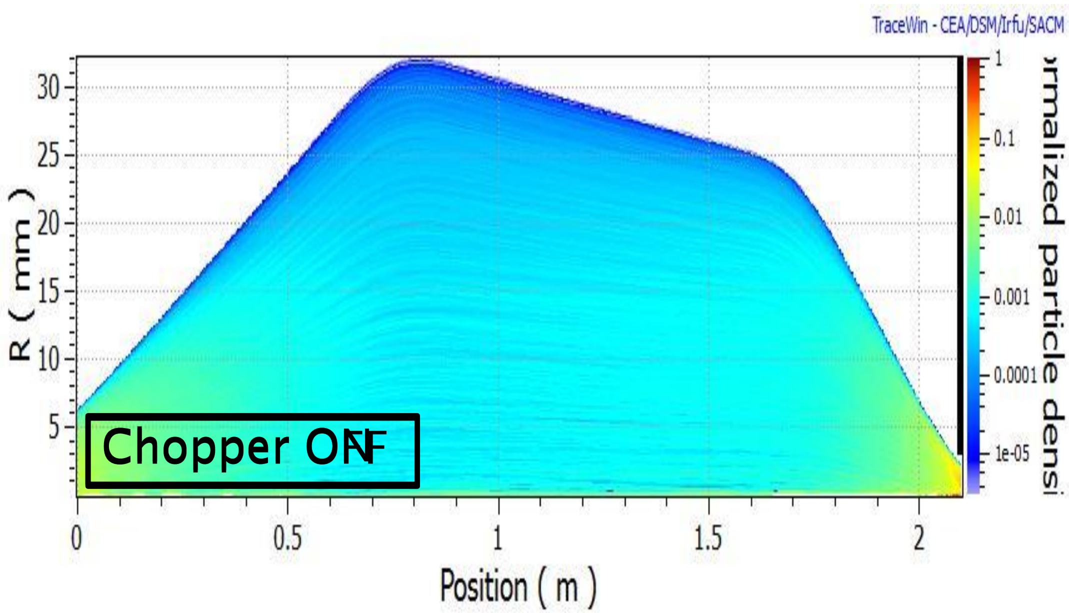

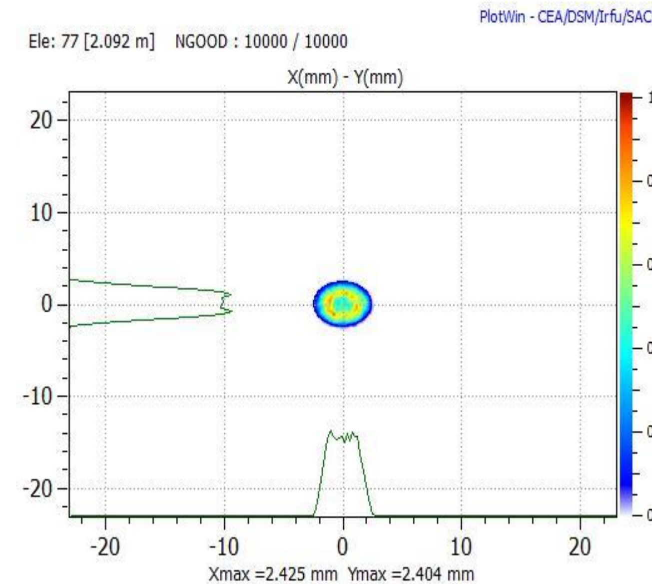

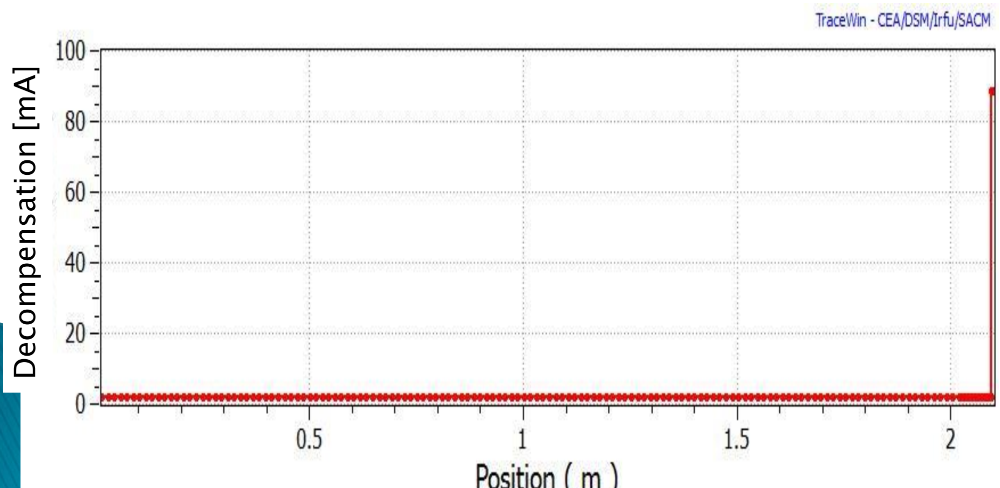

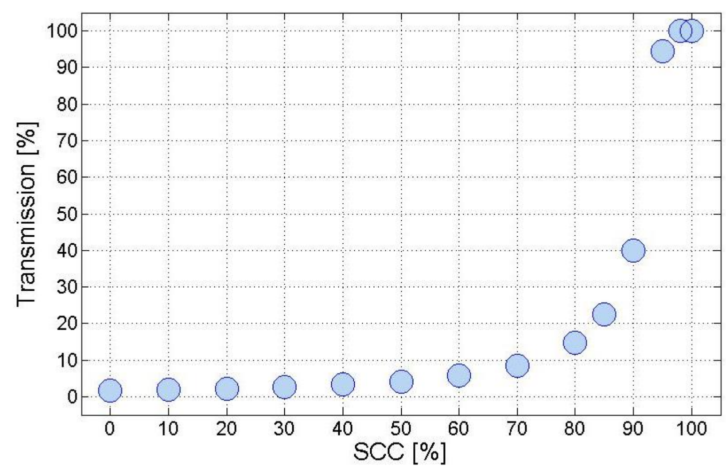

Chopper ON-OFF transition

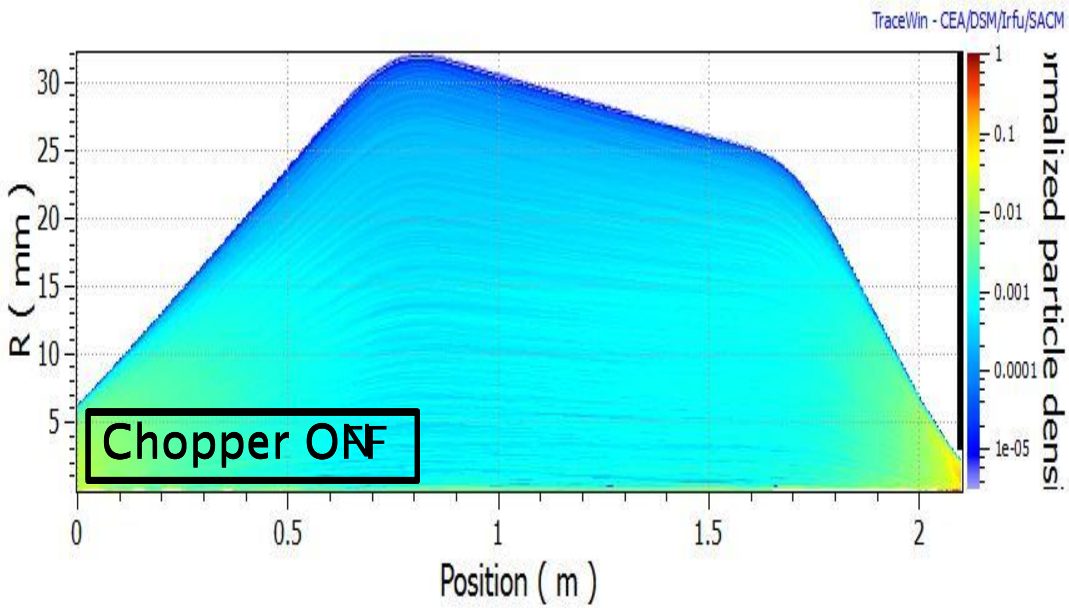

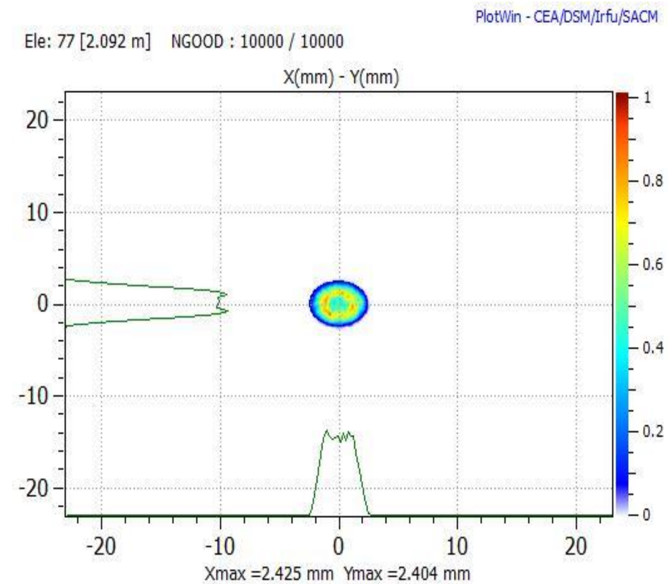

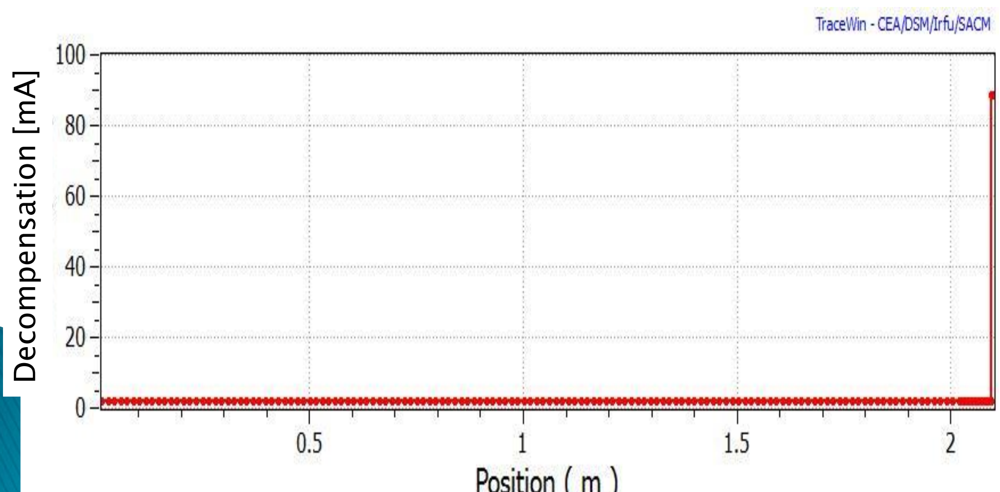

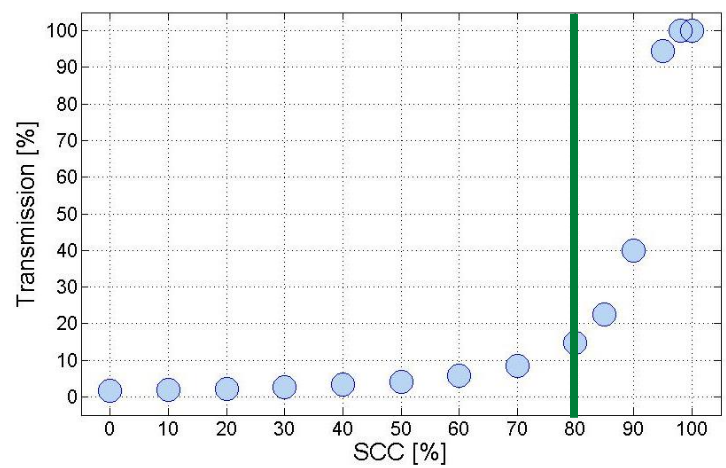

Chopper ON–OFF transition

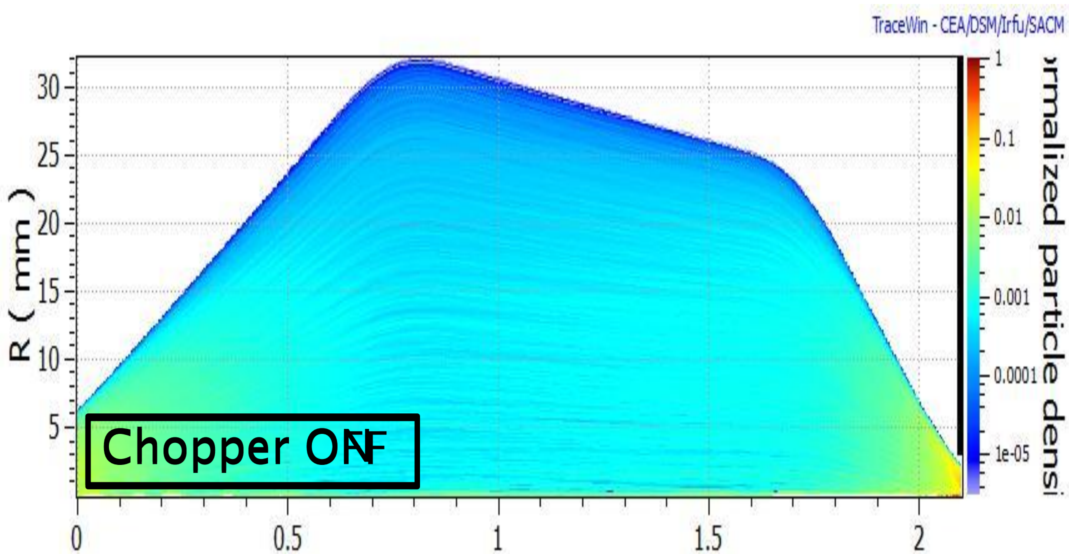

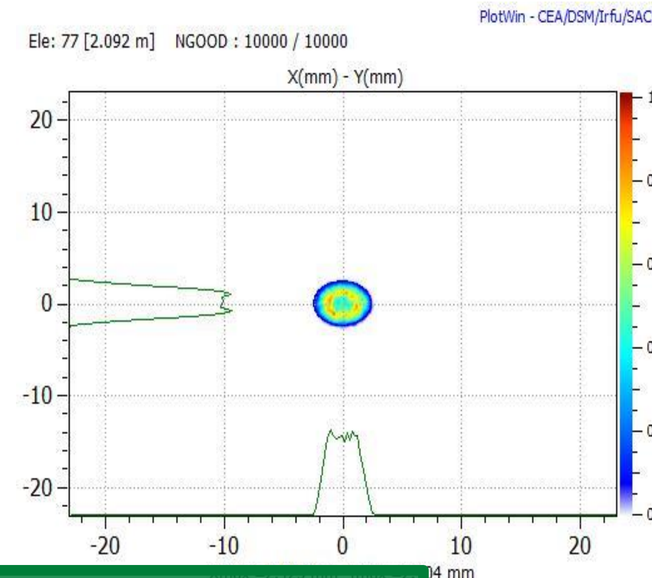

1 meter with reduced SCC means high SCC sensitivity
=>
Low transmission fraction until high SCC is reacted

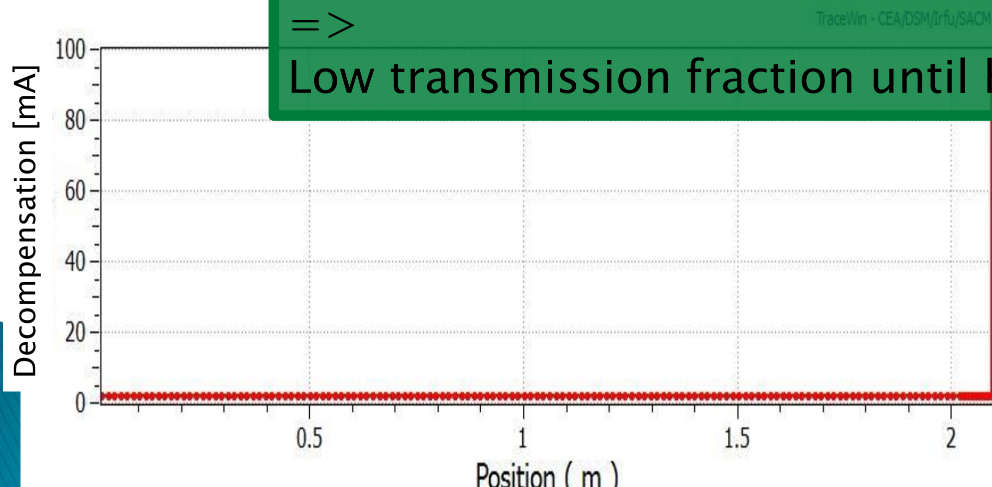

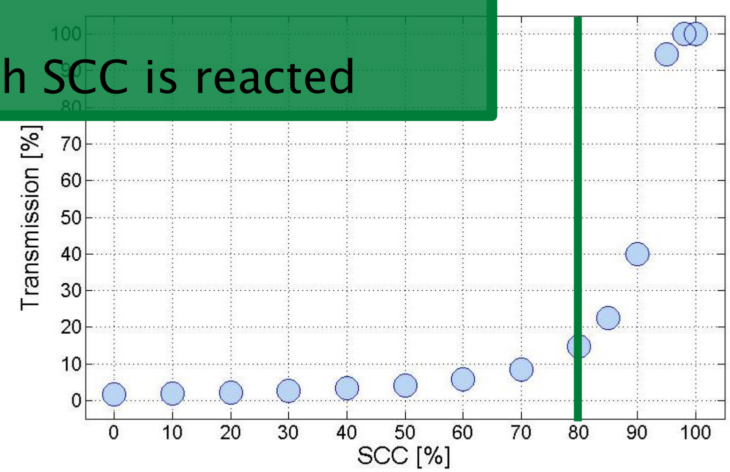

ESS and FPT-VIS sites preparation

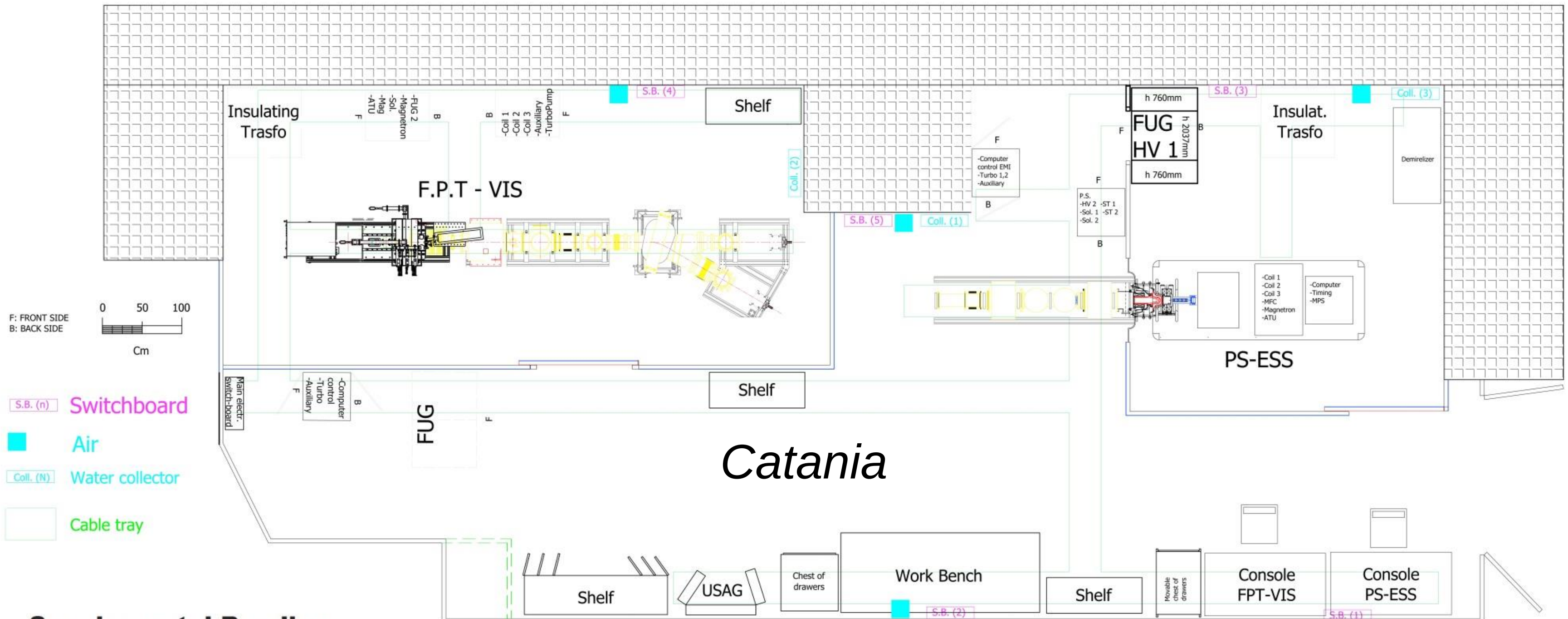

Supplemental Bonding

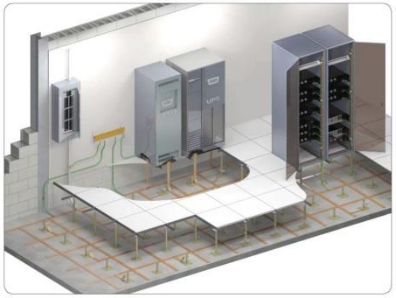

High Frequency Bonding for H.V. sparks

ESS-AB Lund (Sweden)

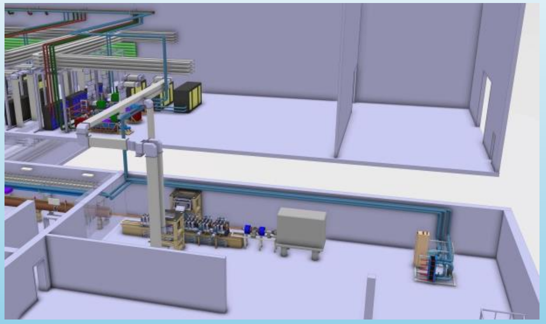

Time schedule

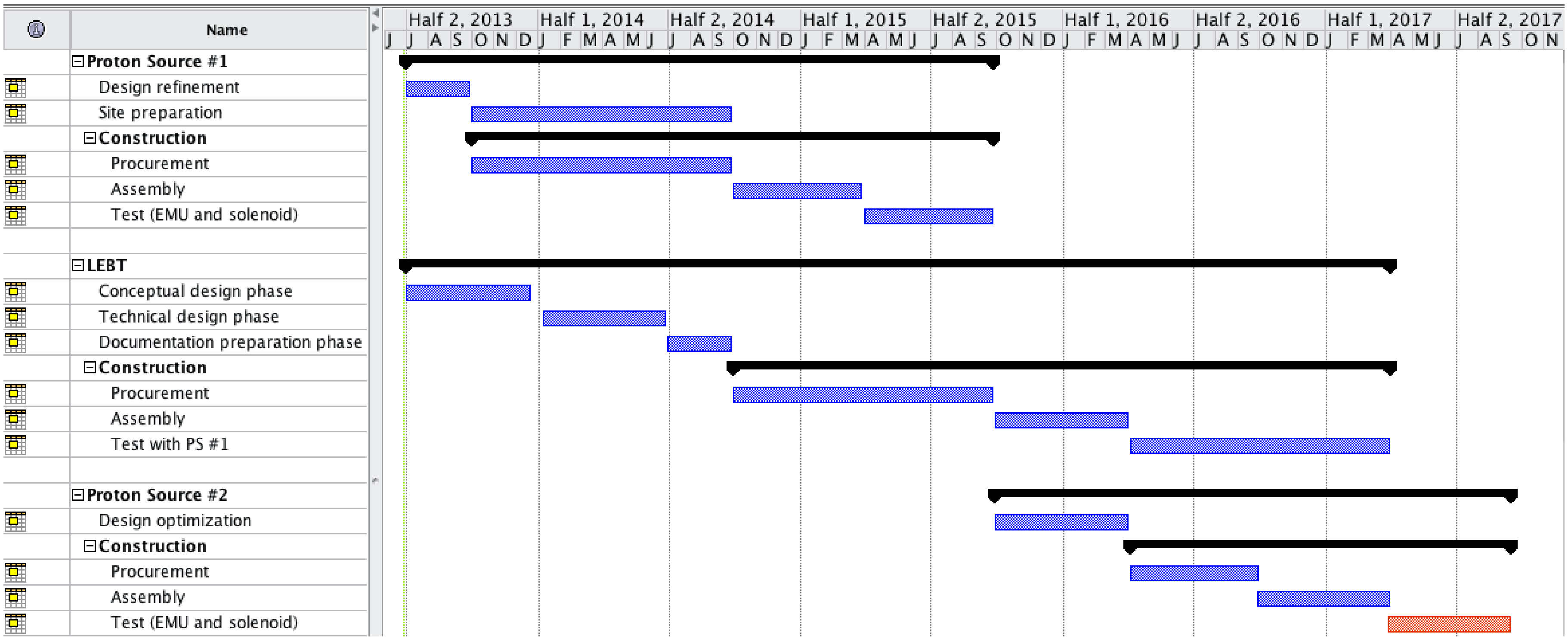

A. Ponton, June 26th 2013

Future developments

- PS-ESS#2 will be designed following the results that will be achieved on PS-ESS#1
- Layout semplification will be pursed trying to avoid instrumentation at potential (only body source) and simplify the controls and the ancillary equipment needed.

R&D activities

- Modelling and full wave computations
- Plasma diagnostic
    - Advances in X-ray spectroscopy
    - Development of microwave interferometer for ECRIS
- Flexible Plasma Trap completion

Non-uniform dielectric tensor

In the cold approximation, the magnetostatic field is always represented with a vector along the z-axis. NOT APPLIABLE FOR ECRIS!!!

Non-symmetric 3D magnetostatic field Equations

$$\begin{cases} B_x = B_1 xz + 2S_{ex}xy \\ B_y = -B_1 yz + S_{ex}(x^2 - y^2) \\ B_z = B_0 + B_1 z^2 \end{cases}$$

Non-uniform dielectric tensor

In the cold approximation, the magnetostatic field is always represented with a vector along the z-axis. NOT APPLIABLE FOR ECRIS!!!

Non-symmetric 3D magnetostatic field Equations

$$\begin{cases} B_x = B_1 xz + 2 S_{ex} xy \\ B_y = - B_1 yz + S_{ex}(x^2 - y^2) \\ B_z = B_0 + B_1 z^2 \end{cases}$$

Assuming a non uniform magnetostatic field the ***dielectric tensor*** *is:*

Non-uniform dielectric tensor

In the cold approximation, the magnetostatic field is always represented with a vector along the z-axis. NOT APPLIABLE FOR ECRIS!!!

Non-symmetric 3D magnetostatic field Equations

$$\begin{cases} B_x = B_1 xz + 2S_{ex}xy \\ B_y = -B_1 yz + S_{ex}(x^2 - y^2) \\ B_z = B_0 + B_1 z^2 \end{cases}$$

Assuming a non uniform magnetostatic field the ***dielectric tensor*** *is:*

$$\bar{\bar{\epsilon}} = \epsilon_0 \bar{\bar{\epsilon}}_r = \epsilon_0 \left(\bar{\bar{\mathrm{I}}} + \frac{\mathrm{i}\bar{\bar{\sigma}}}{\omega\epsilon_0} \right) = \epsilon_0 \left(\bar{\bar{\mathrm{I}}} + \frac{\mathrm{i}\omega_p^2 \bar{\bar{\mathrm{T}}}^{-1}}{\omega} \right) =$$

$$= \epsilon_0 \begin{bmatrix} 1 + \frac{\mathrm{i}\omega_p^2}{\omega} \frac{(-\mathrm{i}\omega+\omega_{\mathrm{eff}})^2 + B_{0x}^2 (\frac{q}{m})^2}{\Delta} & \frac{\mathrm{i}\omega_p^2}{\omega} \frac{B_{0z}\frac{q}{m}(-\mathrm{i}\omega+\omega_{\mathrm{eff}}) + B_{0x}B_{0y}(\frac{q}{m})^2}{\Delta} & \frac{\mathrm{i}\omega_p^2}{\omega} \frac{-B_{0y}\frac{q}{m}(-\mathrm{i}\omega+\omega_{\mathrm{eff}}) + B_{0x}B_{0z}(\frac{q}{m})^2}{\Delta} \\ \frac{\mathrm{i}\omega_p^2}{\omega} \frac{-B_{0z}\frac{q}{m}(-\mathrm{i}\omega+\omega_{\mathrm{eff}}) + B_{0x}B_{0y}(\frac{q}{m})^2}{\Delta} & 1 + \frac{\mathrm{i}\omega_p^2}{\omega} \frac{(-\mathrm{i}\omega+\omega_{\mathrm{eff}})^2 + B_{0y}^2 (\frac{q}{m})^2}{\Delta} & \frac{\mathrm{i}\omega_p^2}{\omega} \frac{B_{0x}\frac{q}{m}(-\mathrm{i}\omega+\omega_{\mathrm{eff}}) + B_{0y}B_{0z}(\frac{q}{m})^2}{\Delta} \\ \frac{\mathrm{i}\omega_p^2}{\omega} \frac{B_{0y}\frac{q}{m}(-\mathrm{i}\omega+\omega_{\mathrm{eff}}) + B_{0x}B_{0z}(\frac{q}{m})^2}{\Delta} & \frac{\mathrm{i}\omega_p^2}{\omega} \frac{-B_{0x}\frac{q}{m}(-\mathrm{i}\omega+\omega_{\mathrm{eff}}) + B_{0z}B_{0y}(\frac{q}{m})^2}{\Delta} & 1 + \frac{\mathrm{i}\omega_p^2}{\omega} \frac{(-\mathrm{i}\omega+\omega_{\mathrm{eff}})^2 + B_{0z}^2 (\frac{q}{m})^2}{\Delta} \end{bmatrix}$$

$$\bar{\bar{\sigma}} = \epsilon_0 \omega_p^2 \bar{\bar{\mathrm{T}}}^{-1}$$

Non-uniform dielectric tensor

In the cold approximation, the magnetostatic field is always represented with a vector along the z-axis. NOT APPLIABLE FOR ECRIS!!!

Non-symmetric 3D magnetostatic field Equations

$$\begin{cases} B_x = B_1 xz + 2S_{ex} xy \\ B_y = -B_1 yz + S_{ex}(x^2 - y^2) \\ B_z = B_0 + B_1 z^2 \end{cases}$$

*Assuming a non uniform magnetostatic field the **dielectric tensor** is:*

$$\bar{\bar{\epsilon}} = \epsilon_0 \bar{\bar{\epsilon}}_r = \epsilon_0 \left(\bar{\bar{\mathrm{I}}} + \frac{\mathrm{i}\bar{\bar{\sigma}}}{\omega \epsilon_0} \right) = \epsilon_0 \left(\bar{\bar{\mathrm{I}}} + \frac{\mathrm{i}\omega_p^2 \bar{\bar{\mathrm{T}}}^{-1}}{\omega} \right) =$$

$$= \epsilon_0 \begin{bmatrix} 1 + \frac{\mathrm{i}\omega_p^2}{\omega} \frac{(-\mathrm{i}\omega + \omega_{\mathrm{eff}})^2 + B_{0x}^2 (\frac{q}{m})^2}{\Delta} & \frac{\mathrm{i}\omega_p^2}{\omega} \frac{B_{0z} \frac{q}{m}(-\mathrm{i}\omega + \omega_{\mathrm{eff}}) + B_{0x} B_{0y} (\frac{q}{m})^2}{\Delta} & \frac{\mathrm{i}\omega_p^2}{\omega} \frac{-B_{0y} \frac{q}{m}(-\mathrm{i}\omega + \omega_{\mathrm{eff}}) + B_{0x} B_{0z} (\frac{q}{m})^2}{\Delta} \\ \frac{\mathrm{i}\omega_p^2}{\omega} \frac{-B_{0z} \frac{q}{m}(-\mathrm{i}\omega + \omega_{\mathrm{eff}}) + B_{0x} B_{0y} (\frac{q}{m})^2}{\Delta} & 1 + \frac{\mathrm{i}\omega_p^2}{\omega} \frac{(-\mathrm{i}\omega + \omega_{\mathrm{eff}})^2 + B_{0y}^2 (\frac{q}{m})^2}{\Delta} & \frac{\mathrm{i}\omega_p^2}{\omega} \frac{B_{0x} \frac{q}{m}(-\mathrm{i}\omega + \omega_{\mathrm{eff}}) + B_{0y} B_{0z} (\frac{q}{m})^2}{\Delta} \\ \frac{\mathrm{i}\omega_p^2}{\omega} \frac{B_{0y} \frac{q}{m}(-\mathrm{i}\omega + \omega_{\mathrm{eff}}) + B_{0x} B_{0z} (\frac{q}{m})^2}{\Delta} & \frac{\mathrm{i}\omega_p^2}{\omega} \frac{-B_{0x} \frac{q}{m}(-\mathrm{i}\omega + \omega_{\mathrm{eff}}) + B_{0z} B_{0y} (\frac{q}{m})^2}{\Delta} & 1 + \frac{\mathrm{i}\omega_p^2}{\omega} \frac{(-\mathrm{i}\omega + \omega_{\mathrm{eff}})^2 + B_{0z}^2 (\frac{q}{m})^2}{\Delta} \end{bmatrix}$$

$$\bar{\bar{\sigma}} = \epsilon_0 \omega_p^2 \bar{\bar{\mathrm{T}}}^{-1}$$

Non-uniform dielectric tensor

In the cold approximation, the magnetostatic field is always represented with a vector along the z-axis. NOT APPLIABLE FOR ECRIS!!!

Non-symmetric 3D magnetostatic field Equations

$$\begin{cases} B_x = B_1 xz + 2S_{ex} xy \\ B_y = -B_1 yz + S_{ex}(x^2 - y^2) \\ B_z = B_0 + B_1 z^2 \end{cases}$$

Assuming a non uniform magnetostatic field the ***dielectric tensor*** *is:*

$$\overline{\overline{\epsilon}} = \epsilon_0 \overline{\overline{\epsilon}}_r = \epsilon_0 \left(\overline{\overline{\mathrm{I}}} + \frac{\mathrm{i}\overline{\overline{\sigma}}}{\omega \epsilon_0} \right) = \epsilon_0 \left(\overline{\overline{\mathrm{I}}} + \frac{\mathrm{i}\omega_p^2 \overline{\overline{\mathrm{T}}}^{-1}}{\omega} \right) =$$

$$= \epsilon_0 \begin{bmatrix} 1 + \frac{\mathrm{i}\omega_p^2}{\omega} \frac{(-\mathrm{i}\omega+\omega_{\mathrm{eff}})^2 + B_{0x}^2 (\frac{q}{m})^2}{\Delta} & \frac{\mathrm{i}\omega_p^2}{\omega} \frac{B_{0z}\frac{q}{m}(-\mathrm{i}\omega+\omega_{\mathrm{eff}}) + B_{0x}B_{0y}(\frac{q}{m})^2}{\Delta} & \frac{\mathrm{i}\omega_p^2}{\omega} \frac{-B_{0y}\frac{q}{m}(-\mathrm{i}\omega+\omega_{\mathrm{eff}}) + B_{0x}B_{0z}(\frac{q}{m})^2}{\Delta} \\ \frac{\mathrm{i}\omega_p^2}{\omega} \frac{-B_{0z}\frac{q}{m}(-\mathrm{i}\omega+\omega_{\mathrm{eff}}) + B_{0x}B_{0y}(\frac{q}{m})^2}{\Delta} & 1 + \frac{\mathrm{i}\omega_p^2}{\omega} \frac{(-\mathrm{i}\omega+\omega_{\mathrm{eff}})^2 + B_{0y}^2 (\frac{q}{m})^2}{\Delta} & \frac{\mathrm{i}\omega_p^2}{\omega} \frac{B_{0x}\frac{q}{m}(-\mathrm{i}\omega+\omega_{\mathrm{eff}}) + B_{0y}B_{0z}(\frac{q}{m})^2}{\Delta} \\ \frac{\mathrm{i}\omega_p^2}{\omega} \frac{B_{0y}\frac{q}{m}(-\mathrm{i}\omega+\omega_{\mathrm{eff}}) + B_{0x}B_{0z}(\frac{q}{m})^2}{\Delta} & \frac{\mathrm{i}\omega_p^2}{\omega} \frac{-B_{0x}\frac{q}{m}(-\mathrm{i}\omega+\omega_{\mathrm{eff}}) + B_{0z}B_{0y}(\frac{q}{m})^2}{\Delta} & 1 + \frac{\mathrm{i}\omega_p^2}{\omega} \frac{(-\mathrm{i}\omega+\omega_{\mathrm{eff}})^2 + B_{0z}^2 (\frac{q}{m})^2}{\Delta} \end{bmatrix}$$

$$\overline{\overline{\sigma}} = \epsilon_0 \omega_p^2 \overline{\overline{\mathrm{T}}}^{-1}$$

Non-uniform dielectric tensor

In the cold approximation, the magnetostatic field is always represented with a vector along the z-axis. NOT APPLIABLE FOR ECRIS!!!

Non-symmetric 3D magnetostatic field Equations

$$\begin{cases} B_x = B_1 xz + 2S_{ex} xy \\ B_y = -B_1 yz + S_{ex}(x^2 - y^2) \\ B_z = B_0 + B_1 z^2 \end{cases}$$

Assuming a non uniform magnetostatic field the ***dielectric tensor*** *is:*

$$\overline{\overline{\epsilon}} = \epsilon_0 \overline{\overline{\epsilon}}_r = \epsilon_0 \left(\overline{\overline{\mathrm{I}}} + \frac{\mathrm{i}\overline{\overline{\sigma}}}{\omega \epsilon_0} \right) = \epsilon_0 \left(\overline{\overline{\mathrm{I}}} + \frac{\mathrm{i}\omega_p^2 \overline{\overline{\mathrm{T}}}^{-1}}{\omega} \right) =$$

$$= \epsilon_0 \begin{bmatrix} 1 + \frac{\mathrm{i}\omega_p^2}{\omega} \frac{(-\mathrm{i}\omega+\omega_{\mathrm{eff}})^2 + B_{0x}^2 (\frac{q}{m})^2}{\Delta} & \frac{\mathrm{i}\omega_p^2}{\omega} \frac{B_{0z}\frac{q}{m}(-\mathrm{i}\omega+\omega_{\mathrm{eff}}) + B_{0x}B_{0y}(\frac{q}{m})^2}{\Delta} & \frac{\mathrm{i}\omega_p^2}{\omega} \frac{-B_{0y}\frac{q}{m}(-\mathrm{i}\omega+\omega_{\mathrm{eff}}) + B_{0x}B_{0z}(\frac{q}{m})^2}{\Delta} \\ \frac{\mathrm{i}\omega_p^2}{\omega} \frac{-B_{0z}\frac{q}{m}(-\mathrm{i}\omega+\omega_{\mathrm{eff}}) + B_{0x}B_{0y}(\frac{q}{m})^2}{\Delta} & 1 + \frac{\mathrm{i}\omega_p^2}{\omega} \frac{(-\mathrm{i}\omega+\omega_{\mathrm{eff}})^2 + B_{0y}^2 (\frac{q}{m})^2}{\Delta} & \frac{\mathrm{i}\omega_p^2}{\omega} \frac{B_{0x}\frac{q}{m}(-\mathrm{i}\omega+\omega_{\mathrm{eff}}) + B_{0y}B_{0z}(\frac{q}{m})^2}{\Delta} \\ \frac{\mathrm{i}\omega_p^2}{\omega} \frac{B_{0y}\frac{q}{m}(-\mathrm{i}\omega+\omega_{\mathrm{eff}}) + B_{0x}B_{0z}(\frac{q}{m})^2}{\Delta} & \frac{\mathrm{i}\omega_p^2}{\omega} \frac{-B_{0x}\frac{q}{m}(-\mathrm{i}\omega+\omega_{\mathrm{eff}}) + B_{0z}B_{0y}(\frac{q}{m})^2}{\Delta} & 1 + \frac{\mathrm{i}\omega_p^2}{\omega} \frac{(-\mathrm{i}\omega+\omega_{\mathrm{eff}})^2 + B_{0z}^2 (\frac{q}{m})^2}{\Delta} \end{bmatrix}$$

$$\overline{\overline{\sigma}} = \epsilon_0 \omega_p^2 \overline{\overline{\mathrm{T}}}^{-1}$$

Non-uniform dielectric tensor

In the cold approximation, the magnetostatic field is always represented with a vector along the z-axis. NOT APPLIABLE FOR ECRIS!!!

Non-symmetric 3D magnetostatic field Equations

$$\begin{cases} B_x = B_1 xz + 2 S_{ex} xy \\ B_y = - B_1 yz + S_{ex}(x^2 - y^2) \\ B_z = B_0 + B_1 z^2 \end{cases}$$

Assuming a non uniform magnetostatic field the ***dielectric tensor*** *is:*

$$\overline{\overline{\epsilon}} = \epsilon_0 \overline{\overline{\epsilon}}_r = \epsilon_0 \left(\overline{\overline{\mathrm{I}}} + \frac{\mathrm{i}\overline{\overline{\sigma}}}{\omega \epsilon_0} \right) = \epsilon_0 \left(\overline{\overline{\mathrm{I}}} + \frac{\mathrm{i}\omega_p^2 \overline{\overline{\mathrm{T}}}^{-1}}{\omega} \right) =$$

$$= \epsilon_0 \begin{bmatrix} 1 + \frac{\mathrm{i}\omega_p^2}{\omega} \frac{(-\mathrm{i}\omega + \omega_{\mathrm{eff}})^2 + B_{0x}^2 (\frac{q}{m})^2}{\Delta} & \frac{\mathrm{i}\omega_p^2}{\omega} \frac{B_{0z} \frac{q}{m} (-\mathrm{i}\omega + \omega_{\mathrm{eff}}) + B_{0x} B_{0y} (\frac{q}{m})^2}{\Delta} & \frac{\mathrm{i}\omega_p^2}{\omega} \frac{-B_{0y} \frac{q}{m} (-\mathrm{i}\omega + \omega_{\mathrm{eff}}) + B_{0x} B_{0z} (\frac{q}{m})^2}{\Delta} \\ \frac{\mathrm{i}\omega_p^2}{\omega} \frac{-B_{0z} \frac{q}{m} (-\mathrm{i}\omega + \omega_{\mathrm{eff}}) + B_{0x} B_{0y} (\frac{q}{m})^2}{\Delta} & 1 + \frac{\mathrm{i}\omega_p^2}{\omega} \frac{(-\mathrm{i}\omega + \omega_{\mathrm{eff}})^2 + B_{0y}^2 (\frac{q}{m})^2}{\Delta} & \frac{\mathrm{i}\omega_p^2}{\omega} \frac{B_{0x} \frac{q}{m} (-\mathrm{i}\omega + \omega_{\mathrm{eff}}) + B_{0y} B_{0z} (\frac{q}{m})^2}{\Delta} \\ \frac{\mathrm{i}\omega_p^2}{\omega} \frac{B_{0y} \frac{q}{m} (-\mathrm{i}\omega + \omega_{\mathrm{eff}}) + B_{0x} B_{0z} (\frac{q}{m})^2}{\Delta} & \frac{\mathrm{i}\omega_p^2}{\omega} \frac{-B_{0x} \frac{q}{m} (-\mathrm{i}\omega + \omega_{\mathrm{eff}}) + B_{0z} B_{0y} (\frac{q}{m})^2}{\Delta} & 1 + \frac{\mathrm{i}\omega_p^2}{\omega} \frac{(-\mathrm{i}\omega + \omega_{\mathrm{eff}})^2 + B_{0z}^2 (\frac{q}{m})^2}{\Delta} \end{bmatrix}$$

$$\overline{\overline{\sigma}} = \epsilon_0 \omega_p^2 \overline{\overline{\mathrm{T}}}^{-1}$$

Non-uniform dielectric tensor

In the cold approximation, the magnetostatic field is always represented with a vector along the z-axis. NOT APPLIABLE FOR ECRIS!!!

Non-symmetric 3D magnetostatic field Equations

$$\begin{cases} B_x = B_1 xz + 2 S_{ex} xy \\ B_y = - B_1 yz + S_{ex}(x^2 - y^2) \\ B_z = B_0 + B_1 z^2 \end{cases}$$

*Assuming a non uniform magnetostatic field the **dielectric tensor** is:*

$$\overline{\overline{\epsilon}} = \epsilon_0 \overline{\overline{\epsilon}}_r = \epsilon_0 \left(\overline{\overline{\mathrm{I}}} + \frac{\mathrm{i}\overline{\overline{\sigma}}}{\omega \epsilon_0} \right) = \epsilon_0 \left(\overline{\overline{\mathrm{I}}} + \frac{\mathrm{i}\omega_p^2 \overline{\overline{\mathrm{T}}}^{-1}}{\omega} \right) =$$

$$= \epsilon_0 \begin{bmatrix} 1 + \frac{\mathrm{i}\omega_p^2}{\omega} \frac{(-\mathrm{i}\omega + \omega_{\mathrm{eff}})^2 + B_{0x}^2 (\frac{q}{m})^2}{\Delta} & \frac{\mathrm{i}\omega_p^2}{\omega} \frac{B_{0z} \frac{q}{m} (-\mathrm{i}\omega + \omega_{\mathrm{eff}}) + B_{0x} B_{0y} (\frac{q}{m})^2}{\Delta} & \frac{\mathrm{i}\omega_p^2}{\omega} \frac{-B_{0y} \frac{q}{m} (-\mathrm{i}\omega + \omega_{\mathrm{eff}}) + B_{0x} B_{0z} (\frac{q}{m})^2}{\Delta} \\ \frac{\mathrm{i}\omega_p^2}{\omega} \frac{-B_{0z} \frac{q}{m} (-\mathrm{i}\omega + \omega_{\mathrm{eff}}) + B_{0x} B_{0y} (\frac{q}{m})^2}{\Delta} & 1 + \frac{\mathrm{i}\omega_p^2}{\omega} \frac{(-\mathrm{i}\omega + \omega_{\mathrm{eff}})^2 + B_{0y}^2 (\frac{q}{m})^2}{\Delta} & \frac{\mathrm{i}\omega_p^2}{\omega} \frac{B_{0x} \frac{q}{m} (-\mathrm{i}\omega + \omega_{\mathrm{eff}}) + B_{0y} B_{0z} (\frac{q}{m})^2}{\Delta} \\ \frac{\mathrm{i}\omega_p^2}{\omega} \frac{B_{0y} \frac{q}{m} (-\mathrm{i}\omega + \omega_{\mathrm{eff}}) + B_{0x} B_{0z} (\frac{q}{m})^2}{\Delta} & \frac{\mathrm{i}\omega_p^2}{\omega} \frac{-B_{0x} \frac{q}{m} (-\mathrm{i}\omega + \omega_{\mathrm{eff}}) + B_{0z} B_{0y} (\frac{q}{m})^2}{\Delta} & 1 + \frac{\mathrm{i}\omega_p^2}{\omega} \frac{(-\mathrm{i}\omega + \omega_{\mathrm{eff}})^2 + B_{0z}^2 (\frac{q}{m})^2}{\Delta} \end{bmatrix}$$

$$\overline{\overline{\sigma}} = \epsilon_0 \omega_p^2 \overline{\overline{\mathrm{T}}}^{-1}$$

Off-diagonal Elements due to 3D Magnetic field

Cold plasma simulations in COMSOL and Matlab

Journal of Electromagnetic Waves and Applications, 2014
Vol. 28, No. 9, 1085–1099, http://dx.doi.org/10.1080/09205071.2014.905245

Taylor & Francis
Taylor & Francis Group

Full-wave FEM simulations of electromagnetic waves in strongly magnetized non-homogeneous plasma

G. Torrisi[a,b*], D. Mascali[a], G. Sorbello[a,c], L. Neri[a], L. Celona[a], G. Castro[a], T. Isernia[b] and S. Gammino[a]

Solution of Maxwell's equations in **COMSOL** using MUMPS direct solver

Full anisotropic dielectric tensor for the magnetized plasma computed in **MATLAB**

Electromagnetic field in ECRIS Plasma

Solution of the wave equation

$$\vec{\nabla}\times\vec{\nabla}\times\vec{E}(\vec{r})+\frac{w^2}{c^2}\bar{\bar{e}}\cdot\vec{E}(\vec{r})=0$$

Conventional PDE which can be solved by **COMSOL**

Full-wave computation: *8 GHz microwaves into the plasma filled chamber*

In-vacuum cavity field

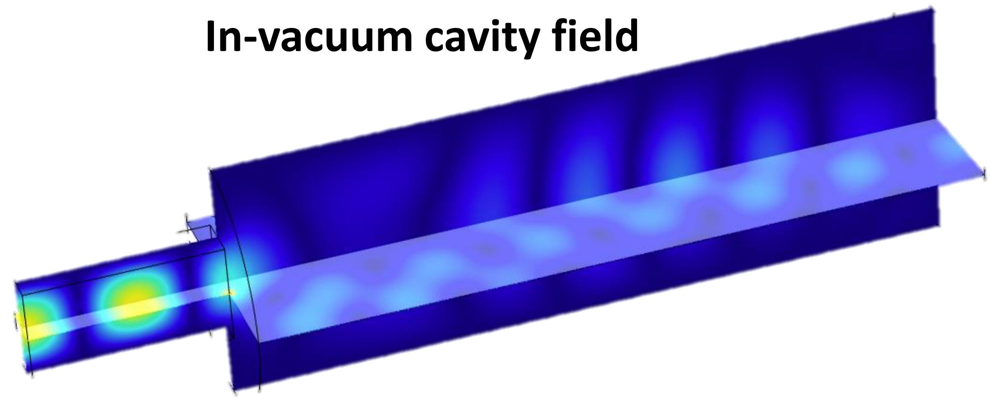

Non-uniform mesh accounting for dielectric tensor elements discontinuity at ECR

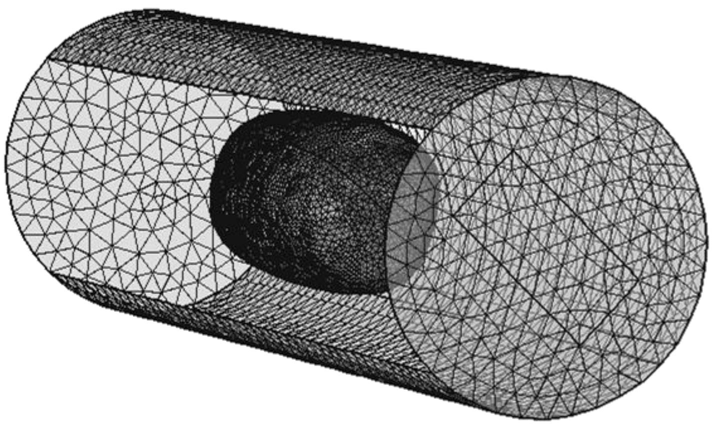

Electromagnetic field distribution inside the plasma filled cavity (cutoff density into the plasmoid)

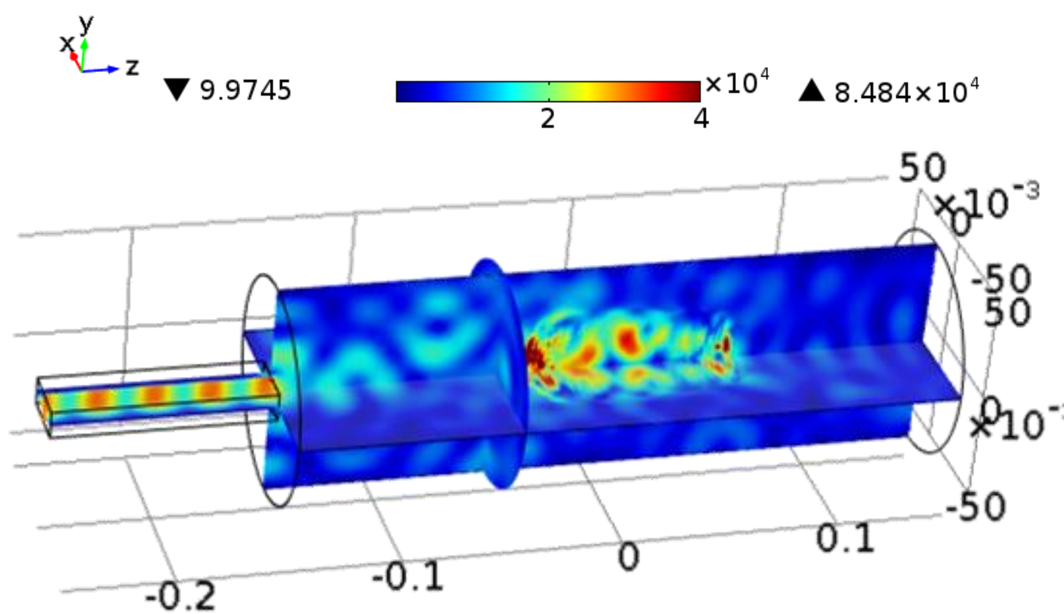

Self-consistency implementation

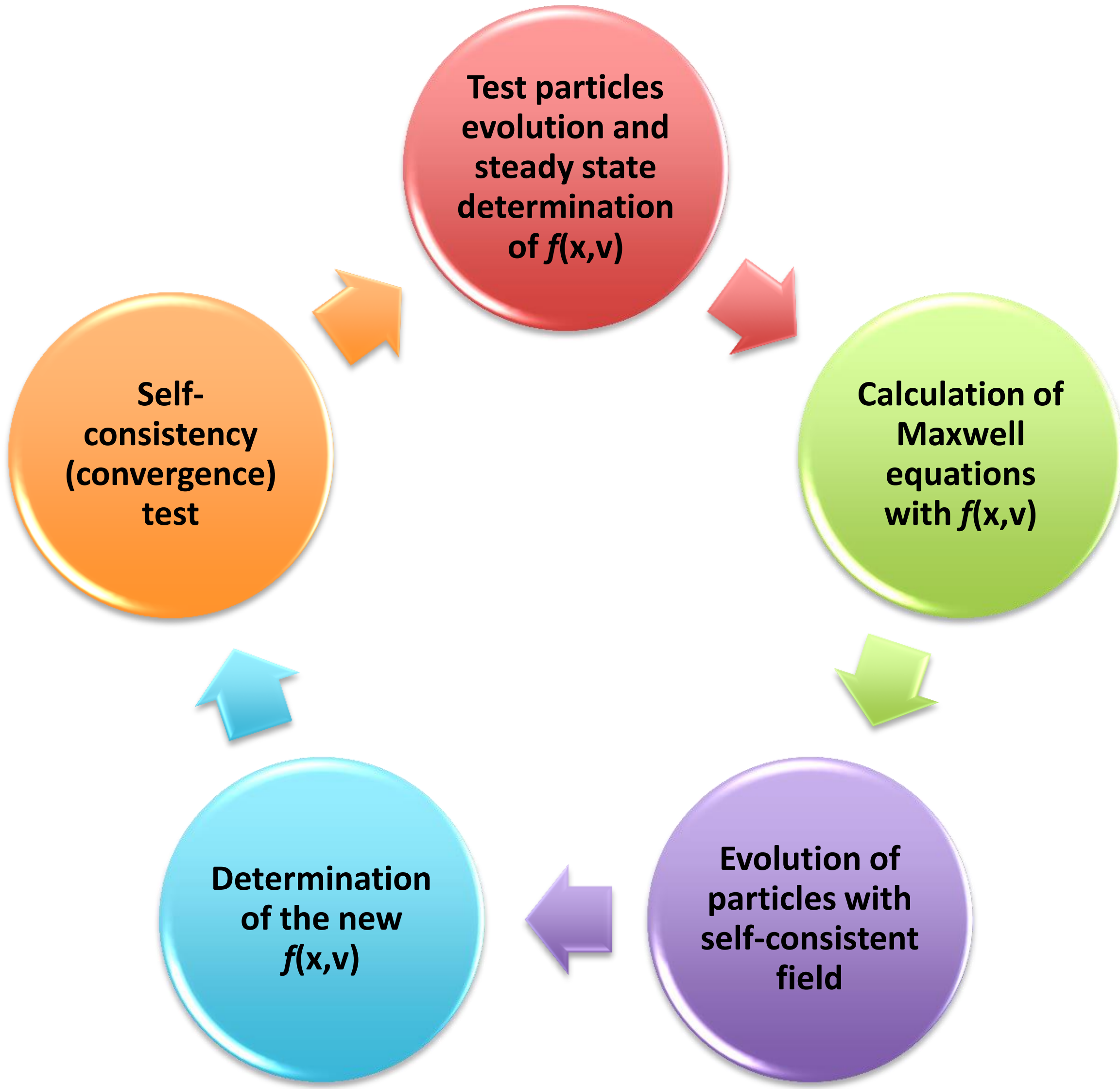

Simulations and modelling: Further Steps towards self-consistency

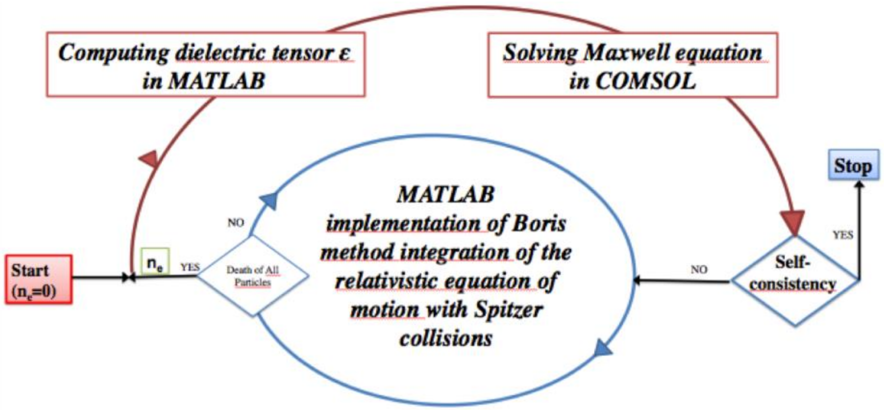

Solution of Maxwell-equations including the plasma inside the resonator: cold dielectric tensor used, accounting for R,L,O,X modes.

RF power deposition on the plasmoid surface

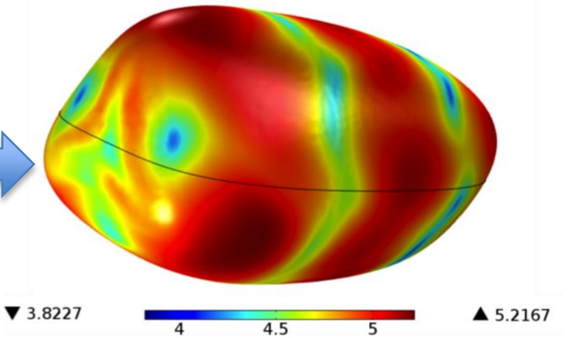

Plasma density structure in different energy domains

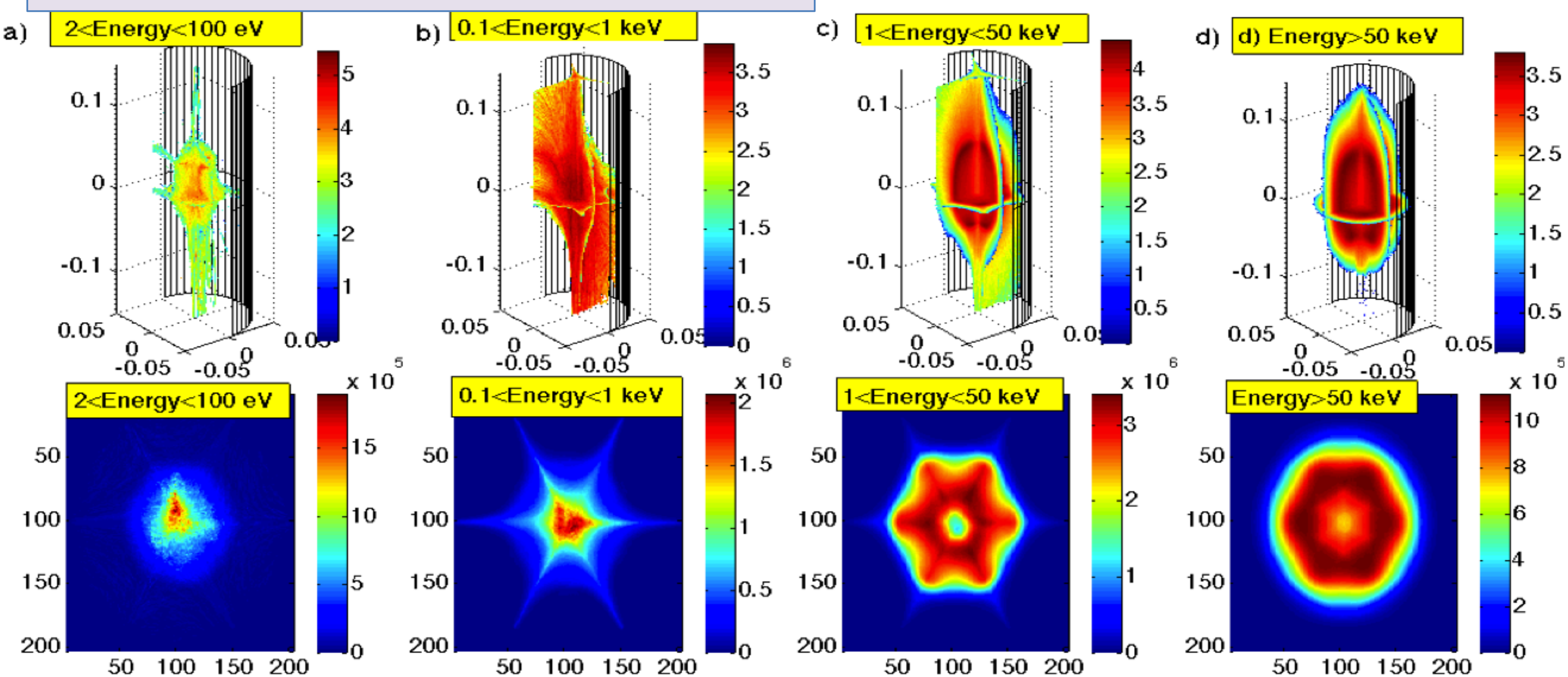

Plasma Diagnostics

- Advancements in X-ray spectroscopy (including space-resolved spectroscopy)
- Development of a new, compact microwave interferometer

Advanced techniques of plasma diagnostics have been already implemented: the X-ray pin-hole camera

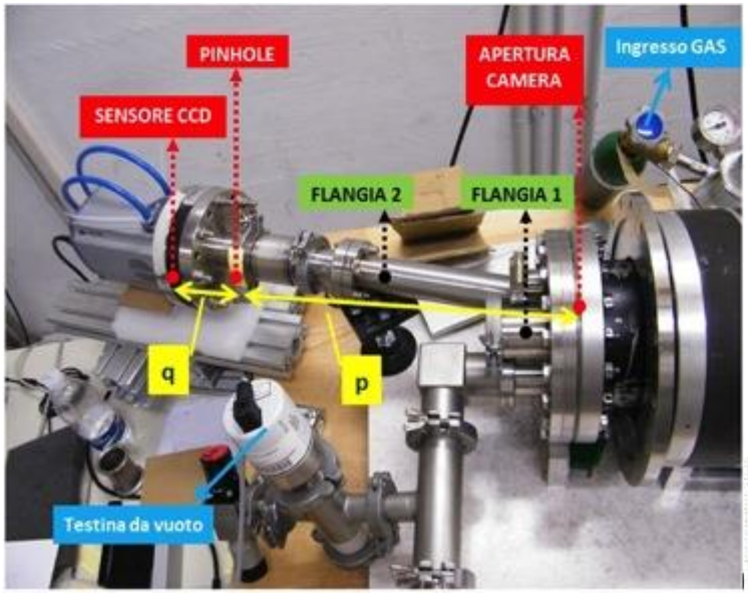

X-ray imaging can be performed with a pin-hole camera technique

The pin-hole is mounted between the plasma and a X-ray sensitive CCD camera having 1024x1024 pixels in the 0.5-15 keV energy domain

X-ray sensitive CCD - camera

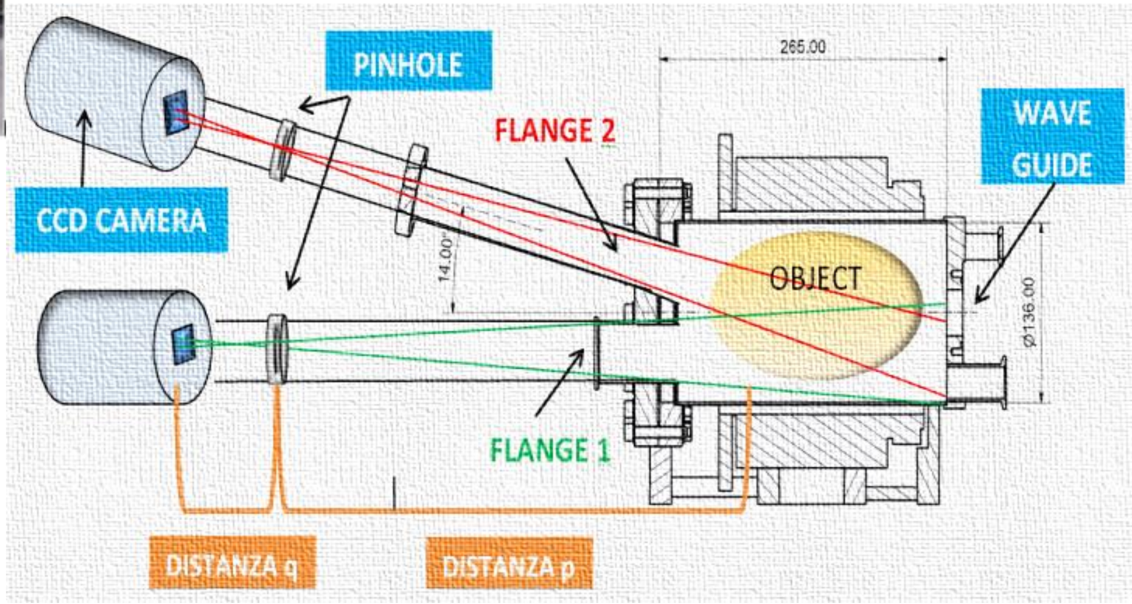

X-ray imaging: detection of the Hot Electron Layer

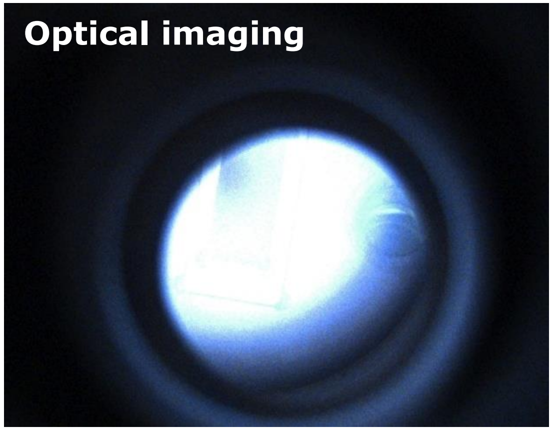

Images in the optical window, taken through an off-axis DN40 flange, evidence the generation of a high-brightness annulus surrounding a dark hole.

X-ray imaging evidences that the pumping power is deposited in the annulus, where the energetic electrons are generated

Transversal reconstruction of the plasma structure in X-ray domain (1-30 keV).

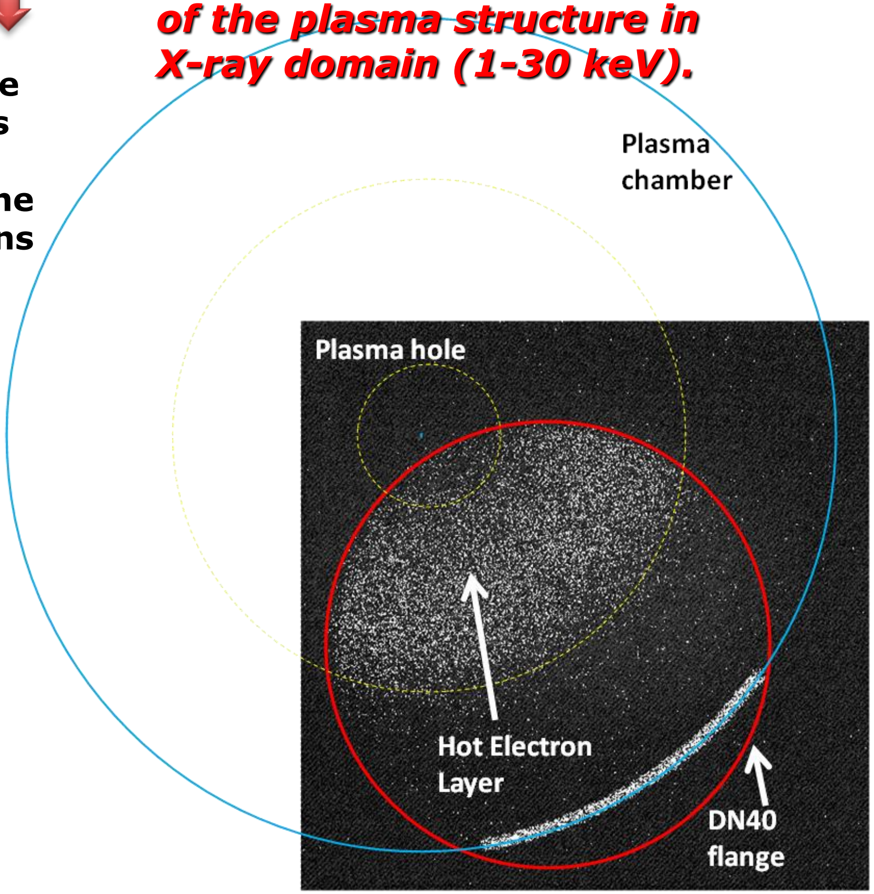

A high brightness strip appears due to electrons impinging on the chamber walls (bremsstrahlung through the stainless steel walls)

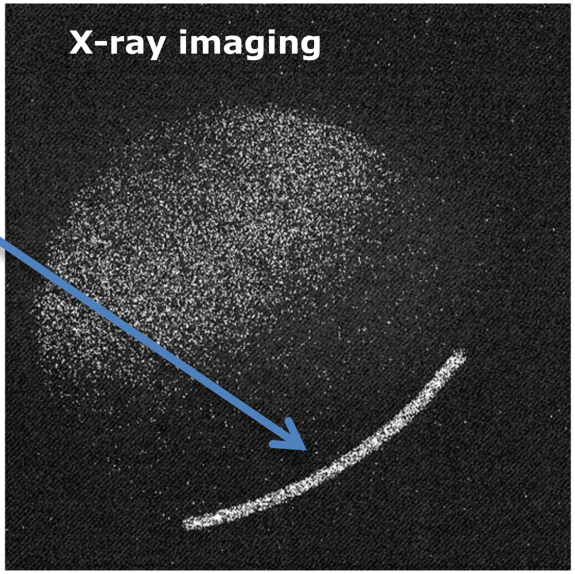

gas:Argon
pressure:3*10-4 mbar
RF power:100W
100 frames - 1sec exposure for each one

Plama Diagnostics: *sophisticated tools for covering the entire EM spectrum*

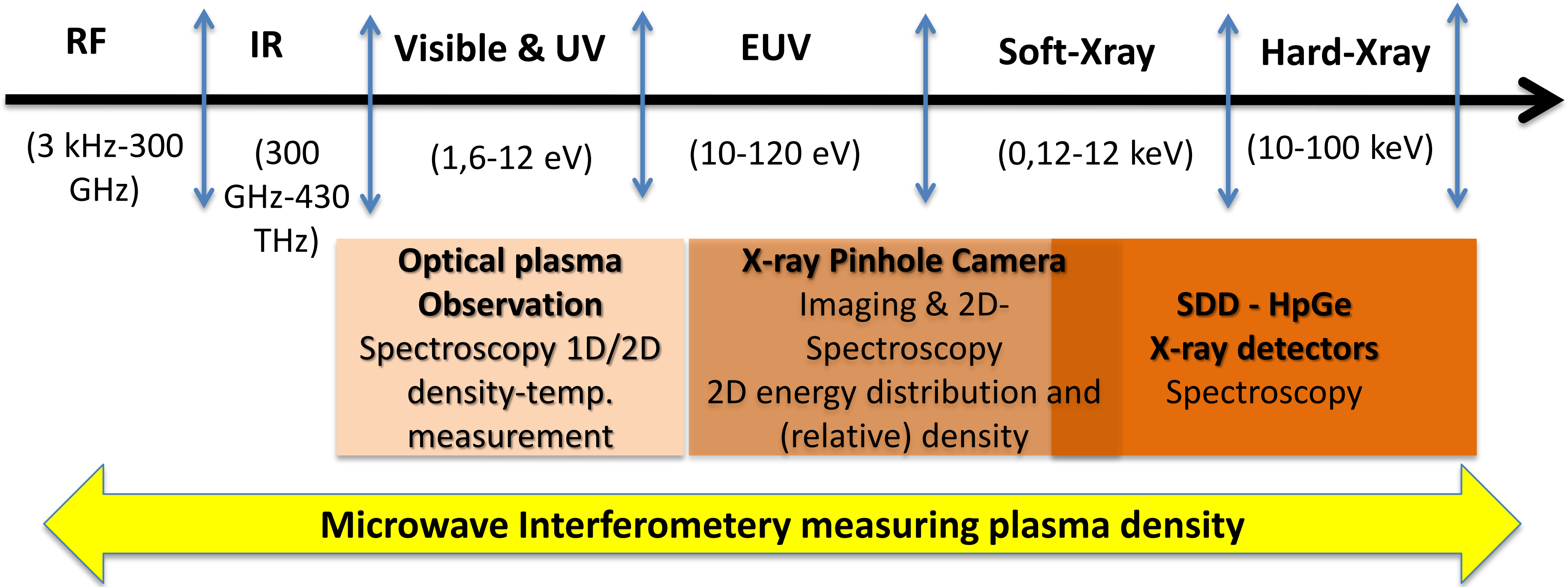

We need a tool able to measure density of electrons with an externally injected "probing" radiation (no perturbation since $P_{probing}/P_{exciting}<1\%$)

→ Density measurement technique no-longer based on plasma emission but on "response-on-transmission" of microwaves through the plasma

MICROWAVE INTERFEROMETRY

Interferometry for plasmas

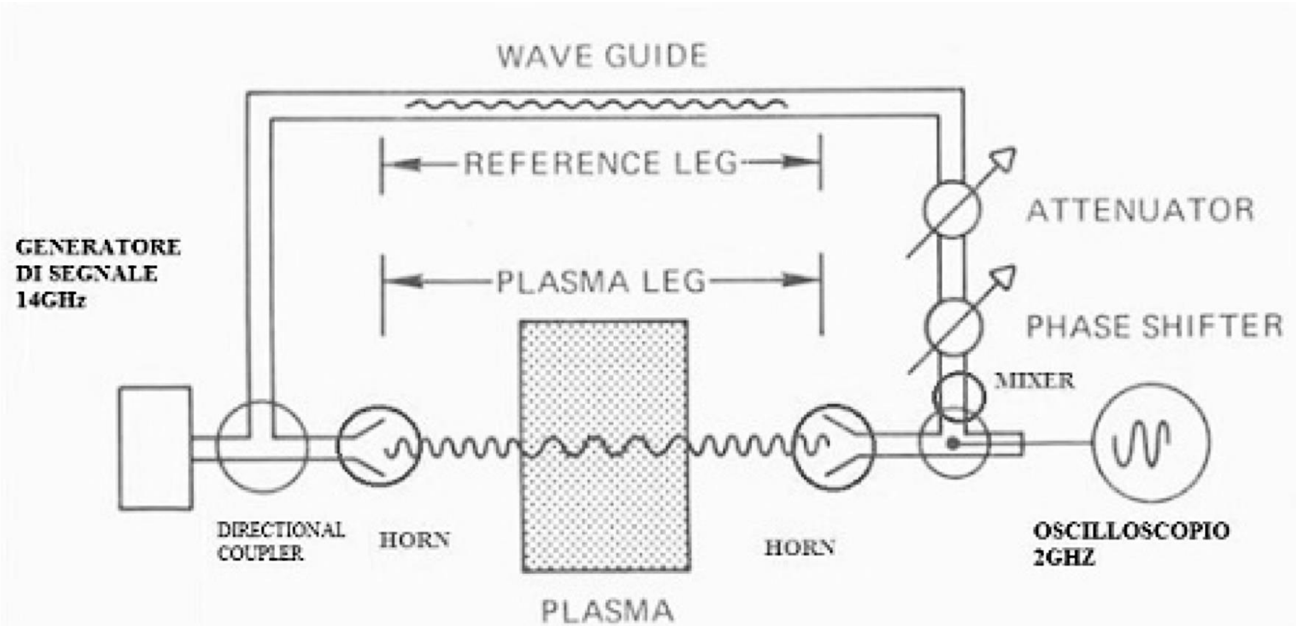

Classical Scheme of Interferometer

$$\Delta\varphi = \frac{\omega}{c}\left[1 - \left(1 - \frac{{\omega_p}^2}{\omega^2}\right)^{\frac{1}{2}}\right]L \quad \Rightarrow \quad {\omega_p}^2 = \frac{4\pi n e^2}{m\varepsilon_0} \quad \Rightarrow$$

In plasmas the phase variation depends on the " natural plasma frequency"

The plasma frequency depends on the density

Microwave interferometry measures plasma density through a measurement of phase shift.

Criticality: multi-paths introduce spurious signals

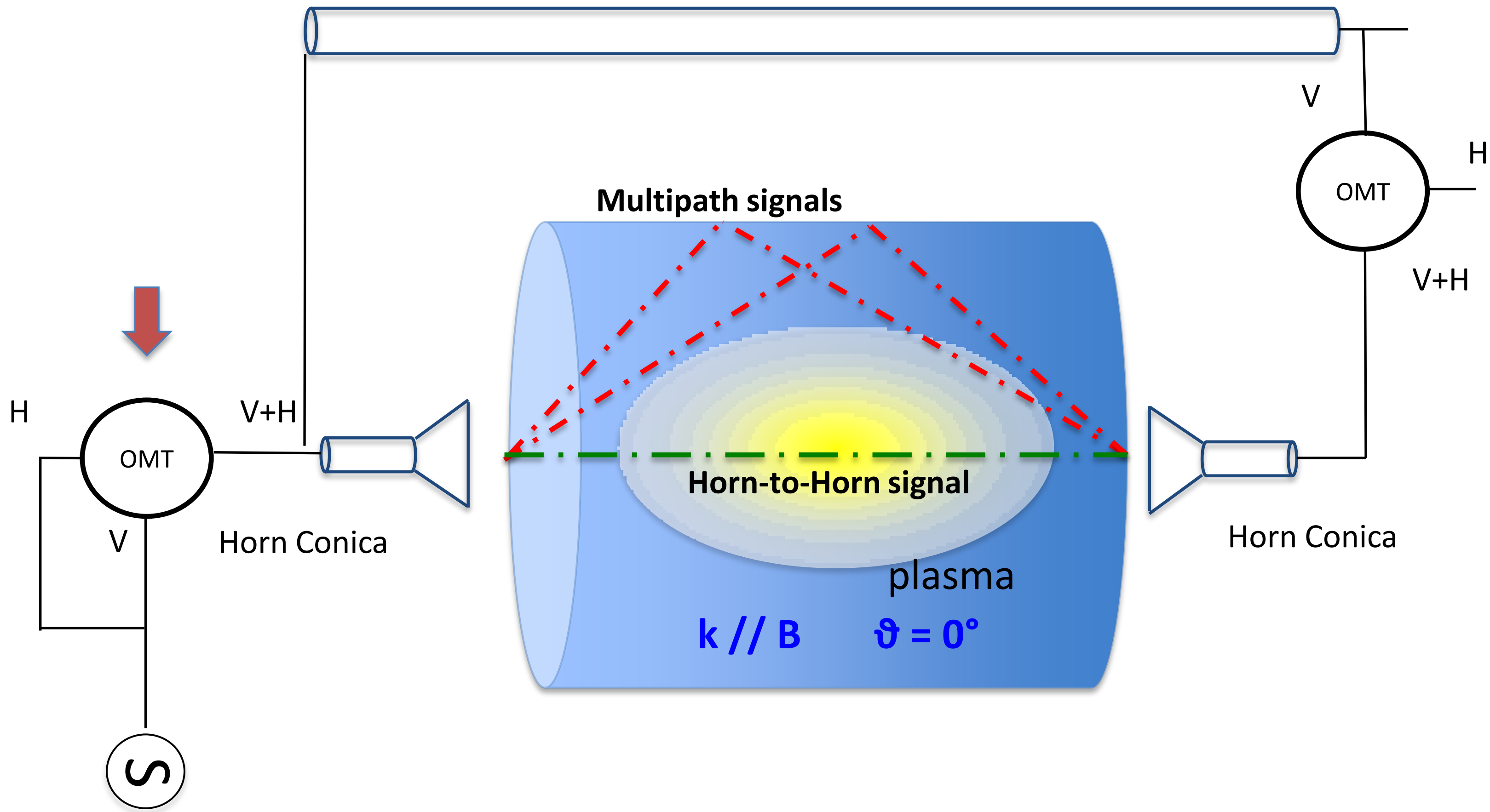

SIMULATION HORN TO HORN TO UNDERSTAND HOW TO DISCRIMINATE CAVITY WALL EFFECTS IN PROGRESS

Flexible Plasma Trap: *a new tool for fundamental plasma physics studies*

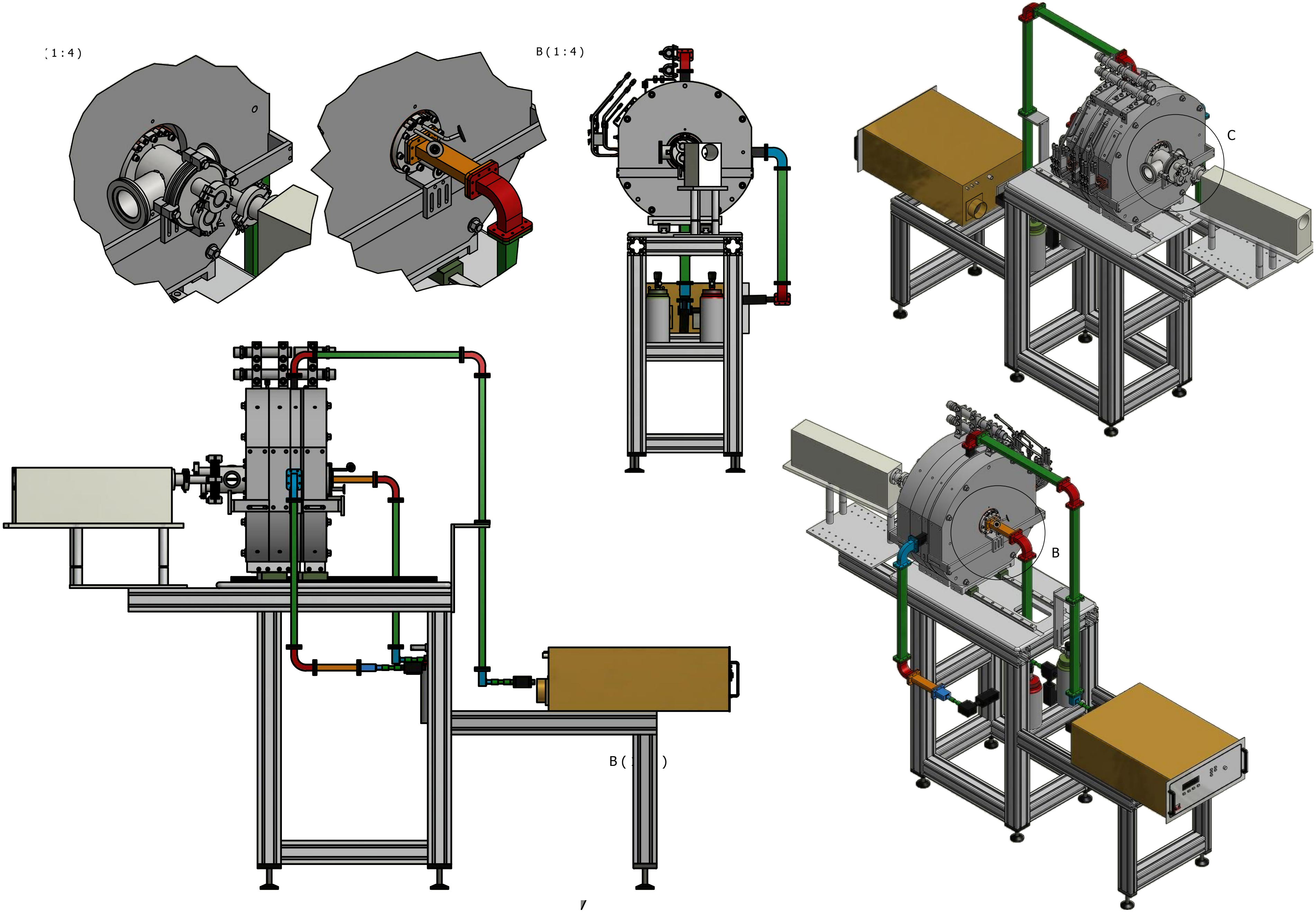

Trap assebly is ongoing…

Diagnostcs box as a prechamber for hosting high sensitive/space resolved X-ray spectrometers

Installation to be completed within September. First plasma late September.

Thank You for Your Attention !!!